

TA7

C6

CER 65-32

COPY 2

ENGINEERING RESEARCH

SEP 4 '74

FOOTHILLS READING ROOM

Final Report

RATE OF QUALITY CHANGE OF DRAIN EFFLUENT  
FROM A SALINE WATER AQUIFER

by

D. E. L. Maasland

With Supplement

COMPARISONS OF VISCOUS ANALOGY MODEL  
RESULTS WITH USBR SAND TANK STUDIES

by

M. W. Bittinger and D. E. L. Maasland

Submitted to the

Bureau of Reclamation

U.S. Department of Interior

Under Contract No. 14-06-D-5254

Engineering Research Center  
Colorado State University  
Fort Collins, Colorado

June, 1965

CER65DELM-MWB32

13  
Final Report

RATE OF QUALITY CHANGE OF DRAIN EFFLUENT  
FROM A SALINE WATER AQUIFER

by

D. E. L. Maasland

With Supplement

COMPARISONS OF VISCOUS ANALOGY MODEL  
RESULTS WITH USBR SAND TANK STUDIES

by

M. W. Bittinger and D. E. L. Maasland

Submitted to the  
Bureau of Reclamation  
U.S. Department of Interior  
Under Contract No. 14-06-D-5254

Engineering Research Center  
Colorado State University  
Fort Collins, Colorado

June 1965

CER65DELM-MWB32



U18401 0594409

DISSERTATION

---

RATE OF QUALITY CHANGE OF DRAIN  
EFFLUENT FROM A SALINE WATER  
AQUIFER

Submitted by

D. E. L. Maasland

In partial fulfillment of the requirements

for the Degree of Doctor of Philosophy

in Civil Engineering

Colorado State University

Fort Collins, Colorado

January, 1965

## ABSTRACT OF DISSERTATION

### RATE OF QUALITY CHANGE OF DRAIN EFFLUENT FROM A SALINE WATER AQUIFER

The effluent from drains in a saline water aquifer, being recharged with fresh water, consists of a mixture of salt and fresh water.

A Hele-Shaw model study was conducted to determine the rate of quality change of drain effluent for various conditions of drain spacing, thickness of aquifer, permeability, and recharge rate. Three aquifer conditions were studied: 1. A uniform aquifer, 2. A layered aquifer (top layer 12 times as permeable as the bottom), 3. A layered aquifer (bottom layer 6 times as permeable as the top).

Results are presented in the form of dimensionless charts, containing the variables drain spacing, thickness of aquifer, permeability, recharge rate, and effective porosity.

The concentration of the effluent at any time was found to be: 1. inversely related to the recharge rate, 2. directly related to the drain spacing only for very small values of the spacing, 3. directly related to the thickness of the aquifer, 4. inversely related to the permeability.

D. E. L. Maasland  
Civil Engineering Department  
Colorado State University  
Fort Collins, Colorado  
January, 1965

## ACKNOWLEDGEMENT

The author wishes to express his sincere thanks and appreciation to his major professor Morton W. Bittinger, Associate Civil Engineer, for his guidance during the course of this study. His ability in stimulating independence and interest as well as his valuable suggestions and contributions have made this dissertation possible.

The author's research and dissertation committee, Dr. A. T. Corey, Professor of Agricultural Engineering, Dr. J. W. F. Fead, Professor of Civil Engineering, Dr. W. D. Kemper, Associate Professor of Agronomy and Soil Scientist, U.S.D.A.-A.R.S.-S.W.C., and Dr. E. Gordon Kruse, Agricultural Engineer, U.S.D.A.-A.R.S.-S.W.C., reviewed and made valuable comments on the dissertation.

G. Palos, initially, and Ray Walchle, during the later stages, assisted with the experimental work. Mr. Gale Lutz offered valuable comments.

Mrs. June Steele, Mrs. Arlene Nelson, Miss Hanae Akari, Mrs. Janice Liggett, Mrs. Vicki Sopher, and Mr. Duayne Barrhart are to be thanked for the typing, drafting and reproduction of the final draft.

The U. S. Bureau of Reclamation provided the financial support for the research and some of the equipment.

The author's most deep felt thanks go to his wife Paula, not only for helping in the analysis of the data, but especially for her patience and acceptance of the many hours away from home.

## TABLE OF CONTENTS

<u>Chapter</u>	<u>Page</u>
I INTRODUCTION.....	1
II REVIEW OF LITERATURE.....	4
Use of Ground Water Models.....	4
The Interface Between Salt and Fresh Water.....	7
III THEORY AND SCALING OF MODEL.....	12
Analysis of Problem.....	12
Model Theory and Scaling.....	15
IV EXPERIMENTAL PROCEDURE.....	22
Experiments with Water.....	23
Experiments with Water-Glycerine Mixture.....	25
V PRESENTATION OF DATA AND RESULTS.....	29
Aquifer of Uniform Permeability.....	29
Two-Part Aquifer. Top Half More Permeable than Bottom Half.....	31
Two-Part Aquifer. Bottom Half More Permeable than Top Half.....	32
VI ANALYSIS OF RESULTS.....	34
Dimensionless Charts.....	34
Effect of Variables on Degree of Aquifer Cleaning.	37
Effect of Variables on Concentration of Effluent...	40
Comparison of Water with Glycerine-Water Experiments.....	44
Continuous versus Intermittent Recharge.....	45

TABLE OF CONTENTS (cont'd)

<u>Chapter</u>		<u>Page</u>
	Effect of Initial Concentration.....	47
VII	CONCLUSIONS AND RECOMMENDATIONS.....	49
	BIBLIOGRAPHY .....	52
	APPENDIX A--Figures.....	55

## LIST OF FIGURES

<u>Figure</u>		<u>Page</u>
1	Refraction of flow lines near a water table with accretion.....	56
2	Sketch of Hele-Shaw model.....	57
3	Example of change of salt-fresh water interface with time.....	58
4	Conductivity cell arrangement and conductivity recorder.....	59
5	Concentration versus time (Run 1, initial concentration 10,000 ppm, uniform aquifer).....	60
6	Concentration versus time (Run 10, initial concentration 10,000 ppm, uniform aquifer).....	61
7	Concentration versus time (Run 9, initial concentration 10,000 ppm, uniform aquifer).....	62
8	Concentration versus time (Run 5, initial concentration 10,000 ppm, uniform aquifer).....	63
9	Concentration versus time (Run 8, initial concentration 10,000 ppm, uniform aquifer).....	64
10	Concentration versus time (Run 7, initial concentration 10,000 ppm, uniform aquifer).....	65
11	Concentration versus time (Run 11, initial concentration 10,000 ppm, uniform aquifer).....	66
12	Concentration versus time (Run 6, initial concentration 10,000 ppm, uniform aquifer).....	67
13	Concentration versus time (Run 4, initial concentration 10,000 ppm, uniform aquifer).....	68
14	Concentration versus time (Run 2, initial concentration 10,000 ppm, uniform aquifer).....	69
15	Concentration versus time (Run 3, initial concentration 10,000 ppm, uniform aquifer).....	70

LIST OF FIGURES (cont'd)

<u>Figure</u>		<u>Page</u>
16	Concentration versus time (Run 1, initial concentration 15,000 ppm, uniform aquifer).....	71
17	Concentration versus time (Run 8, initial concentration 15,000 ppm, uniform aquifer).....	72
18	Concentration versus time (Run 2, initial concentration 15,000 ppm, uniform aquifer).....	73
19	Concentration versus time (Run 3, initial concentration 15,000 ppm, uniform aquifer).....	74
20	Concentration versus time (Run 12, initial concentration 15,000 ppm, uniform aquifer).....	75
21	Concentration versus time (Run 4, initial concentration 15,000 ppm, uniform aquifer).....	76
22	Concentration versus time (Run 11, initial concentration 15,000 ppm, uniform aquifer).....	77
23	Concentration versus time (Run 5, initial concentration 15,000 ppm, uniform aquifer).....	78
24	Concentration versus time (Run 9, initial concentration 15,000 ppm, uniform aquifer).....	79
25	Concentration versus time (Run 6, initial concentration 15,000 ppm, uniform aquifer).....	80
26	Concentration versus time (Run 7, initial concentration 15,000 ppm, uniform aquifer).....	81
27	Concentration versus time (Run 10, initial concentration 15,000 ppm, uniform aquifer).....	82
28	Concentration versus time (Run 13, initial concentration 15,000 ppm, uniform aquifer).....	83
29	Concentration versus time (Run 6, initial concentration 30,000 ppm, uniform aquifer).....	84
30	Concentration versus time (Run 5, initial concentration 30,000 ppm, uniform aquifer).....	85

LIST OF FIGURES (cont'd)

<u>Figure</u>		<u>Page</u>
31	Concentration versus time (Run 13, initial concentration 30,000 ppm, uniform aquifer).....	86
32	Concentration versus time (Run 10, initial concentration 30,000 ppm, uniform aquifer).....	87
33	Concentration versus time (Run 9, initial concentration 30,000 ppm, uniform aquifer).....	88
34	Concentration versus time (Run 12, initial concentration 30,000 ppm, uniform aquifer).....	89
35	Concentration versus time (Run 11, initial concentration 30,000 ppm, uniform aquifer).....	90
36	Concentration versus time (Run 8, initial concentration 30,000 ppm, uniform aquifer).....	91
37	Concentration versus time (Run 3, initial concentration 30,000 ppm, uniform aquifer).....	92
38	Concentration versus time (Run 4, initial concentration 30,000 ppm, uniform aquifer).....	93
39	Concentration versus time (Run 7, initial concentration 30,000 ppm, uniform aquifer).....	94
40	Concentration versus time (Run 1, initial concentration 30,000 ppm, uniform aquifer).....	95
41	Concentration versus time (Run 2, initial concentration 30,000 ppm, uniform aquifer).....	96
42	Concentration versus time (Run 8, initial concentration 15,000 ppm, layered aquifer $K_1/K_2 = 12/1$ )....	97
43	Concentration versus time (Run 5, initial concentration 15,000 ppm, layered aquifer $K_1/K_2 = 12/1$ )....	98
44	Concentration versus time (Run 10, initial concentration 15,000 ppm, layered aquifer $K_1/K_2 = 12/1$ )....	99

LIST OF FIGURES (cont'd)

<u>Figure</u>		<u>Page</u>
45	Concentration versus time (Run 6, initial concentration 15,000 ppm, layered aquifer $K_1/K_2 = 12/1$ ) . . . .	100
46	Concentration versus time (Run 3, initial concentration 15,000 ppm, layered aquifer $K_1/K_2 = 12/1$ ) . . . .	101
47	Concentration versus time (Run 7, initial concentration 15,000 ppm, layered aquifer $K_1/K_2 = 12/1$ ) . . . .	102
48	Concentration versus time (Run 4, initial concentration 15,000 ppm, layered aquifer $K_1/K_2 = 12/1$ ) . . . .	103
49	Concentration versus time (Run 9, initial concentration 15,000 ppm, layered aquifer $K_1/K_2 = 12/1$ ) . . . .	104
50	Concentration versus time (Run 2, initial concentration 15,000 ppm, layered aquifer $K_1/K_2 = 12/1$ ) . . . .	105
51	Concentration versus time (Run 1, initial concentration 15,000 ppm, layered aquifer $K_1/K_2 = 12/1$ ) . . . .	106
52	Concentration versus time (Run 4, initial concentration 30,000 ppm, layered aquifer $K_1/K_2 = 12/1$ ) . . . .	107
53	Concentration versus time (Run 8, initial concentration 30,000 ppm, layered aquifer $K_1/K_2 = 12/1$ ) . . . .	108
54	Concentration versus time (Run 5, initial concentration 30,000 ppm, layered aquifer $K_1/K_2 = 12/1$ ) . . . .	109
55	Concentration versus time (Run 7, initial concentration 30,000 ppm, layered aquifer $K_1/K_2 = 12/1$ ) . . . .	110
56	Concentration versus time (Run 2, initial concentration 30,000 ppm, layered aquifer $K_1/K_2 = 12/1$ ) . . . .	111
57	Concentration versus time (Run 9, initial concentration 30,000 ppm, layered aquifer $K_1/K_2 = 12/1$ ) . . . .	112
58	Concentration versus time (Run 6, initial concentration 30,000 ppm, layered aquifer $K_1/K_2 = 12/1$ ) . . . .	113
59	Concentration versus time (Run 3, initial concentration 30,000 ppm, layered aquifer $K_1/K_2 = 12/1$ ) . . . .	114

LIST OF FIGURES (cont'd)

<u>Figure</u>		<u>Page</u>
60	Concentration versus time (Run 1, initial concentration 30,000 ppm, layered aquifer $K_1/K_2 = 12/1$ ).....	115
61	Concentration versus time (Run 3, initial concentration 15,000 ppm, layered aquifer $K_1/K_2 = 1/6$ ).....	116
62	Concentration versus time (Run 1, initial concentration 15,000 ppm, layered aquifer $K_1/K_2 = 1/6$ ).....	117
63	Concentration versus time (Run 7, initial concentration 15,000 ppm, layered aquifer $K_1/K_2 = 1/6$ ).....	118
64	Concentration versus time (Run 5, initial concentration 15,000 ppm, layered aquifer $K_1/K_2 = 1/6$ ).....	119
65	Concentration versus time (Run 12, initial concentration 15,000 ppm, layered aquifer $K_1/K_2 = 1/6$ ).....	120
66	Concentration versus time (Run 6, initial concentration 15,000 ppm, layered aquifer $K_1/K_2 = 1/6$ ).....	121
67	Concentration versus time (Run 2, initial concentration 15,000 ppm, layered aquifer $K_1/K_2 = 1/6$ ).....	122
68	Concentration versus time (Run 10, initial concentration 15,000 ppm, layered aquifer $K_1/K_2 = 1/6$ ).....	123
69	Concentration versus time (Run 9, initial concentration 15,000 ppm, layered aquifer $K_1/K_2 = 1/6$ ).....	124
70	Concentration versus time (Run 8, initial concentration 15,000 ppm, layered aquifer $K_1/K_2 = 1/6$ ).....	125
71	Concentration versus time (Run 11, initial concentration 15,000 ppm, layered aquifer $K_1/K_2 = 1/6$ ).....	126
72	Concentration versus time (Run 4, initial concentration 15,000 ppm, layered aquifer $K_1/K_2 = 1/6$ ).....	127
73	Concentration versus time (Run 2, initial concentration 30,000 ppm, layered aquifer $K_1/K_2 = 1/6$ ).....	128
74	Concentration versus time (Run 13, initial concentration 30,000 ppm, layered aquifer $K_1/K_2 = 1/6$ ).....	129

LIST OF FIGURES (cont'd)

<u>Figure</u>	<u>Page</u>
75 Concentration versus time (Run 3, initial concentration 30,000 ppm, layered aquifer $K_1/K_2 = 1/6$ ).....	130
76 Concentration versus time (Run 5, initial concentration 30,000 ppm, layered aquifer $K_1/K_2 = 1/6$ ).....	131
77 Concentration versus time (Run 9, initial concentration 30,000 ppm, layered aquifer $K_1/K_2 = 1/6$ ).....	132
78 Concentration versus time (Run 7, initial concentration 30,000 ppm, layered aquifer $K_1/K_2 = 1/6$ ).....	133
79 Concentration versus time (Run 6, initial concentration 30,000 ppm, layered aquifer $K_1/K_2 = 1/6$ ).....	134
80 Concentration versus time (Run 8, initial concentration 30,000 ppm, layered aquifer $K_1/K_2 = 1/6$ ).....	135
81 Concentration versus time (Run 4, initial concentration 30,000 ppm, layered aquifer $K_1/K_2 = 1/6$ ).....	136
82 Concentration versus time (Run 1, initial concentration 30,000 ppm, layered aquifer $K_1/K_2 = 1/6$ ).....	137
83 Concentration versus time (Run 10, initial concentration 30,000 ppm, layered aquifer $K_1/K_2 = 1/6$ ).....	138
84 Concentration versus time (Run 11, initial concentration 30,000 ppm, layered aquifer $K_1/K_2 = 1/6$ ).....	139
85 Dimensionless chart of $(hx_p^2) / (K_{xp} z_p^2)$ versus $(z_p K_{xp} t) / (n x_p^2)$ (uniform aquifer, initial concentration 10,000 ppm).....	140
86 Dimensionless chart of $(hx_p^2) / (K_{xp} z_p^2)$ versus $(z_p K_{xp} t) / (n x_p^2)$ (uniform aquifer, initial concentration 15,000 ppm).....	141

LIST OF FIGURES (cont'd)

<u>Figure</u>		<u>Page</u>
87	Dimensionless chart of $(hx_p^2) / (K_{xp} z_p^2)$ versus $(z_p K_{xp} t) / (n_p x_p^2)$ (uniform aquifer, initial concentration 30,000 ppm).....	142
88	Dimensionless chart of $(hx_p^2) / (K_{xp} z_{p1}^2)$ versus $(z_{p1} K_{xp} t) / (n_p x_p^2)$ (layered aquifer, $K_1/K_2 = 12/1$ , initial concentration 15,000 ppm).....	143
89	Dimensionless chart of $(hx_p^2) / (K_{xp} z_{p1}^2)$ versus $(z_{p1} K_{xp} t) / (n_p x_p^2)$ (layered aquifer, $K_1/K_2 = 12/1$ , initial concentration 30,000 ppm).....	144
90	Dimensionless chart of $(hx_p^2) / (K_{xp} z_{p1}^2)$ versus $(z_{p1} K_{xp} t) / (n_p x_p^2)$ (layered aquifer, $K_1/K_2 = 1/6$ , initial concentration 15,000 ppm).....	145
91	Dimensionless chart of $(hx_p^2) / (K_{xp} z_{p1}^2)$ versus $(z_{p1} K_{xp} t) / (n_p x_p^2)$ (layered aquifer, $K_1/K_2 = 1/6$ , initial concentration 30,000 ppm).....	146
92	Percent of aquifer thickness cleaned versus $(hx_p^2) / (K_{xp} z_p^2)$ (uniform aquifer).....	147
93	Percent of aquifer thickness cleaned versus $(hx_p^2) / (K_{xp} z_{p1}^2)$ (layered aquifer $K_1/K_2 = 12/1$ ).....	148
94	Concentration versus time for some specific conditions (uniform aquifer, initial concentration, 10,000 ppm).....	149
95	Model discharge versus model time (uniform aquifer, water experiments).....	150

LIST OF FIGURES (cont'd)

<u>Figure</u>		<u>Page</u>
96	Model discharge versus model time (10.5/1 aquifer, water experiments).....	151
97	Model discharge versus model time (1/11.5 aquifer, water experiments).....	152
98	Effluent concentration versus time.....	153
99	Effluent concentration versus time (intermittent versus continuous recharge, initial concentration 15,000 ppm).....	154
100	Effluent concentration versus time (intermittent versus continuous recharge, initial concentration 30,000 ppm).....	155
101	Effluent concentration versus $(z \frac{K_p}{x p} t) / (n \frac{x}{p} p^2)$ for different values of initial concentration.....	156
102	Effluent concentration versus $(z \frac{K_p}{x p} t) / (n \frac{x}{p} p^2)$ for different values of initial concentration.....	157

## LIST OF SYMBOLS

<u>SYMBOL</u>	<u>DIMENSION</u>	<u>DESCRIPTION</u>
b	L	Interspace width of model
$b_p$	L	Width in prototype
g	$L/T^2$	Acceleration of gravity
h	L/T	Rate of recharge
K	L/T	Permeability
k	$L^2$	Intrinsic permeability
$K_x, K_z$	L/T	Permeability in horizontal and vertical direction
$K_1$	L/T	Permeability of upper layer
$K_2$	L/T	Permeability of lower layer
m		Subscript used in conjunction with a variable denoting the magnitude of the variable in the model
n	Dimensionless	Effective porosity
p		Subscript used in conjunction with a variable denoting the magnitude of the variable in the prototype
p	$ML/L^2T^2$	Pressure
q	L/T	Flux
Q	$L^3/T$	Rate of flow
r		Subscript used in conjunction with a variable denoting the scale factor of the variable
s	L	Average direction of flow
S	Dimensionless	Storage coefficient
t	T	Time

LIST OF SYMBOLS (cont'd)

<u>SYMBOL</u>	<u>DIMENSION</u>	<u>DESCRIPTION</u>
T	$L^2/T$	Transmissivity
v	$L/T$	Average velocity
x, y, z	L	Coordinates
$x_m$	L	Length of model
$x_p$	L	Half spacing between drains
$z_m$	L	Height in model
$z_p$	L	Thickness of aquifer
$z_{pl}$	L	Thickness of top part of aquifer (two-part aquifer)
$\rho$	$M/L^3$	Density
$\nu$	$L^2/T$	Kinematic viscosity
$\mu$	$M/L/T$	Dynamic viscosity
$\phi$	L	Piezometric head
$\Psi$	$L^2/T$	Stream function
$\gamma$	$ML/L^3T^2$	Specific weight

## CHAPTER I

### INTRODUCTION

The quality of ground water in arid and semi-arid regions is frequently poor as a result of the presence of salt. Dissolved salt may be present because of geologic conditions, such as dissolution from rocks, or man-made reasons, such as leaching by irrigation water from the upper strata of soil towards ground water.

When irrigation water is applied to land, the water table will generally rise, and water logging and soil salinity may result. These undesirable features may be prevented or corrected by installing drainage systems, such as drainage wells, tile drains or open drains. When tile drains are used, the quality of effluent from the drains will be dependent upon the ratio of the amounts of salt and fresh water flowing into the drain. The quality of effluent at any time depends upon the following factors: quality of both the recharge water and water present in the aquifer, spacing between drains, saturated thickness of the aquifer, permeability in horizontal and vertical directions, rate of recharge, effective porosity and the degree of homogeneity of the aquifer.

Most of the drainage effluent will in time find its way back to a stream, thus contaminating its water. In 1945 water use in the United States amounted to 160 billion gallons of water daily. Presently the daily water use has more than doubled to 355 billion gallons.

With a rather fixed supply of fresh water available, more water will have to be re-used in the future.

Clapper (1963) quotes Public Health Service estimates that the total flow of the Ohio River is being used 3.7 times before it reaches the Mississippi River. By the time the water in the Mahoning River reaches Youngstown, Ohio, it has been re-used more than eight times.

Although much contamination of river water is due to industrial wastes and raw sewage from population centers, the Western United States will increasingly be bothered by contamination due to drainage effluents. For example, the soluble salts in the Rio Grande increase from about 180 parts per million at Otowi Bridge, New Mexico, to 780 parts per million at El Paso, Texas, and 1770 parts per million at Fort Quitman, Texas. The concentration of salt in the lower Rio Grande, however, drops because of the lower concentration of salts in some of the tributaries, so that at Rio Grande City, Texas, more than 900 miles down the river from Fort Quitman, the amount of soluble salts is only about 525 parts per million. (Fireman and Hayward, 1955)

It is therefore of great interest to be able to predict how the quality of effluent from drain tiles will change in time when an aquifer containing saline water is recharged with fresh irrigation water under different conditions of ground water and recharge water salinity, drain

spacing, and aquifer characteristics. It is also of interest to know the depth to which the aquifer will eventually be flushed clear of salt water. Except for some work by Peterka and Glover (1963) no one is known to have studied this problem.

There are basically three ways in which this problem may be studied; i.e. by field experiments, analytical solutions, or model studies. Field experiments are of long duration, often expensive and with little control. Moreover it is often difficult, if not impossible, to change variables in the field in order to obtain answers to questions of interest. Analytical solutions are desirable under many conditions. However, even though the problem can be stated in the form of a differential equation with appropriate initial and boundary equations, frequently an exact solution will not be available. In addition, if an exact solution may be obtained, the assumptions and simplifications required are sometimes so severe that application to field conditions is questionable. The third technique then, model studies, is often the only practical manner of obtaining desired answers.

The purpose of this study was to determine the rate of quality change of drain effluent as influenced by various physical factors using a viscous analogy model. The study was financed through a contract with the U. S. Bureau of Reclamation.

## CHAPTER II

### REVIEW OF LITERATURE

To the knowledge of this writer little work directly related to the present work has been done. Thus in this chapter literature is reviewed which indirectly was an aid to this study.

#### Use of groundwater models

In principle any ground water problem can be solved by means of an analytical solution. An analytical solution is always obtained by solving one or more differential equations with a set of appropriate initial and boundary conditions. Frequently it is difficult, if not impossible, to obtain the equations and boundary conditions, or when they can be obtained, to find the exact solutions of the equations and boundary conditions.

In that case, model studies are generally the practical way of obtaining answers to specific problems. Several types of models have been used in ground water research. Santing (1963) reviewed the various types of ground water models, particularly in connection with their applicability to different problems. The most commonly used models are the sand model, the Hele-Shaw model, the head model, the electrical model and the membrane model. All of these are based upon the similarity between the law governing ground water flow through porous media and the laws determining the motion of various physical quantities. The law governing ground

water flow is Darcy's Law (Darcy, 1856)

$$v = -K \frac{\partial \phi}{\partial s} \quad (2.1)$$

where  $v$  (the apparent velocity of flow) and  $\phi = p/\gamma + z$  (the piezometric head) are continuous functions of  $s$  (the distance along the average direction of flow). The permeability  $K$  is a characteristic of both the medium and the liquid flowing through it and may be expressed as

$$K = k \frac{\rho g}{\mu} \quad (2.2)$$

where  $k$  is the intrinsic permeability (characteristic of the porous medium only),  $\rho$  the density of the liquid and  $\mu$  the dynamic viscosity.

Laws similar to Darcy's Law describe the laminar flow of a viscous liquid between parallel plates, the flow of heat, the flow of electricity, and deflection of a rubber membrane. These laws may all be expressed by

$$q = -K \frac{\partial \phi}{\partial s} \quad (2.3)$$

where  $q$  is the flux,  $K$  a capacity factor and  $\frac{\partial \phi}{\partial s}$  a potential gradient. Adapted from Santing (1963) we present Table I

TABLE I

## Similarity of Flow Equations

Phenomenon	q	K	$\frac{\partial \phi}{\partial s}$
laminar flow of a liquid between parallel plates at distance b	v = average velocity of flow	$\frac{g}{12} \frac{\rho b^2}{\mu}$	$\frac{\partial \phi}{\partial s}$ = hydraulic gradient
flow of heat	q = heat flow per unit cross-sectional area	$\lambda$ = conductivity of medium	$\frac{\partial t}{\partial s}$ = temperature gradient
flow of electricity	i = current per unit of cross-sectional area	C = conductivity of conductor	$\frac{\partial E}{\partial s}$ = potential gradient
Deflection of rubber membrane	$S_z$ = deflection of membrane	C = tension in membrane	$\frac{\partial z}{\partial x}$ = slope of the membrane at any point

The proper choice of a model to be used in an investigation is dependent on the nature of the problem. The present study is basically a problem of determining the change in position of the salt-fresh water interface in time. In the types of analogies mentioned above, liquid density differences can be simulated only in a sand tank and in the viscous flow analogy (Santing, 1963). The latter has distinct advantages for 2-dimensional flow problems. Permeability may be changed by merely changing the width of the interspace between the plates or by employing a liquid of different kinematic viscosity. Since glass or plastic plates are used the flow is easily

visualized. No porous medium is used, eliminating side effects such as enclosed air, non-uniformity of packing and dispersion. Smaller quantities of liquid are needed, because the total amount of liquid stored in the model is small. Boundaries in the model may be adapted readily to the prototype geometry. The greatest advantage of the Hele-Shaw model over the sand model is the magnitude of the time-scale. Experiments which may take several days in a sand model, can often be performed in the viscous flow analogy in a period of a few hours. Its greatest disadvantage is, that it can be used to study 2-dimensional flow problems only.

The first viscous flow model was developed in England by H. S. Hele-Shaw (1898 and 1899), for the study of flow patterns around variously shaped bodies. It was named the Hele-Shaw model in his honor. It was not until 1936 that this model was used for groundwater studies by Dachler (1936) in Austria. Mme. Polubarinova-Kochina (1962) quotes a paper by Aravin in which is described the use of the parallel plate model for both two-dimensional and radial flow problems in ground water hydraulics. Santing (1951) reported the use of the Hele-Shaw model for the study of a salt-fresh water interface in a coastal aquifer.

#### The interface between salt and fresh water

From a search of the existing literature it becomes clear that the interest in the salt-fresh water interface has been centered

around problems occurring in coastal aquifers. A land mass bordering an ocean receives precipitation, a portion of which reaches the ground water system, thus creating a gradient towards the ocean. The flow of fresh water, due to this gradient occurs above a wedge of salt water. When left alone, a dynamic balance between the fresh ground water flow and the intruded salt water wedge is established. Todd (1960) quotes Badon Ghyben and Herzberg who found that salt water along the coast occurred at a depth below sea level of about forty times the height of fresh water above sea level. This distribution was attributed to a hydrostatic equilibrium existing between the two fluids of different density, and is now generally known as the Ghyben-Herzberg relation.

Glover (1959) states that when static conditions alone prevail the fresh water body tapers to a knife edge at the shore allowing no way for the fresh water to escape. He postulates a theory whereby the salt water edge is static and the fresh water above it flows towards the ocean. He then gives an equation for the interface location for a horizontal outcropping of fresh water.

Cooper (1959) states that in a coastal region neither the fresh water nor the salt water is in equilibrium. He visualizes a circulation of salt water from the sea to a zone of diffusion (zone of dispersion would be a more appropriate name) and back to the sea. Above this zone of diffusion the fresh water flows to the sea. This zone of diffusion may be as thick as 1000 ft such as measured below

the Pearl Harbor area. The approach of this paper is entirely qualitative in that no attempt is made to quantitatively define the zone of diffusion.

Bear and Dagan (1964) attempted to determine the shape and position of the interface in a coastal aquifer along the coast under various steady and unsteady exploitation conditions of wells. They also studied the phenomenon of local upconing towards a collector operating above the interface and the development of a transition zone along the interface due to hydrodynamic dispersion. The investigations were carried out in two stages: in the first stage the assumption was made that the two fluids were immiscible and that an abrupt interface existed. The second stage included the problems of hydrodynamic dispersion and the transition zone. They solved some steady-state conditions by means of the hodograph method and by the use of the Dupuit assumptions. These solutions were compared with results obtained with Hele-Shaw model tests. Good agreement was obtained. The same paper also pays some attention to the moving interface. Non-linear equations are obtained which make exact analytic solution almost impossible unless special linearization techniques are employed.

The problem of the moving interface has also received the attention of investigators in the oil-industry. The interface must be construed to be the interface between two immiscible fluids (e.g. oil and water). Kidder (1956,1) was concerned with the problem of

"fingering". Fingering refers to problems in which the permeable stratum is sufficiently thin that the flow of fluids can be treated as a two-dimensional flow in the plane of the stratum. He determined an exact solution at which oil may be produced without drawing water into the wells. The position of the interface between oil and water was only given in its terminal state. In another paper Kidder (1956, 2) obtained a general solution to a two-dimensional problem of the movement of the interface between two immiscible liquids of unequal density in a porous solid. The motion of the interface was the result of the force of gravity acting on the two liquids. The solution was obtained by direct potential theory methods and a method of approximation was employed similar to that used in the linear theory of water waves. The elevation of the interface above its equilibrium position was shown to satisfy a nonoscillatory wave equation.

Josselin de Jong (1960) studied the simultaneous flow of fluids of different properties by substituting the fluids by one hypothetical fluid and applying singularities at those points where the properties of the actual fluids change. The motion of the hypothetical fluid is taken identical to the movement of the different fluids. The solution is given in the form of an integral for which the region of integration is that part of the aquifer where weight differences are present. In most practical cases the interface will have a form which prohibits a mathematically convenient calculation of the integral in closed form. The author also states that "model studies provide the only means of

studying the location and movement of interfaces for general problems involving movement of both fluids."

Biggar and Nielsen (1964) discuss the conditions for which the interface between two liquids of unequal density and viscosity is unstable. For steady movement upwards the interface is unstable when

$$(\mu_2 - \mu_1) v + k (\rho_2 - \rho_1) g < 0 \quad (2.4)$$

where  $\rho$  is the density,  $\mu$  the viscosity,  $g$  the acceleration of gravity and the subscripts 1 and 2 refer to the displaced and displacing solutions, respectively. Whenever a dilute NaCl solution is displaced by an equal or more concentrated NaCl solution (upward flow) the interface was stable. Conversely, when a dilute solution displaced a more concentrated one, unstable flow existed. Instability was caused by fingers of displacing fluid running ahead of the average displacement.

Hubbert (1953) discusses a case in which flowing fresh water is in contact with static salt water. If at rest, the fresh water overlies the salt water with the interface horizontal, but if the fresh water is set in motion, this interface will tilt upward in the direction of flow at an angle whose tangent is given by

$$\tan \alpha = \frac{\rho_f}{\rho_f - \rho_s} \frac{dh}{dx} \quad (2.5)$$

where  $\rho_f$  and  $\rho_s$  are the densities of fresh and salt water respectively and  $\frac{dh}{dx}$  is the gradient of piezometric head.

## CHAPTER III

## THEORY AND SCALING OF MODEL

Analysis of problem:

Analytical solutions to groundwater problems involving flow in isotropic media have been successfully obtained by use of the Laplace equation:

$$\frac{\partial^2 \phi}{\partial x^2} + \frac{\partial^2 \phi}{\partial y^2} + \frac{\partial^2 \phi}{\partial z^2} = 0 \quad (3.1)$$

for steady state flow and the equation

$$\frac{\partial^2 \phi}{\partial x^2} + \frac{\partial^2 \phi}{\partial y^2} + \frac{\partial^2 \phi}{\partial z^2} = \frac{S}{T} \frac{\partial \phi}{\partial t} \quad (3.2)$$

for transient flow. The relative difficulty of solution of these equations depends entirely on the initial and boundary conditions used in conjunction with the two equations. If we have a free surface or water table the problem becomes increasingly difficult. This is true because not only does the water table determine the distribution of flow in the system, but also the shape of the water table depends upon the distribution of flow. In general, therefore, free surface flow problems are solved using an approximate theory, utilizing the Dupuit-Forchheimer assumptions. For the situation in which no accretion to the water table occurs, i.e., where the water table is a streamline, the Dupuit-Forchheimer assumptions may be stated as

- 1) the velocity of flow along the water table is proportional to the slope (the tangent) of the water table, and

2) the flow is everywhere horizontal and uniform throughout the entire saturated thickness.

By utilizing these assumptions many approximate solutions have been obtained. Generally these solutions take the form of  $\phi = f(x, y, z)$  for steady flow and  $\phi = g(x, y, z, t)$  for unsteady flow and from these solutions the flow at different points and times may be evaluated.

The principal interest of this study was the position of the interface at any time rather than the shape of the free surface. The position of the interface is determined by the component of flow normal to the interface.

Suppose that in Figure 1 (see Jacob (1950)) water is being added to the water table at a rate  $W$ . The distance between the two flow lines is  $\frac{\Delta\psi}{W}$  and the difference between the piezometric head at A and B is  $\Delta\phi = \frac{\Delta\psi}{W} \tan \beta$ . This head difference  $\Delta\phi$  occurs over a distance  $\frac{\Delta\psi}{V} \tan(\alpha + \beta)$  where  $V$  is the velocity of flow below the water table. The gradient of piezometric head  $\frac{V}{K}$  may then be expressed by

$$\frac{V}{K} = \frac{\Delta\psi/W \tan \beta}{\Delta\psi/V \tan(\alpha + \beta)} \quad (3.3)$$

or

$$\alpha = \arctan \left( \frac{K}{W} \tan \beta \right) - \beta \quad (3.4)$$

In equation (3.4) the limit of  $\alpha$ , if  $W$  approaches zero, is  $(90-\beta)$ , or in other words the water table is a streamline. When water is added to the free surface, the flow lines will be at an angle with the

water table. The magnitude of this angle depends on the slope of the water table, the saturated permeability and the recharge rate. The same phenomenon of refraction of streamlines also occurs at the boundary of two layers having different permeabilities. This was discussed by Todd (1961).

From the foregoing it becomes clear that an analysis utilizing the Dupuit-Forchheimer assumptions is inapplicable for the present problem, since it is precisely the normal component of flow (due to recharge) which causes the interface to move.

A second approach to the problem is an attempt to determine the differential equation governing the shape of the fresh-salt water interface at any time. The equation governing the shape of the interface may be written as

$$f(x, z, t) = 0, \quad (3.5)$$

and thus

$$\frac{df}{dt} = \frac{\partial f}{\partial x} \frac{dx}{dt} + \frac{\partial f}{\partial z} \frac{dz}{dt} + \frac{\partial f}{\partial t} = 0. \quad (3.6)$$

Defining the piezometric head as

$$\phi = p/\gamma + z, \text{ or } \phi - p/\gamma - z = 0, \quad (3.7)$$

and combining equations (3.5) and (3.7)

$$f = \phi - p/\gamma - z \quad (3.8)$$

Substituting equation (3.8) into equation (3.6) gives

$$\frac{\partial \phi}{\partial x} \frac{dx}{dt} + \frac{\partial \phi}{\partial z} \frac{dz}{dt} + \frac{\partial \phi}{\partial t} - \frac{\partial p/\gamma}{\partial x} \frac{dx}{dt} - \frac{\partial p/\gamma}{\partial z} \frac{dz}{dt} - \frac{\partial p/\gamma}{\partial t} - \frac{dz}{dt} = 0 \quad (3.9)$$

From Darcy's law:

$$\frac{dx}{dt} = -\frac{K}{n} \frac{\partial \phi}{\partial x} \quad \text{and} \quad \frac{dz}{dt} = -\frac{K}{n} \frac{\partial \phi}{\partial z} \quad (3.10)$$

Substituting equations (3.10) into (3.9) yields

$$-\frac{K}{n} \left[ \left( \frac{\partial \phi}{\partial x} \right)^2 - \frac{\partial p/\gamma}{\partial x} \frac{\partial \phi}{\partial x} \right] - \frac{K}{n} \left[ \left( \frac{\partial \phi}{\partial z} \right)^2 - \frac{\partial p/\gamma}{\partial z} \frac{\partial \phi}{\partial z} + \frac{\partial \phi}{\partial z} \right] + \frac{\partial \phi}{\partial t} - \frac{\partial p/\gamma}{\partial t} = 0. \quad (3.11)$$

Solution of this non-linear equation would be extremely difficult.

The remainder of this chapter is devoted to the theory of the model and scaling.

#### Model theory and scaling

In order to adequately simulate prototype conditions in a model it is necessary to relate every model variable to its counterpart in the prototype. Two methods of doing this are known. The first is dimensional analysis, mainly developed and used by British and American scientists. Dimensional analysis entails the reduction of the number of variables by the creation of dimensionless variables. In the second method, model laws are derived from the differential equations that govern flow phenomena. When laws of similarity are desired for distorted models, the second method is desirable. Since in the present study the differential equations governing the flow in prototype and model are known the latter method has been used. Bear (1960) derived the scales of viscous analogy models for ground water studies.

An alternative method is used here.

If the function  $f(x, z, t) = 0$  describes the position of the water table, then any increments  $(dx, dz, dt)$  in  $(x, z, t)$  are related by the equation

$$df = \frac{\partial f}{\partial x} dx + \frac{\partial f}{\partial z} dz + \frac{\partial f}{\partial t} dt = 0, \quad (3.12)$$

or

$$\frac{df}{dt} = \frac{\partial f}{\partial x} \frac{dx}{dt} + \frac{\partial f}{\partial z} \frac{dz}{dt} + \frac{\partial f}{\partial t} = 0. \quad (3.13)$$

Since the potential  $\phi = p/\gamma + z$  for the water table reduces to  $\phi = z$  one may write for the water table

$$\phi - z = 0 = f \quad (3.14)$$

or

$$\frac{\partial \phi}{\partial x} \frac{dx}{dt} + \frac{\partial \phi}{\partial z} \frac{dz}{dt} - \frac{dz}{dt} + \frac{\partial \phi}{\partial t} = 0 \quad (3.15)$$

Substituting for  $\frac{dx}{dt}$  and  $\frac{dz}{dt}$  by use of Darcy's Law

$$-\frac{K_x}{n} \frac{\partial \phi}{\partial x}, \quad -\frac{K_z}{n} \frac{\partial \phi}{\partial z}$$

respectively, the following equation is obtained for the prototype

$$K_{xp} \left( \frac{\partial \phi_p}{\partial x_p} \right)^2 + K_{zp} \left( \frac{\partial \phi_p}{\partial z_p} \right)^2 - K_{zp} \frac{\partial \phi_p}{\partial z_p} = n_p \frac{\partial \phi_p}{\partial t_p} \quad (3.16)$$

Similarly for the model (keeping in mind that  $K_{xm} = K_{zm} = K_m$ ) one finds

$$K_m \left( \frac{\partial \phi_m}{\partial x_m} \right)^2 + K_m \left[ \left( \frac{\partial \phi_m}{\partial z_m} \right)^2 - \frac{\partial \phi_m}{\partial z_m} \right] = n_m \frac{\partial \phi_m}{\partial t_m} \quad (3.17)$$

Equations (3.16) and (3.17) may be expressed in dimensionless form

by defining the following dimensionless variables:

$$\begin{aligned} \overline{K}_{xp} &= \frac{K_{xp}}{A}, & \overline{\phi}_p &= \frac{\phi_p}{B}, & \overline{x}_p &= \frac{x_p}{C}, & \overline{K}_{zp} &= \frac{K_{zp}}{D}, \\ \overline{z}_p &= \frac{z_p}{E}, & \overline{n}_p &= \frac{n_p}{F}, & \overline{t}_p &= \frac{t_p}{G} \end{aligned} \quad (3.18)$$

where  $A, B, C, D, E, F,$  and  $G$  are the characteristic values of  $K_{xp}, \phi_p, x_p, K_{zp}, z_p, n_p,$  and  $t_p$  respectively, and the dimensionless variables are designated with a bar.

Equation (3.16) may now be written

$$\frac{AB^2}{C^2} \overline{K}_{xp} \left( \frac{\partial \overline{\phi}_p}{\partial \overline{x}_p} \right)^2 + \frac{DB^2}{E^2} \overline{K}_{zp} \left( \frac{\partial \overline{\phi}_p}{\partial \overline{z}_p} \right)^2 - \frac{DB}{E} \overline{K}_{zp} \frac{\partial \overline{\phi}_p}{\partial \overline{z}_p} = \frac{FB}{G} \overline{n}_p \frac{\partial \overline{\phi}_p}{\partial \overline{t}_p} \quad (3.19)$$

Similarly equation (3.17) may be expressed in dimensionless form by defining the dimensionless variables

$$\begin{aligned} \overline{K}_m &= \frac{K_m}{A'}, & \overline{\phi}_m &= \frac{\phi_m}{B'}, & \overline{x}_m &= \frac{x_m}{C'}, \\ \overline{z}_m &= \frac{z_m}{E'}, & \overline{n}_m &= \frac{n_m}{F'}, & \overline{t}_m &= \frac{t_m}{G'} \end{aligned} \quad (3.20)$$

where  $A', B', C', E', F,$  and  $G'$  are the characteristic values of  $K_m, \phi_m, x_m, z_m, n_m,$  and  $t_m$  respectively.

Equation (3.17) then becomes

$$\frac{A'B'^2}{C'^2} \overline{K}_m \left( \frac{\partial \overline{\phi}_m}{\partial \overline{x}_m} \right)^2 + \frac{A'B'^2}{E'^2} \overline{K}_m \left( \frac{\partial \overline{\phi}_m}{\partial \overline{z}_m} \right)^2 - \frac{A'B'}{E'} \overline{K}_m \frac{\partial \overline{\phi}_m}{\partial \overline{z}_m} = \frac{F'B'}{G'} \overline{n}_m \frac{\partial \overline{\phi}_m}{\partial \overline{t}_m} \quad (3.21)$$

Corresponding dimensionless variables must have the same value for both model and prototype. For the systems to be similar the corresponding coefficients (composed of the characteristic values) of equations (3.19) and (3.21) must be equal, thus

$$\frac{AB^2}{C^2} = \frac{A'B'^2}{C'^2}, \quad \frac{DB^2}{E^2} = \frac{A'B'^2}{E'^2}, \quad \frac{DB}{E} = \frac{A'B'}{E'}, \quad \frac{FB}{G} = \frac{F'B'}{G'} \quad (3.22)$$

Denoting the scale factors of the variables with a subscript  $r$  we finally obtain

$$\frac{K_{xr} \phi_r^2}{x_r^2} = 1 \quad (3.23)$$

$$\frac{K_{zr} \phi_r^2}{z_r^2} = 1 \quad (3.24)$$

$$\frac{K_{zr} \phi_r}{z_r} = 1 \quad (3.25)$$

$$\frac{n_r \phi_r}{t_r} = 1 \quad (3.26)$$

From equation (3.24) and (3.25) it may be concluded that  $\phi_r = z_r$ .

Thus equations (3.23), (3.24), (3.25) and (3.26) may be rewritten as

$$\frac{K_{xr} z_r^2}{x_r^2} = K_{zr} = \frac{n_r z_r}{t_r} \quad (3.27)$$

The scale factor for time is therefore given by

$$t_r = \frac{n_r x_r^2}{K_{xr} z_r} \quad (3.28)$$

or since  $n_m = 1$  and  $K_m = \frac{g}{12} \frac{b^2}{v}$

$$t_m = \frac{12 \nu}{g n_p} \frac{x_m^2}{x_p^2} \frac{z_p}{z_m} \frac{K_{xp}}{b^2} t_p \quad (3.29)$$

Equation (3.27) also shows

$$\frac{K_{xr}}{K_{zr}} = \frac{x_r^2}{z_r^2} \quad (3.30)$$

Equation (3.30) states that the ratio of scale factors of horizontal and vertical permeability equals the square of the scale factor ratio of dimensions  $x$  and  $z$ . In other words geometrical distortion of the model implies anisotropy. This is in direct contradiction to findings by De Wiest (1961); De Wiest's equations (115a) and (115b) may be written in our terminology

$$\frac{n_r}{K_r} \frac{x_r^2}{z_r} \frac{1}{t_r} = 1 \quad (3.31)$$

and

$$\frac{n_r}{K_r} \frac{z_r}{t_r} = 1 \quad (3.32)$$

De Wiest states: "From equations (115) it follows that, in order to have a unique time scale one must have  $x_r = z_r$ . This means that the model cannot be distorted, which it was, to our knowledge at least, in most of the previously constructed models of this kind. The distortion of the model is a direct consequence of the Dupuit assumption, which was not made in the present analysis."

Taking the first and third identity of equation (3.27) one finds

$$\frac{n_r x_r^2}{K_{xr} t_r} = 1 \quad (3.33)$$

and taking the second and third identity gives

$$\frac{n_r z_r}{K_{zr} t_r} = 1 \quad (3.34)$$

Equations (3.33) and (3.34) are equivalent to De Wiest's equations (3.31) and (3.32), differing from his equations only in the inequality of  $K_{xr}$  and  $K_{zr}$ . If  $K_{xr}$  equals  $K_{zr}$  equations (3.33) and (3.34) are identical to De Wiest's equations. Since Dupuit's assumptions were not made in the derivations herein it must be concluded that De Wiest's statement is not correct and the model may be distorted. Distortion, however, does imply anisotropy.

The discharge scale may be obtained by comparison of Darcy's and Poiseuille's Law:

$$Q_{xp} = -K_{xp} b_p z_p \frac{\partial \phi_p}{\partial x_p} \quad (3.35)$$

and

$$Q_{xm} = -K_{xm} b_m z_m \frac{\partial \phi_m}{\partial x_m} \quad (3.36)$$

Thus

$$Q_{xr} = \frac{K_{xr} b_r z_r^2}{x_r} \quad (3.37)$$

and similarly

$$Q_{zr} = K_{zr} b_r x_r \quad (3.38)$$

However, because of equation (3.30) it may be shown that

$$Q_{xr} = Q_{zr} = Q_r \quad (3.39)$$

Substituting the appropriate value of  $K_{xr}$  in equation (3.37) the discharge scale becomes

$$Q_r = \frac{g}{12} \frac{b^3}{\nu} \frac{1}{K_{xp} b_p} \frac{z_r^2}{x_r} \quad (3.40)$$

In part of this study it was desired to model a layered aquifer system with permeability in one half of the aquifer 10 times the other half. The discharge scale for both parts of the aquifer must be unique. Denoting the two layers of different permeability by subscripts 1 and 2 we obtain, using equation (3.40).

$$\left( \frac{g}{12} \frac{b^3}{\nu} \frac{1}{K_{xp} b_p} \frac{z_r^2}{x_r} \right)_1 = \left( \frac{g}{12} \frac{b^3}{\nu} \frac{1}{K_{xp} b_p} \frac{z_r^2}{x_r} \right)_2 \quad (3.41)$$

Since  $\nu$ ,  $g$  and  $b_p$  are constant and  $z_r$  and  $x_r$  are fixed throughout the model equation (3.41) may be written as

$$\left( \frac{b^3}{K_{xp}} \right)_1 = \left( \frac{b^3}{K_{xp}} \right)_2 \quad (3.42)$$

To obtain layer permeability ratios of 1 to 10,  $b_2$  must be approximately  $2.16b_1$ ,  $[(2.16)^3 = 10]$ .

In order to satisfy both equation (3.42) and the requirement of a unique time scale (equation (3.29)) the ratio  $b_m/n_p$  must be constant. Therefore, changes in interspace width in the model and changes in effective porosity in the prototype cannot be made independently.

## CHAPTER IV

## EXPERIMENTAL PROCEDURE

The Hele-Shaw model consists in its simplest form of two parallel plates separated by a narrow interspace. A sketch of the model is shown in Figure 2. The dimensions of the two plates were 96 x 20 x 3/8 inches. The tops of both plates were beveled at an angle of 45 degrees (A) in order to provide a larger catchment surface for the recharge liquid. The plates were held together with bolts and nuts (B). Correct separation of the plates was maintained at these points by means of small spacers of appropriate thickness. The spacers were small so as to cause little interference with the flow through the model. Spacer strips (C) one inch wide and 1/32 inch thick were also inserted along the bottom and sides of the model. Two cylinders (D) attached to the rear plate allowed movement of the liquid into or out of the model interspace through small holes (E) drilled through the contact between cylinder and plate. The plexiglass plates were held with C-clamps in the aluminum frame (F). Before placing the plates in the frame a bead of plasticine\* was inserted in the interspace next to and outside the spacer strips. Of the different methods tried for sealing, plasticine proved to be effective and easy to use.

---

\* Harbutt's Plasticine Ltd, Bathampton, Bath, England.

Recharge liquid was applied by means of the recharge tube (G), which was fastened to the aluminum frame by means of the adjustable tube holder (H). The recharge tube consisted of "one inch" diameter plexiglass fastened to an aluminum T-beam. A series of small plexiglass tubes (I), spaced at two inches were glued to the large tube. Calibrated glass capillaries were connected to each of the small plexiglass tubes with rubber tubing. When being filled, the recharge tube was inverted by means of pivots, thus preventing air from being entrapped in the tube. For operation the recharge tube was connected to a Mariotte-syphon in an 18 liter carboy, containing the recharge liquid.

#### Experiments with water

The first series of experiments was conducted using water as the model liquid. Saline water in the aquifer was simulated by dissolving 1.5 gms. of sodium chloride in each 100 gms of salt. Added to this was a trace of potassium-permanganate to color the water.

The model was used in such a manner as to simulate only half the distance between drain tiles. This procedure is correct since there is theoretically no flow across the planes midway between the drains and through the middle of the drain itself. Before assembling the model all holes (E) except two were covered with electrical tape. One hole near the top of the model remained open to serve as a drain. On the other end of the model the bottom hole was used to

to fill and drain the interspace at the beginning and end of each run.

Before starting a series of runs the width of the interspace was determined by admitting known volumes of water and noting the height to which it filled the interspace. Since the volume of water admitted was equal to the height of rise times the known length of the model times the width of the interspace, the width could be calculated.

Each run consisted of the following steps. The model interspace was filled with colored salt water through the inlet hole. After filling, the water table was allowed to establish a near horizontal position. The inflow from the Mariotte syphon into the recharge tube was adjusted to a desired rate by means of a clamp and the run started. Photographs were taken at suitable intervals in order to obtain a record of the salt-fresh water interface with time. An example of such a record is shown in Figure 3. The recharge rate was determined by continuous measurement of the drain discharge of a standard stand to discharge into the same capillary tube (inflow equals outflow).

Three different systems were studied, i.e.,

1. Parallel drains in an aquifer of uniform permeability,
2. Parallel drains in a two-part aquifer. (Permeability of the lower half of the aquifer 11.5 times the permeability of the upper half).

3. Parallel drains in a two-part aquifer, (permeability of the upper half of the aquifer 10.5 times the permeability of the lower half).

The set up for the first system was as described above. For the second and third system a different front plate was used. Part of the plate was machined in such a manner, that one half of the plate was  $1/32$  inch thicker than the other half.

#### Experiments with glycerine-water mixture

In order to slow down the time scale in the model a mixture of 60 percent glycerine and 40 percent water by weight was used in the next series of experiments. The viscosity of the mixture was determined with an Ostwald viscometer. This viscometer measures the relative viscosity of a liquid. The determination consists of measuring the time for a known volume of liquid to flow through a capillary tube and comparing this with the time for an equal volume of a standard liquid to flow through the same capillary tube. Twice distilled water was used as the standard. After determining the times, the viscosity of the glycerine-water liquid was calculated. The density of each mixture was determined with a pycnometer.

The same model as described above was used for the glycerine-water experiments. To prevent the cumbersome computations resulting from using photographs, the procedure for determining the salt content of the effluent was changed. The effluent from the drain

was funneled into a conductivity cell as shown in Figure 4. The conductivity cell used was a glass flow cell (CEL-JD)\* with a constant of 20. The cell was connected to a Type 153 ELECTRONIK six-point recorder and self-balancing Wheatstone bridge. Only one point of the recorder was used. The other five points were connected to a fixed resistance, to indicate proper operation of the bridge. In this manner a continuous record of conductivity versus time was obtained.

The drain outflow rate was measured at suitable time intervals depending upon the flow rate. Since the viscosity of a glycerine-water mixture is dependent on the temperature, periodic temperature measurements were taken. During the course of a run the temperature of the liquid varied less than two and normally less than one degree centigrade.

Using the glycerine-water mixture the following systems were studied:

1. Parallel drains in an aquifer of uniform permeability.
  - a) Initial concentration of ground water 10,000 ppm of salt
  - b) Initial concentration of ground water 15,000 ppm of salt

---

\* Industrial Instruments Inc., Cedar Grove, New Jersey.

- c) Initial concentration of ground water 30,000 ppm of salt
2. Parallel drains in a two-part aquifer (permeability of the lower half of the aquifer approximately twelve times the permeability of the upper half).
    - a) Initial concentration of ground water 15,000 ppm of salt
    - b) Initial concentration of ground water 30,000 ppm of salt
  3. Parallel drains in a two-part aquifer (permeability of lower half of the aquifer approximately one sixth the permeability of the upper half).
    - a) Initial concentration of ground water 15,000 ppm of salt
    - b) Initial concentration of ground water 30,000 ppm of salt.

For each arrangement of the model a series of runs was performed covering a range of values of model discharge. A total of 80 uniform recharge runs was performed with the glycerine-water mixture with the above seven model setups.

After completion of the runs with continuous, uniform recharge rates, a few runs were made with intermittent recharge. The time scale (equation 3.29), is a function of the geometric

distortion of the model, the permeability and effective porosity in the prototype and the width of the model interspace. Likewise, the model discharge is a function of the geometric distortion of the model the permeability and application rate in the prototype and the width of the model interspace (equation 3.38). Thus specific values of these variables in the prototype were chosen in order to obtain the model time intervals during which the glycerine-water mixture should be admitted to the model. The intermittent recharge runs were performed by intercepting recharge liquid with an aluminum trough at the computed time intervals.

## CHAPTER V

### PRESENTATION OF DATA AND RESULTS

The conductivity recorder provides a record of conductivity of the solution versus time. The conductivity of the solution is related to the amount of salt in solution. The chart used on the recorder is calibrated such that when the conductivity values of the chart are plotted on Cartesian graph paper, a straight line relationship between concentration and conductivity is obtained. For different temperatures the slope of the line is different. No automatic temperature compensator was used with the conductivity recorder, therefore the conductivity was converted to concentration in the following manner: For each run, the highest conductivity value (equivalent to the known initial concentration) was divided by ten, thus giving the values at which the concentration was 10, 20, 30, etc., percent of the initial concentration.

#### Aquifer of uniform permeability

The results of the runs with an aquifer of uniform permeability are shown in Figures 5 through 41. The width of the interspace  $b$  was 0.085 cms, the length  $x_m$  of the model 236 cms, and the saturated thickness in the model 42.0 cms.

The runs with initial concentration of 10,000 ppm are represented in Figures 5 through 15 in order of decreasing discharge. Each graph is a representation of the concentration of effluent

expressed as a fraction of the initial concentration versus time in minutes. The model discharge was varied from  $0.346 \text{ cm}^3/\text{sec}$  to  $0.0115 \text{ cm}^3/\text{sec}$ . Each run was discontinued when the concentration of the effluent was approximately one tenth of the original concentration. The duration of each run was indirectly proportional to the discharge and varied from about two hours for a discharge of  $0.346 \text{ cm}^3/\text{sec}$  to about 33 hours for a discharge rate of  $0.0115 \text{ cm}^3/\text{sec}$ .

In addition to the discharge rate each figure also shows the measured dynamic viscosity at  $20^\circ\text{C}$  of the particular glycerine-water mixture used for the run and the average temperature in degrees centigrade at which the run was performed.

The values of the computed kinematic viscosity used in subsequent calculations are also shown. These values were obtained in the following manner: A curve relating the dynamic viscosity to temperature was drawn for a true 60 percent glycerine-40 percent water mixture. From this curve the value of the viscosity was obtained for the temperature at which the run was performed. The value of the viscosity was then expressed as a percentage of the value of the viscosity of the 60 percent mixture at  $20^\circ\text{C}$ . The measured viscosity was divided by this percentage and the measured density of the mixture to give the kinetic viscosity.

Figures 16 through 28 show the results for the uniform aquifer with initial concentration of 15,000 ppm. The discharge rate varied

from 0.357 cm<sup>3</sup>/sec to 0.024 cm<sup>3</sup>/sec and the resulting durations of the runs varying from about two hours to about 20 hours.

The final experiments with the uniform aquifer and initial concentration of 30,000 ppm of salt are shown in Figures 29 through 41. In this set the discharge rate varied from 0.334 cm<sup>3</sup>/sec to 0.0286 cm<sup>3</sup>/sec. The runs varied in duration from approximately 2 hours to about 13 hours.

As shown by the curves, the concentration dropped rapidly during the first part of each run and then gradually leveled off. The runs having low rate of discharge were less concave than the runs with high discharge. The smoothness of the curves indicated good performance of the model and the measuring equipment.

Two-part aquifer (top half more permeable than bottom half).

The results of the non-uniform layered aquifer, with the top half of the aquifer more permeable than the bottom are shown in Figures 42 through 60.

The width of the interspace in the top half of the model was 0.190 cms and in the bottom half the width was 0.0828 cms. The width ratio was thus 2.295 which implies a field permeability ratio of 12.1 to 1. The length of the model was 235 cms, the height from the impermeable boundary at the bottom to the separation between the zones of unequal permeability was 20 cms and the height from this separation to the center line of the drain 20.2 cms.

Figures 42 through 51 show the results for this set-up with initial concentration of 15,000 ppm of salt. The drain discharge rates varied from 0.328 cm<sup>3</sup>/sec to 0.0188 cm<sup>3</sup>/sec. The lengths of the runs ranged from approximately two hours to approximately 18 hours. Figures 52 through 60 contain the data for the same conditions and with initial concentration of 30,000 ppm. Discharge ranged from 0.336 cm<sup>3</sup>/sec to 0.0183 cm<sup>3</sup>/sec and resulting durations ranged from 2-1/2 hours to about 12 hours.

As with the results obtained from the uniform aquifer, the smoothness of the data was reassuring. The shape of the curves was similar to that obtained with the uniform aquifer runs.

Two part aquifer (bottom half more permeable than top-half)

Figures 61 through 84 present the results for the reverse permeability condition. For these runs the interspace width for the top half of the aquifer was 0.0905 cms and for the bottom half 0.165 cms. The ratio of interspace widths was 1 to 1.82 which results in a field permeability ratio of 1 to 6.1. The length of the model was 235 cms. The distance from the bottom of the model to the boundary between layers of different permeability was 20.3 cms. and from this boundary to the center line between drains 19.8 cms.

The results of this set-up with initial concentration of 15,000 ppm are presented in Figures 61 through 72. The flow rates for these runs varied from 0.293 cm<sup>3</sup>/sec to 0.0155 cm<sup>3</sup>/sec with resulting

durations ranging from three hours to 18 hours.

Finally, Figures 73 through 84 show the results for the same non-uniform condition with an initial concentration of 30,000 ppm dissolved salt. The model drain discharge rates ranged from  $0.275 \text{ cm}^3/\text{sec}$  to  $0.0156 \text{ cm}^3/\text{sec}$  and lengths of the runs varied from 3-1/2 hours to 19 hours.

The appearance of the curves in Figures 61 through 84 was quite different from those obtained in the previous setups. Rather than the typical concave curves of Figure 5 through 60, those obtained with the one to six permeability ratio showed double curvature. The shape of the curves is similar at low values of time, until the fresh-salt water interface reaches the boundary between layers of low and high permeability. When fresh water begins to enter the layer of high permeability, mixing between fresh and salt water takes place and the interface in the high permeability layer becomes undefined. Water entering the drain above the interface in the upper layer is thus a mixture of salt and fresh water for some time and the concentration curve becomes convex. When eventually the sharp interface is re-established the curve regains its normal concave shape. In a number of runs (for example Figures 67, 68, 69, 70) it was very difficult to draw a smooth curve through the data.

CHAPTER VI  
ANALYSIS OF RESULTS

Dimensionless charts

In the previous chapter the results of the experiments were shown in graphical form in Figures 5 through 84. Each figure was a plot of the effluent concentration versus model time for particular values of drain discharge or rate of application. In Chapter III it was shown (equation 3.29) that the model time was related to the other variables by

$$t_m = \frac{12}{g} \frac{v}{n_p} \frac{x_m^3}{x_p^2} \frac{z_p}{z_m} \frac{K_{xp}}{b^2} t_p \quad (6.1)$$

which may be rewritten as

$$\frac{g}{12} \frac{z_m}{v} \frac{b^3}{x_m^2} t_m = \frac{z_p K_{xp} t_p}{n_p x_p^2} \quad (6.2)$$

Both sides of equation (6.2) are dimensionless.

Similarly for the model discharge it was found that

$$Q_{xm} = \frac{g}{12} \frac{b^3}{v} \frac{h}{K_{xp}} \frac{z_m^2}{z_p^2} \frac{x_p^2}{x_m} \quad (6.3)$$

which may be written as

$$\frac{12}{g} \frac{v}{b^3} \frac{x_m}{z_m^2} Q_{xm} = \frac{h}{K_{xp}} \frac{x_p^2}{z_p^2} \quad (6.4)$$

Both sides of this equation are also dimensionless.

The values of  $g$ ,  $b$ ,  $x_m$ , and  $z_m$  are known and constant for each series of runs so that one may write for the left-hand side of equations (6.2) and (6.4),  $C_1(t_m/\nu)$  and  $C_2\nu Q_{xm}$  respectively, where

$$C_1 = \frac{g}{12} \frac{z_m}{x_m^2} b^2 \quad (6.5)$$

and

$$C_2 = \frac{12}{g} \frac{x_m}{z_m^2} \frac{1}{b^3} \quad (6.6)$$

Equations (6.2) and (6.4) may then be written as:

$$C_1 \frac{t_m}{\nu} = \frac{z_p K_{xp} t}{n_p x_p^2} \quad (6.7)$$

$$C_2 \nu Q_{xm} = \frac{h}{K_{xp}} \frac{x_p^2}{z_p^2} \quad (6.8)$$

Once the value of the kinematic viscosity of the liquid is computed it is possible to compute the values of  $C_1(t_m/\nu)$  and  $C_2\nu Q_{xm}$  for each run. Dimensionless charts of  $(z_p K_{xp} t)/(n_p x_p^2)$  versus  $(h_{xp}^2)/(K_{xp} z_p^2)$  were obtained by determining the time  $t_m$  required to reach effluent salt concentrations of 90, 80, 70, etc. percent of the initial concentration. These charts are shown in Figures 85 through 91. The figures are composite in the sense that they show the results of a series of runs in one graph. To reduce scatter several points indicated on the chart were obtained by averaging two adjacent points in both directions. In the lower parts of the curves

in Figures 85 through 91 this was quite beneficial, because considerable scatter was encountered there. This scatter was due to two reasons: (1) the low discharge runs represented by the lower part of the curves were of relatively long duration, thus temperature variations affected these runs to a greater degree than those with a high discharge. Temperature variations affect the results by changing the viscosity and the concentration-conductivity relationship of the liquid, (2) constant flow rate became more difficult to maintain at low discharges.

Figures 85, 86 and 87 are charts obtained from the results of the experiments with the uniform aquifer for original salt concentrations of 10,000, 15,000 and 30,000 ppm respectively. The value of  $z_p$  in the dimensionless parameters on the abscissa and ordinate represents the total depths of the prototype aquifer.

Results of runs for the 12/1 layered aquifer are summarized in Figure 88 and 89 for initial concentration of 15,000 and 30,000 ppm respectively. The value of  $z_{p1}$  refers, in this case, to the thickness in the prototype of the high permeability layer of the prototype aquifer. It was impossible in this case to use  $z_p$ , the entire depth of the aquifer. The reason for this may be seen in equations (6.2) and (6.4) where the spacing ( $b$ ) between the plates occurs in the left hand side of each equation. Since the scale factor for  $z$  has to be the same in both layers of the aquifer, the prototype thickness of the lower layer

is automatically determined by the choice of the thickness of the upper layer in the prototype and the thickness ratio in the model. In this case the thickness ratio was 1/0.95 (upper part to lower part).

The composite graphs resulting from the runs with the non-uniform aquifer, (bottom half six times as permeable as the top) are shown in Figures 90 and 91 for initial concentrations of 15,000 ppm and 30,000 ppm respectively. Again  $z_{p1}$  represents the thickness of the upper member of the aquifer. The thickness ratio of the upper part of the model to the lower was 0.91/1. As could be expected from the appearance of the curves in Figures 61 through 84, the composite points in the composite charts showed considerably more scatter than for the previous setups.

#### Effect of variables on degree of aquifer cleaning

At the end of each run, the position of the water table and the fresh-salt water interface was recorded and plotted. By means of a planimeter, the areas between the water table and the fresh-salt water interface and between the water table and the bottom of the aquifer was determined. The ratio between the two areas is the fraction of the aquifer volume flushed free of salt water, or more conveniently the average depth to which fresh water has replaced salt water.

Figure 92 is a plot of the dimensionless parameter  $(hx_p^2)/(K_{xp} z_p^2)$  versus the average percentage of aquifer thickness cleaned free of salt water for the uniform aquifer. The curve was

drawn through points obtained with an initial concentration of 30,000 ppm. It is not surprising that the points in this figure show a considerable amount of scatter since all runs were discontinued before a true steady state had been reached. In fact, when the runs were discontinued the concentration of the effluent was not the same in each case. Thus, some runs were closer to a terminal state than others.

Nevertheless, Figure 92 shows some interesting features.

The curve rises steeply initially with an increase of the dimensionless parameter and then approaches 100 percent asymptotically. The practical significance of this may be seen by assuming constant values of  $h$ ,  $K_{xp}$ , and  $z_p$  and varying the half distance  $x_p$  between drains. If the drains are very closely spaced (small  $x_p$ ) the depth of flow and thus the percent of aquifer cleaned is small. When the spacing is increased, the depth of flow becomes greater and at very large drain spacings the depth approaches the total depth of the aquifer. This is in agreement with findings by Bouwer (1963) who distinguishes between an active zone and a passive zone. The active zone is the portion of the aquifer in which flow takes place. In the passive zone no flow occurs, thus no salt water is removed from it.

The Dupuit-Forchheimer theory assumes that flow occurs through the entire thickness of the aquifer. From Figure 92 it is clearly evident that this is not true for every combination of the drain spacing, thickness of aquifer, permeability and rate of recharge.

The figure thus suggests that the Hele-Shaw model could be used nicely to determine through which range of the parameter  $(hx_p^2)/(K_{xp} z_p^2)$  the Dupuit-Forchheimer assumptions are valid.

Another interesting feature of Figure 92 is the location of the points denoting the three initial concentrations used. In order for the three sets of points to be truly comparable, the circled points (representing initial concentration of 30,000 ppm) should be lower in the figure than indicated and the squared points (representing initial concentration of 10,000 ppm) should be higher than indicated. The reason for this is the following: The experimental runs were discontinued when the reading on the chart of the conductivity recorder showed a value of 0.1. This means that the runs with high initial concentration were closer to the terminal state than the runs with the low initial concentration.

Figure 92 shows that even without adjustment the percent of aquifer thickness cleaned was inversely related to the initial concentration. The reason for this is the difference in density between fresh and salt water. In order for two flow situations to reach the same terminal state, the piezometric head has to be larger for a more dense liquid than for a less dense liquid. Or, alternatively, for the same piezometric head, the aquifer would be flushed clear of salt water to a greater degree in the case of the less dense liquid compared to the more dense liquid.

Figure 93 presents a similar graph for the 12/1 layered aquifer. However, the depth to which the aquifer is flushed free from salt water is considerably smaller than in the uniform permeability cases. In fact, in the range of values used in the tests, little flow in the lower member occurred. Use of the Dupuit theory does not seem justified in a layered aquifer of this type. Again the depth of flow was less for the case of high initial concentration than for the case of low initial concentration.

#### Effect of variables on concentration of effluent

The dimensionless charts, discussed under the first heading of this chapter, make it possible to predict the quality of effluent from drains under various conditions. By substituting values of the prototype aquifer characteristics, (permeability and specific yield) aquifer dimensions (drain spacing and thickness of aquifer) and recharge rate, one can determine the concentration of effluent at any time. Since  $K_x$ ,  $x$ , and  $z$  occur in the variables of both abscissa and ordinate it is difficult to make an immediate judgment on how their variation changes the quality of effluent in time. Therefore a few quantitative examples are illustrated in Figure 94.

The curve A in Figure 94 shows the change of effluent concentration for the following conditions: (1) horizontal permeability of 15,000 ft/year, (2) recharge rate of 3 ft/year, (3) aquifer thickness of 80 ft, (4) half distance between drains of 800 ft and (5)

effective porosity 0.2. Under these conditions it requires 13.5 years for the effluent concentration to reach one tenth of the original concentration of 10,000 ppm. The effect of a twofold increase of recharge rate (6 ft/year) is shown by curve B. The effluent concentration at any time is considerably lower than in the first case and the time required to reach the 0.1 level is decreased to 6.5 years. The efficiency of flushing was in both cases approximately the same. In case A a total amount of water of  $(3) (13.5) (800) (1) = 32,500 \text{ ft}^3/\text{ft}$  width is required to replace approximately  $(800) (80) (1) (0.2) = 12,800 \text{ ft}^3/\text{ft}$  width. In case B these figures amount to 31,200 and approximately 12,800  $\text{ft}^3/\text{ft}$  width respectively.

Curve C differs from curve A only in the half spacing between drains which has been increased by a factor  $\sqrt{2}$  to 1130 ft. The effect of this increase is negligible, in fact the curves A and C are almost identical. The fact that curve C falls below A must be attributed to experimental inaccuracies. A further increase in spacing by a factor  $\sqrt{3}$  to 1385 ft, or decrease by a factor  $\sqrt{2}$  to 566 ft (not shown in Figure 94) gives the same result. If, however, the half spacing of the drains is decreased to 461 ft the rate of concentration drop is more rapid. The explanation for this is as follows: If half the distance between drains is greater than 566 ft the values of  $(hx_p^2) / (K_{xp} z_p^2)$  are equal to or greater than 0.01. Figure 92 indicates that for these values the depth of flushing becomes nearly

constant. Below the value of 0.01, the aquifer will not be cleaned as extensively. Thus less water is displaced and for the same application rate the effluent concentration drops to the one tenth level more rapidly.

Finally, curve D in Figure 94 shows the decrease in concentration with time for the same situation as A, except the aquifer thickness is reduced by a factor  $\sqrt{2}$  to 57 ft. The effect of a smaller aquifer thickness results in a more rapid reduction in effluent concentration. This is to be expected, since  $z_p$  occurs in the parameter on the abscissa of Figure 85 only to the first power.

The tendencies displayed by the previous examples are true for all aquifer situations investigated in this study. For specific values of the variables the effluent concentration at any time can be determined for the prototype from Figures 85 through 91.

A few additional comments should be made at this point. As was discussed in Chapter III, distortion of the model implies anisotropy according to the relation

$$\frac{K_{xr}}{K_{zr}} = \frac{x_r^2}{z_r^2} \quad (6.9)$$

Since  $K_{xm} = K_{zm}$  and  $x_m/z_m$  is constant one may write equation (6.9) as

$$\frac{K_{zp}}{K_{xp}} = C \frac{z_p^2}{x_p^2} \quad (6.10)$$

This expression shows that, for example, curves A, C and D in Figure 94 are not strictly comparable since the degree of anisotropy for these aquifer and spacing conditions is not the same. In the field the x-dimension is generally large compared to the z-dimension, thus most of the flow is in the horizontal direction. The error incurred by the different degree of anisotropy should be small.

A more serious criticism may be leveled at the use of the dimensionless charts for the layered aquifers. The scale factors  $Q_r$  and  $t_r$  must be equal for both layers of the aquifer. In order to satisfy both conditions, the ratio  $b/n_p$  must be equal for both layers. For the 12/1 layered aquifer this is not serious since the flow occurred almost exclusively in the top part of the aquifer. The effective porosity in the prototype of the more permeable layer may be used in the dimensionless parameter as the disproportionately small assumed effective porosity of the bottom layer of the aquifer has little effect upon the result. The requirement of the constant  $b/n_p$  ratio is more serious in case of the 1/6 layered aquifers. Under field conditions the effective porosity is reasonably constant for two layers of different permeability. When the correct prototype value of effective porosity for the top layer is used in the parameter  $(z_p K_{xp} t) / (n_p x_p^2)$ , the value of the effective porosity in the bottom layer is specified by the constant  $b/n_p$  ratio. This value is then necessarily too large. Thus in the prototype less water must be

displaced than in the model and the concentration time curve obtained from the model will give a conservative estimate.

#### Comparison of water with glycerine-water experiments

The results of the experiments with water as the model liquid have been reported in an earlier paper by Maasland and Bittinger (1964). Figures 85, 86 and 87 have been taken from this report. They are equivalent to Figures 86, 88 and 90 in this work, although the labeling of the axes is slightly different; namely,  $Q_m$  has been plotted against  $t_m$ . The parameter on the curves is the concentration in ppm. The initial concentration was 15,000 ppm.

The range of values covered by the water experiments is considerably smaller than the range in the glycerine-water experiments. For example, the range of values of  $(hx_p^2) / (K_{xp} z_p^2)$  covered in Figure 95 is only from 0.008 to 0.033. The general appearance of the curves is very similar to the ones in Figures 86, 88 and 90.

Figure 98 illustrates the difference between the curves obtained from Figures 86 and 95. The assumed half spacing between drains is 800 ft, the depth of the aquifer 80 ft, effective porosity 0.2, permeability 15,000 ft/year and recharge rate 3 ft/year. Curve A was obtained from the experiments using water as the liquid and curve B from the glycerine-water experiments. The agreement is reassuring in view of the different methods used in obtaining the dimensionless charts in Figures 86 and 95.

### Continuous versus intermittent recharge

Thus far only runs in which recharge water was applied continuously have been discussed. This is contrary to field practice. Generally, water is applied only during a period of three or four months during each year. To check the feasibility of using the Hele-Shaw model for intermittent recharge work and to compare the results so obtained with the results obtained by continuous applications, a few runs were performed with intermittent recharge.

When water is applied intermittently the following sequence of events takes place. When water first reaches the water table, a gradient builds up towards the drain and water starts flowing out of the drain. The effluent consists of a mixture of fresh and salt water. The origin of the fresh water entering the drain is that portion of the recharge water entering the water table close to the drain. The remaining portion of the recharge water is used to raise the water table farther away from the drain. This rise causes the salt water to be pushed ahead of the fresh water towards the drain. The result is the formation of the fresh-salt water interface. The interface is horizontal near the mid-point between drains and slowly curves upward towards the drain. Above the interface fresh water enters the drain, below it salt water. As time goes on the interface is displaced downward and the proportion of fresh water entering the drain increases.

When recharge is discontinued the water table slowly approaches a horizontal position and the interface also begins to level out. Then a new cycle of recharge starts. Since the salt water has dropped below the drain the concentration of the effluent will initially be low as the recharge begins. Soon the salt water wedge reaches the drain again and the concentration increases rapidly until the normal pattern of flow has been established after the concentration again decreases. This cycle repeats itself over and over, the average concentration becoming ever smaller.

Figure 99 shows an example of an intermittent recharge run with initial concentration of 15,000 ppm. Water was applied in the sequence of 8 minutes on and 24 minutes off. The interspace width was 0.0875 cms, the discharge  $0.0675 \text{ cm}^3/\text{sec}$ , kinematic viscosity  $0.0805 \text{ cm}^2/\text{sec}$ , length of model 235 cms and model height 42 cms. The value of  $(hx_p^2) / (K_{xp} z_p^2)$  is therefore 0.0132. Comparison with a similar situation of uniform recharge is indicated by curve A  $\left[ (hx_p^2) / (K_{xp} z_p^2) \text{ is equal to } 0.0115 \right]$ . A direct comparison between the two curves is difficult to make. The sawtooth graph resulting from the intermittent recharge does show the concentration of effluent at any time. However, it does not show the fact that the volume of flow is concentrated around the peaks of the curve when water is being applied. If we keep this in mind the agreement between the two curves is remarkable. As might be expected, initially there is

considerable discrepancy between the two curves.

The same aquifer situation, but for initial concentration of 30,000 ppm, is shown in Figure 100. As before, the on-off sequence was 8 and 24 minutes. The interspace width was 0.0875 cms, the discharge 0.0675 cc/sec, kinematic viscosity 0.0805 cm<sup>2</sup>/sec, length of model 235 cms and model aquifer thickness 42 cms, again giving a value of  $(hx_p^2) / (K_{xp} z_p^2)$  of 0.0132. For comparison the curve of run 8, 30,000 ppm (see Figure 36) for which  $(hx_p^2) / (K_{xp} z_p^2)$  is 0.0122, is shown as curve A. In this case curve A lies somewhat lower at later times than the saw-tooth curve but the agreement is quite good.

It may be concluded that for studies of this kind the simplified procedure of continuous recharge may be used instead of the experimentally more difficult procedure of intermittent recharge.

#### Effect of initial concentration

It was shown earlier in this chapter that an aquifer is flushed clean of salt water to a greater extent when the initial concentration of the salt water is lower. The reason for this was shown to be the difference in density which accompanies a change in concentration.

The concentration of the effluent at any time is obviously higher when the initial concentration is higher. However, when one expresses the concentration of effluent as a fraction of the initial concentration there is little difference. For example Figure 101

shows this fraction as a function of the parameter  $(z_p K_{xp} t) / (n_p x_p^2)$  for the uniform aquifer and initial concentrations of 10,000 and 15,000 ppm of salt. The value of  $(hx_p^2) / (K_{xp} z_p^2)$  is equal to 0.03 in both cases. The curve for 30,000 ppm, which was not drawn in this figure virtually coincided with the other curves. In the range of values of  $(hx_p^2) / (K_{xp} z_p^2)$  of 0.03 and higher there is little effect of initial concentration.

When we take a value of 0.005 for  $(hx_p^2) / (K_{xp} z_p^2)$  as is shown in Figure 102 for initial concentrations of 10,000 and 30,000 ppm, differences do exist. For higher values of initial concentration the salt concentration of the effluent is relatively lower at equivalent times. This is in agreement with Figure 92, where at low values of discharge, the amount of aquifer cleaning is larger for low values of initial concentration.

In the present study fresh water was used for recharge. Since the effect of initial concentration on the concentration effluent curves is small, it seems justified to use the results obtained in this study also in cases for which the concentration of the recharge water is greater than zero. The concentration of the drain effluent, expressed as a fraction of the initial concentration, is determined by the proportion of flow into the drain above and below the interface. Thus, appropriate corrections may be made to take in account the concentration of recharge water.

## CHAPTER VII

## CONCLUSIONS AND RECOMMENDATIONS

Based on the data presented and the analysis in the previous chapters, the following conclusions are drawn.

1. The Hele-Shaw model is a useful tool for the study of the rate of quality change of drain effluent from a saline water aquifer.

2. The relative depth to which an aquifer will be flushed clear of salt water will depend upon the drain spacing, thickness of aquifer, permeability and recharge rate. An increase of the recharge rate and/or drain spacing increases the depth to which the aquifer will be cleaned. An increase of the permeability and/or aquifer thickness has the reverse effect.

3. The relative depth to which an aquifer is flushed clear of salt water also depends upon aquifer stratification. In the 12/1 layered aquifer little flow occurs in the lower member. In the 1/6 layered aquifer and also in the uniform aquifer flow also takes place in the lower part. The extent to which this takes place depends upon the magnitude of the parameter  $(hx_p^2) / (K_{xp} z_p^2)$ .

4. The concentration of the effluent at any time is:

- a) inversely related to the recharge rate
- b) directly related to the drain spacing only for very small values of the spacing

c) directly related to the thickness of the aquifer

d) inversely related to the permeability

5. Whether water or a glycerine-water mixture is used, the results obtained with the model are the same. With a glycerine-water mixture it is possible to cover a larger range of values of the parameter  $(hx_p^2) / (K_{xp} z_p^2)$ .

6. It is experimentally possible to simulate intermittent recharge with the model. The experimental technique is more difficult and elaborate, and the results more difficult to interpret.

7. The procedure of using continuous recharge rather than the more realistic intermittent recharge is justified.

8. The effect of the initial concentration or concentration of effluent (expressed as a fraction of the initial concentration) is small.

9. A Hele-Shaw model may not conform to field conditions when a layered system is investigated, because of scaling requirements.

Recommendations for further work on this subject may consist of:

1. A study similar to the one reported here should be made eliminating the variable anisotropy. In this work none of the results involving changes of drain spacing and aquifer depth are truly comparable, since they involve differences in anisotropy. The effect of anisotropy is increasingly important when the ratio between drain

spacing and aquifer depth becomes smaller. A study of this type could be performed by changing the model geometry rather than the discharge.

2. The results obtained suggest the use of the Hele-Shaw model for determining under which conditions the Dupuit-Forchheimer assumptions are valid. This could be easily accomplished by varying the ratio between drain spacing and aquifer depth. The results of this type of experiment would give correction factors to be applied to the aquifer thickness for different ratios of drain spacing and aquifer thickness.

## BIBLIOGRAPHY

- Bear, Jacob, (1960), Scales of viscous analogy models for ground water studies: Am. Soc. Civil Engineers Proc., v. 86, no. HY 2, p. 11-23.
- Bear, Jacob, and Dagan, Gedeon, (1964), Intercepting fresh water above the interface in a coastal aquifer: Intern. Assoc. Scientific Hydrology, Publ. 64, p. 154-181.
- Biggar, J. W., and Nielsen, D. R., (1964), Chloride - 36 diffusion during stable and unstable flow through glass beads: Soil Science Soc. America Proc., v. 28, p. 591-595.
- Bouwer, H., (1963), Limitations of Dupuit-Forchheimer assumptions in recharge and drainage in Proc. Symp. Transient Ground Water Hydraulics, edited by D. E. L. Maasland and M. W. Bittinger, Colorado State University, Dept. of Civil Engineering, Fort Collins, Civil Engineering Report 1963, no. 70.
- Clapper, L. S., (1963), America's shame, water pollution: National Wildlife, v. 1, no. 6, p. 17-20.
- Cooper, H. H., (1959), A hypothesis concerning the dynamic balance of fresh water and salt water in a coastal aquifer: Jour. Geophys. Research, v. 64, p. 461-467.
- Dachler, R., (1936), in Grundwasserstromung, Vienna, Julius Springer, 320 p.
- Darcy, H., (1856), Les fontaines publiques de la ville de Dijon, Paris, V. Dalmont.
- De Josselin de Jong, G., (1960), Singularity distribution for the analysis of multiple-fluid flow through porous media: Journ. Geophys. Research, v. 65, p. 3739-3758.
- De Wiest, R. J. M., (1961), Free surface flow in homogeneous porous medium: Am. Soc. Civil Engineers Proc., v. 87, no. HY4 p. 181-220.
- Fireman, M., and Hayward, H. E., (1955), Irrigation water and saline and alkali salts: Water, Yearbook of Agriculture, p. 321-327.

## BIBLIOGRAPHY (cont'd)

- Glover, R. E. , (1959), The pattern of fresh-salt water flow in a coastal aquifer: Jour. Geophys. Research, v. 64, p. 457-459.
- Hele-Shaw, H. S. , (1898), Experiments on the nature of surface resistance of water and of stream line motion under certain experimental conditions: Trans. Inst. Naval Architects, v. 40, p.21-46.
- Hele-Shaw, H. S. , (1899), Streamline motion of a viscous film: Report 68th meeting British Assoc. Advancement of Science, p. 136-142.
- Jacob, C. E. , (1950), Flow of ground water in Proc. 4th Hydraulics Conference, University of Iowa, New York, John Wiley and Sons.
- Kidder, R. E. , (1956), Flow of immiscible fluids in porous media: Exact solution of a free boundary problem: Jour. Applied Physics, v. 27, p. 867-869.
- Kidder, R. E. , (1956), Motion of the interface between two immiscible liquids of unequal density in a porous solid: Jour. Applied Physics, v. 27, p. 1546-1548.
- Maasland, D. E. L. , and Bittinger, M. W. , (1964), Quality of effluent from drains in an aquifer containing saline water, Colorado State University, Dept. of Civil Engineering, Fort Collins, Civil Engineering Report 1964, no. 17.
- Peterka, A. J. , and Glover, R. E. , (1963), Laboratory investigation of the removal of salt water from a two-part aquifer using tile drains installed in the top member: U. S. Dept. Interior, Bureau of Reclamation, Hydraulic Laboratory Report no. 520, 12 p.
- Santing, G. , (1951), Modele pour l' etude des problemes de l' ecoulement simultane des eaux souterraine douces et saluees: Intern. Assoc. Scientific Hydrology, Publ. 33, p. 184-193.
- Santing, G. , (1963), Modelonderzoek, in Nederlandse Centrale Organisatie voor toegepast - natuurwetenschappelijk onderzoek, Commissie voor hydrologisch onderzoek. Verslag van de Technische bijeenkomst 17, Verslagen en mededelingen no. 8, 85p.
- Todd, D. K. , (1959), Ground water hydrology: New York, John Wiley and Sons. 336 p.

## BIBLIOGRAPHY (cont'd)

- Todd, D. K., (1961), Seepage through layered anisotropic porous media: Am. Soc. Civil Engineers Proc., v. 87, no. HY 3, p. 31-57.
- Hubbert, M. King, (1953), Entrapment of petroleum under hydrodynamic conditions: Bulletin Am. Assoc. Petroleum Geologists, v. 37, p. 1954-2026.

APPENDIX A

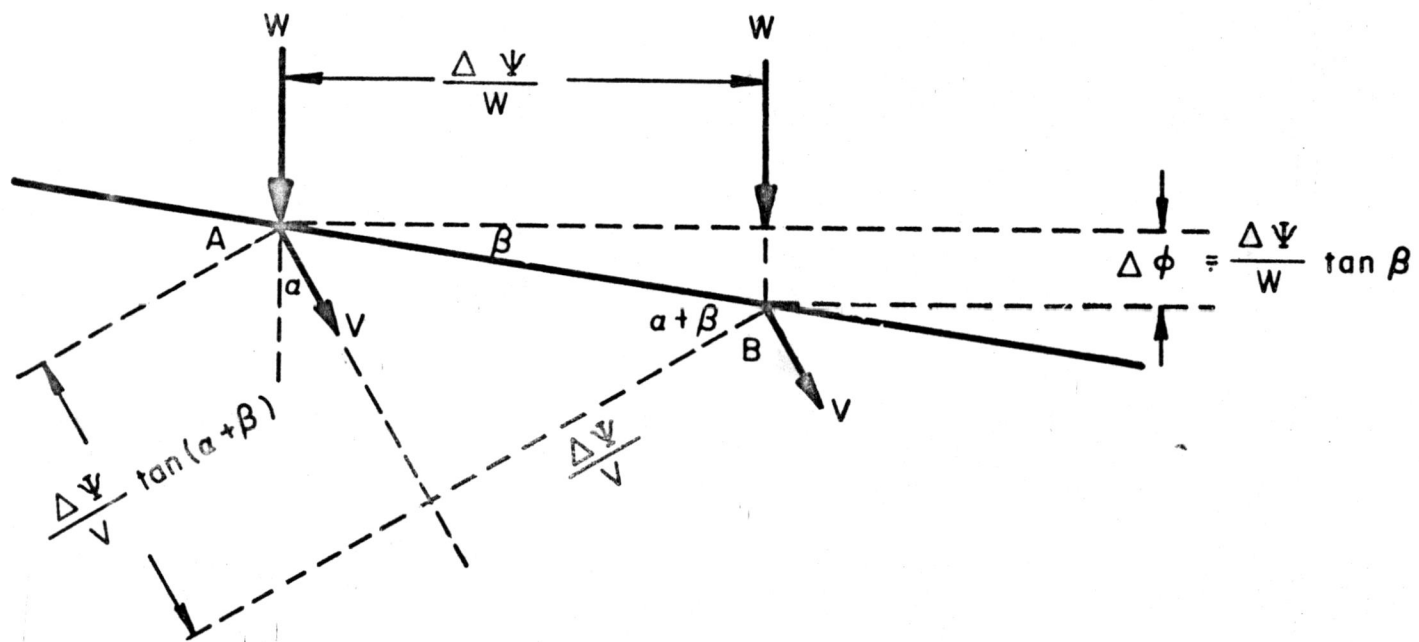


Fig. 1. Refraction of flow lines near a water table with accretion.

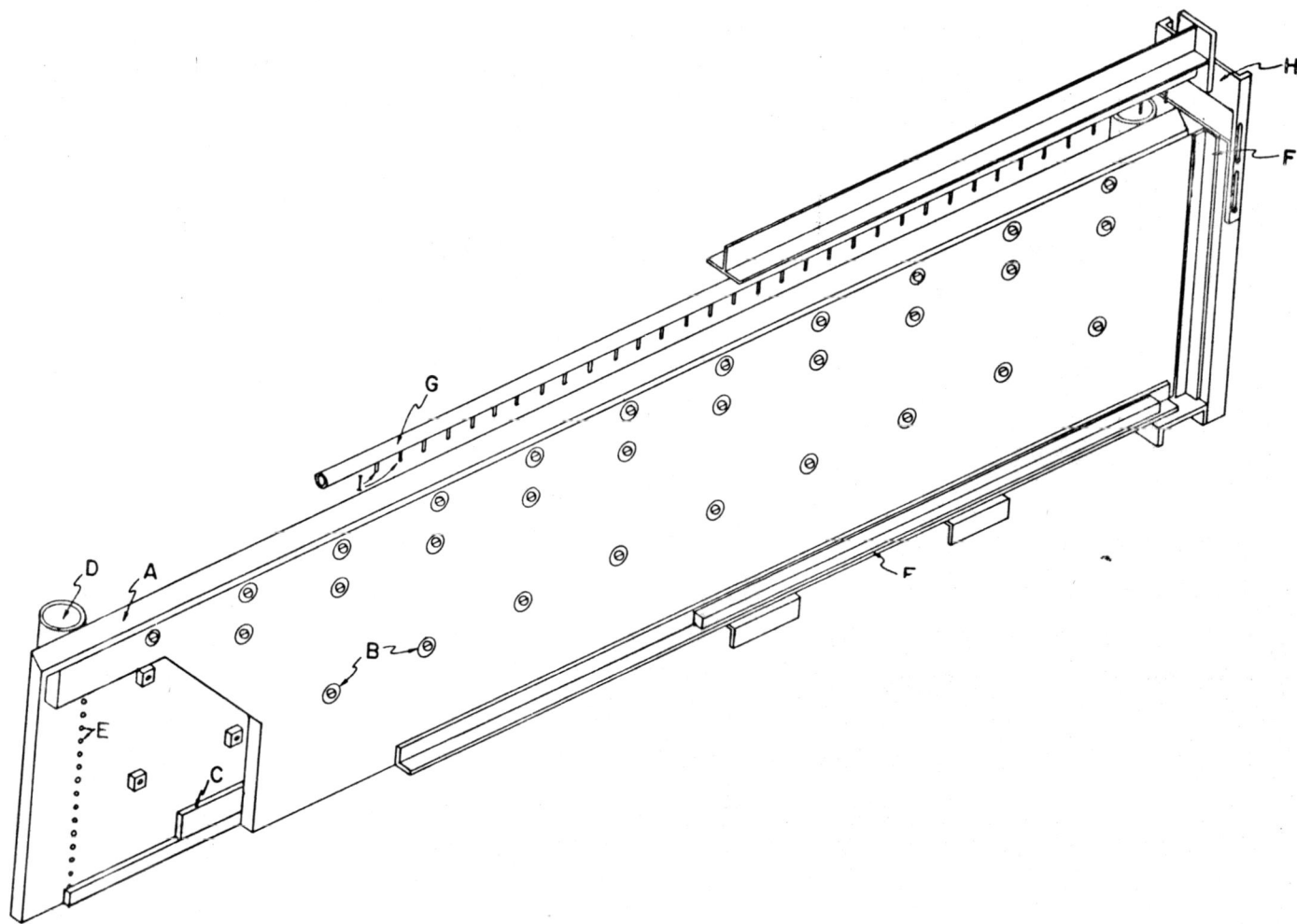


Fig. 2. Sketch of Hele-Shaw model.

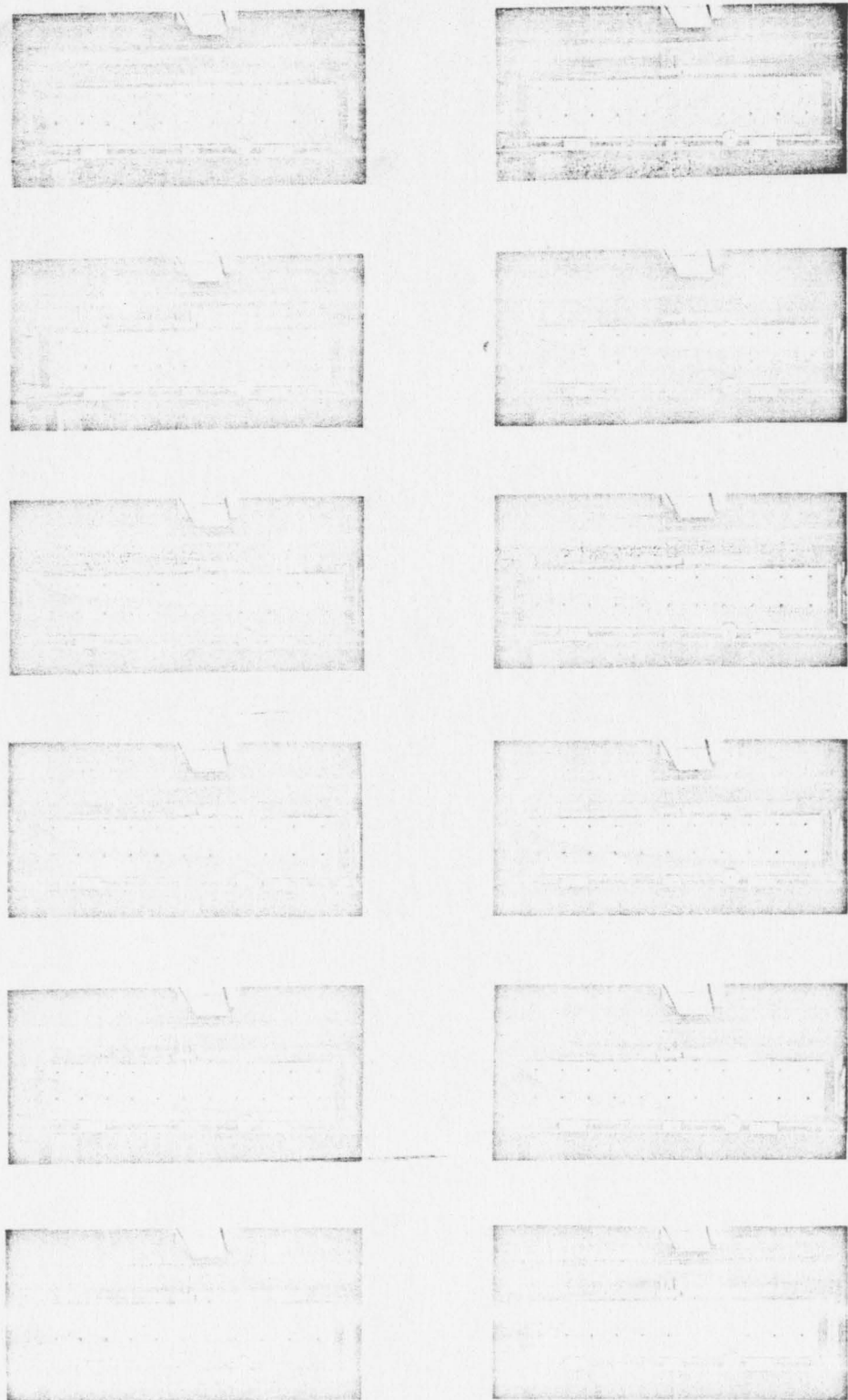


Fig. 3. Example of change of salt-fresh water interface with time.



Fig. 4. Conductivity cell arrangement and conductivity recorder.

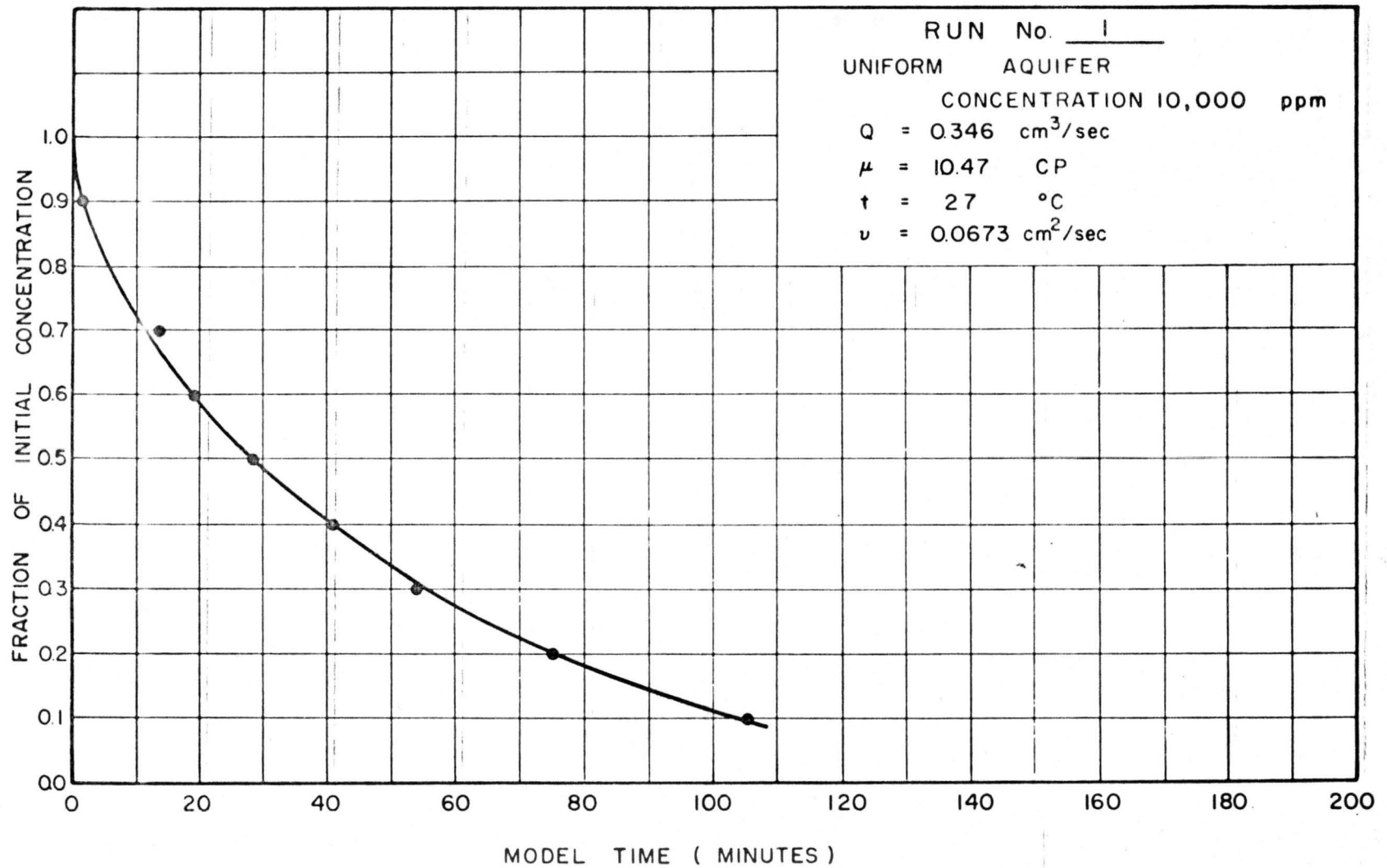


Fig. 5. Concentration versus time (Run 1, initial concentration 10,000 ppm, uniform aquifer).

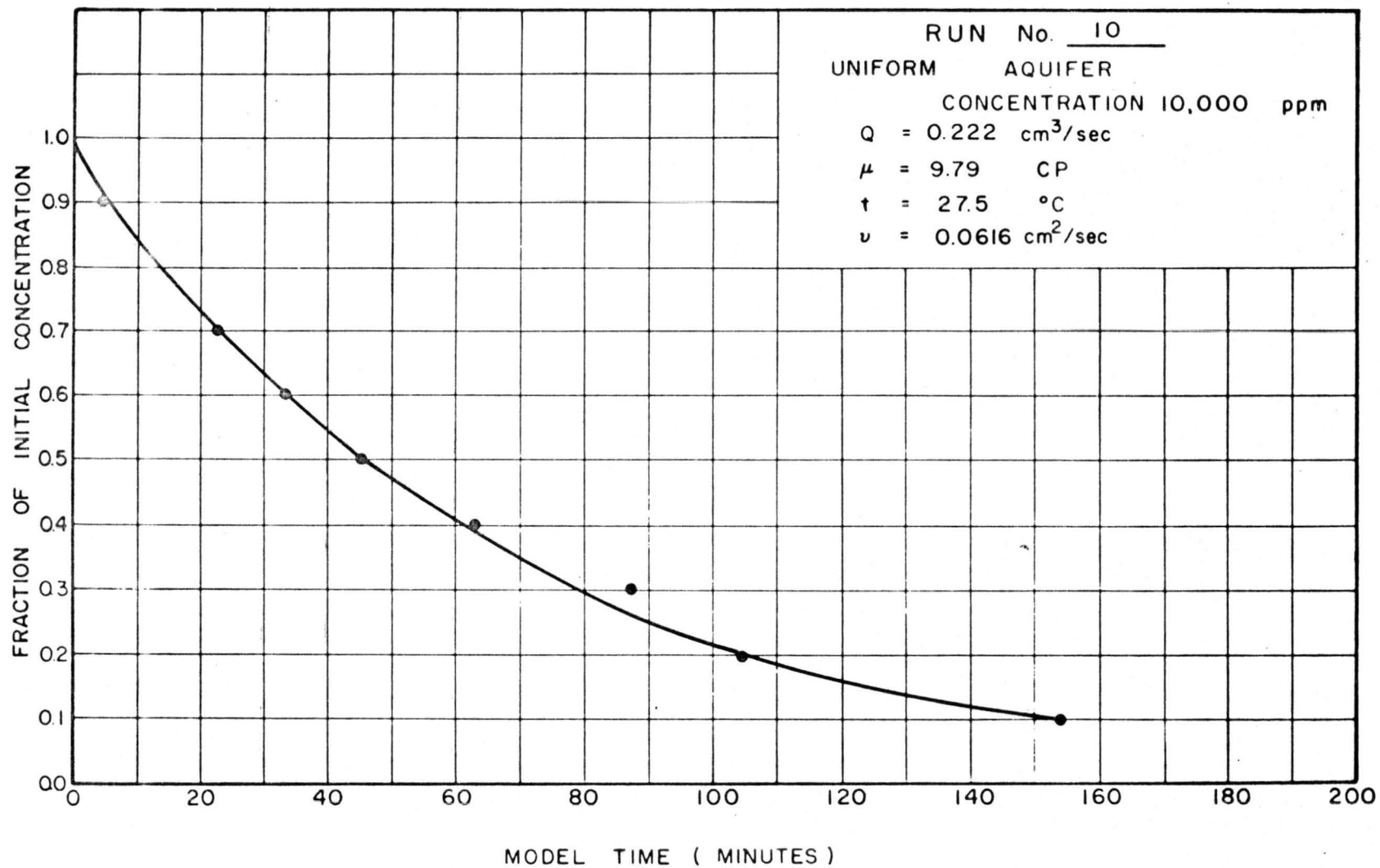


Fig. 6. Concentration versus time (Run 10, initial concentration 10,000 ppm, uniform aquifer).

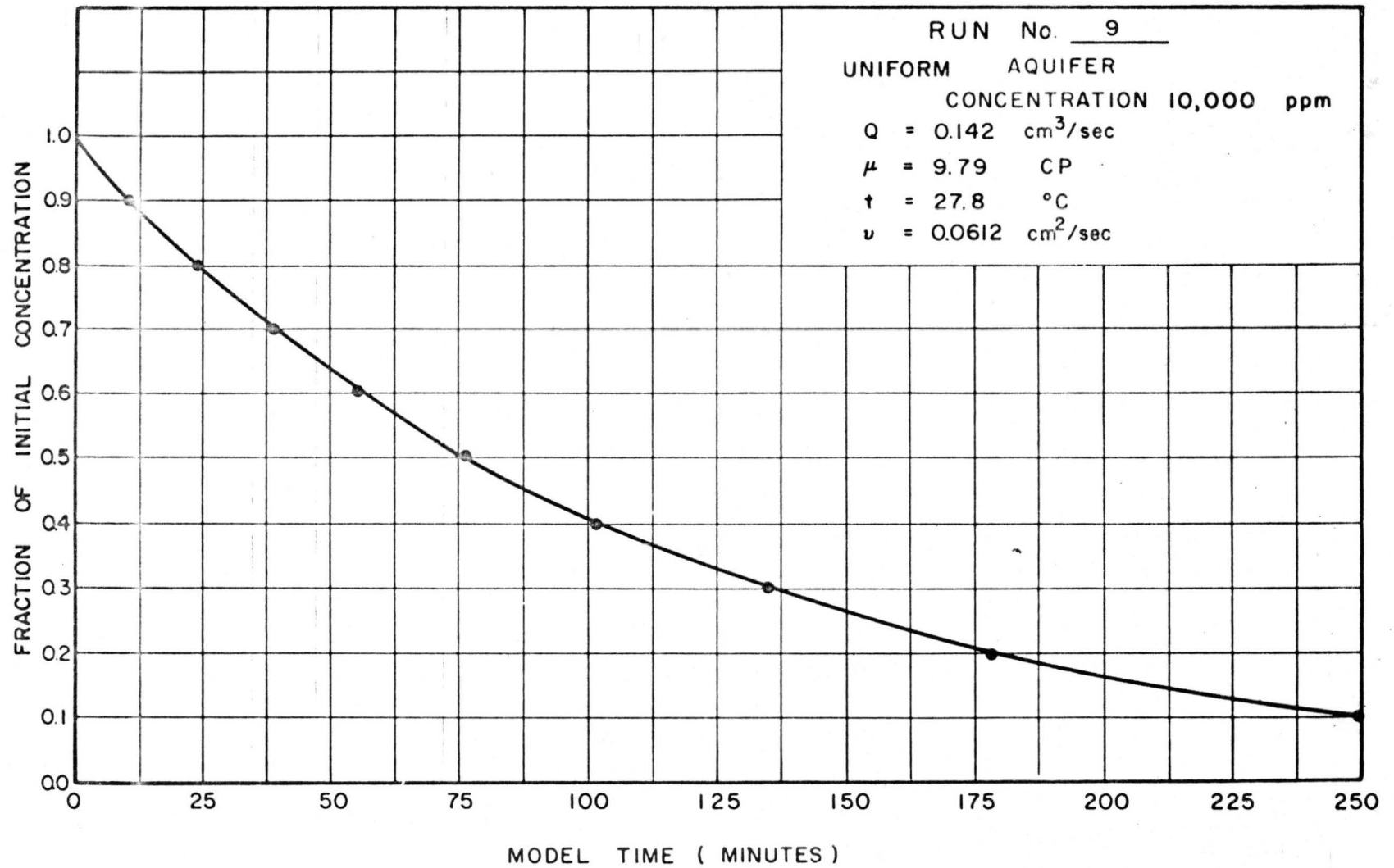


Fig. 7. Concentration versus time (Run 9, initial concentration 10,000 ppm, uniform aquifer).

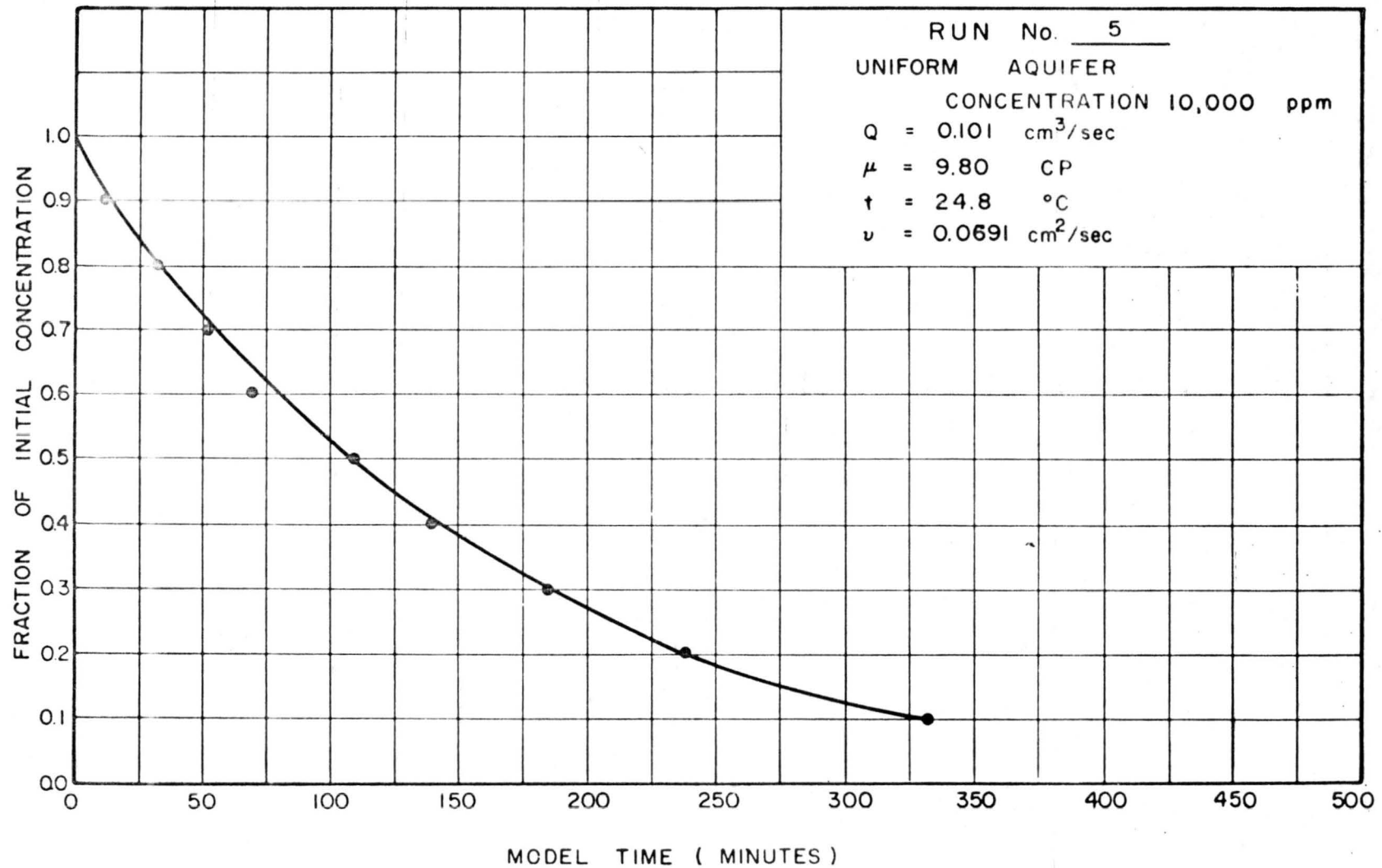


Fig. 3. Concentration versus time (Run 5, initial concentration 10,000 ppm, uniform aquifer).

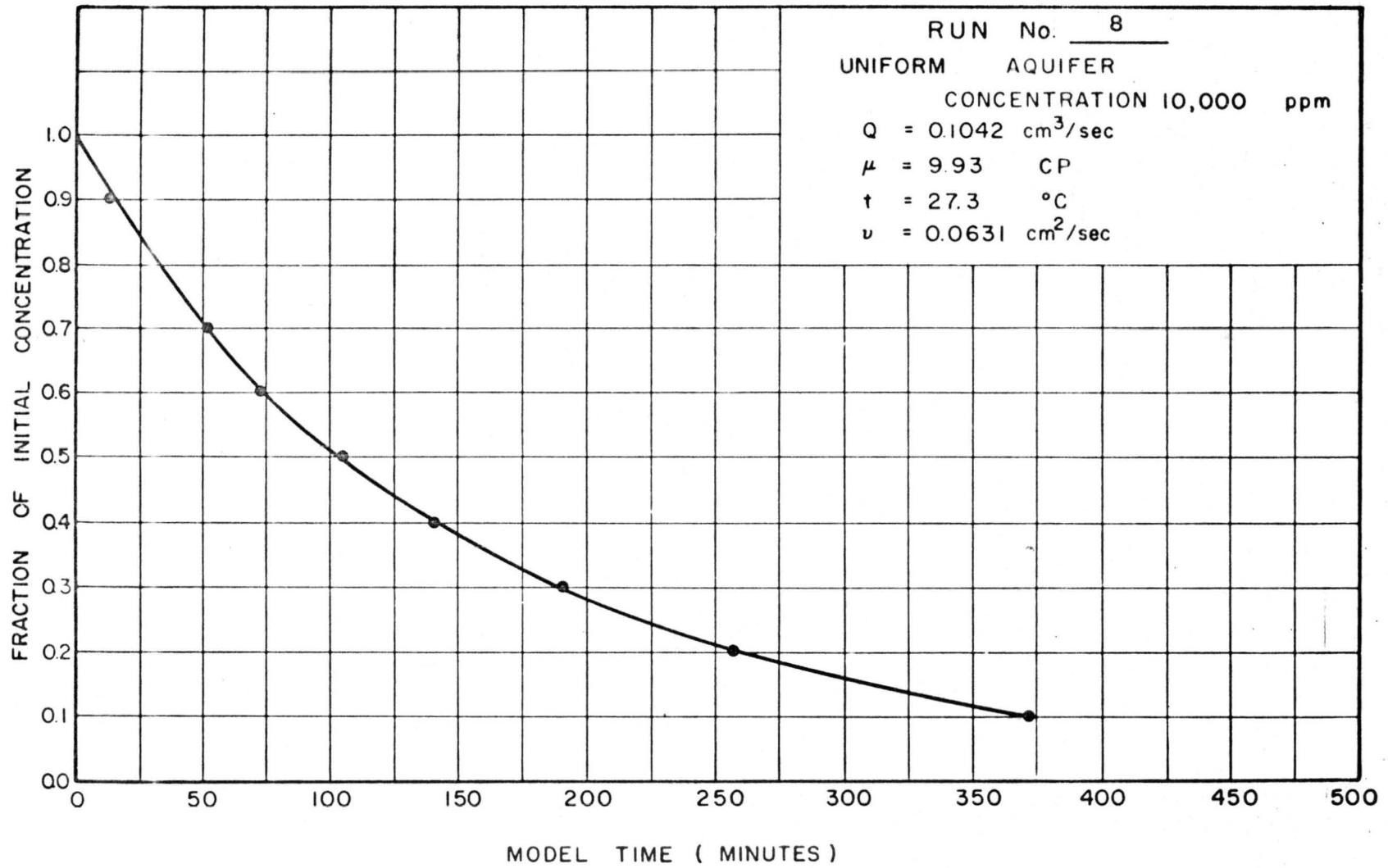


Fig. 9. Concentration versus time (Run 3, initial concentration 10,000 ppm, uniform aquifer).

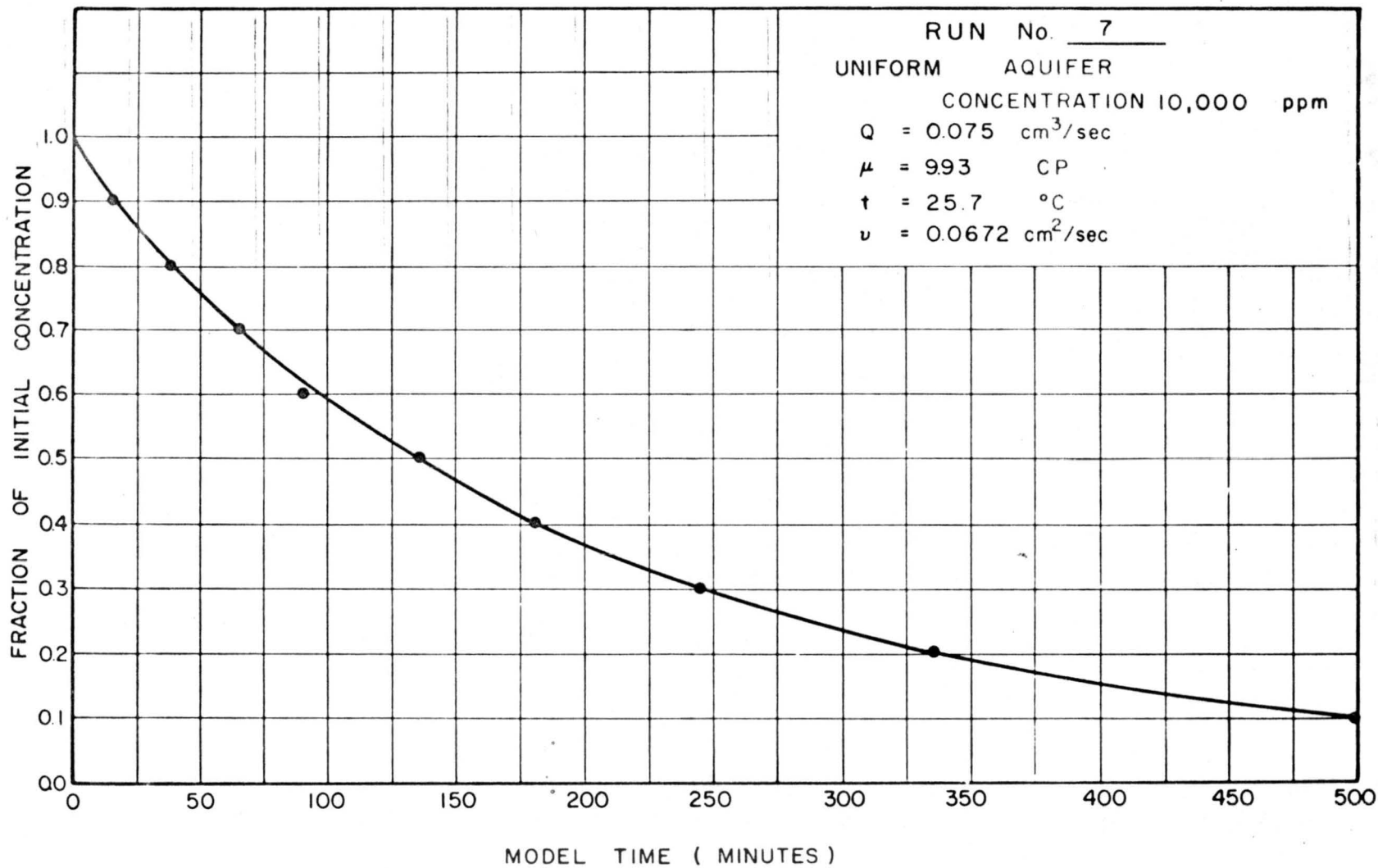


Fig. 10. Concentration versus time (Run 7, initial concentration 10,000 ppm, uniform aquifer).

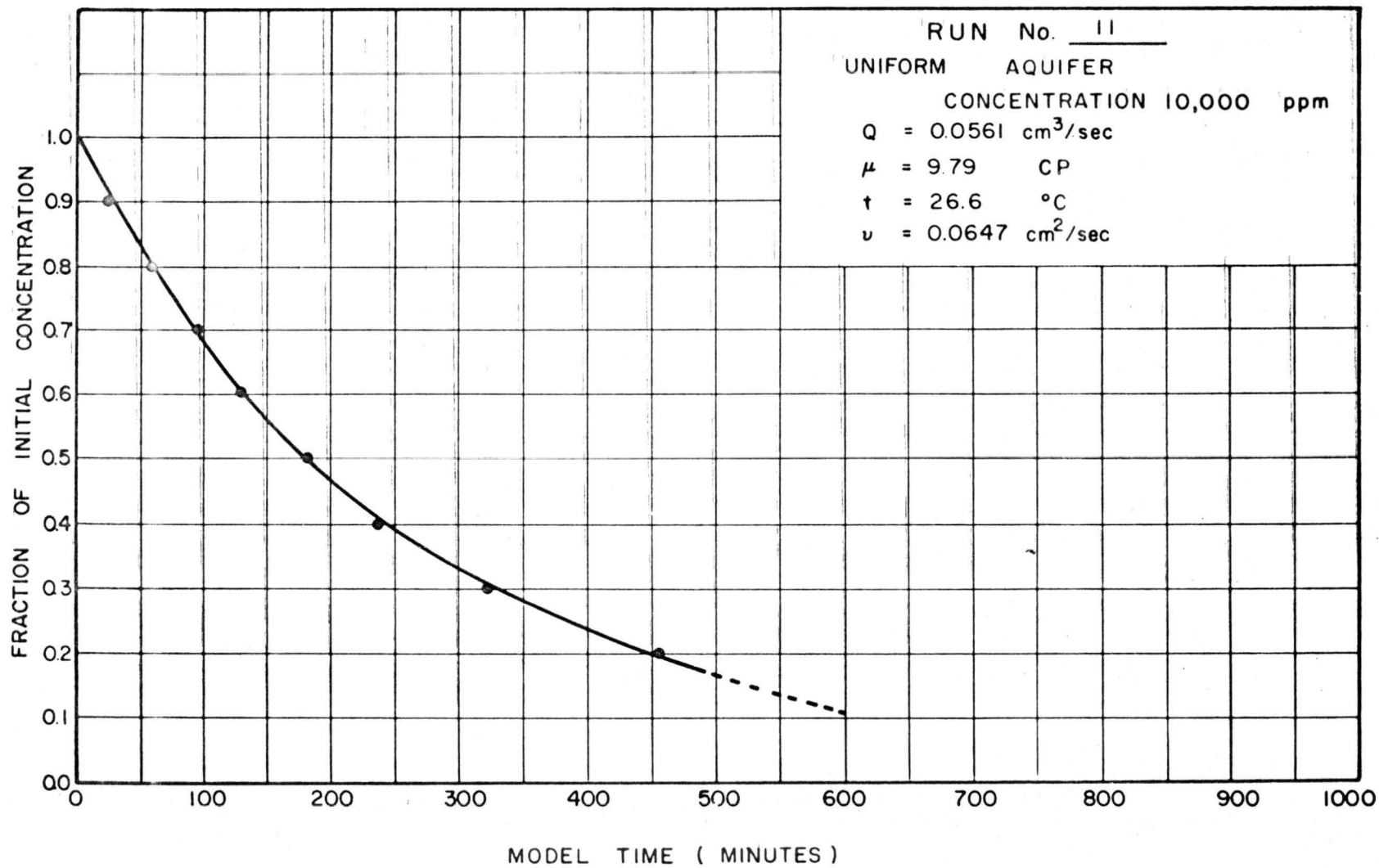


Fig. 11. Concentration versus time (Run 11, initial concentration 10,000 ppm, uniform aquifer).

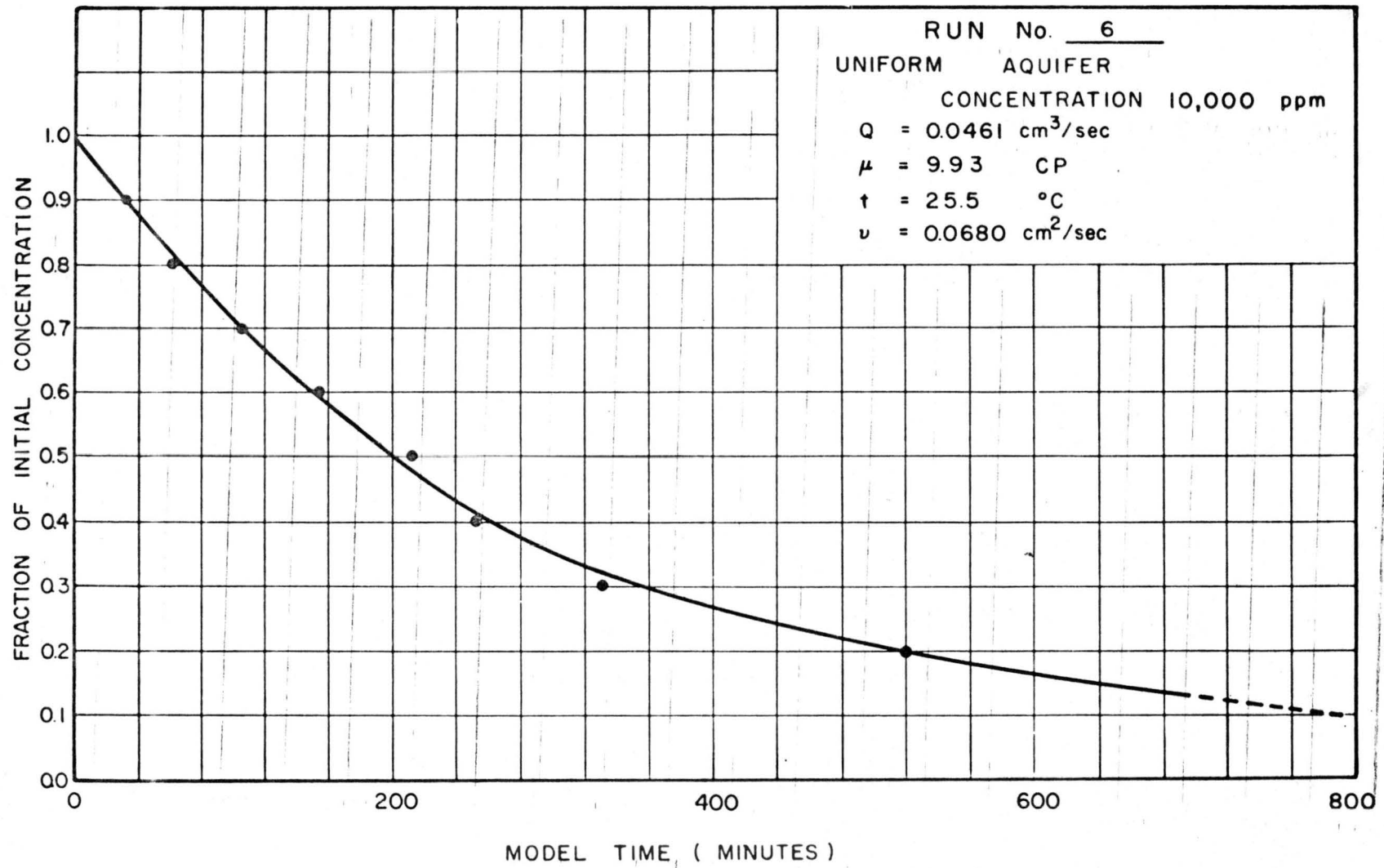


Fig. 12. Concentration versus time (Run 6, initial concentration 10,000 ppm, uniform aquifer) .

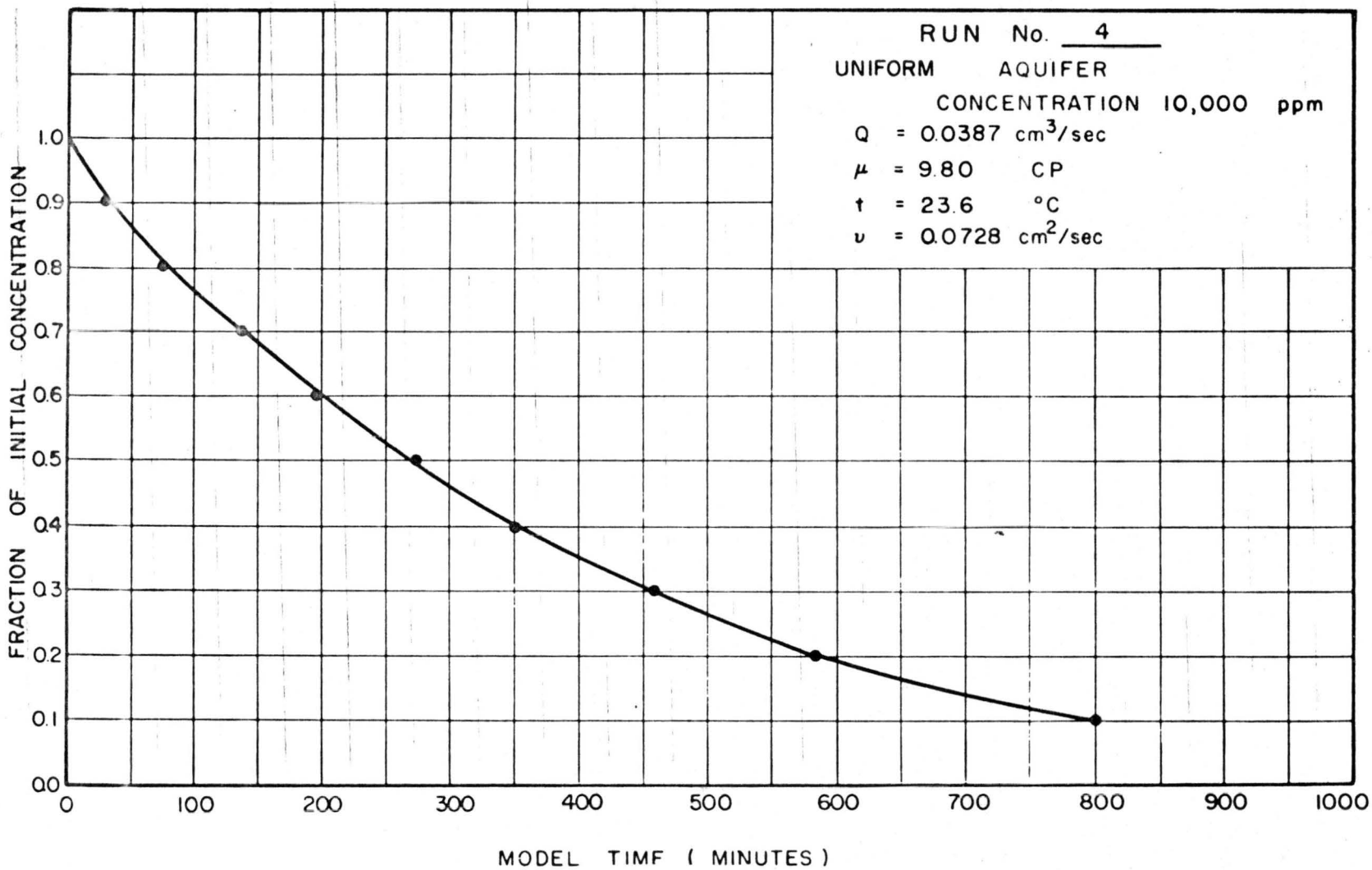


Fig. 13. Concentration versus time (Run 4, initial concentration 10,000 ppm, uniform aquifer).

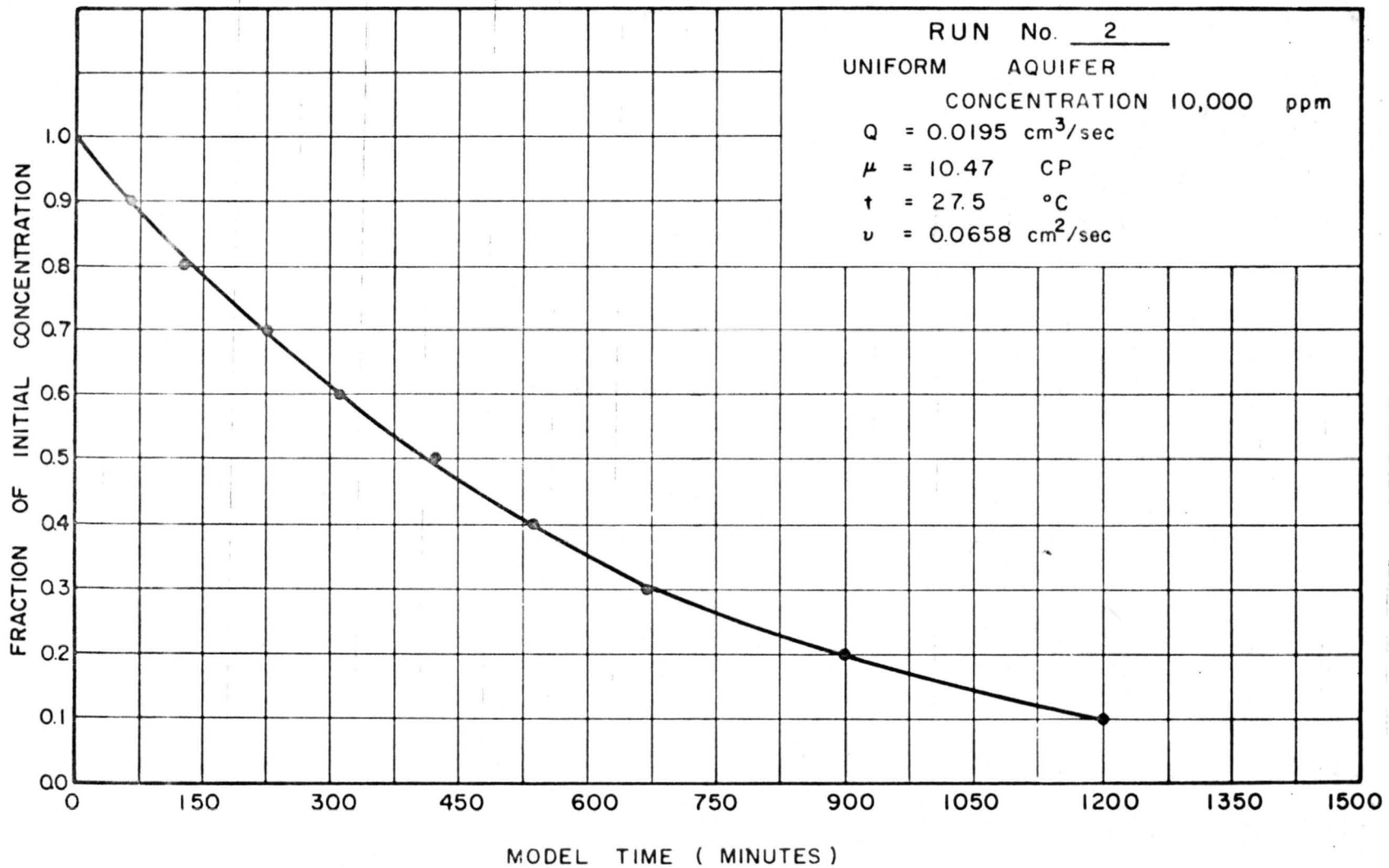


Fig. 14. Concentration versus time (Run 2, initial concentration 10,000 ppm, uniform aquifer).

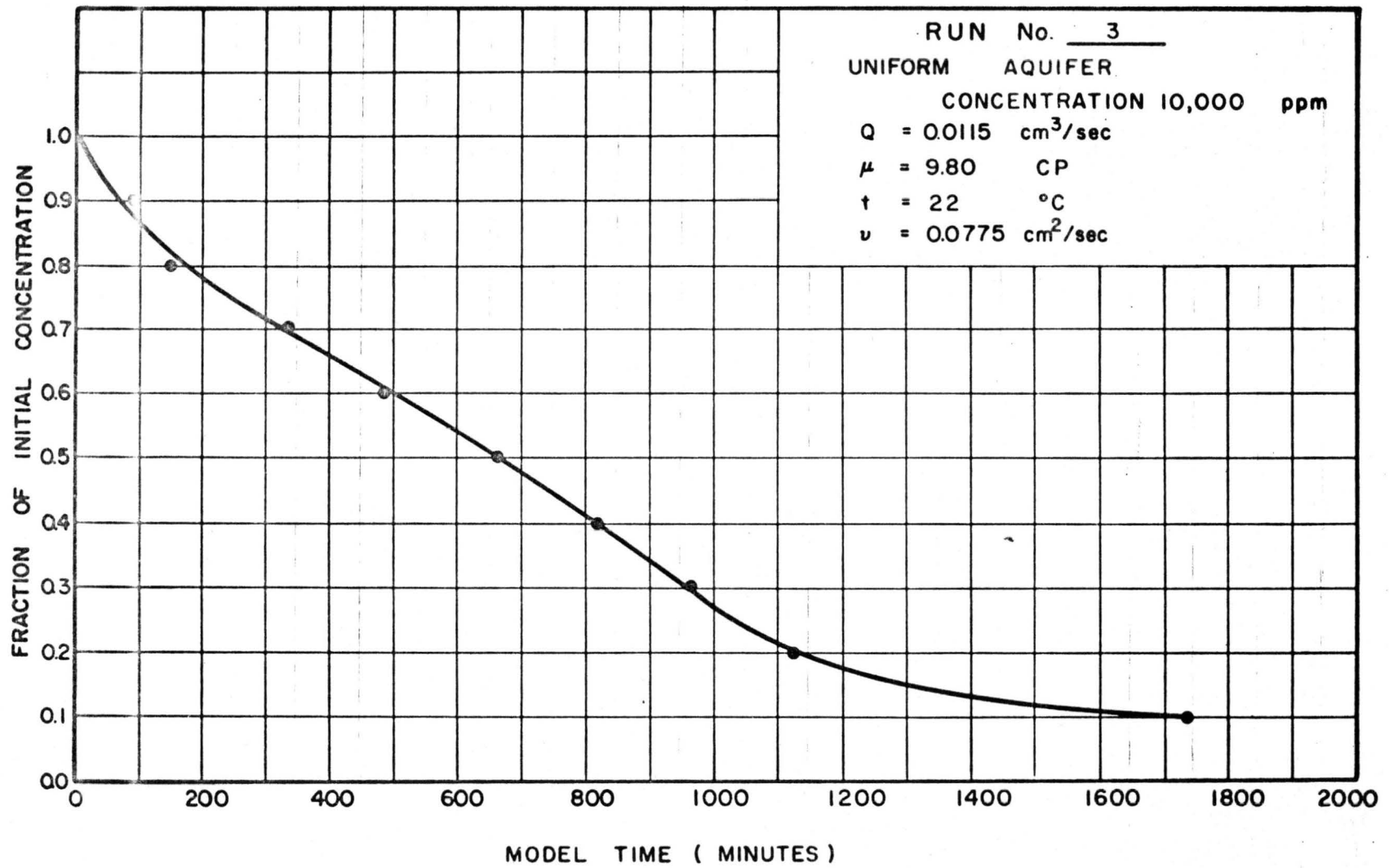


Fig. 15. Concentration versus time (Run 3, initial concentration 10,000 ppm, uniform aquifer).

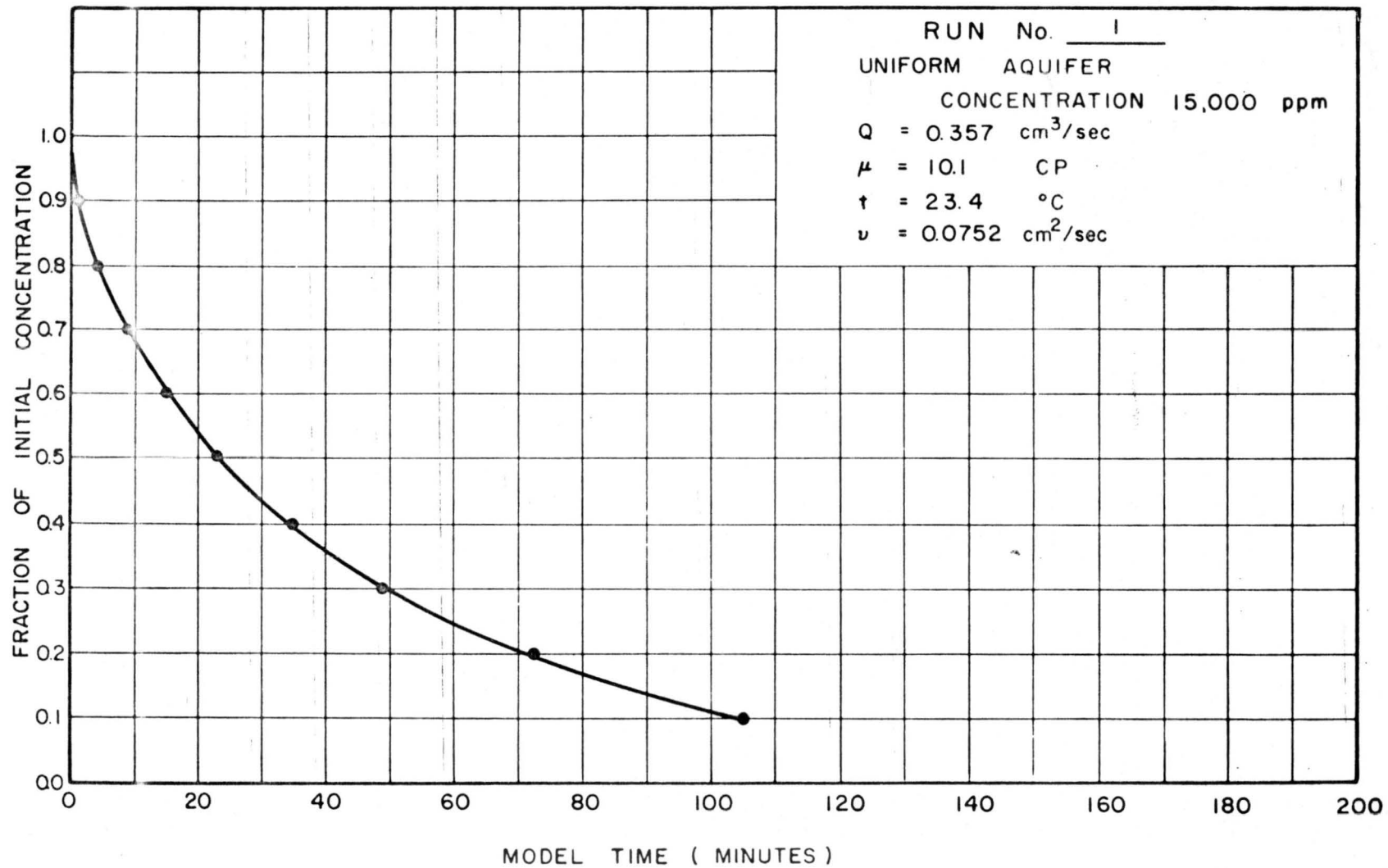


Fig. 16. Concentration versus time (Run 1, initial concentration 15,000 ppm, uniform aquifer).

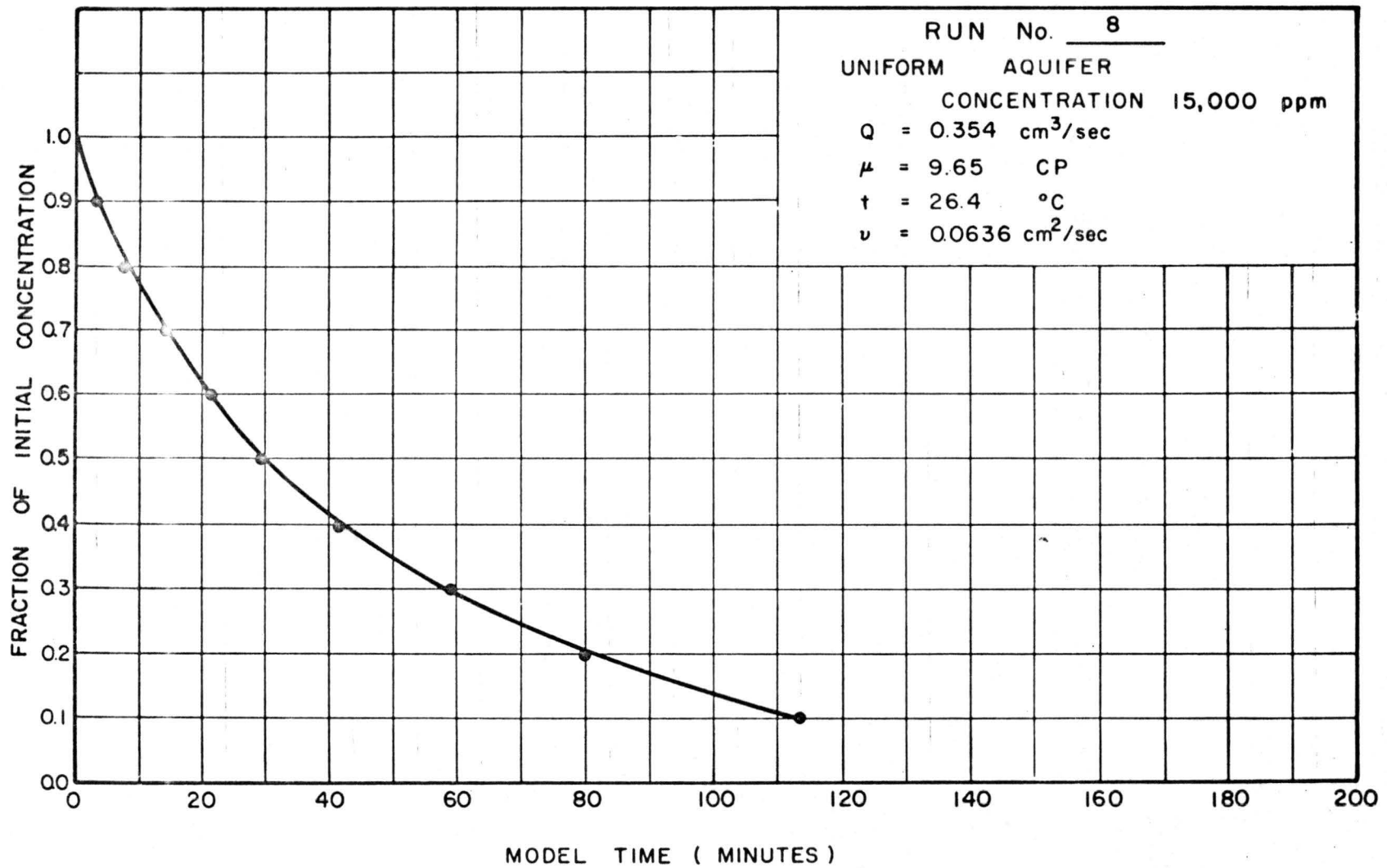


Fig. 17. Concentration versus time (Run 3, initial concentration 15,000 ppm, uniform aquifer).

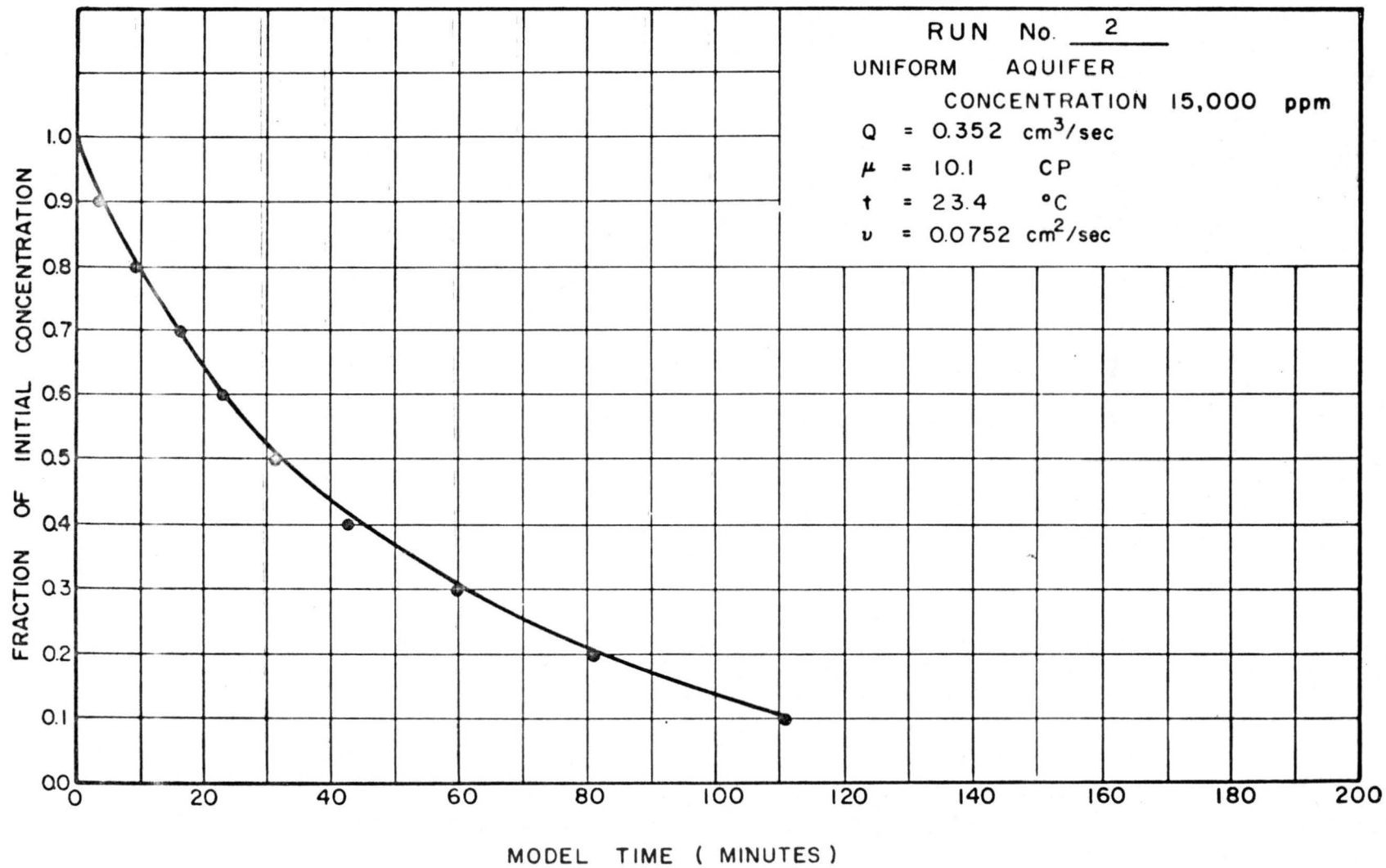


Fig. 13. Concentration versus time (Run 2, initial concentration 15,000 ppm, uniform aquifer).

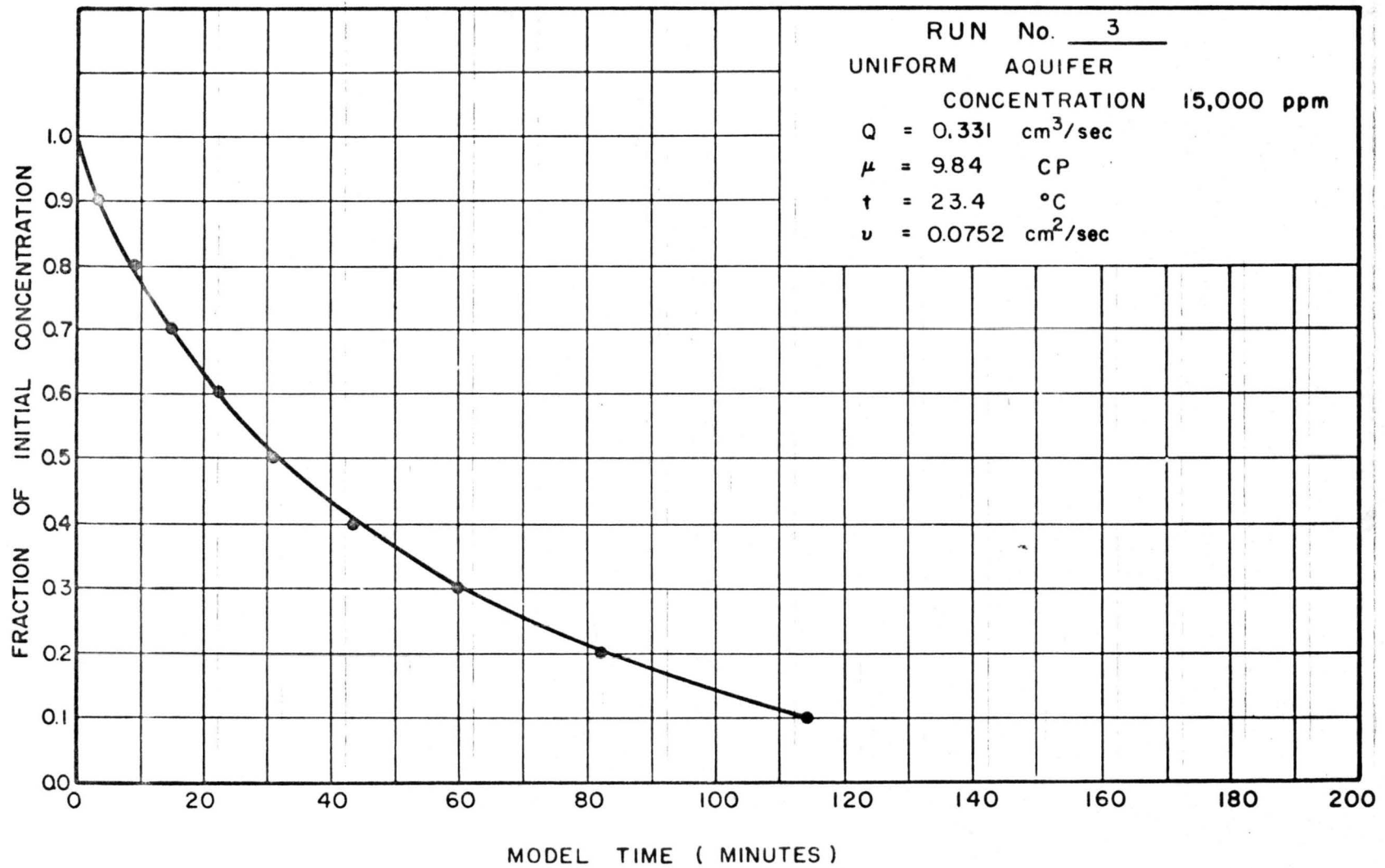


Fig. 19. Concentration versus time (Run 3, initial concentration 15,000 ppm, uniform aquifer).

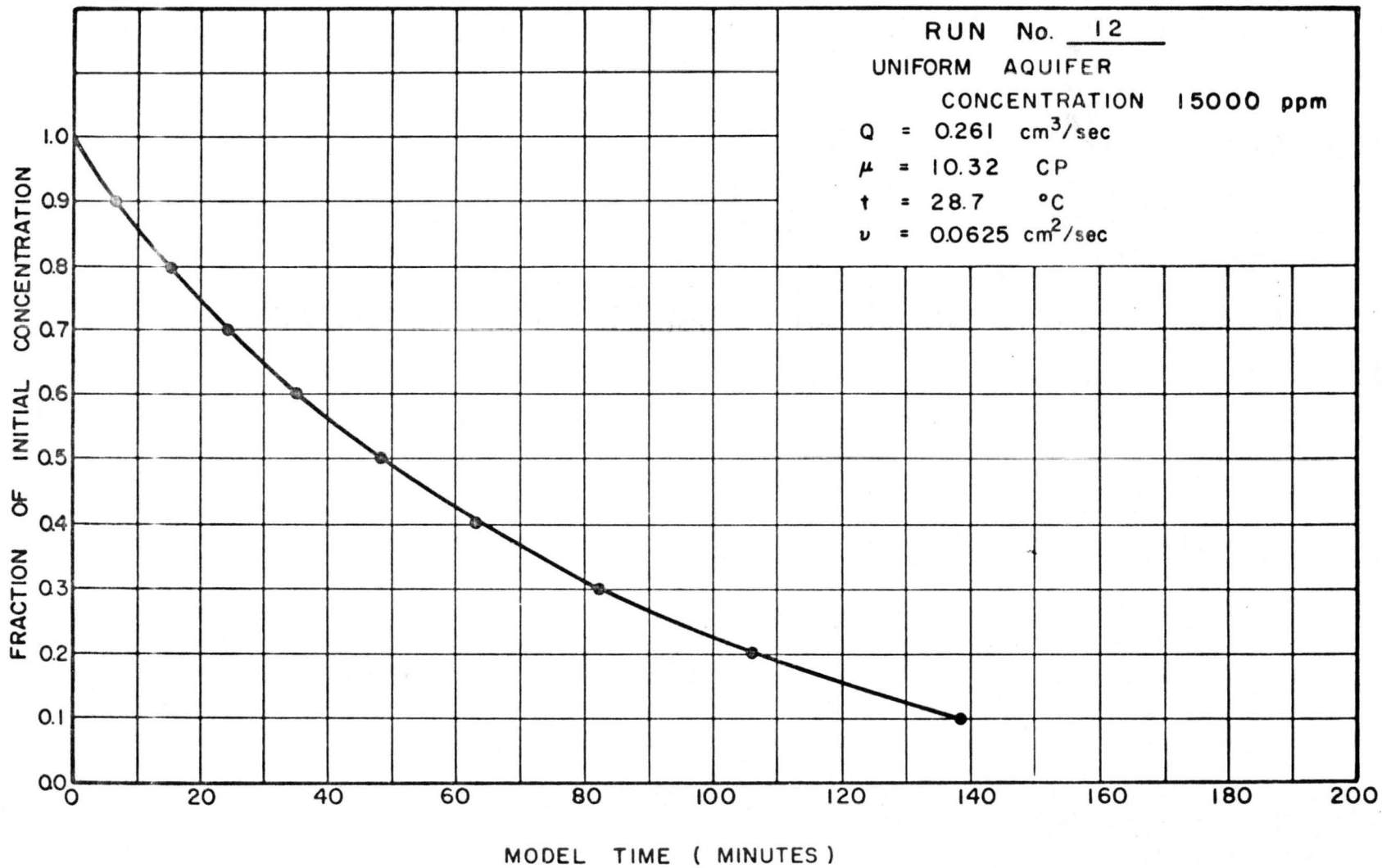


Fig. 20. Concentration versus time (Run 12, initial concentration 15,000 ppm, uniform aquifer).

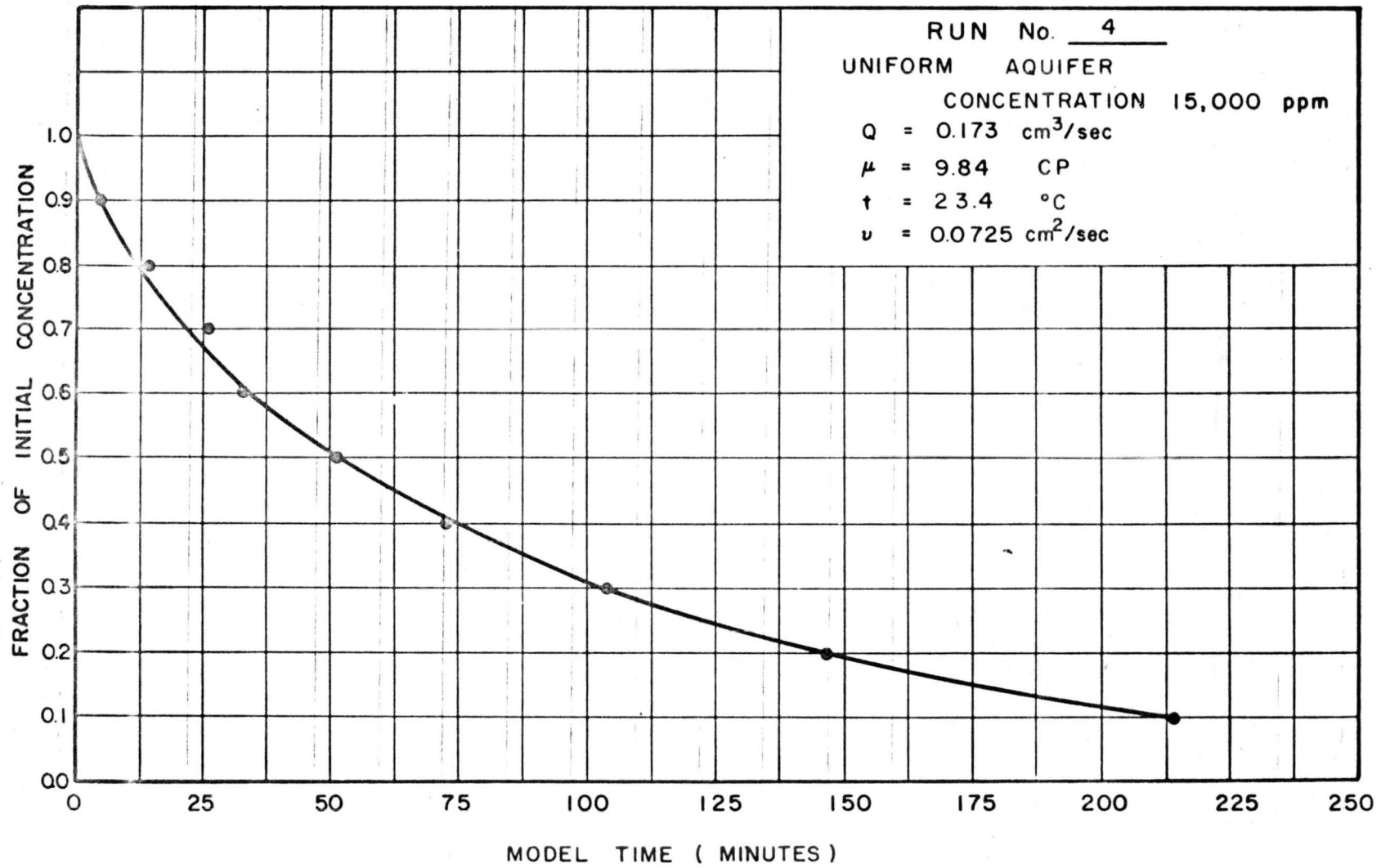


Fig. 21. Concentration versus time (Run 4, initial concentration 15,000 ppm, uniform aquifer).

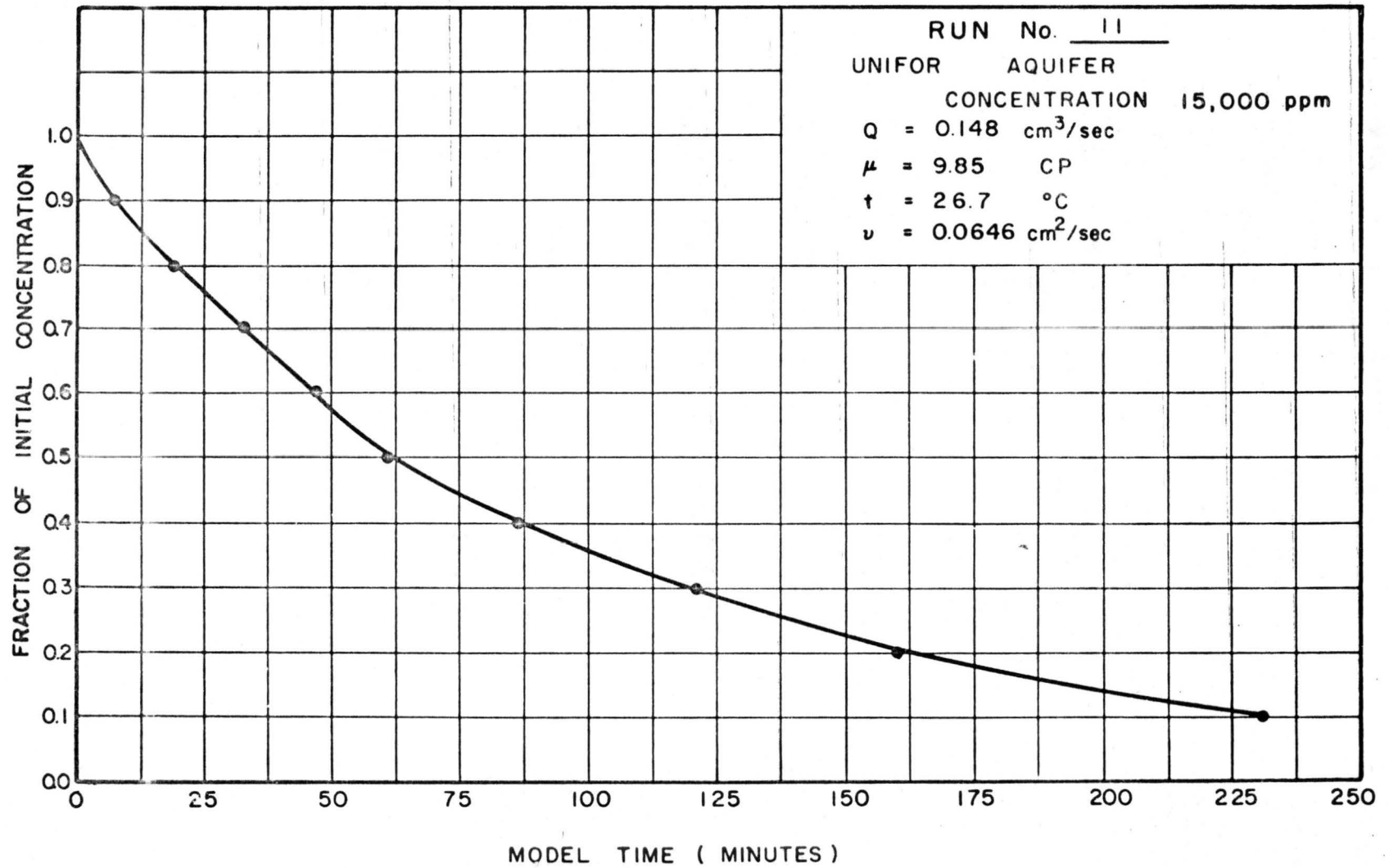


Fig. 22. Concentration versus time (Run 11, initial concentration 15,000 ppm, uniform aquifer).

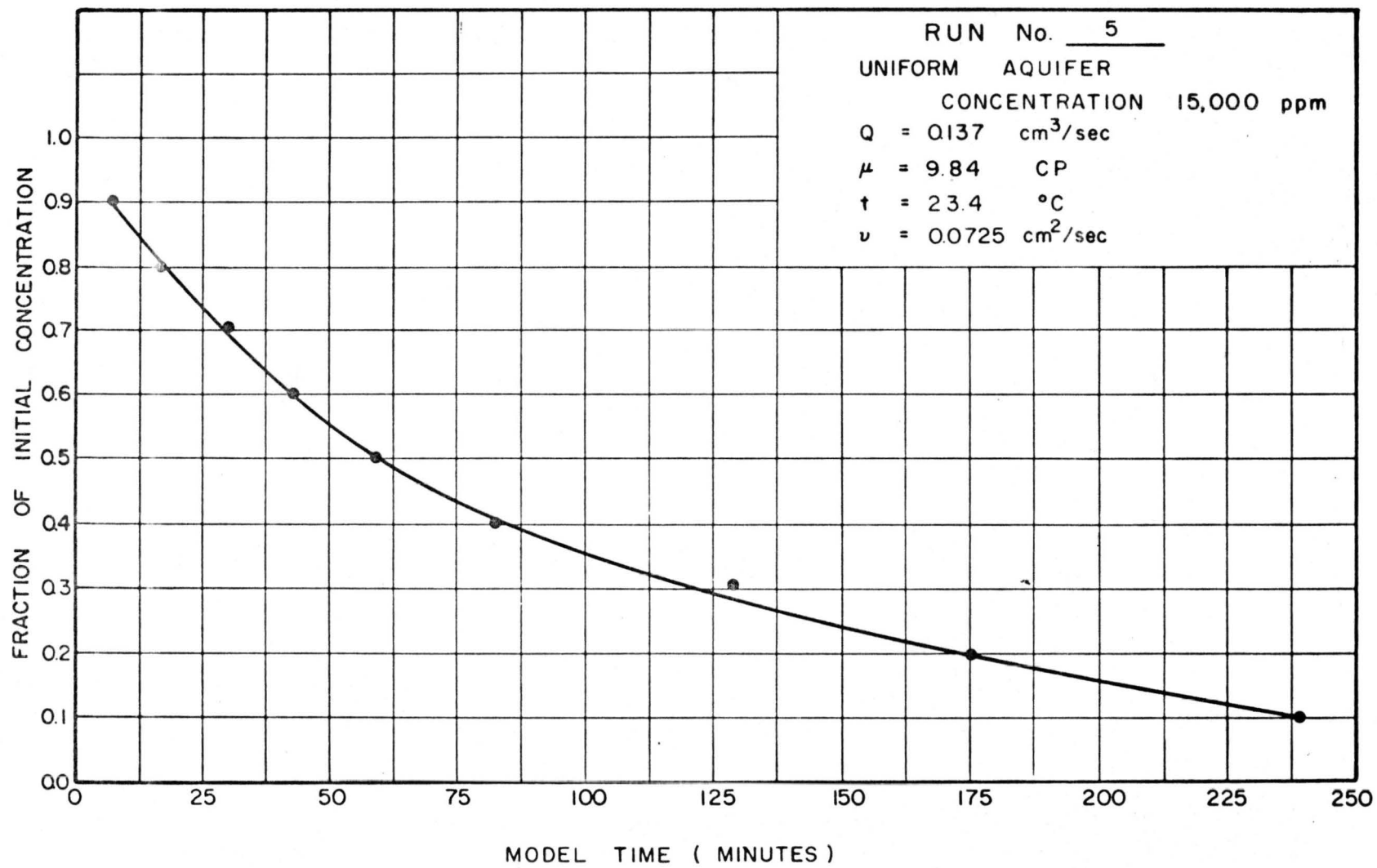


Fig. 23. Concentration versus time (Run 5, initial concentration 15,000 ppm, uniform aquifer).

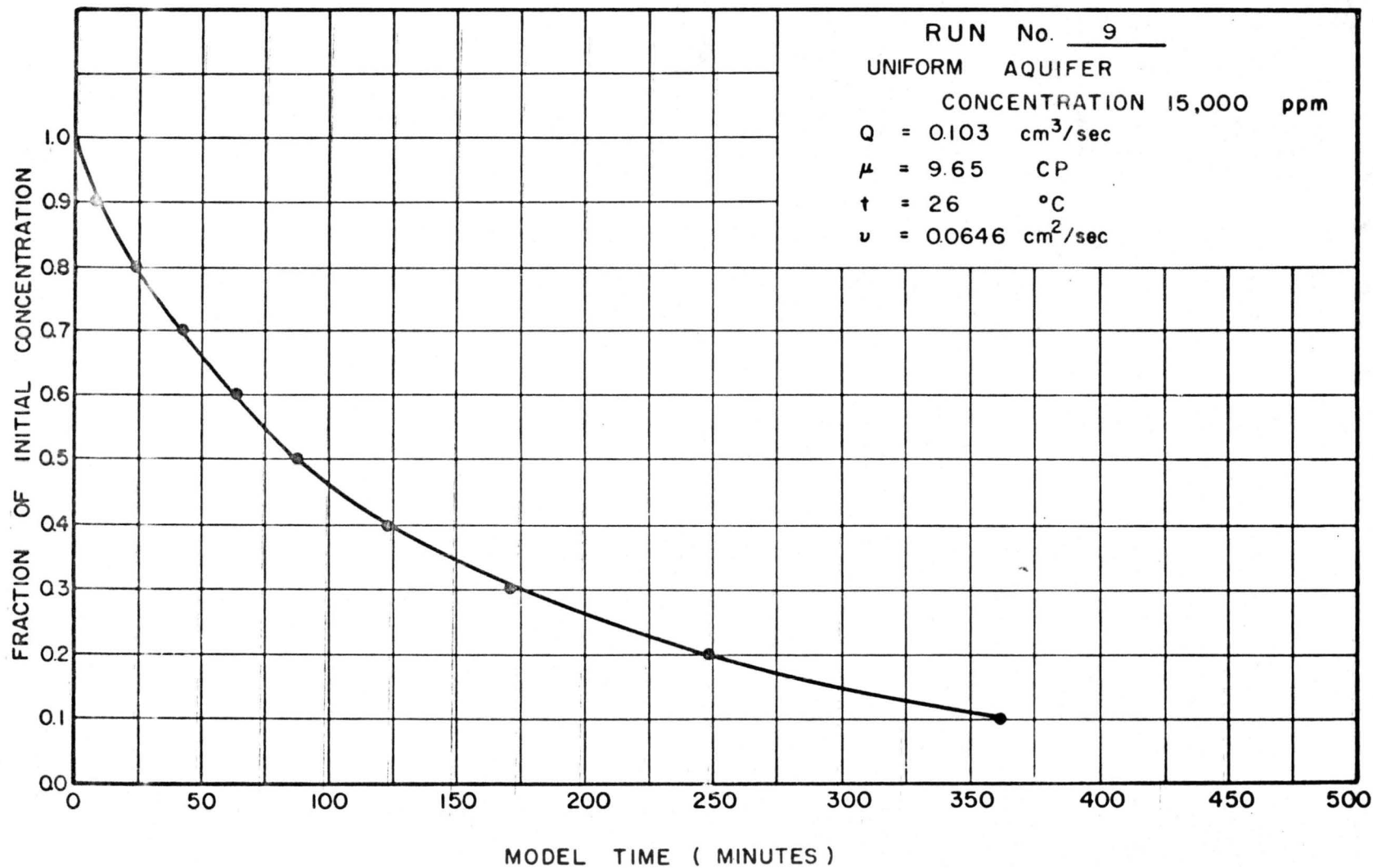


Fig. 24. Concentration versus time (Run 9, initial concentration 15,000 ppm, uniform aquifer).

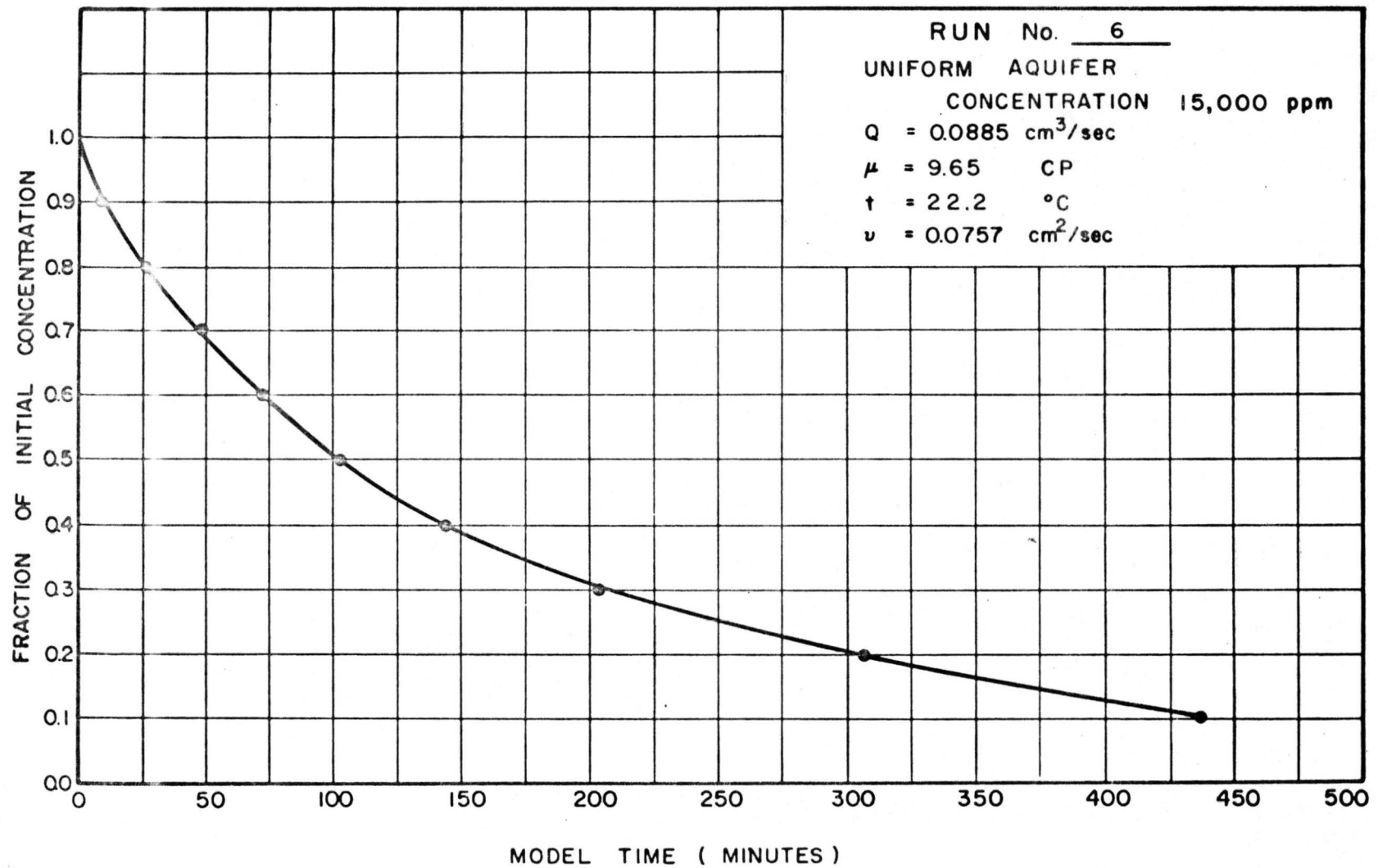


Fig. 25. Concentration versus time (Run 6, initial concentration 15,000 ppm, uniform aquifer).

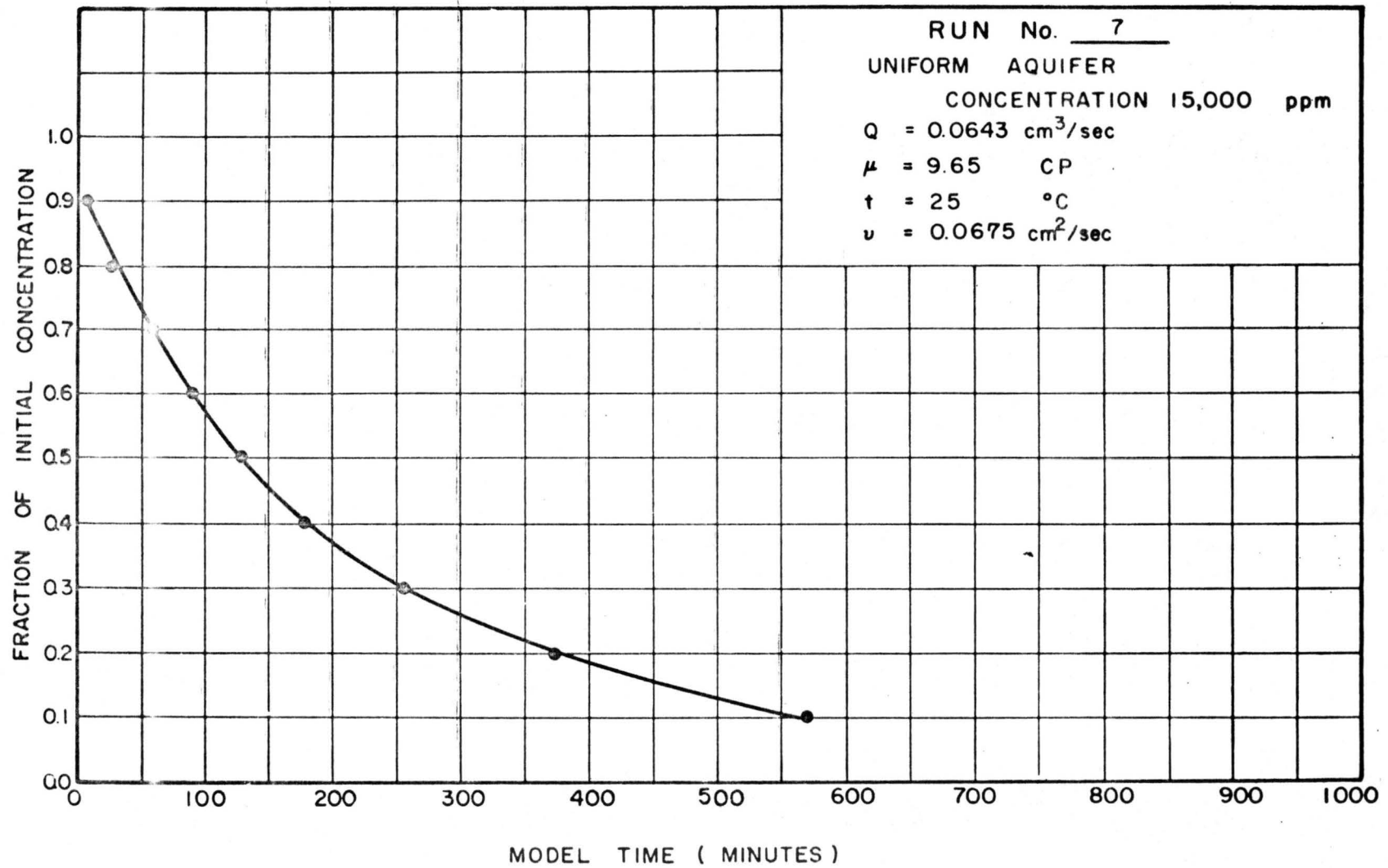


Fig. 26. Concentration versus time (Run 7, initial concentration 15,000 ppm, uniform aquifer).

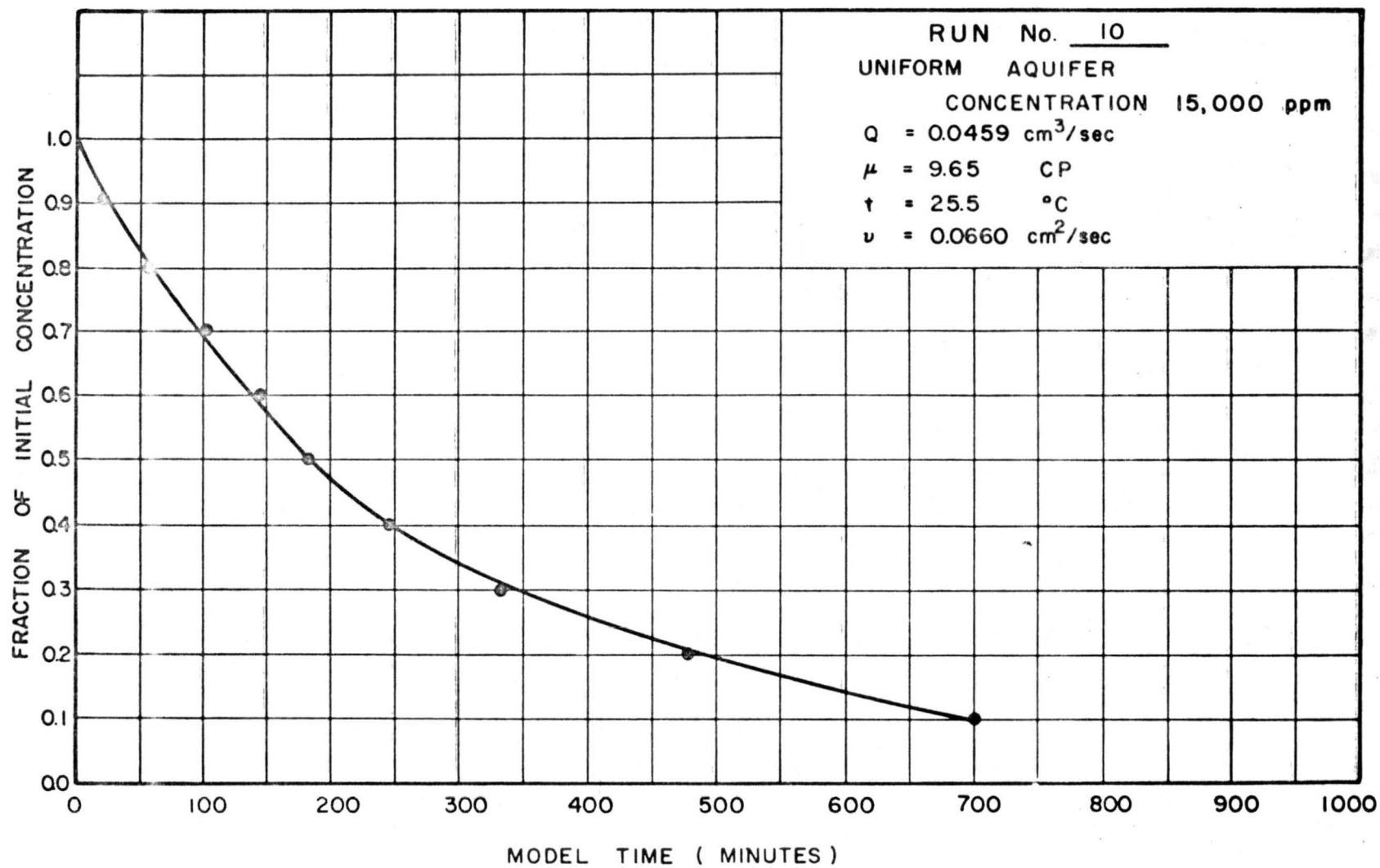


Fig. 27. Concentration versus time (Run 10, initial concentration 15,000 ppm, uniform aquifer).

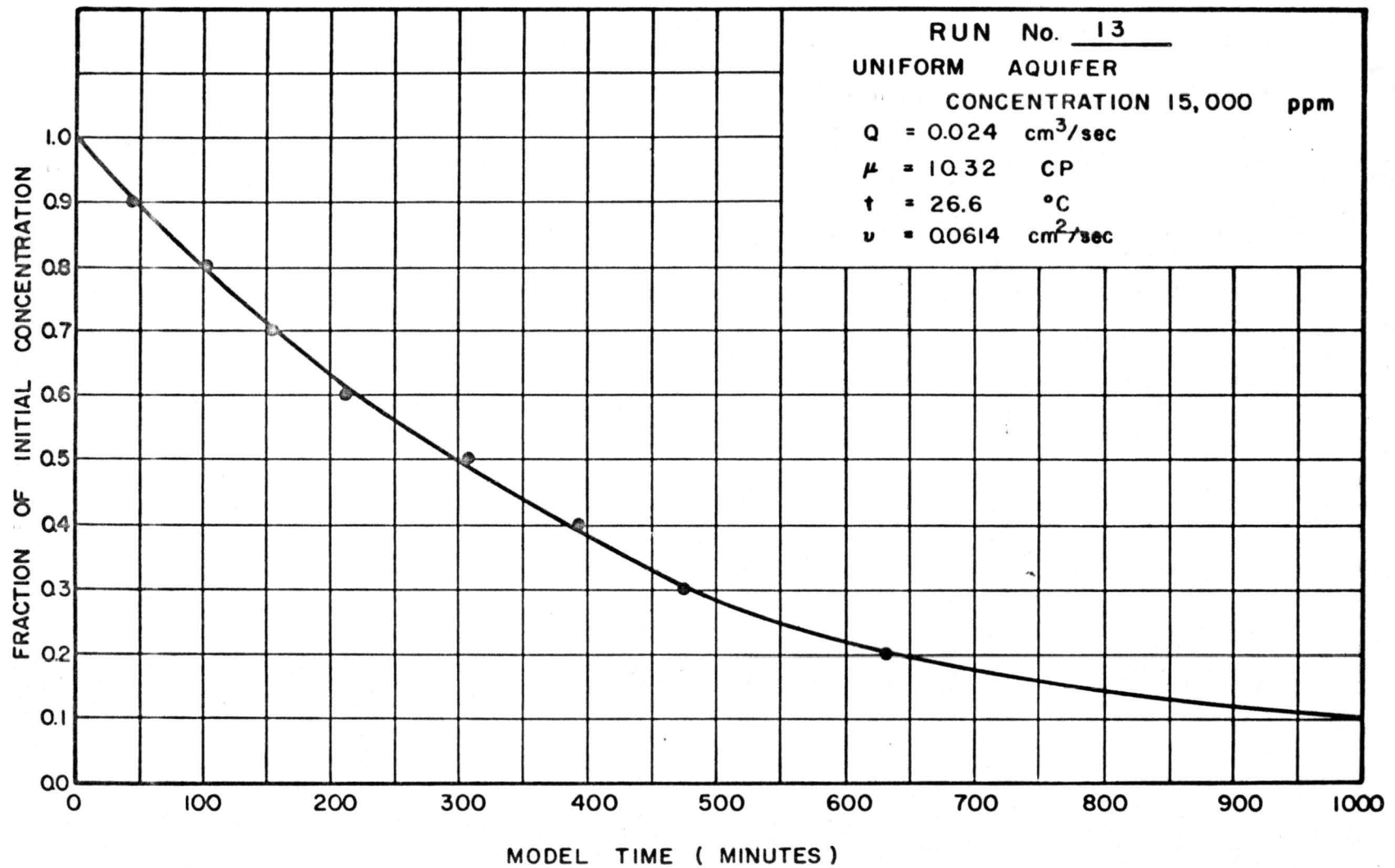


Fig. 23. Concentration versus time (Run 13, initial concentration 15,000 ppm, uniform aquifer).

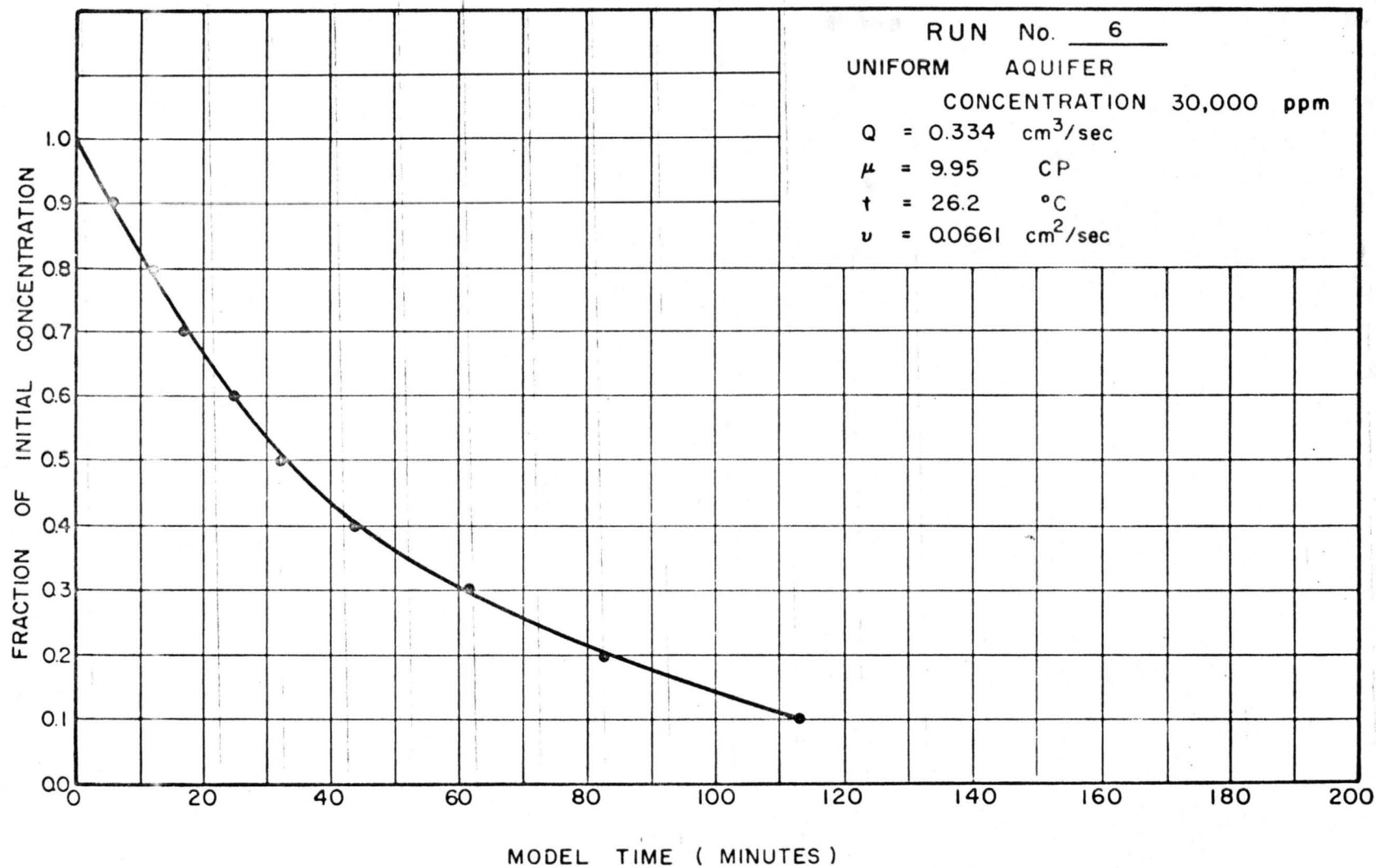


Figure 29. Concentration versus time (Run 6, initial concentration 30,000 ppm, uniform aquifer).

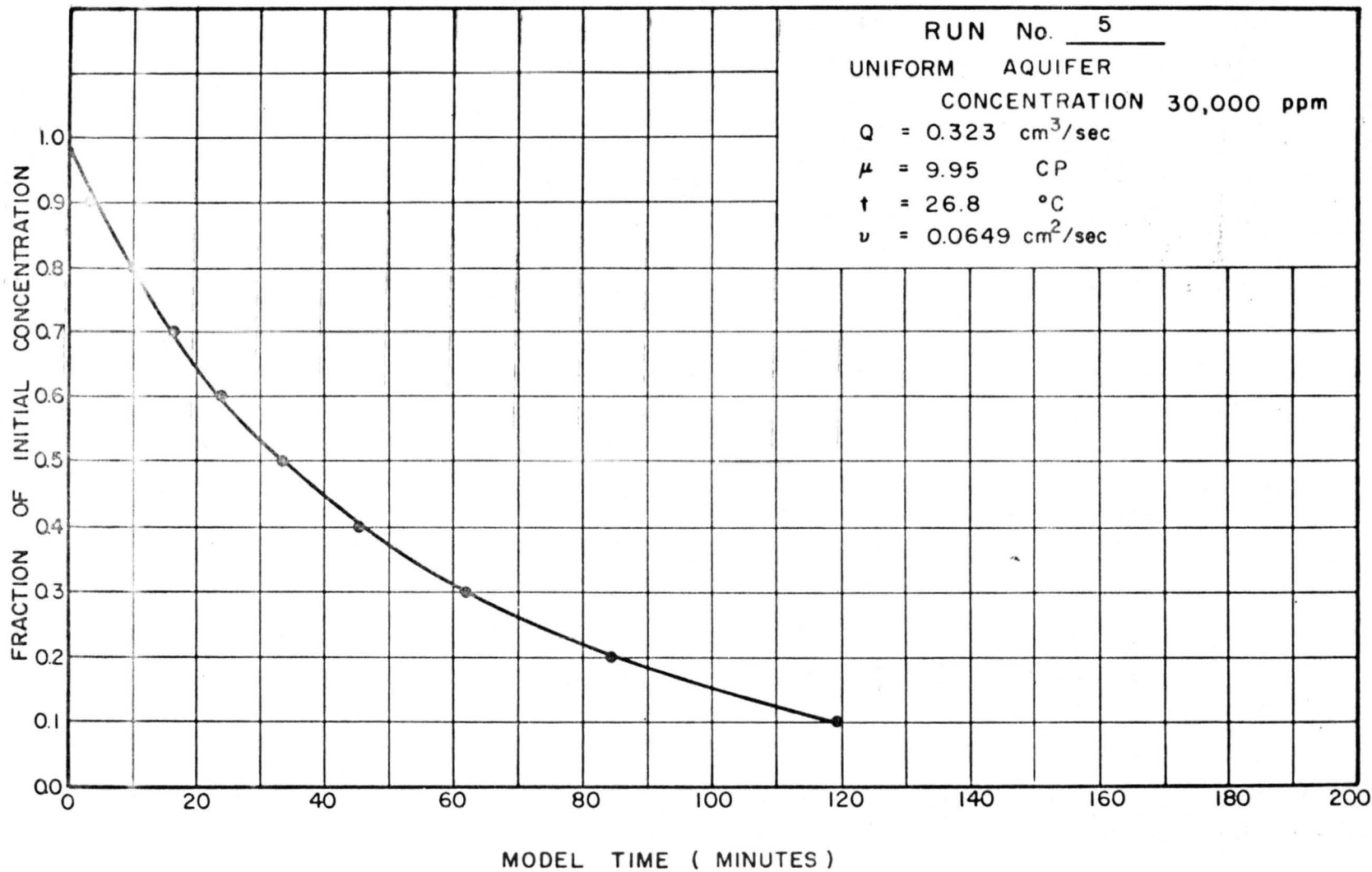


Fig. 30. Concentration versus time (Run 5, initial concentration 30,000 ppm, uniform aquifer).

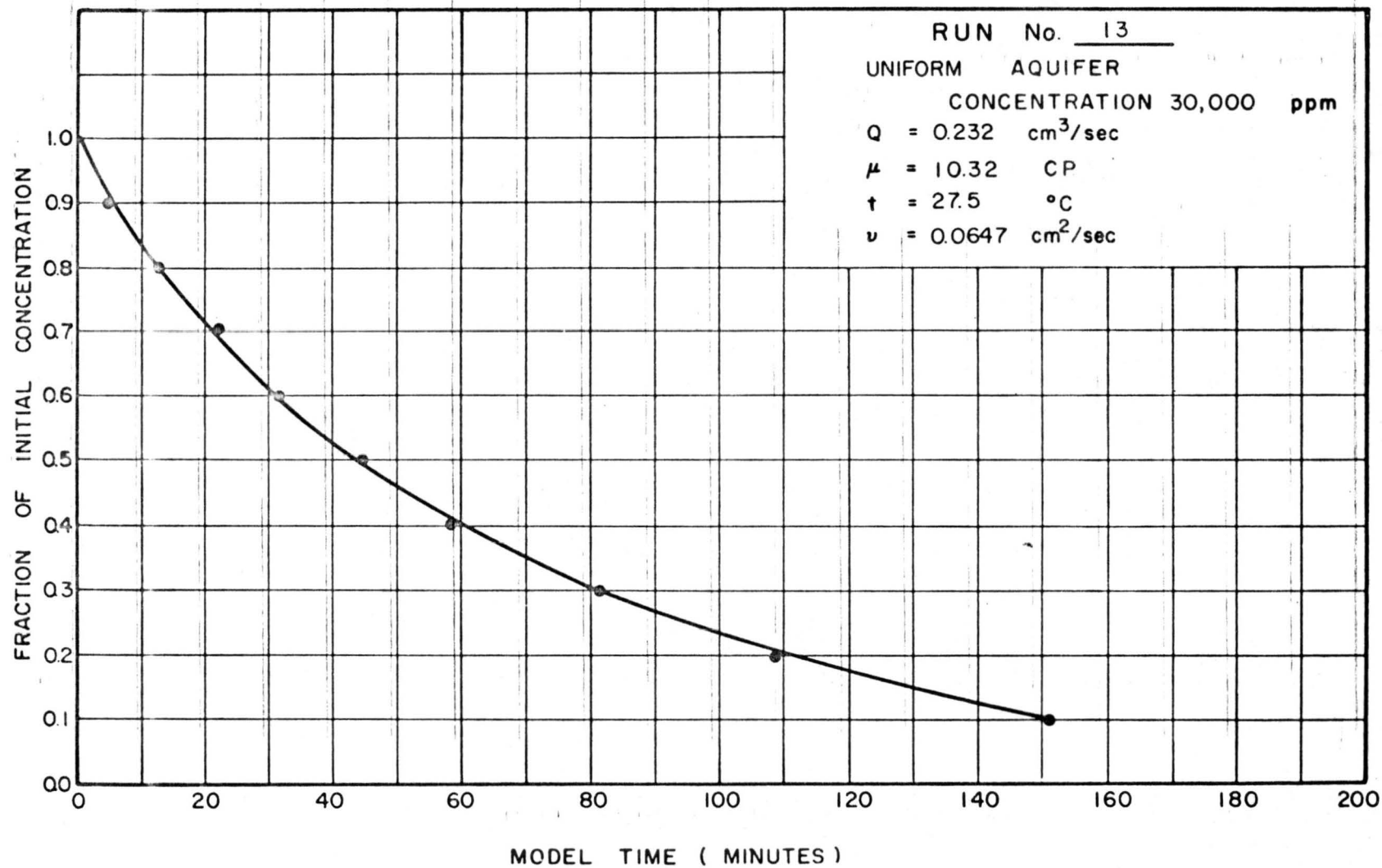


Fig. 31. Concentration versus time (Run 13, initial concentration 30,000 ppm, uniform aquifer).

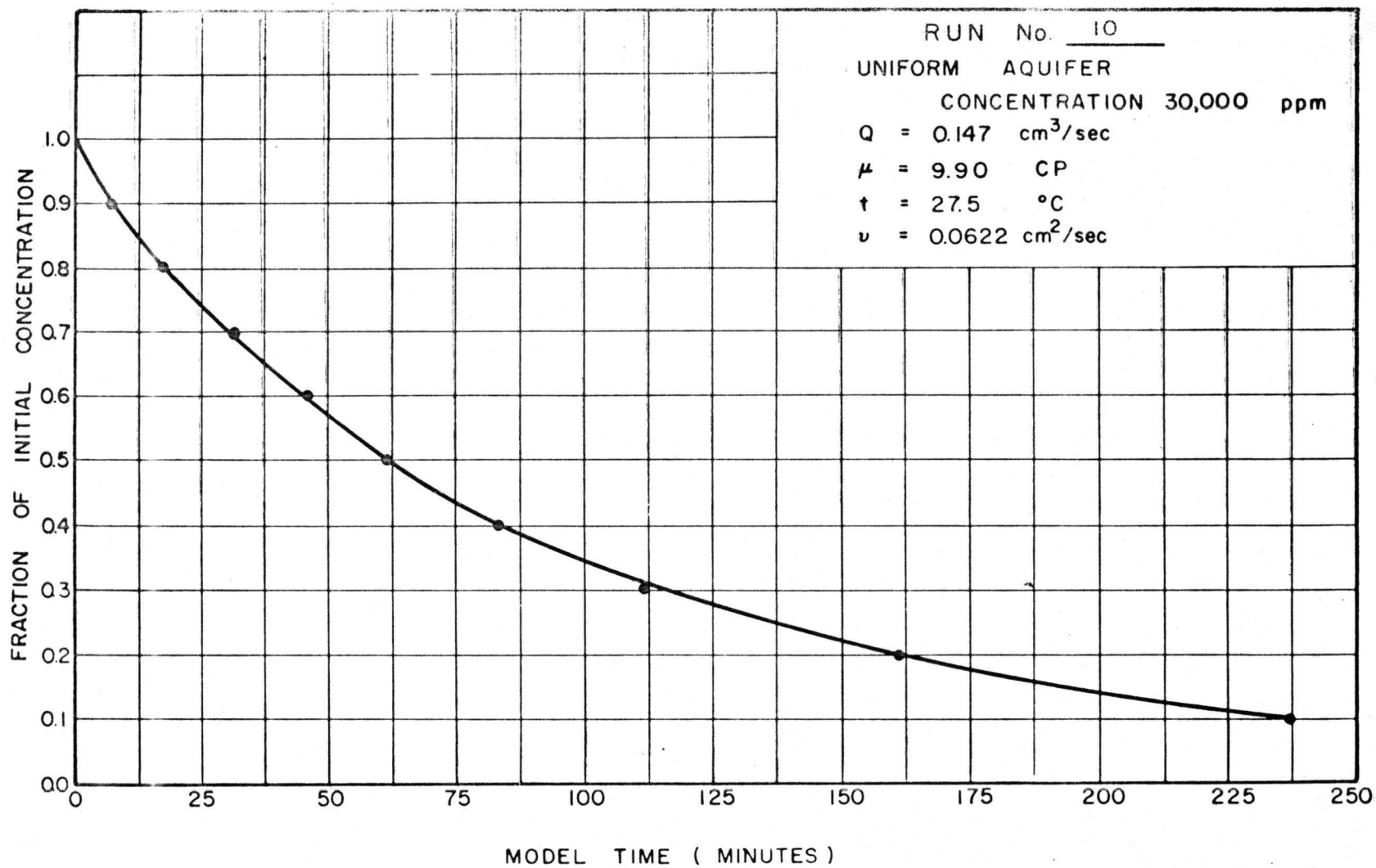


Fig. 32. Concentration versus time (Run 10, initial concentration 30,000 ppm, uniform aquifer).

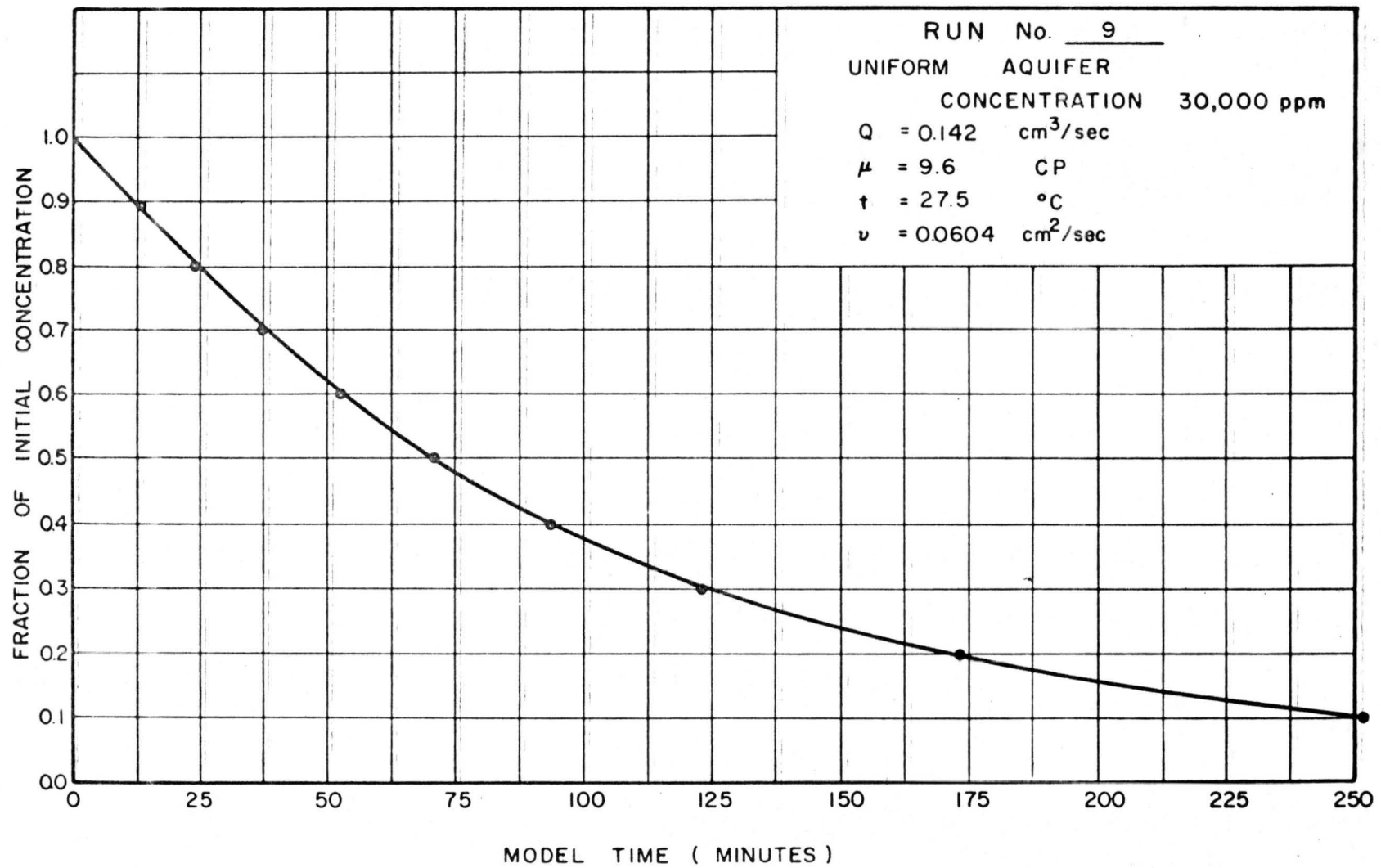


Fig. 33. Concentration versus time (Run 9, initial concentration 30,000 ppm, uniform aquifer.)

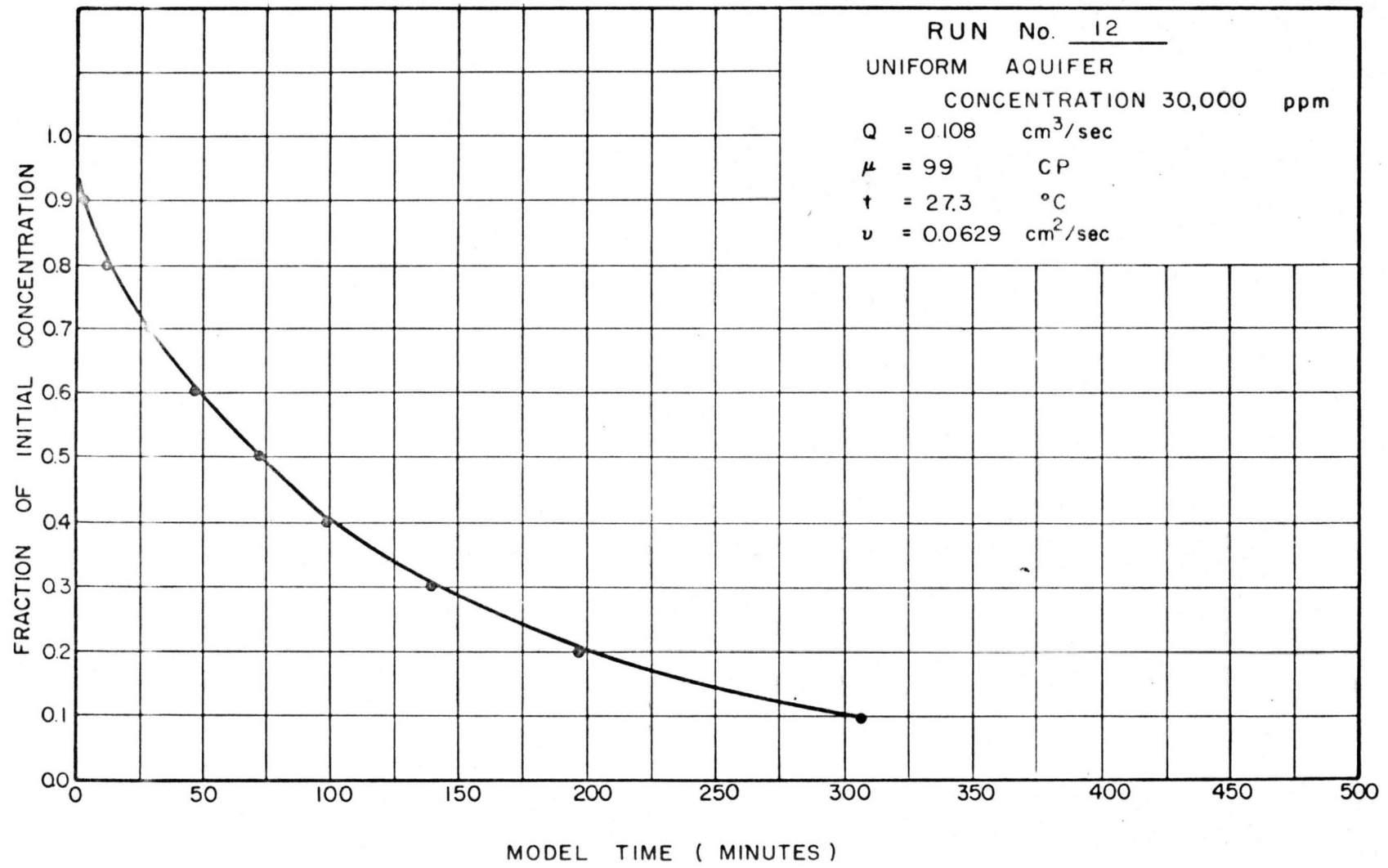


Fig. 34. Concentration versus time (Run 12, initial concentration 30,000 ppm, uniform aquifer).

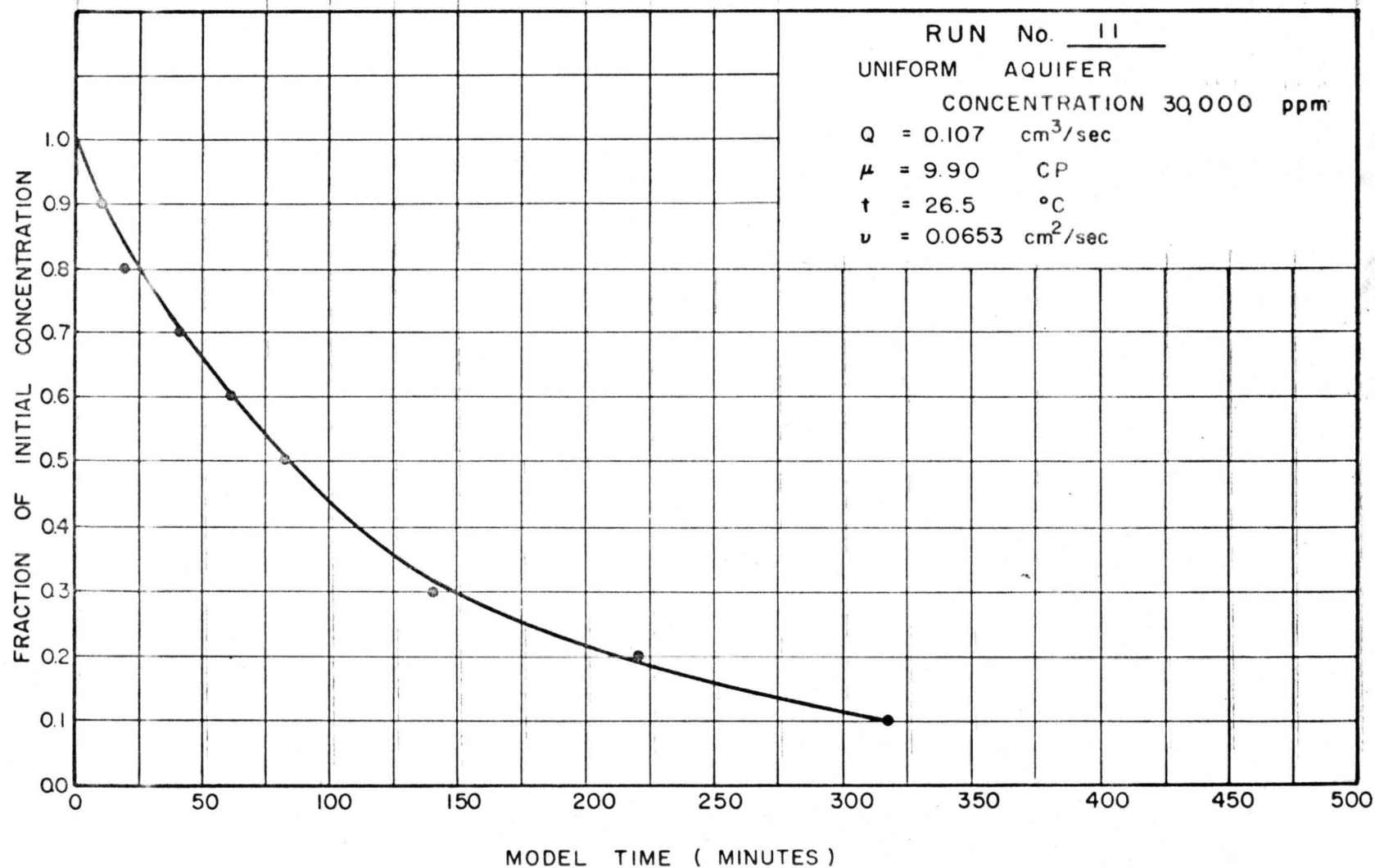


Fig. 35. Concentration versus time (Run 11, initial concentration 30,000 ppm, uniform aquifer).

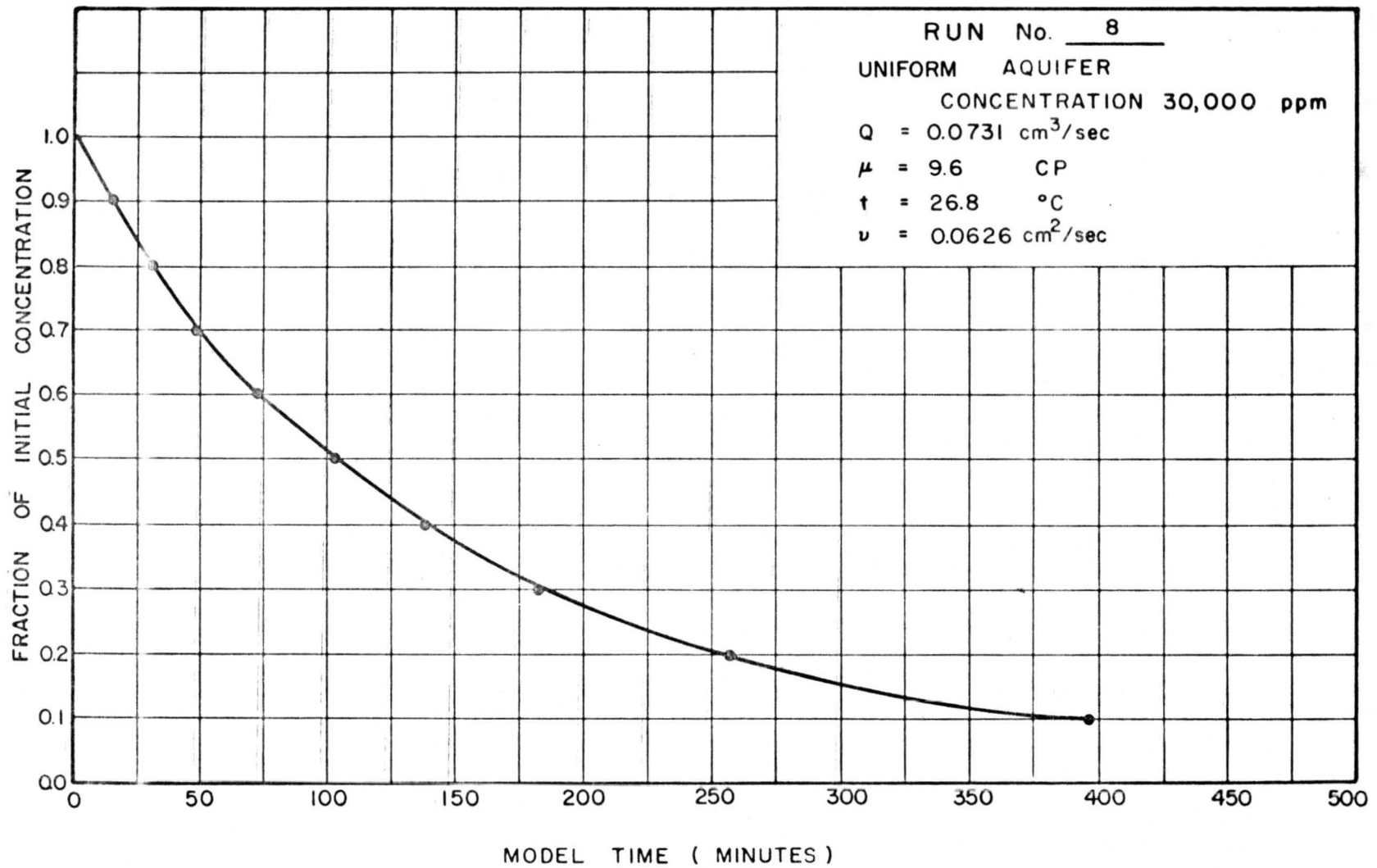


Fig. 36. Concentration versus time (Run 3, initial concentration 30,000 ppm, uniform aquifer).

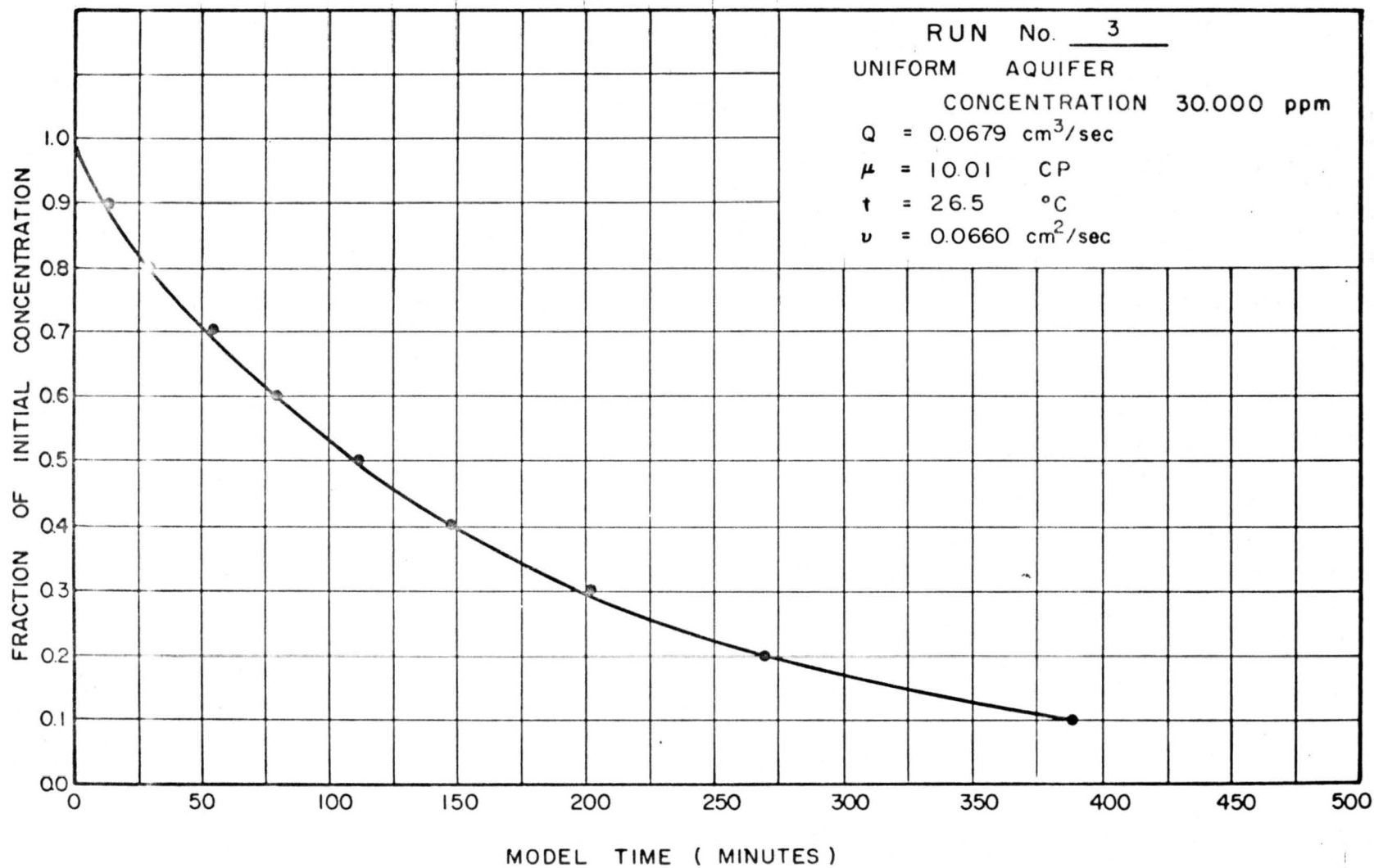


Fig. 37. Concentration versus time (Run 3, initial concentration 30,000 ppm, uniform aquifer).

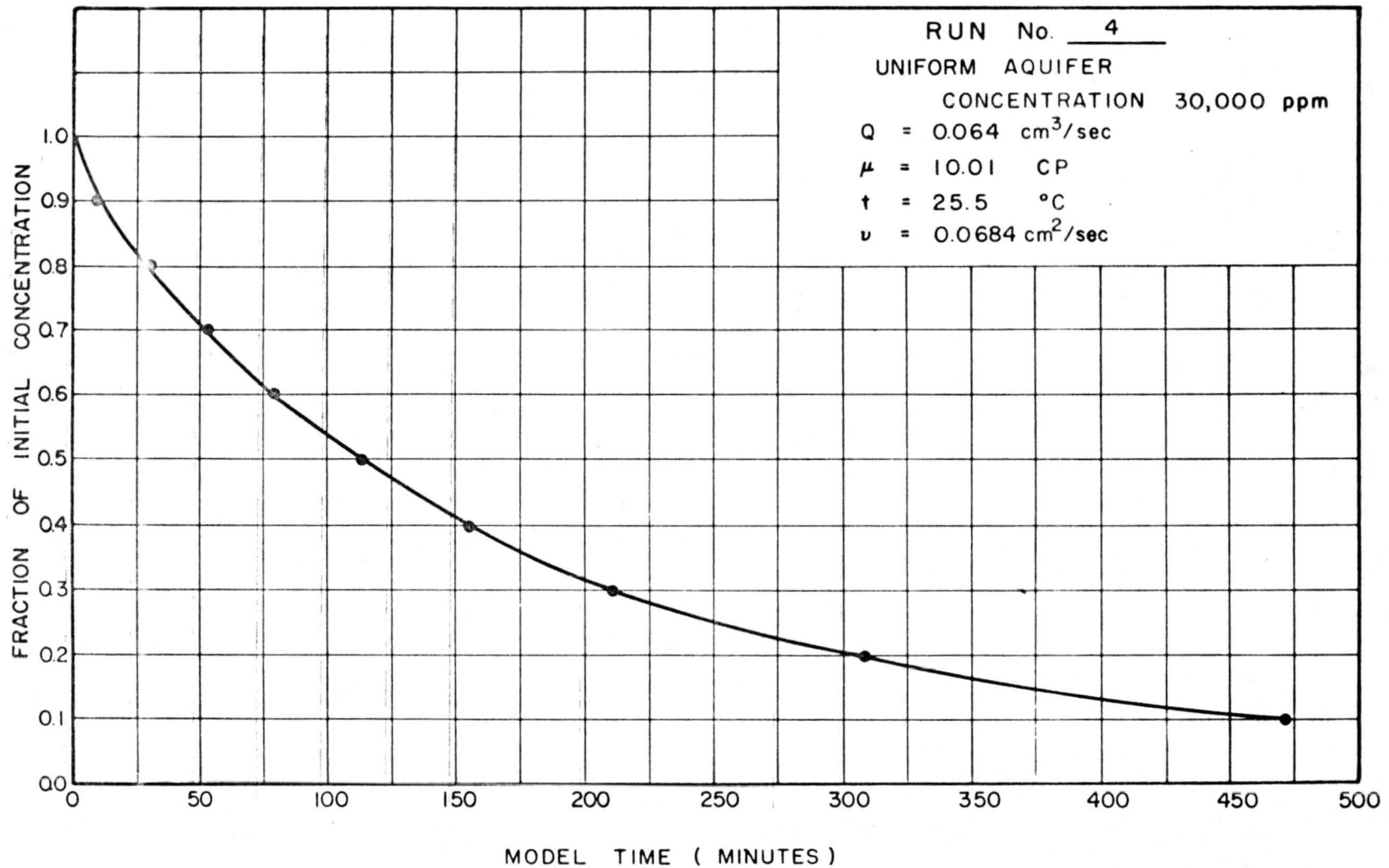


Fig. 33. Concentration versus time (Run 4, initial concentration 30,000 ppm, uniform aquifer).

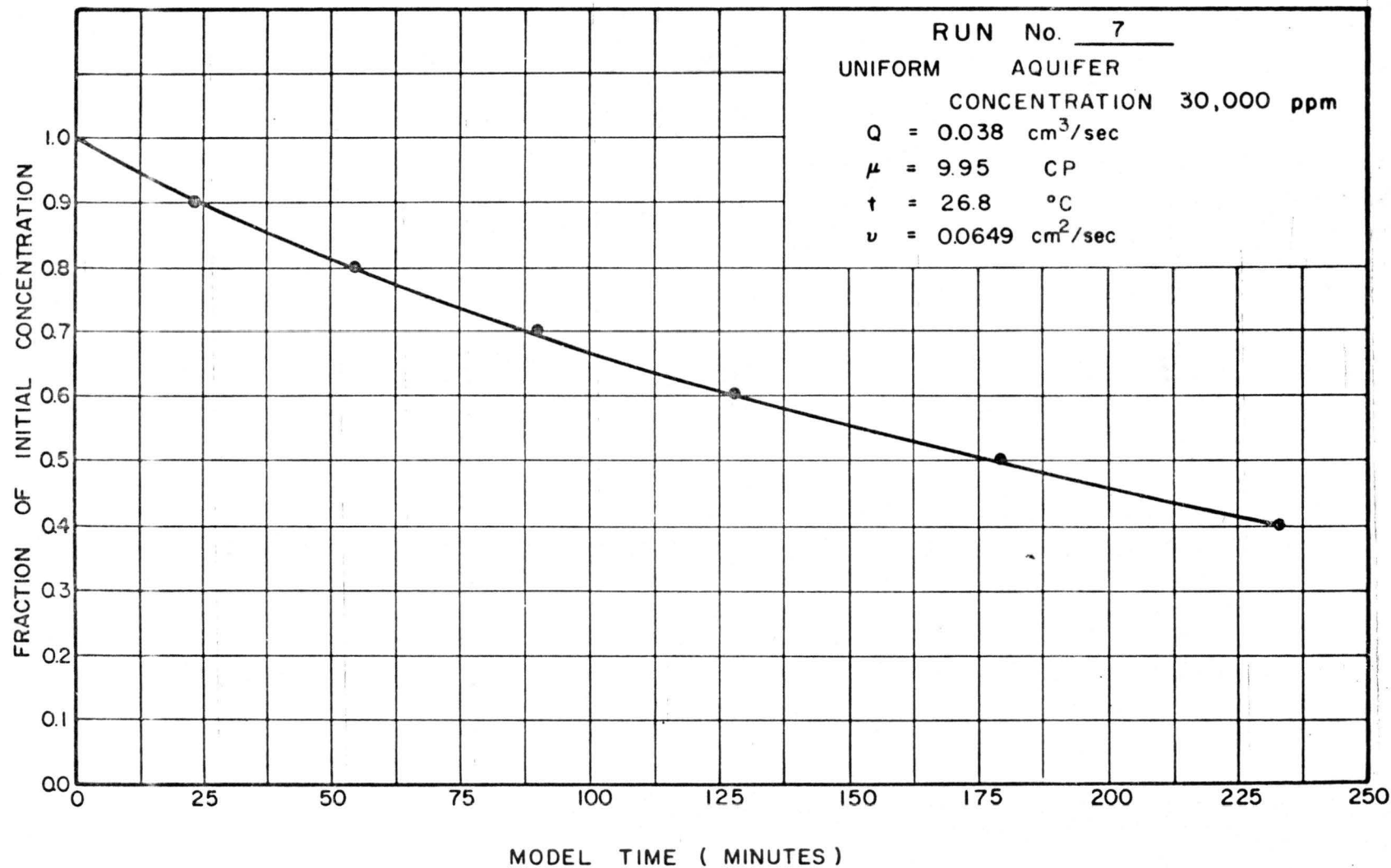


Fig. 39. Concentration versus time (Run 7, initial concentration 30,000 ppm, uniform aquifer).

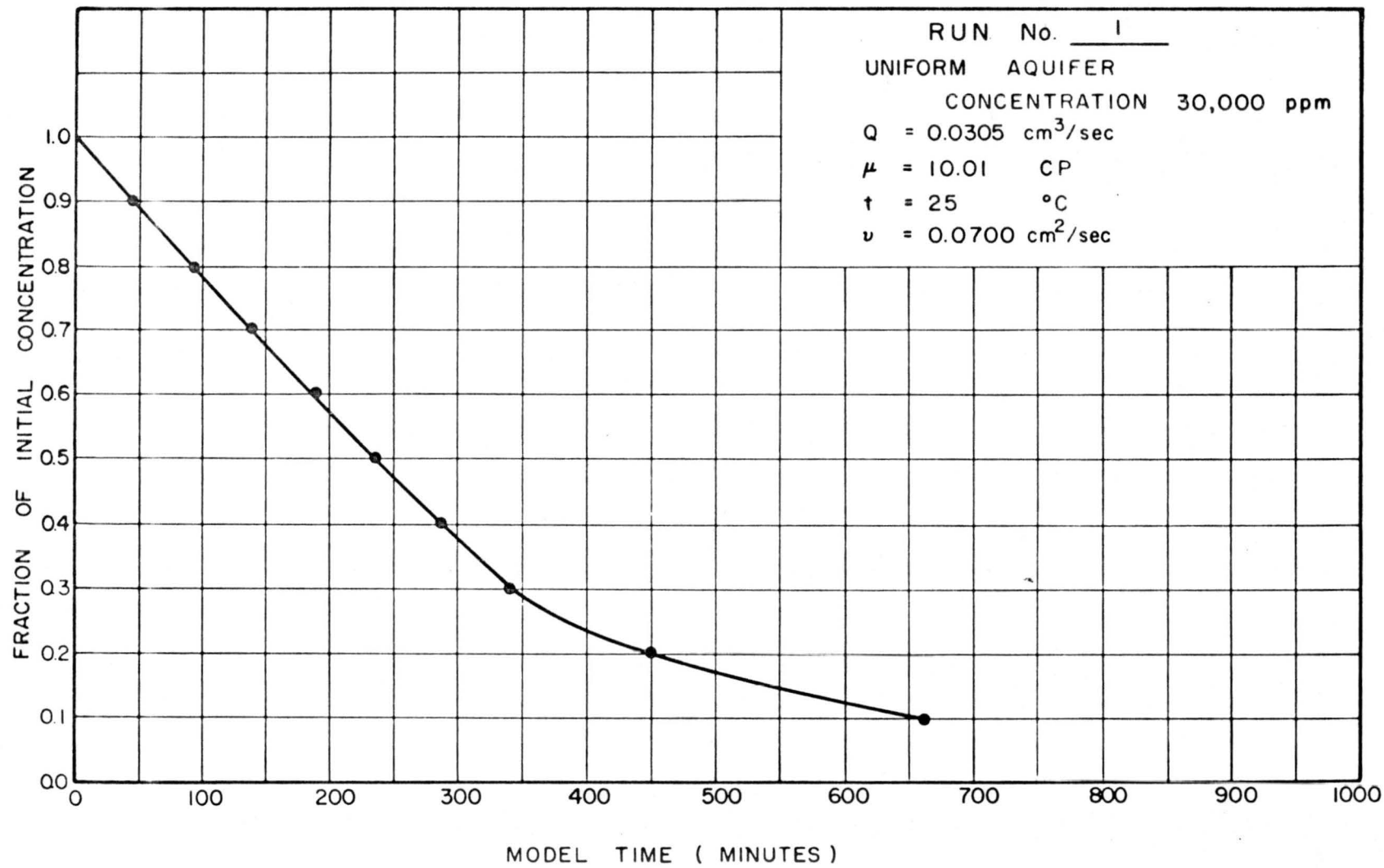


Fig. 40. Concentration versus time (Run 1, initial concentration 30,000 ppm, uniform aquifer).

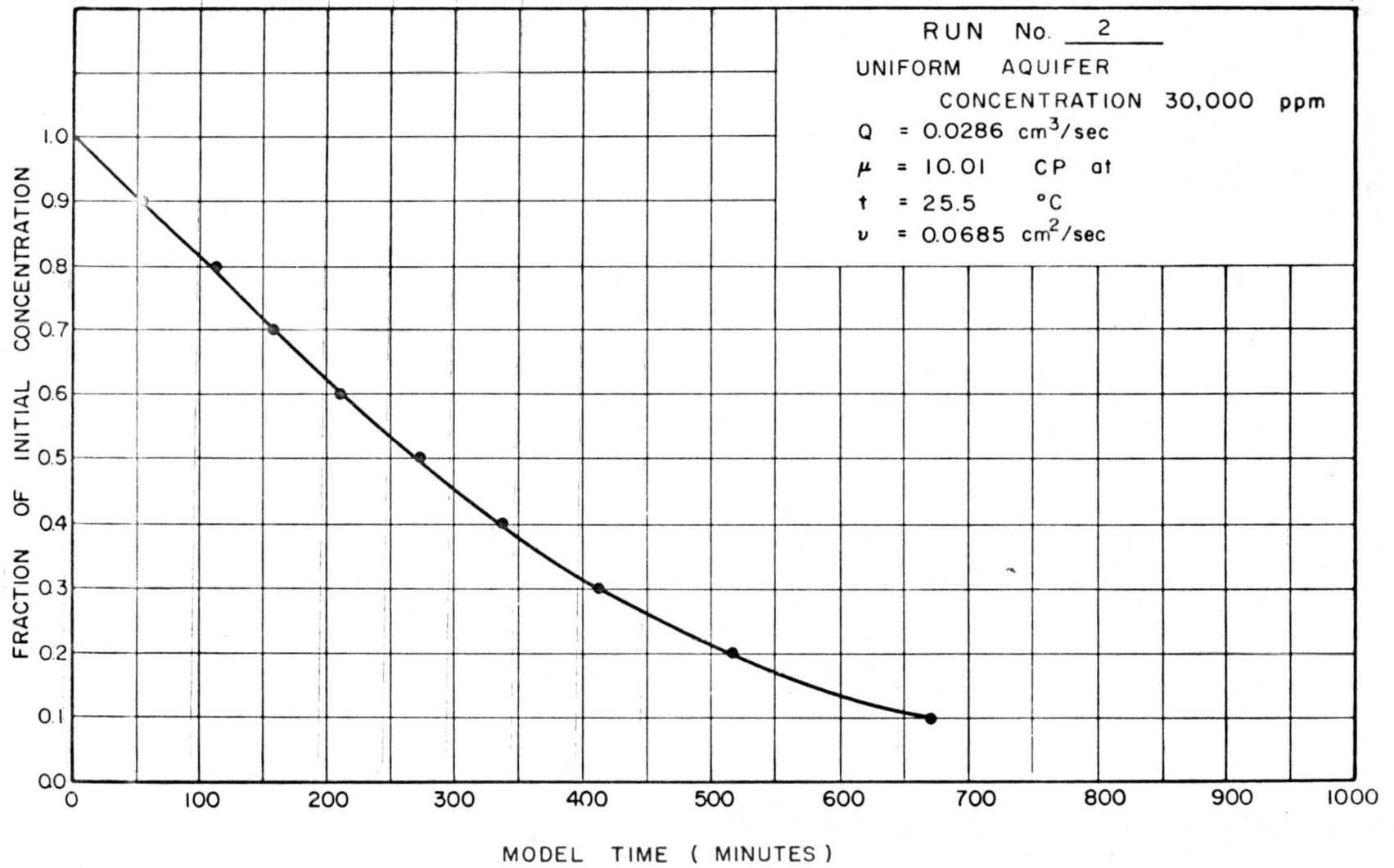


Fig. 41. Concentration versus time (Run 2, initial concentration 30,000 ppm, uniform aquifer).

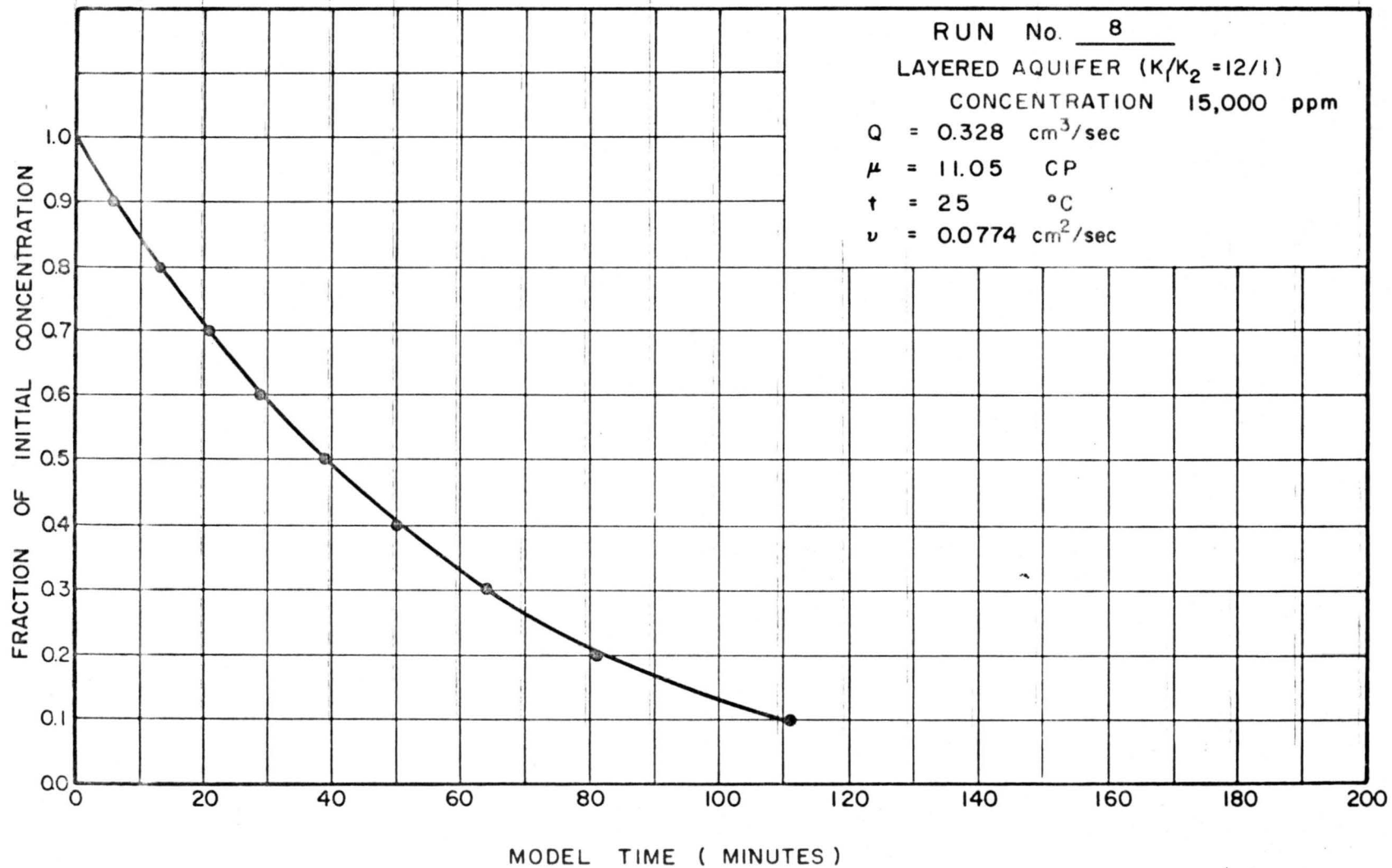


Fig. 42. Concentration versus time (Run 3, initial concentration 15,000 ppm, layered aquifer,  $K_1/K_2 = 12/1$ ).

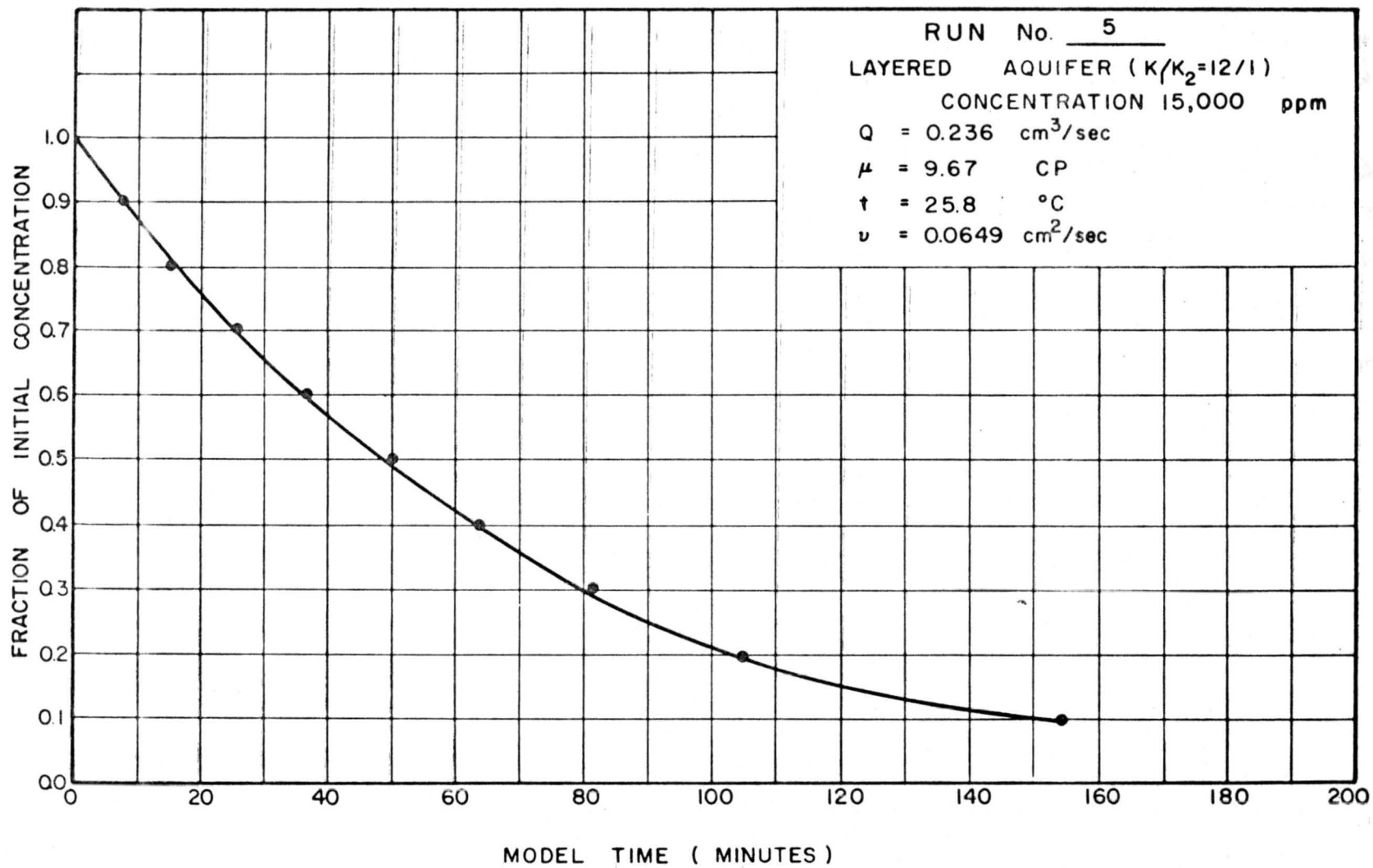


Fig. 43. Concentration versus time (Run 5, initial concentration 15,000 ppm, layered aquifer,  $K_1/K_2 = 12/1$ ).

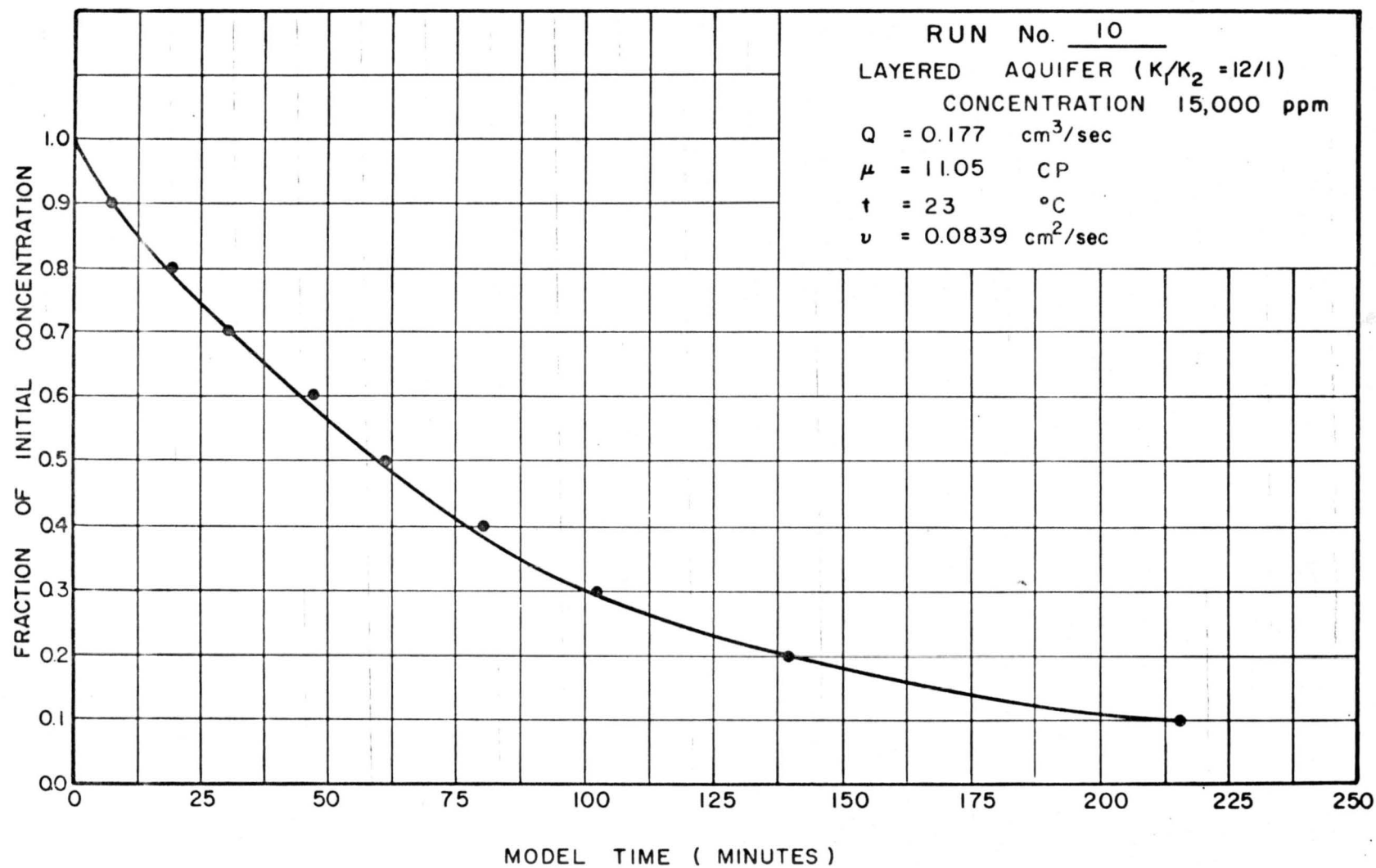


Fig. 44. Concentration versus time (Run 10, initial concentration 15,000 ppm, layered aquifer,  $K_1/K_2 = 12/1$ ).

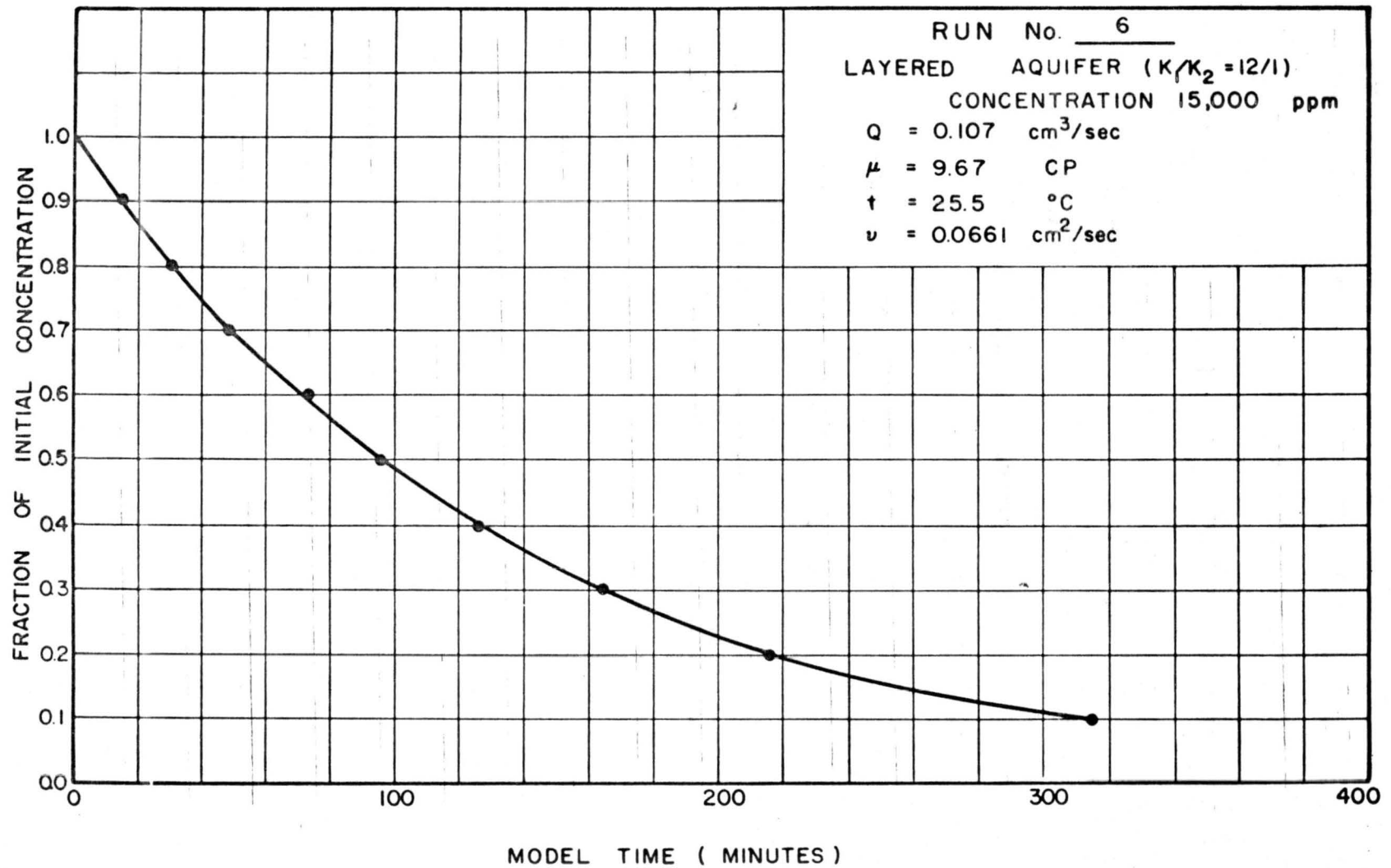


Fig. 45. Concentration versus time (Run 6, initial concentration 15, 000 ppm; layered aquifer,  $K_1/K_2 = 12/1$ ).

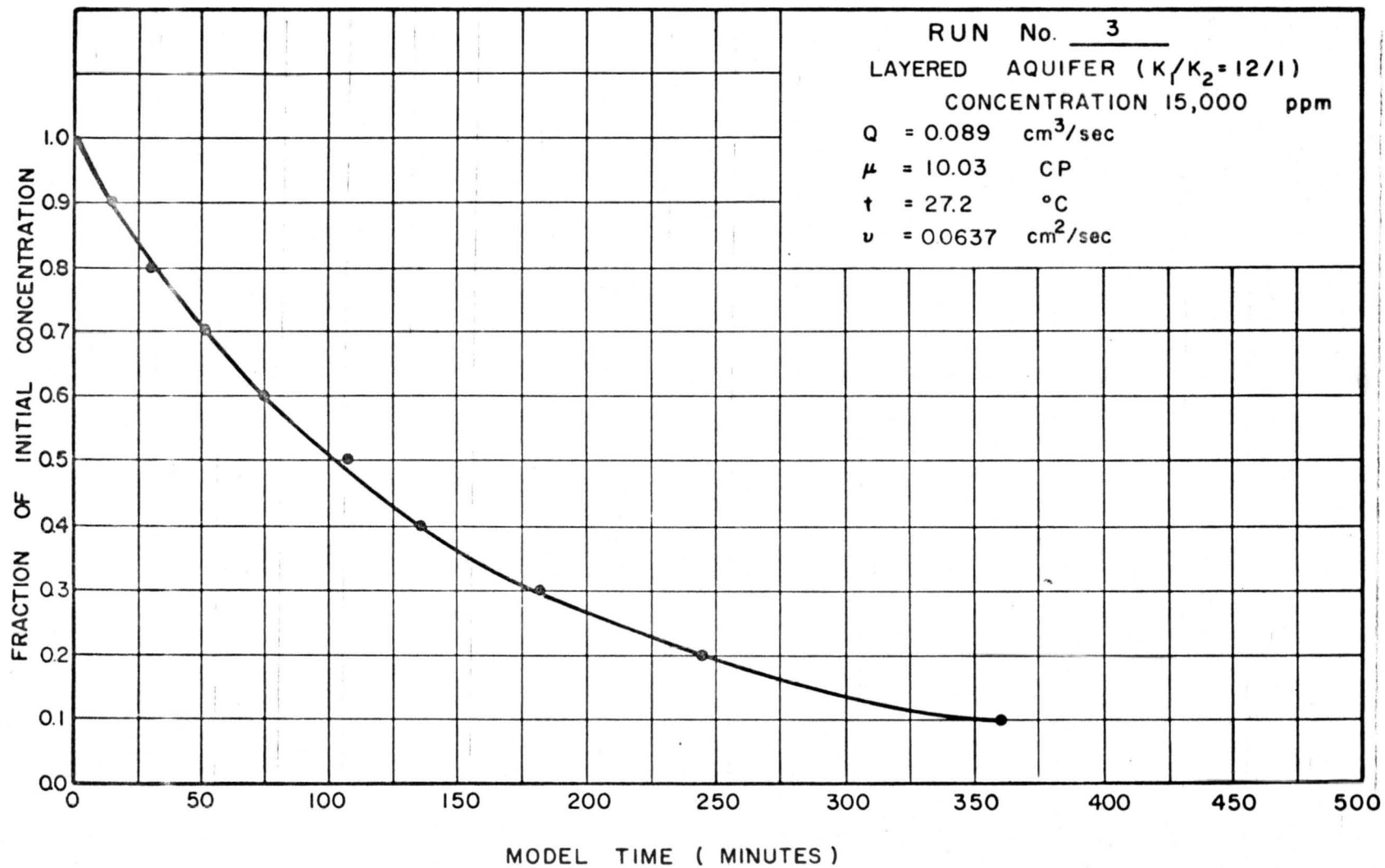


Fig. 46. Concentration versus time (Run 3, initial concentration 15,000 ppm, layered aquifer,  $K_1/K_2 = 12/1$ ).

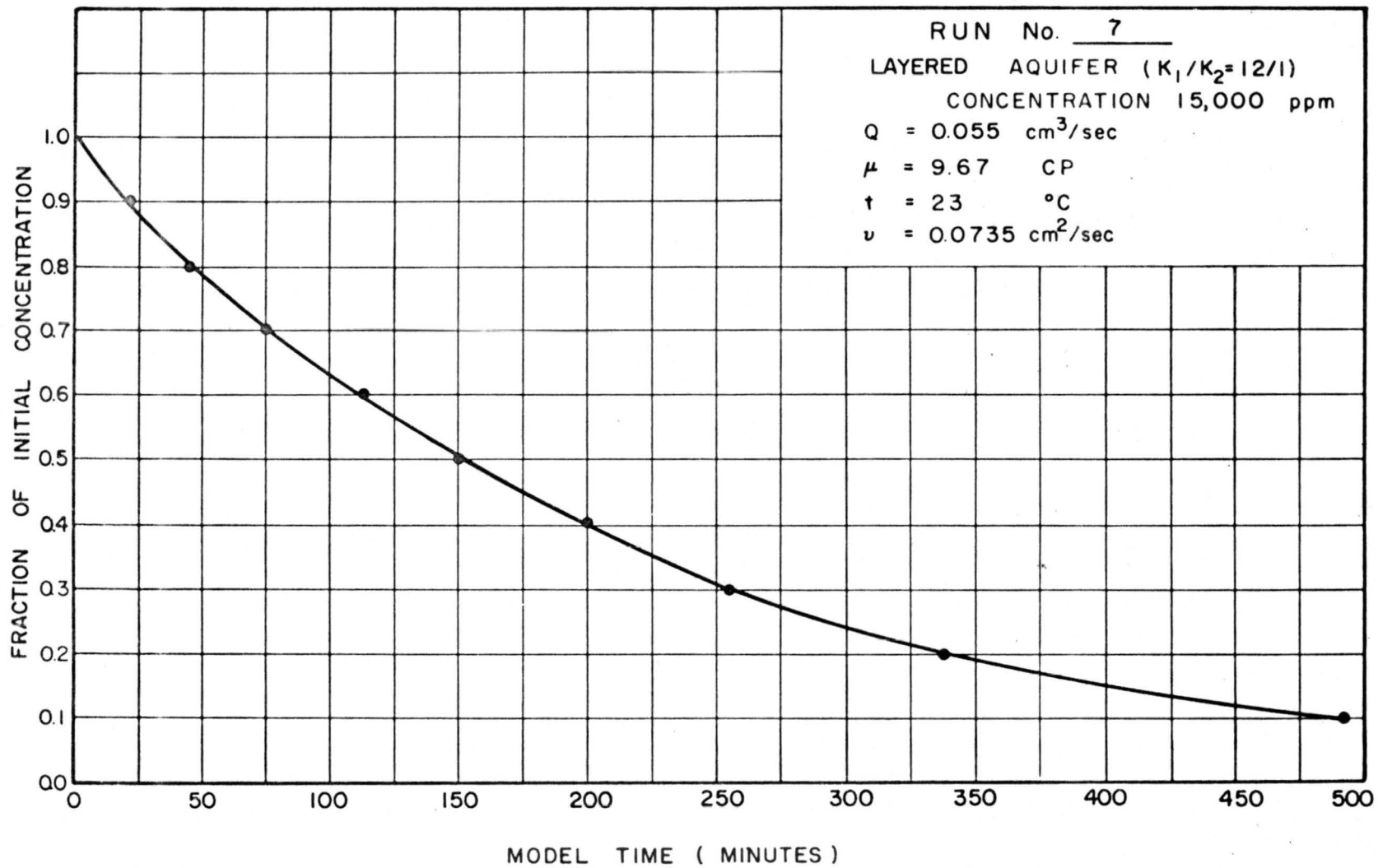


Fig. 47. Concentration versus time (Run 7, initial concentration 15,000 ppm, layered aquifer,  $K_1/K_2 = 12/1$ ).

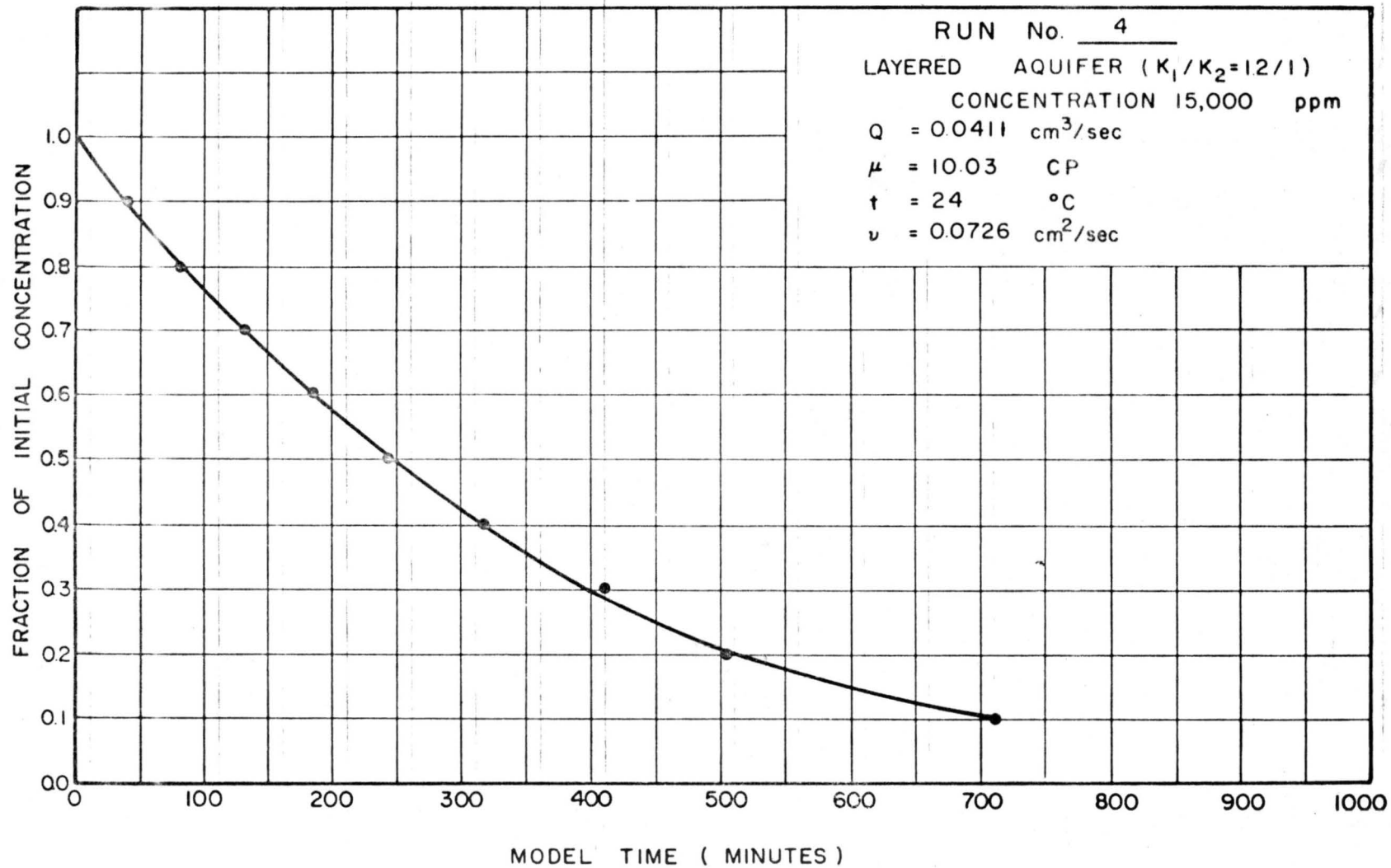


Fig. 48. Concentration versus time (Run 4, initial concentration 15,000 ppm, layered aquifer,  $K_1/K_2 = 12/1$ ).

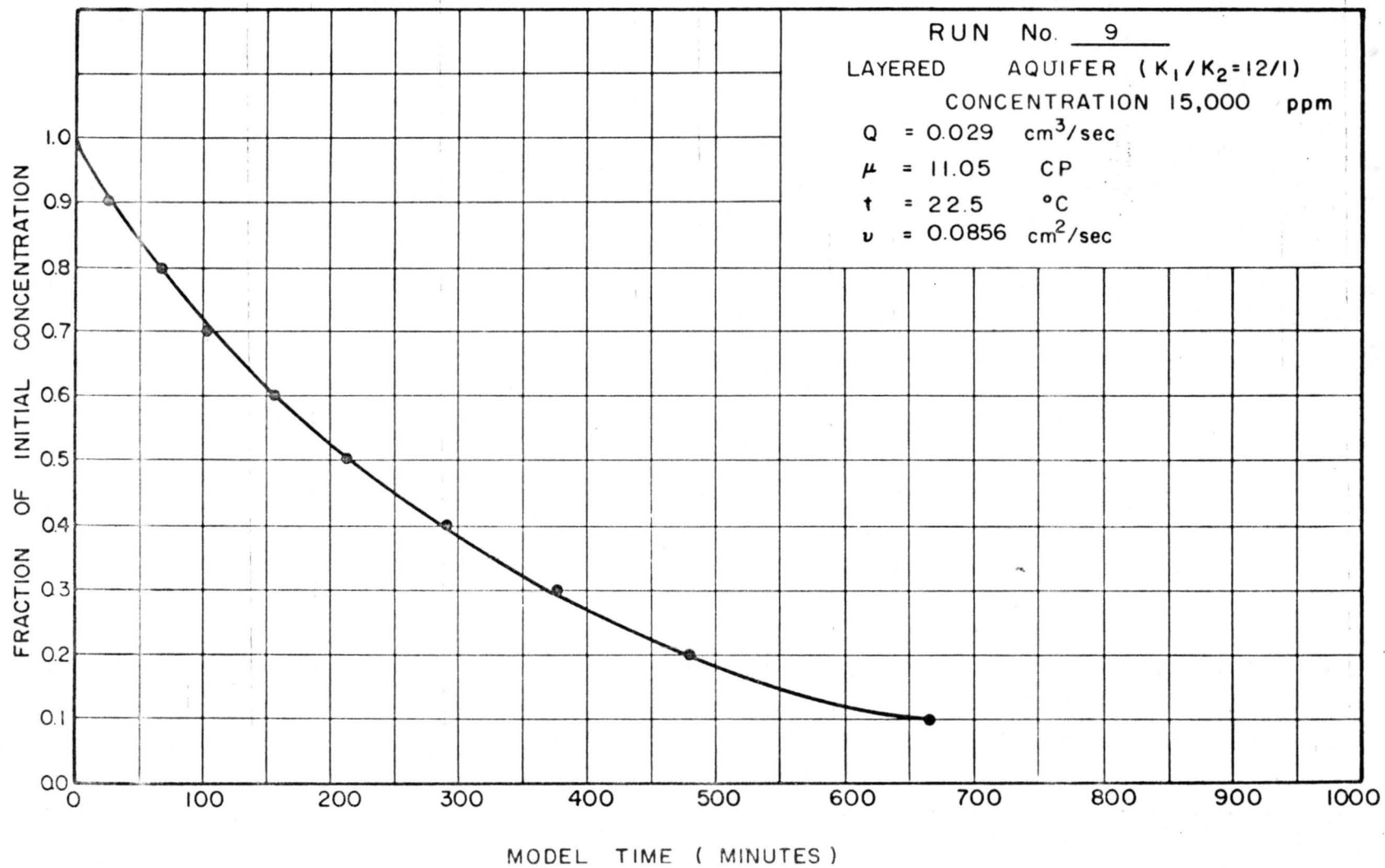


Fig. 49. Concentrated versus time (Run 9, initial concentration 15,000 ppm, layered aquifer,  $K_1/K_2 = 12/1$ ).

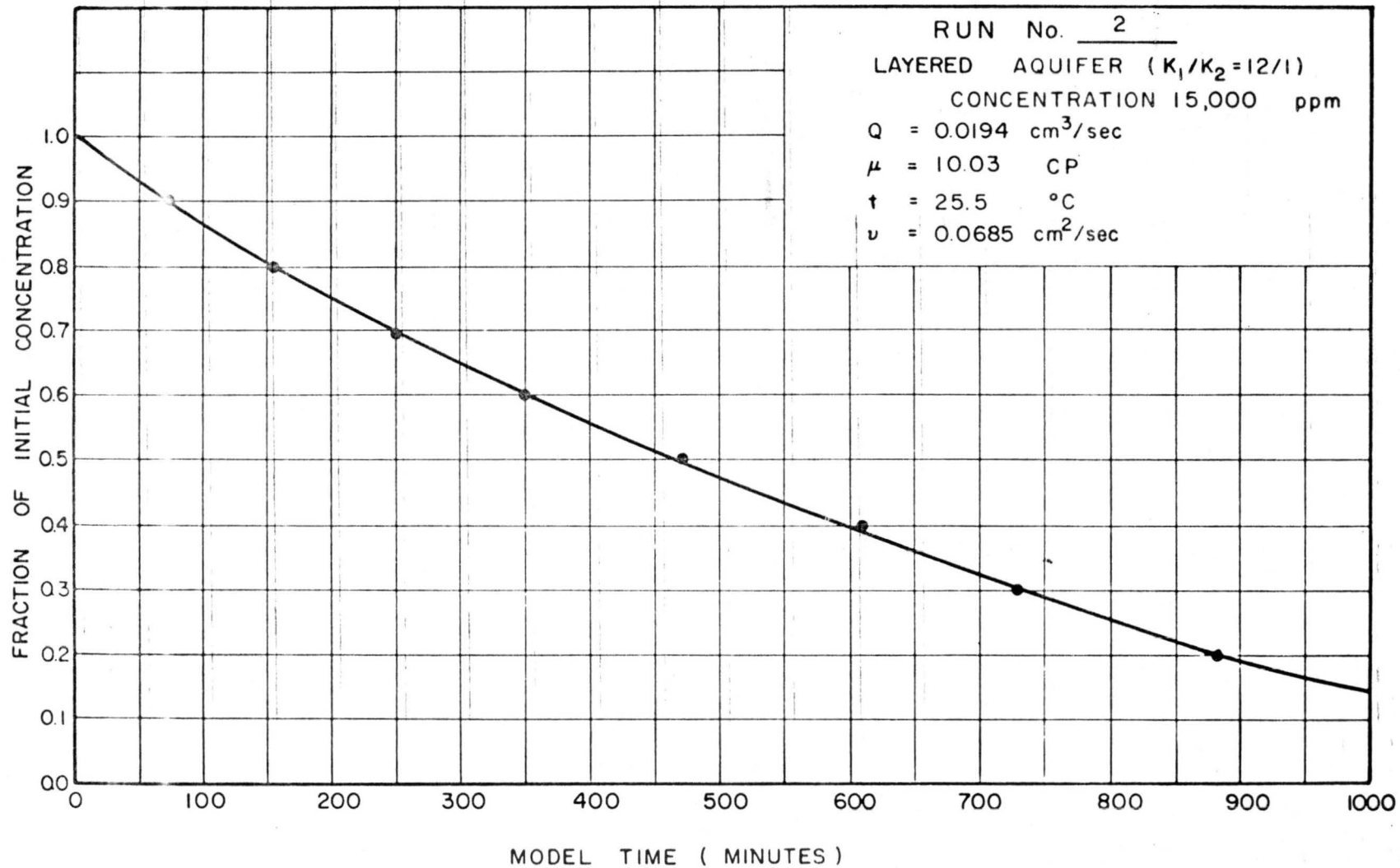


Fig. 50. Concentration versus time (Run 2, initial concentration 15,000 ppm, layered aquifer,  $K_1/K_2 = 12/1$ ).

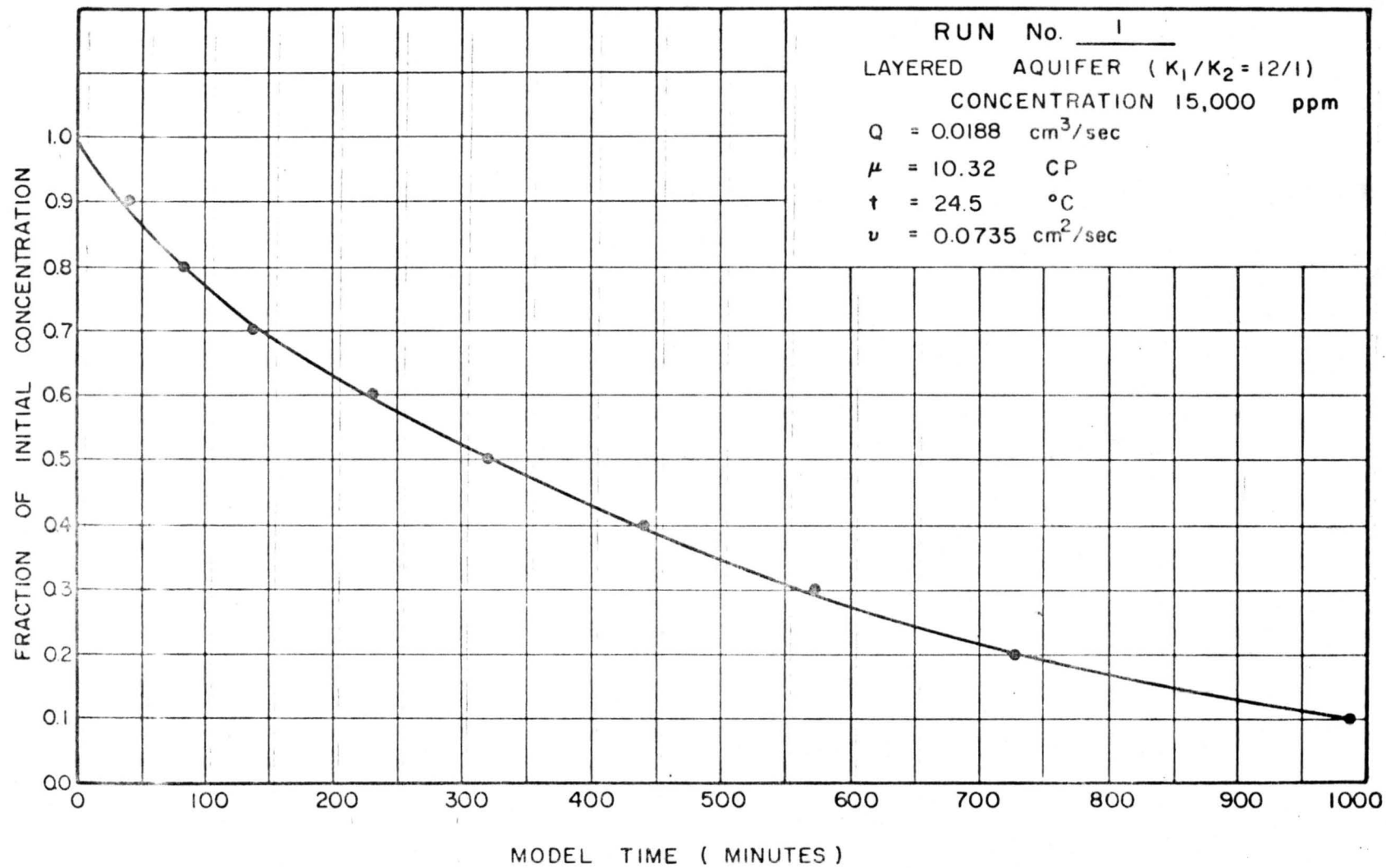


Fig. 51. Concentration versus time (Run 1, initial concentration 15,000 ppm, layered aquifer,  $K_1/K_2 = 12/1$ ).

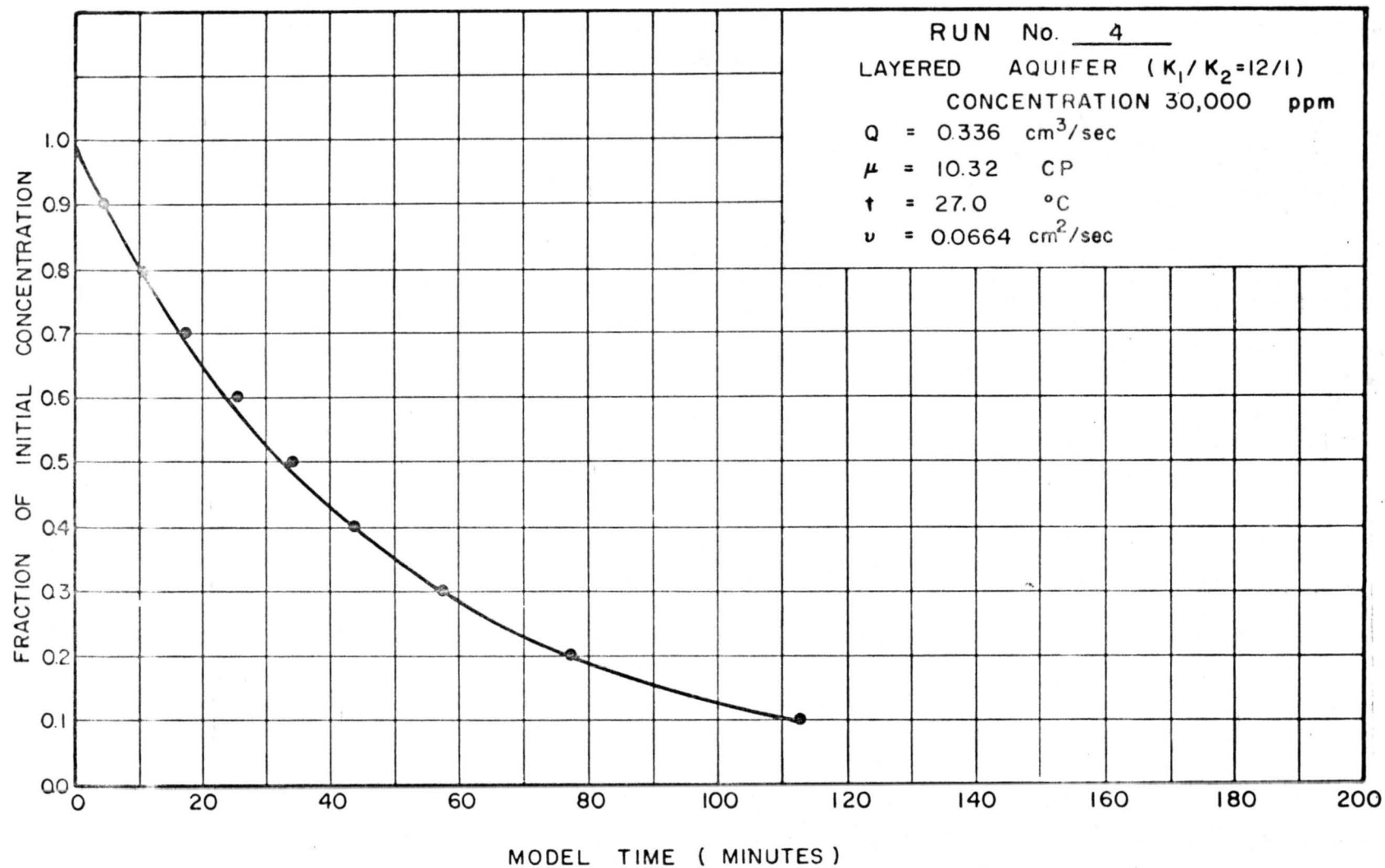


Fig. 52. Concentration versus time (Run 4, initial concentration 30,000 ppm, layered aquifer,  $K_1/K_2 = 12/1$ ).

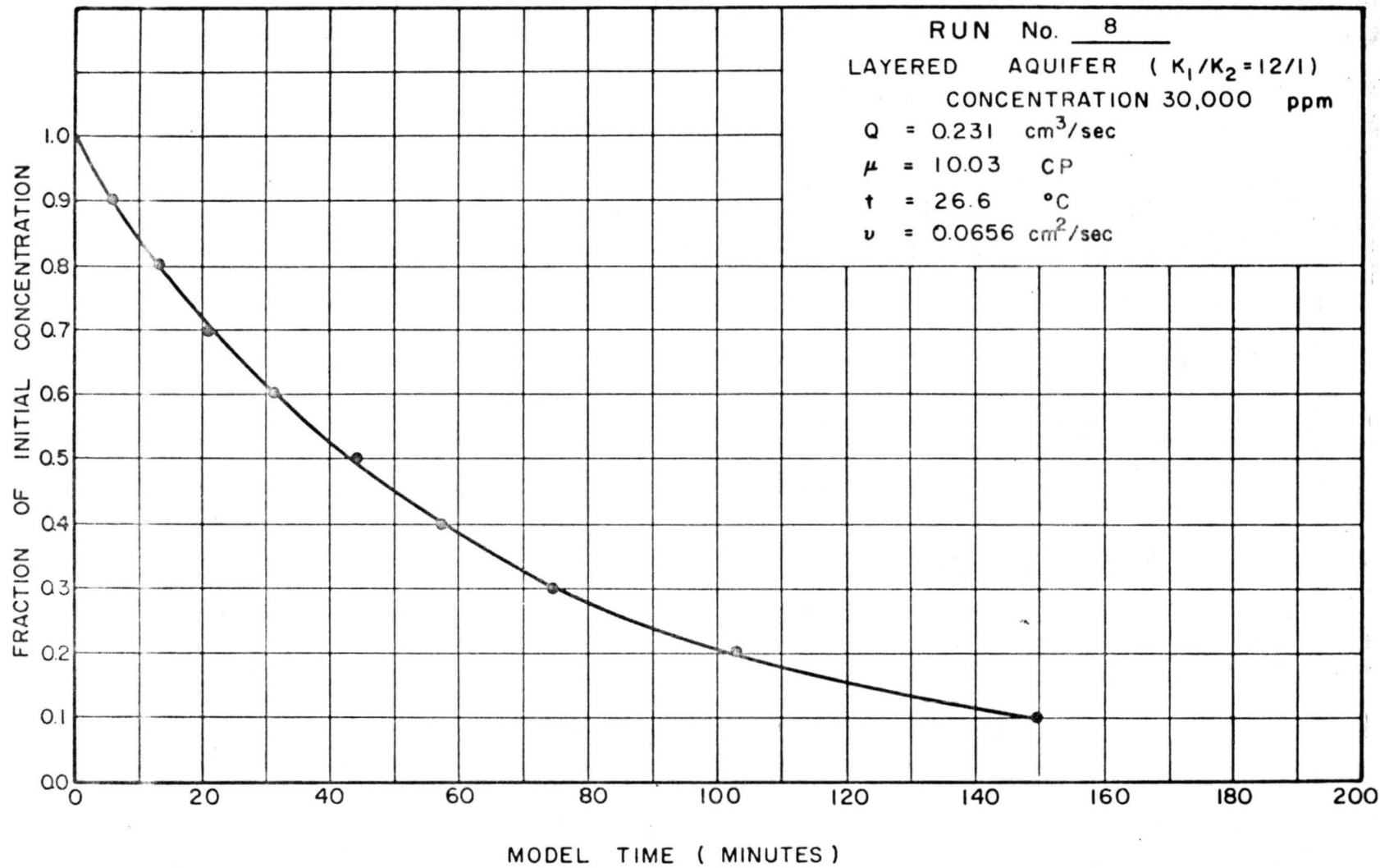


Fig. 53. Concentration versus time (Run 3, initial concentration 30,000 ppm, layered aquifer,  $K_1/K_2 = 12/1$ ).

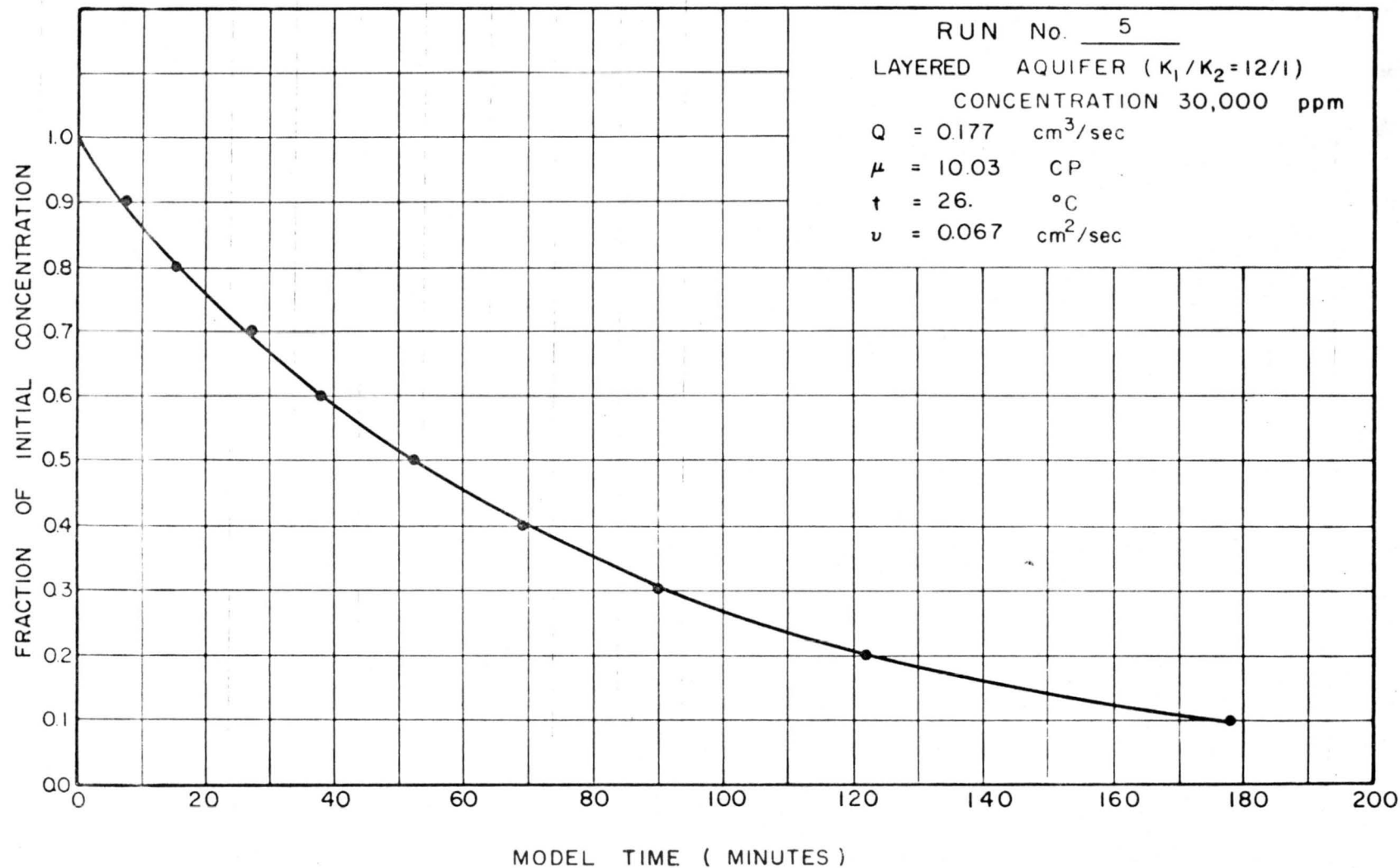


Fig. 54. Concentration versus time (Run 5, initial concentration 30,000 ppm, layered aquifer,  $K_1/K_2 = 12/1$ ).

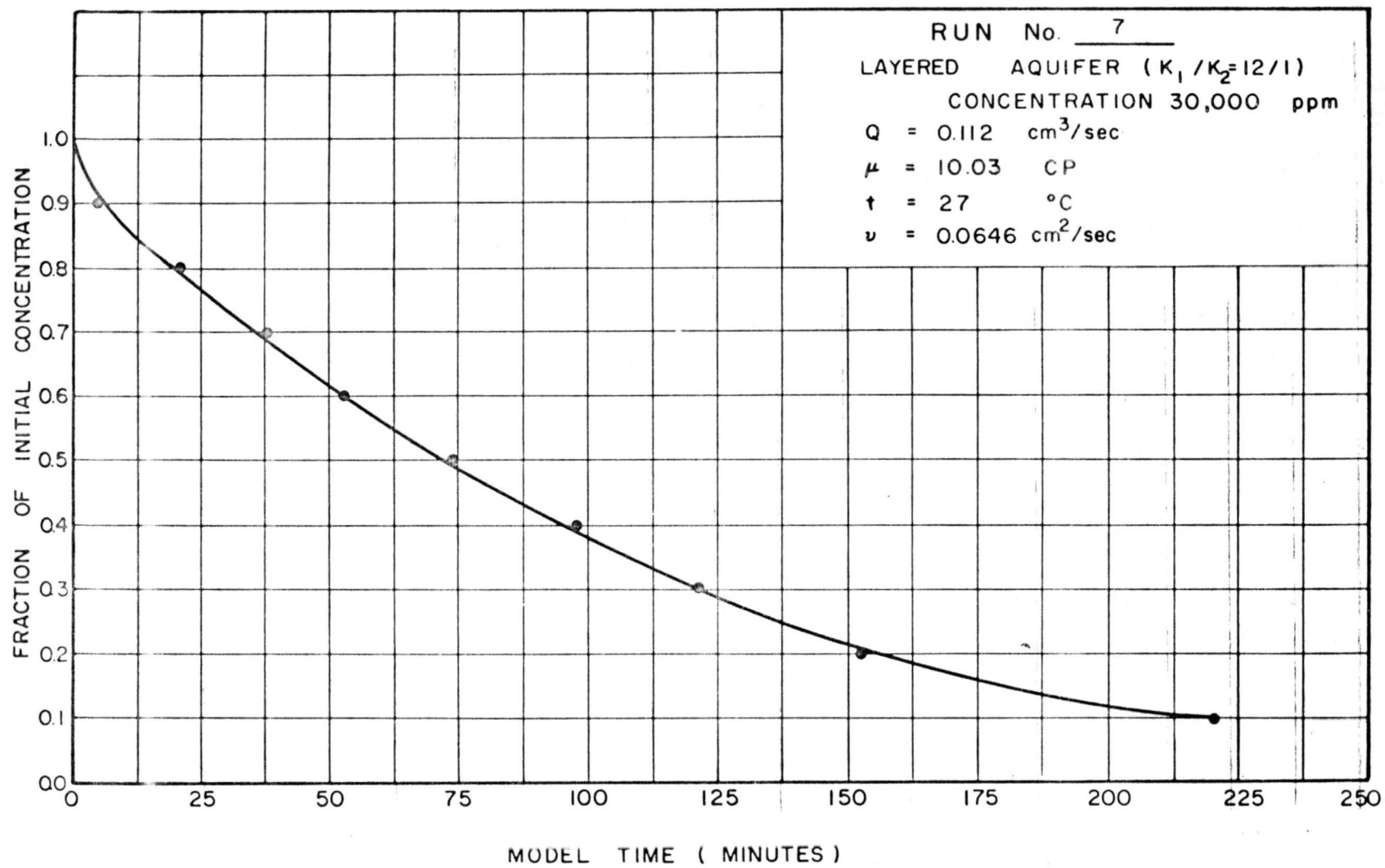


Fig. 55. Concentration versus time (Run 7, initial concentration 30,000 ppm, layered aquifer,  $K_1/K_2 = 12/1$ ).

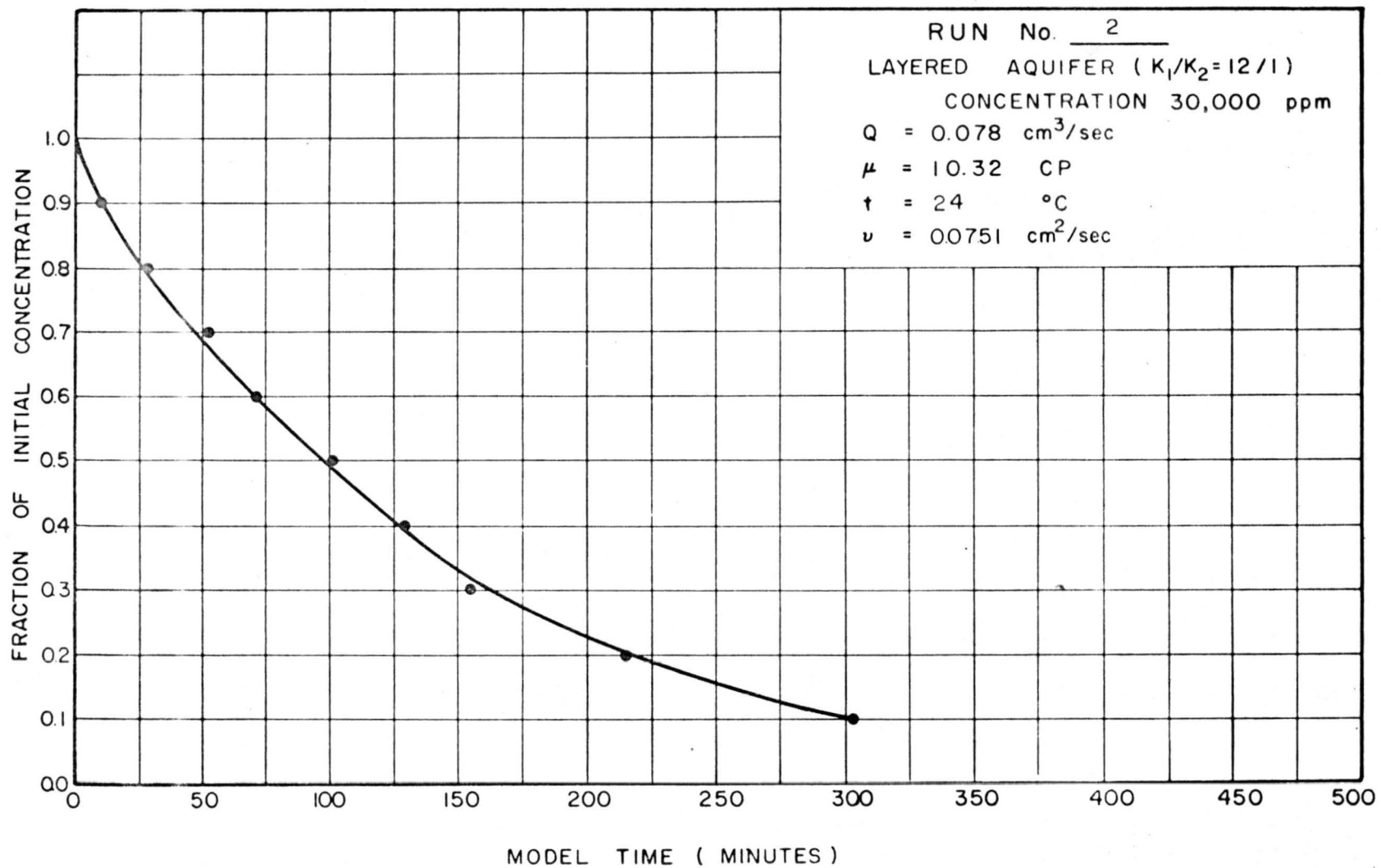


Fig. 56. Concentration versus time (Run 2, initial concentration 30,000 ppm, layered aquifer,  $K_1/K_2 = 12/1$ ).

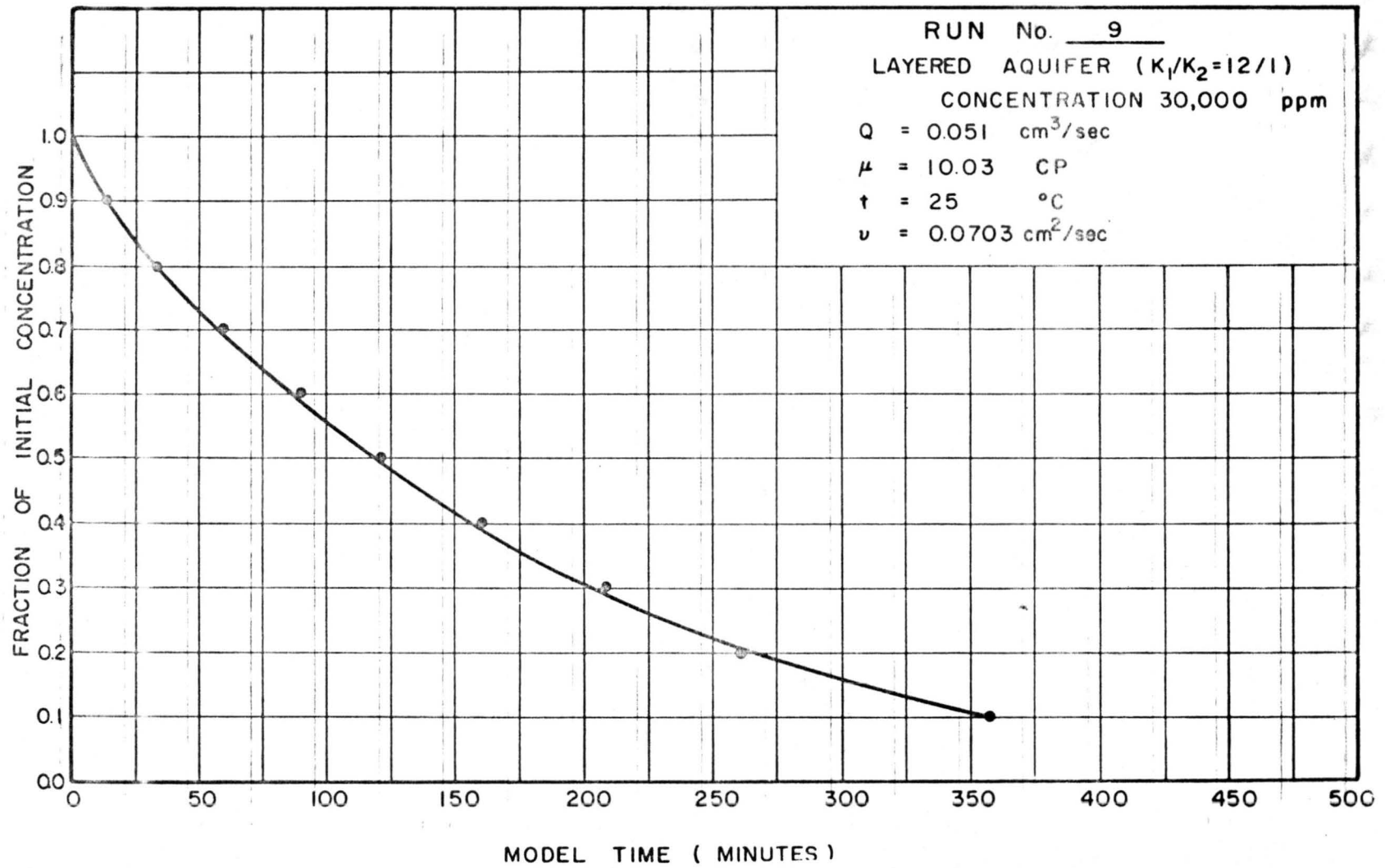


Fig. 57. Concentration versus time (Run 9, initial concentration 30,000 ppm, layered aquifer,  $K_1/K_2 = 12/1$ ).

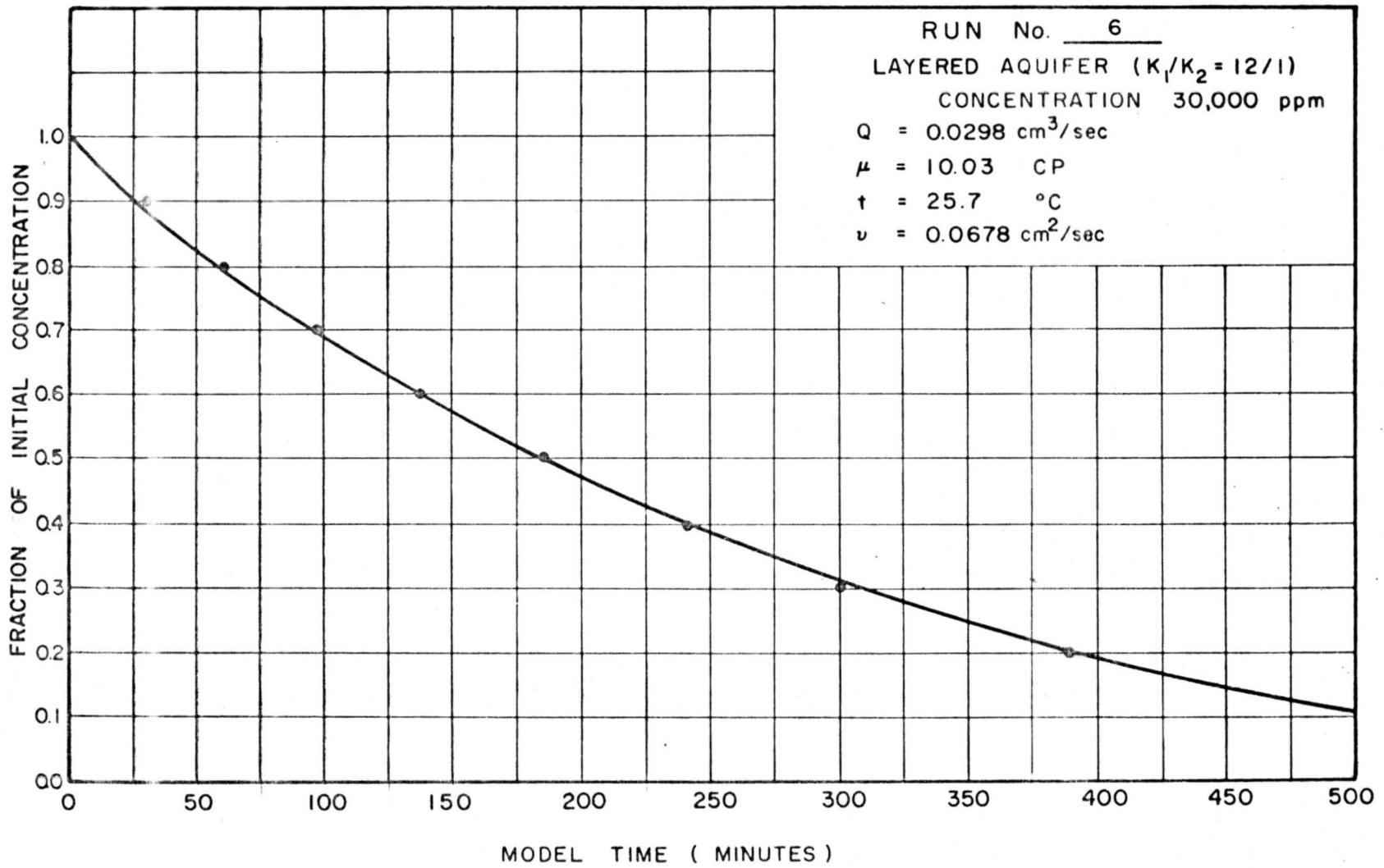


Fig. 55. Concentration versus time (Run 6, initial concentration 30,000 ppm, layered aquifer,  $K_1/K_2 = 12/1$ ).

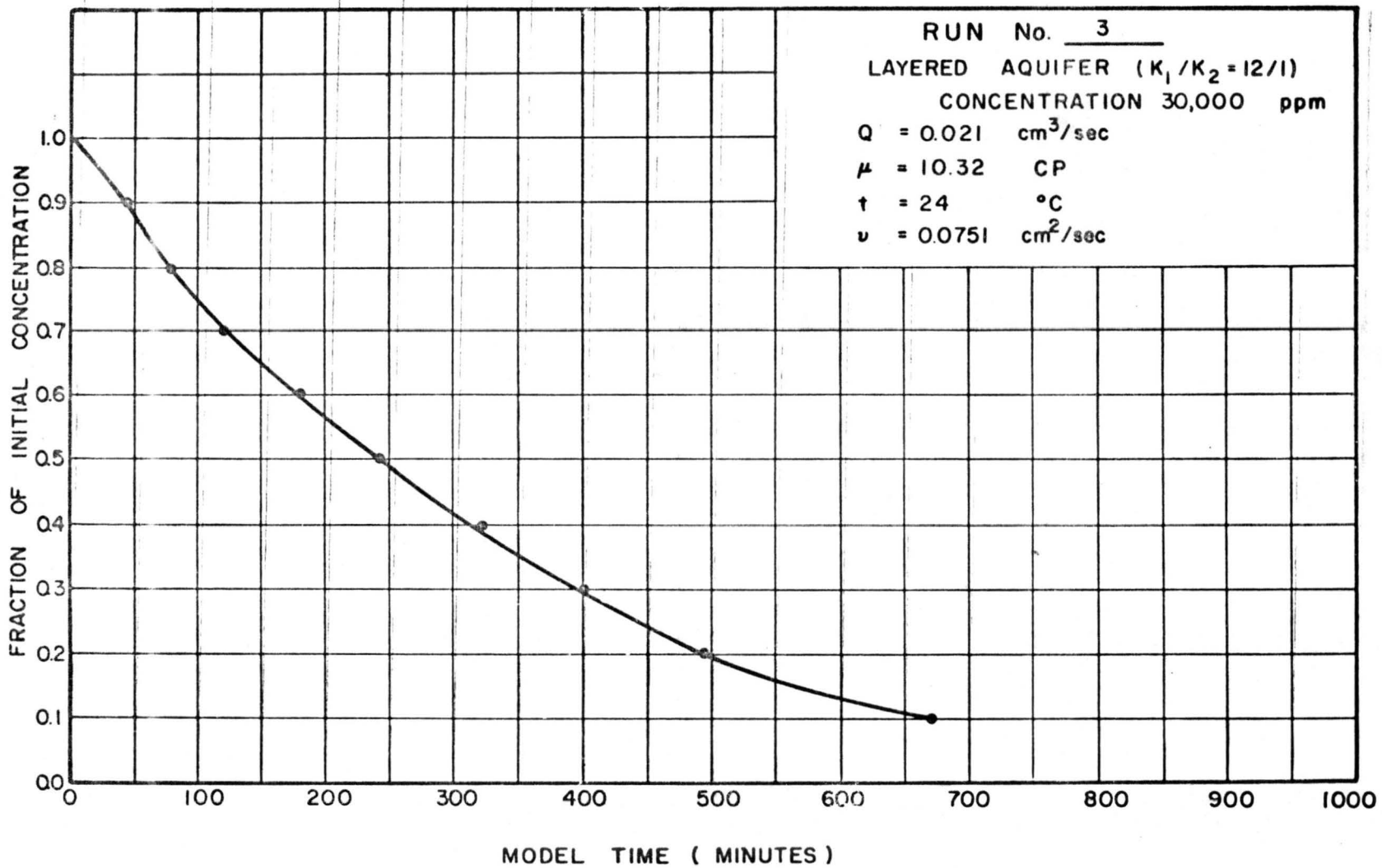


Fig. 59. Concentration versus time (Run 3, initial concentration 30,000 ppm, layered aquifer,  $K_1/K_2 = 12/1$ ).

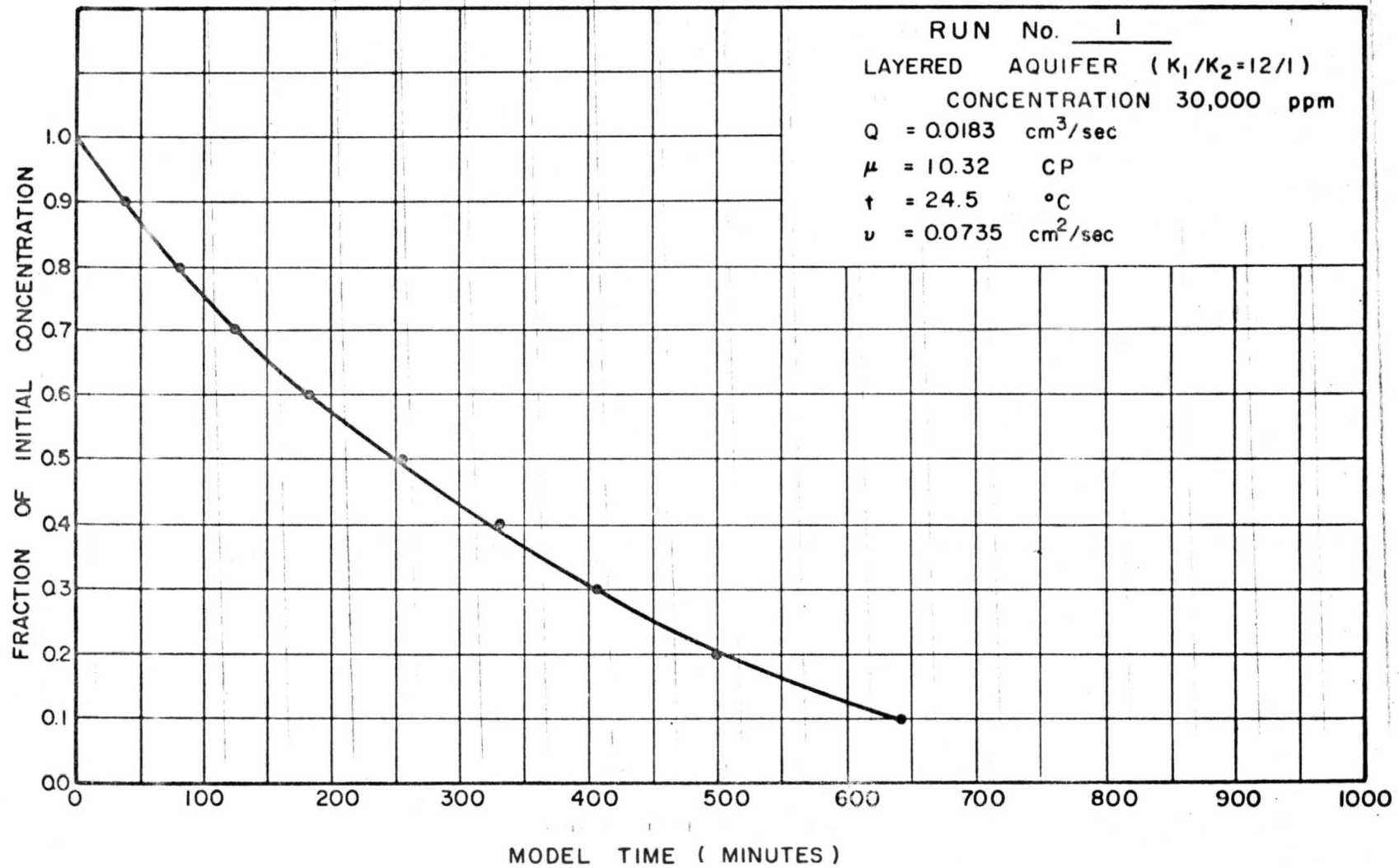


Fig. 69. Concentration versus time (Run 1, initial concentration 30,000 ppm, layered aquifer,  $K_1/K_2 = 12/1$ ).

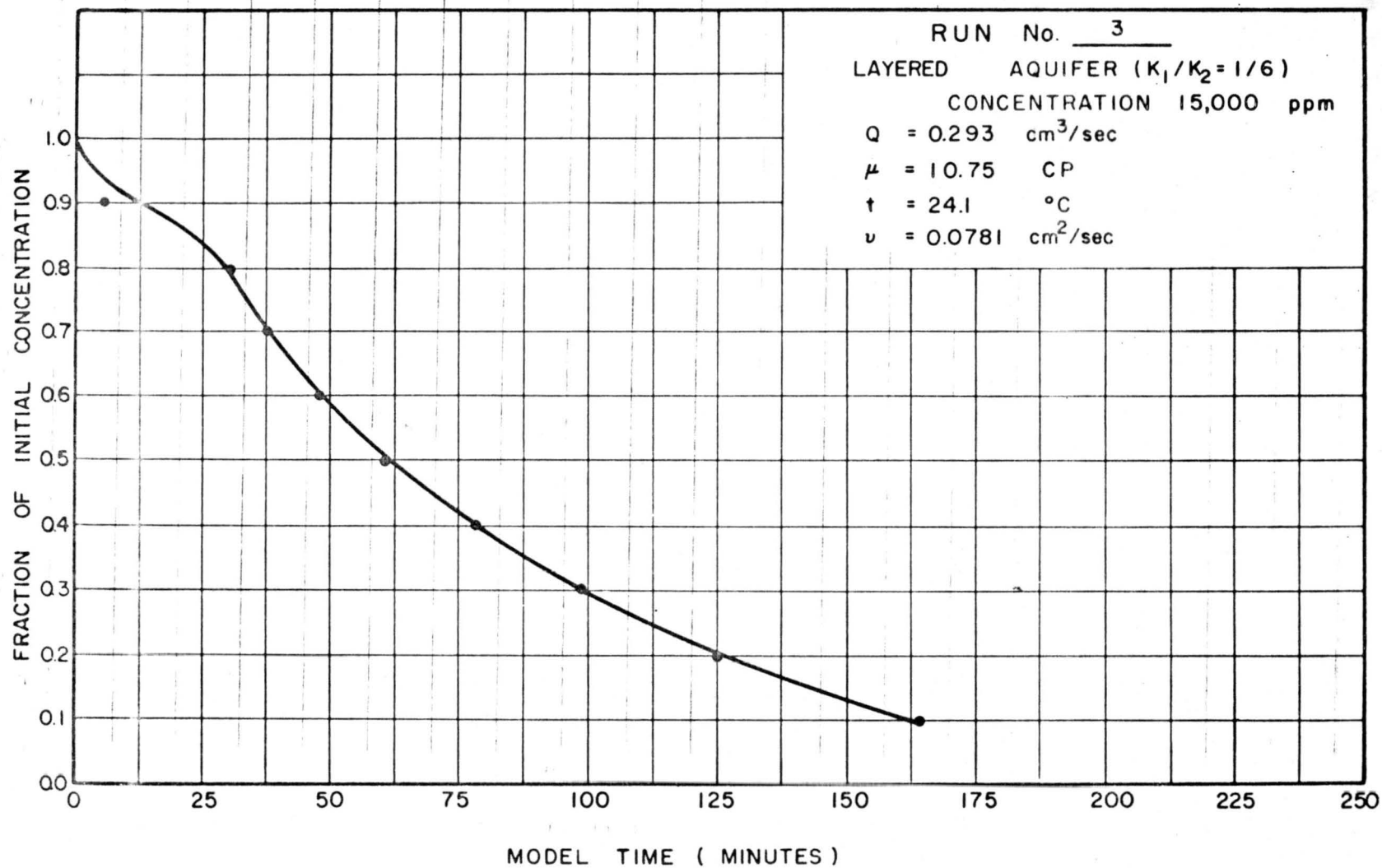


Fig. 61. Concentration versus time (Run 3, initial concentration 15,000 ppm, layered aquifer,  $K_1/K_2 = 1/6$ ).

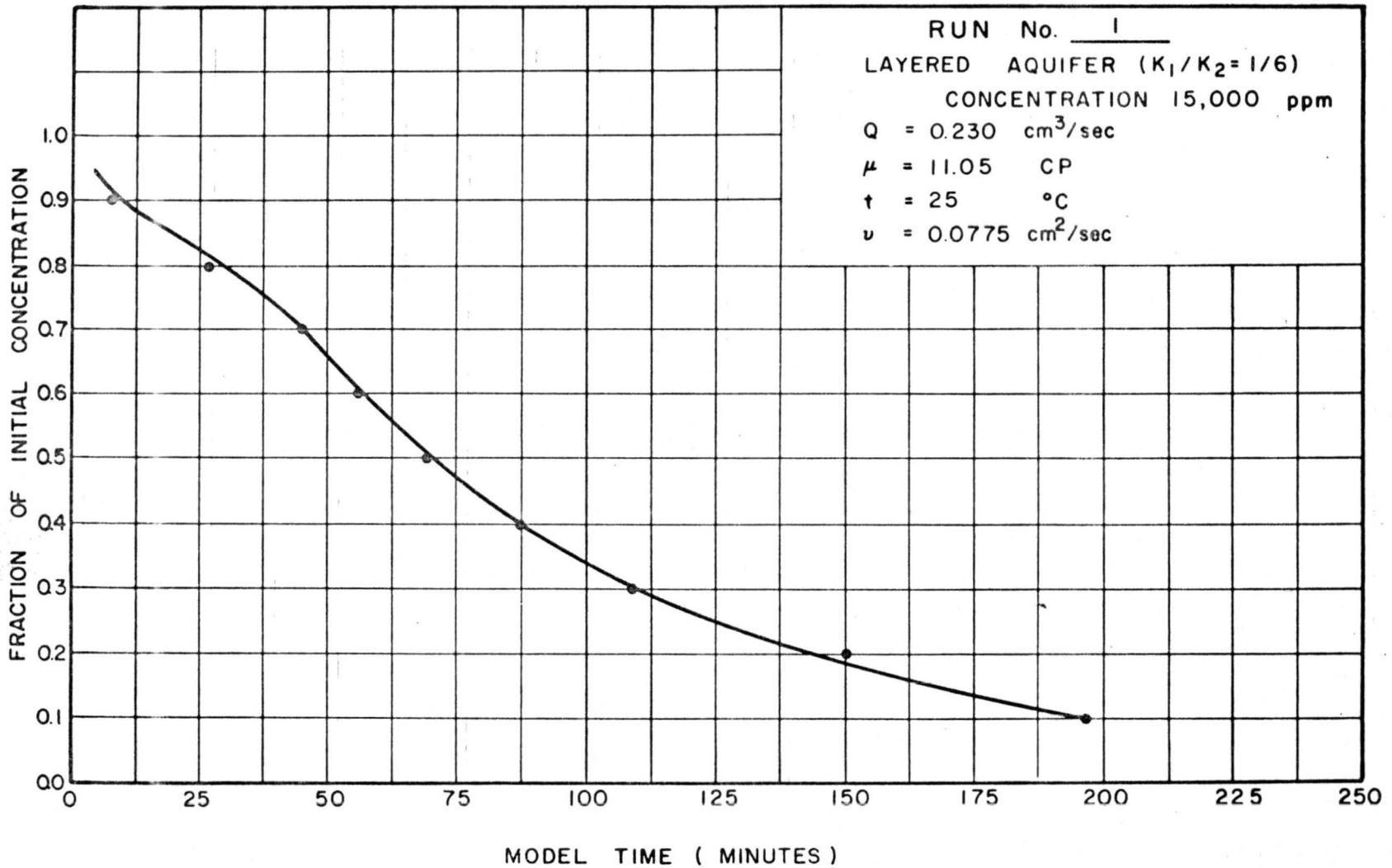


Fig. 62. Concentration versus time (Run 1, initial concentration 15,000 ppm, layered aquifer,  $K_1/K_2 = 1/6$ ).

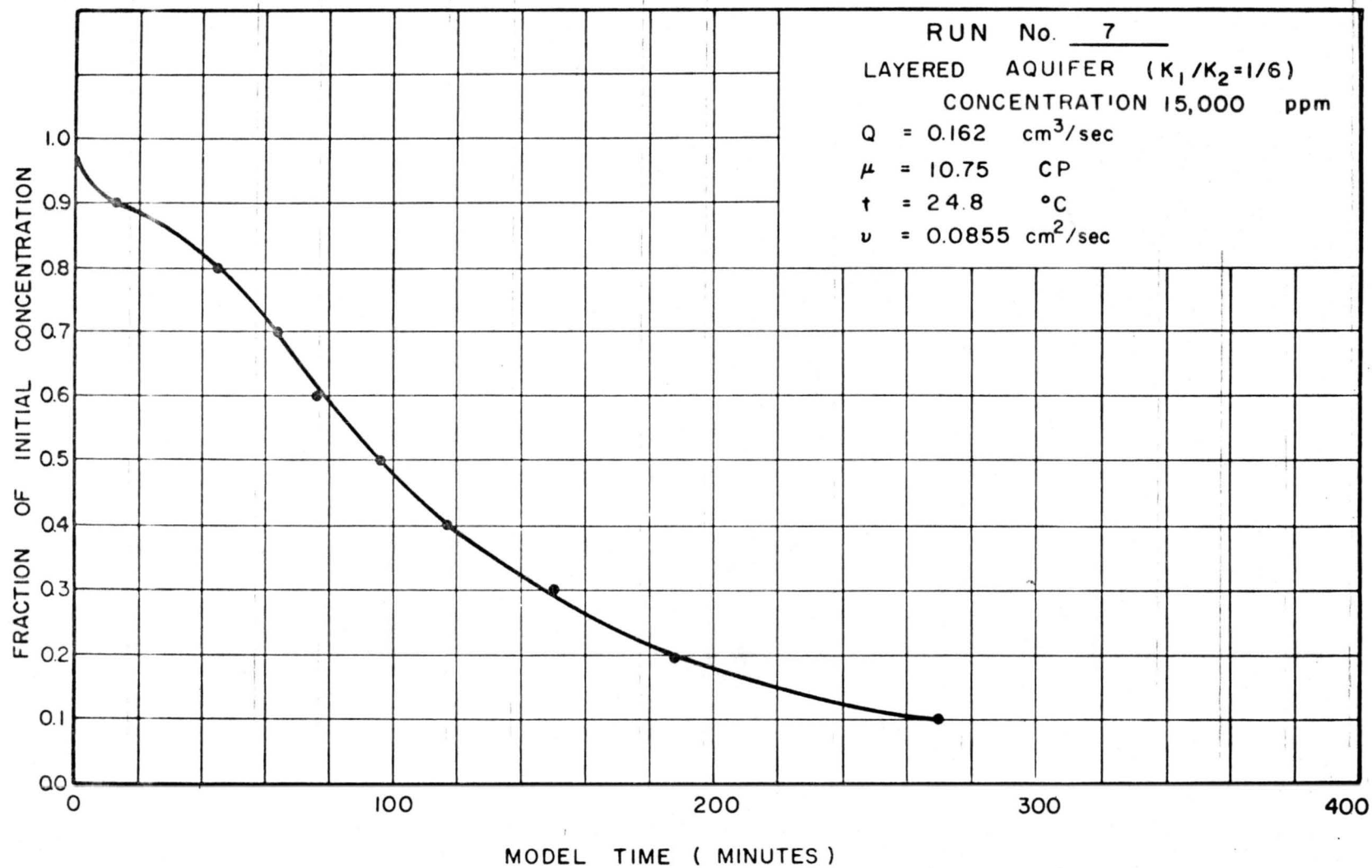


Fig. 63. Concentration versus time (Run 7, initial concentration 15,000 ppm, layered aquifer,  $K_1/K_2 = 1/6$ ).

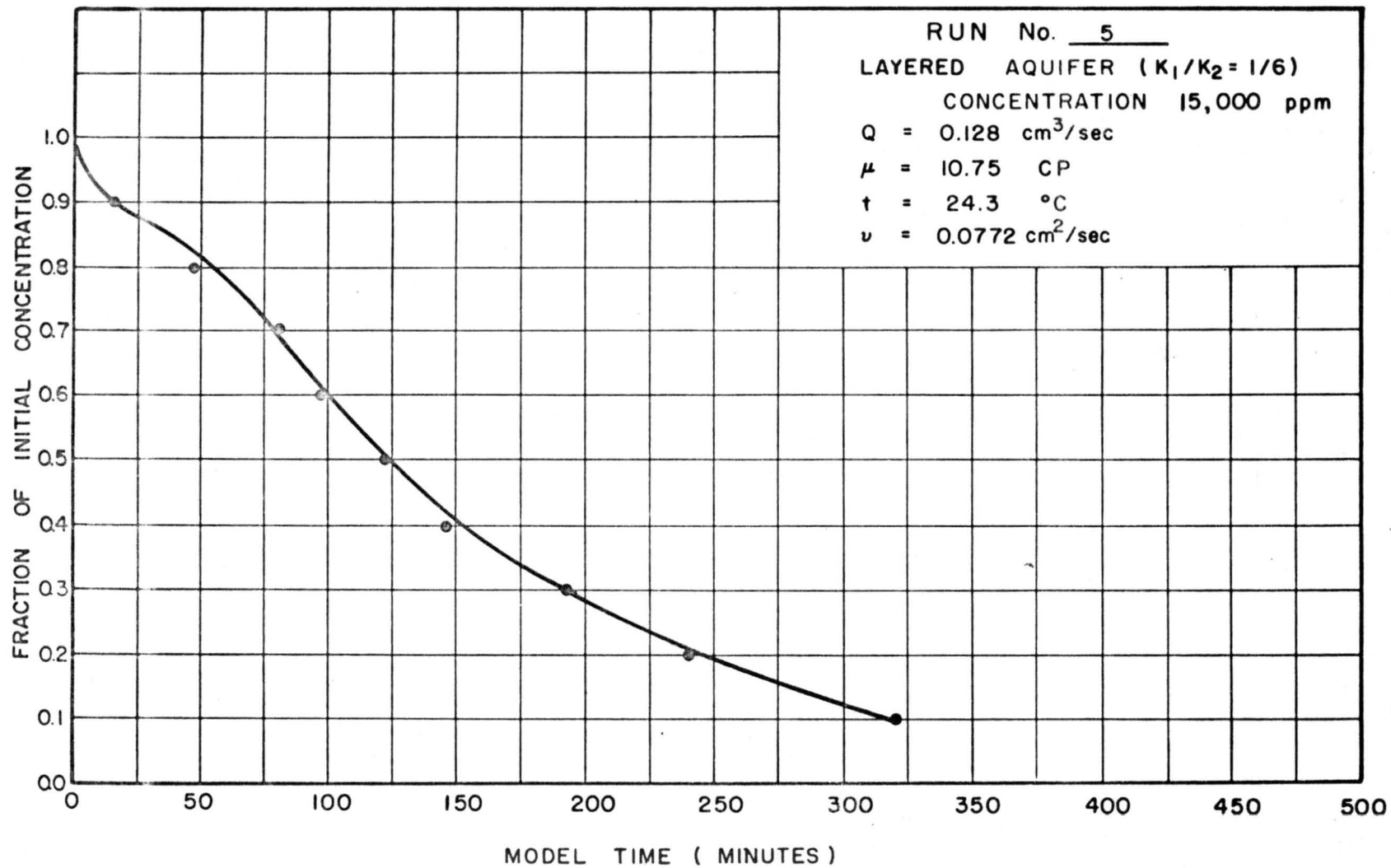


Fig. 64. Concentration versus time (Run 5, initial concentration 15,000 ppm, layered aquifer,  $K_1/K_2 = 1/6$ ).

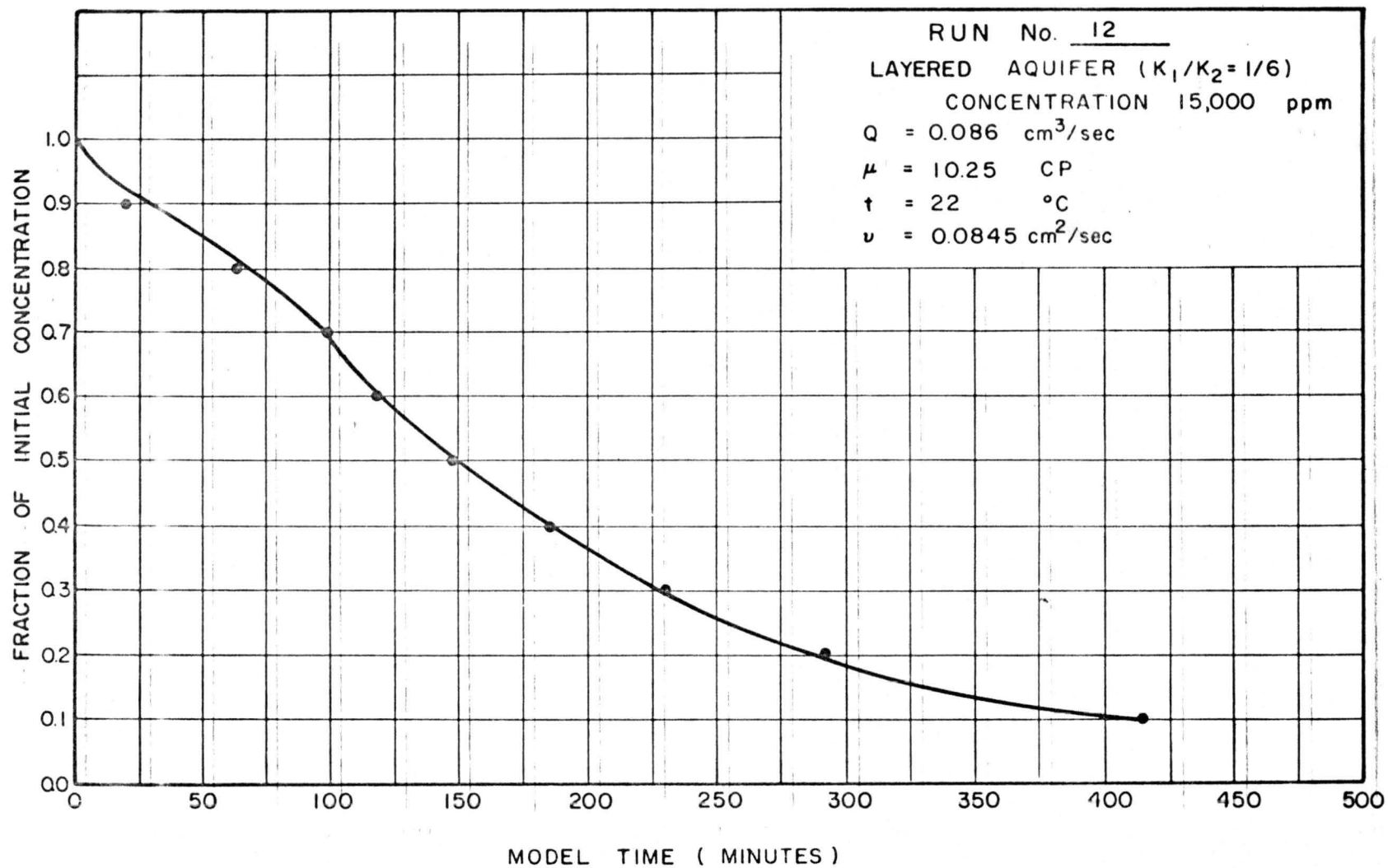


Fig. 65. Concentration versus time (Run 12, initial concentration 15,000 ppm, layered aquifer,  $K_1/K_2 = 1/6$ ).

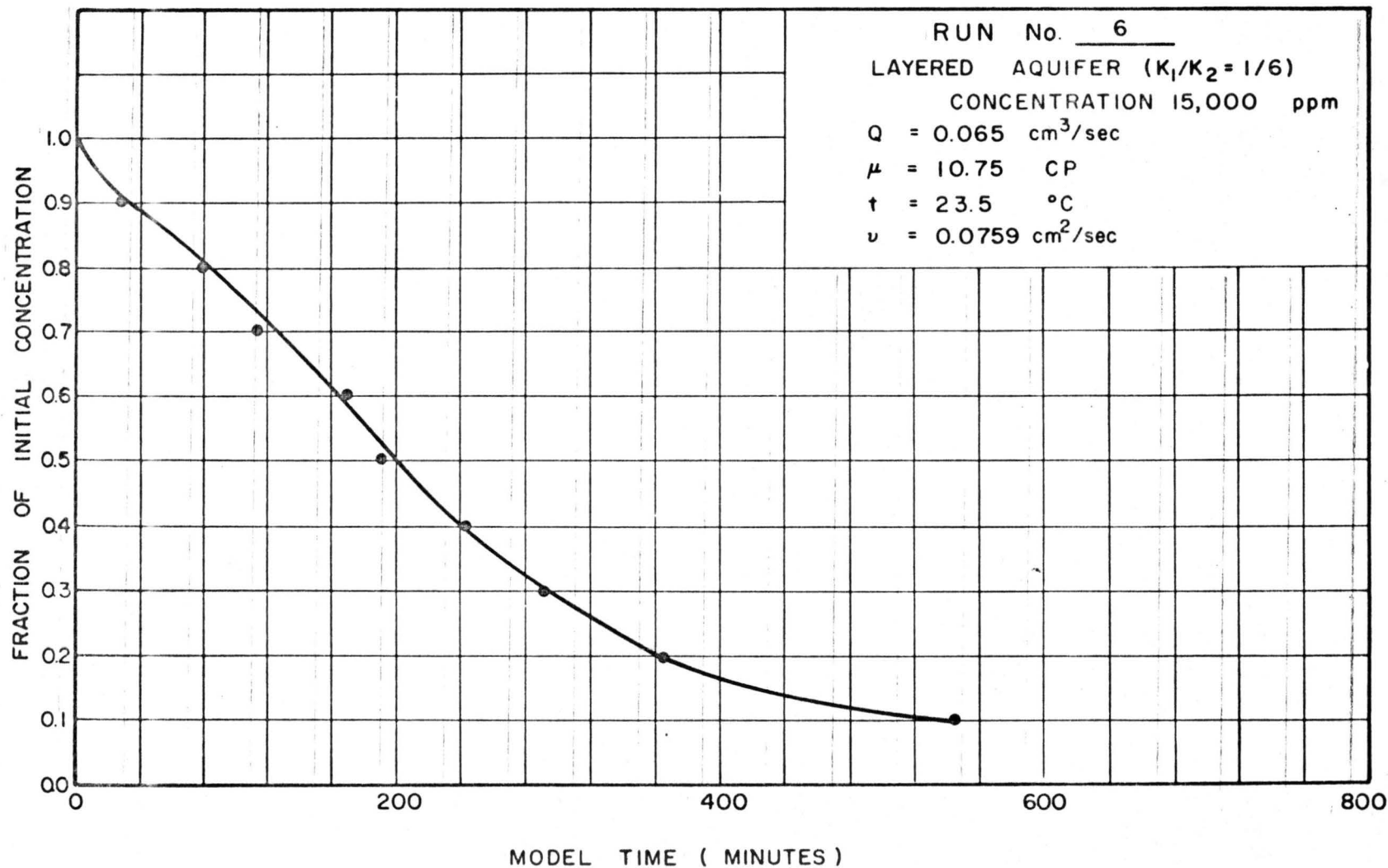


Fig. 66. Concentration versus time (Run 6, initial concentration 15,000 ppm, layered aquifer,  $K_1/K_2 = 1/6$ ).

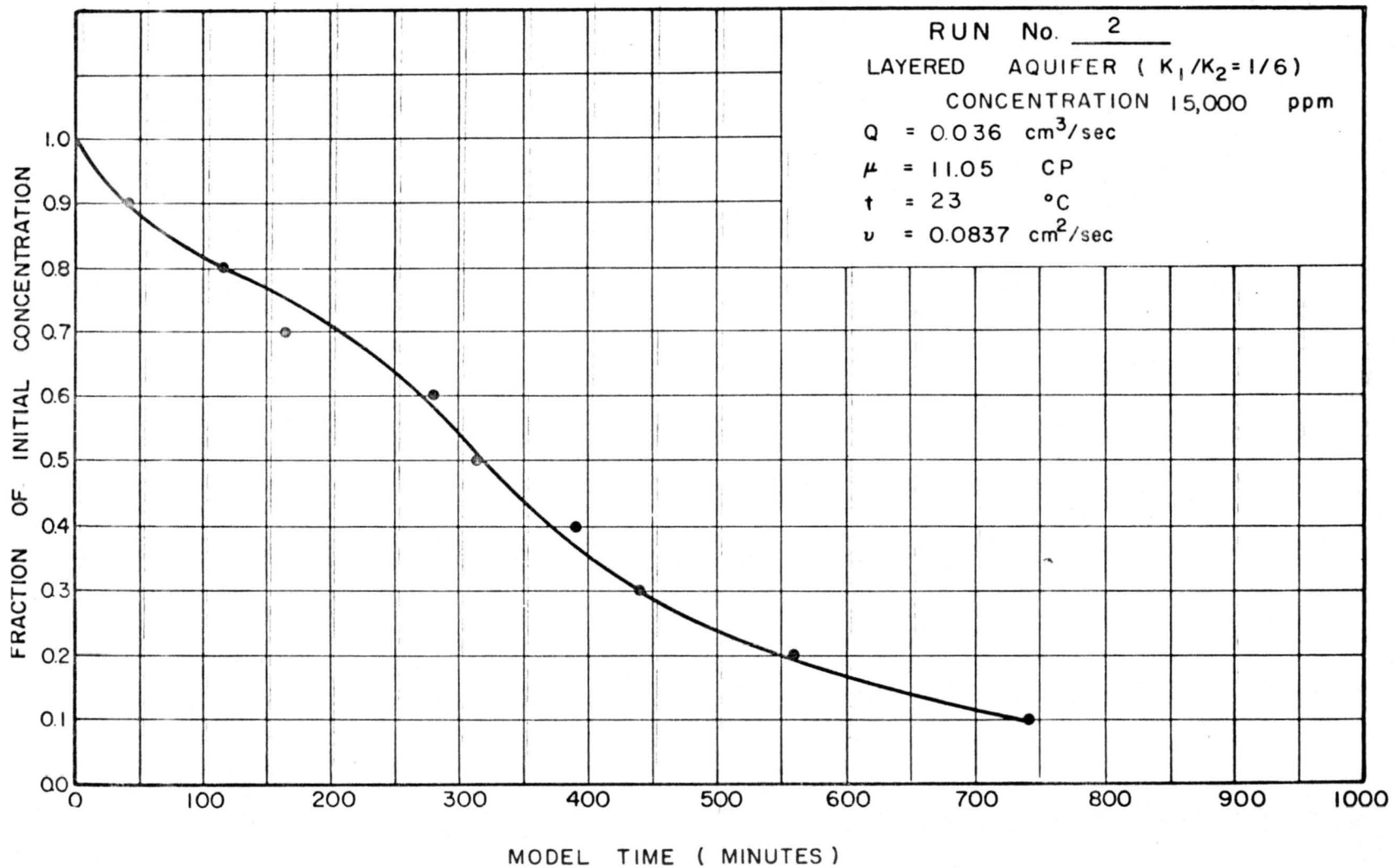


Fig. 67. Concentration versus time (Run 2, initial concentration 15,000 ppm, layered aquifer,  $K_1/K_2 = 1/6$ ).

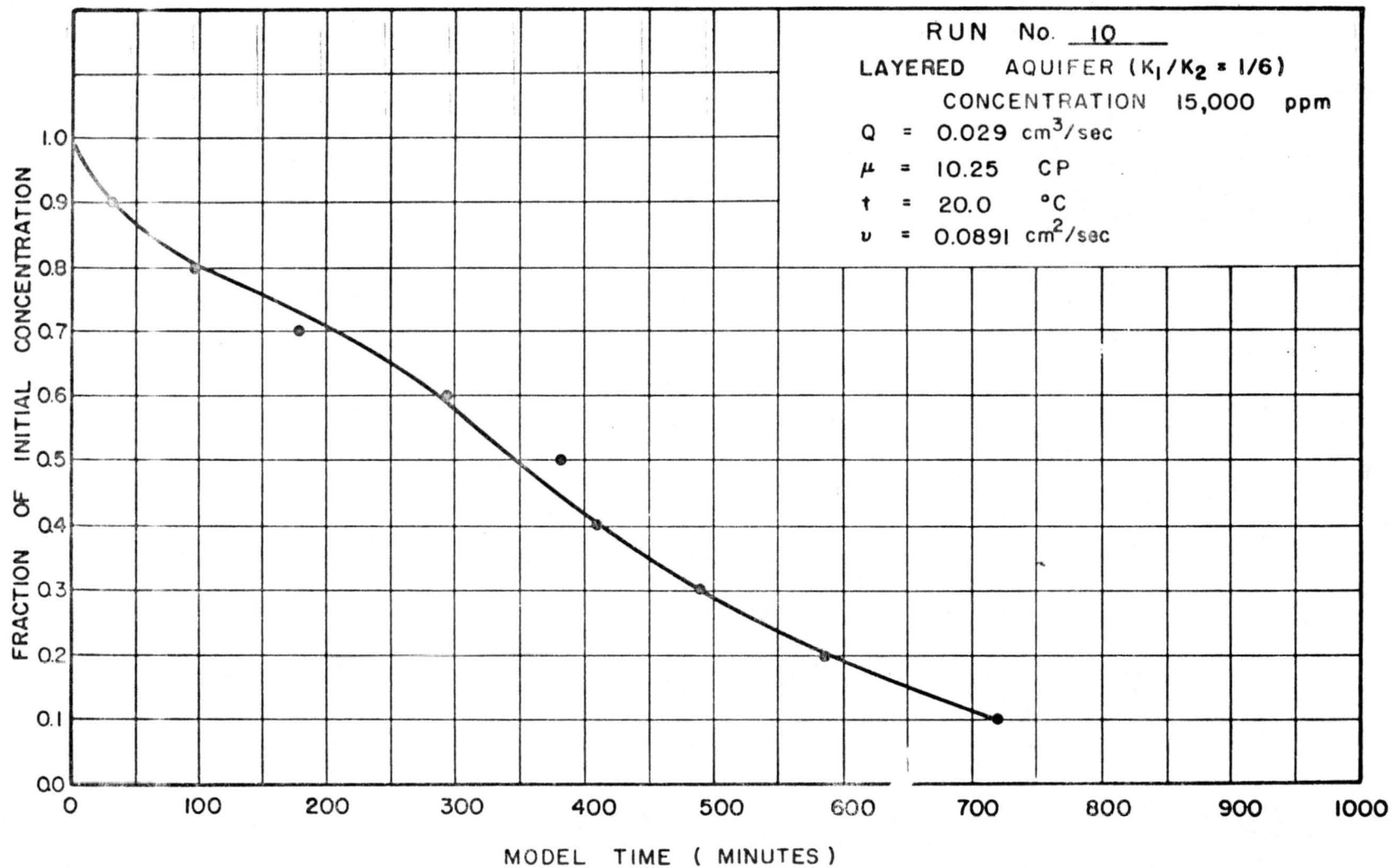


Fig. 63. Concentration versus time (Run 10, initial concentration 15,000 ppm, layered aquifer,  $K_1/K_2 = 1/6$ ).

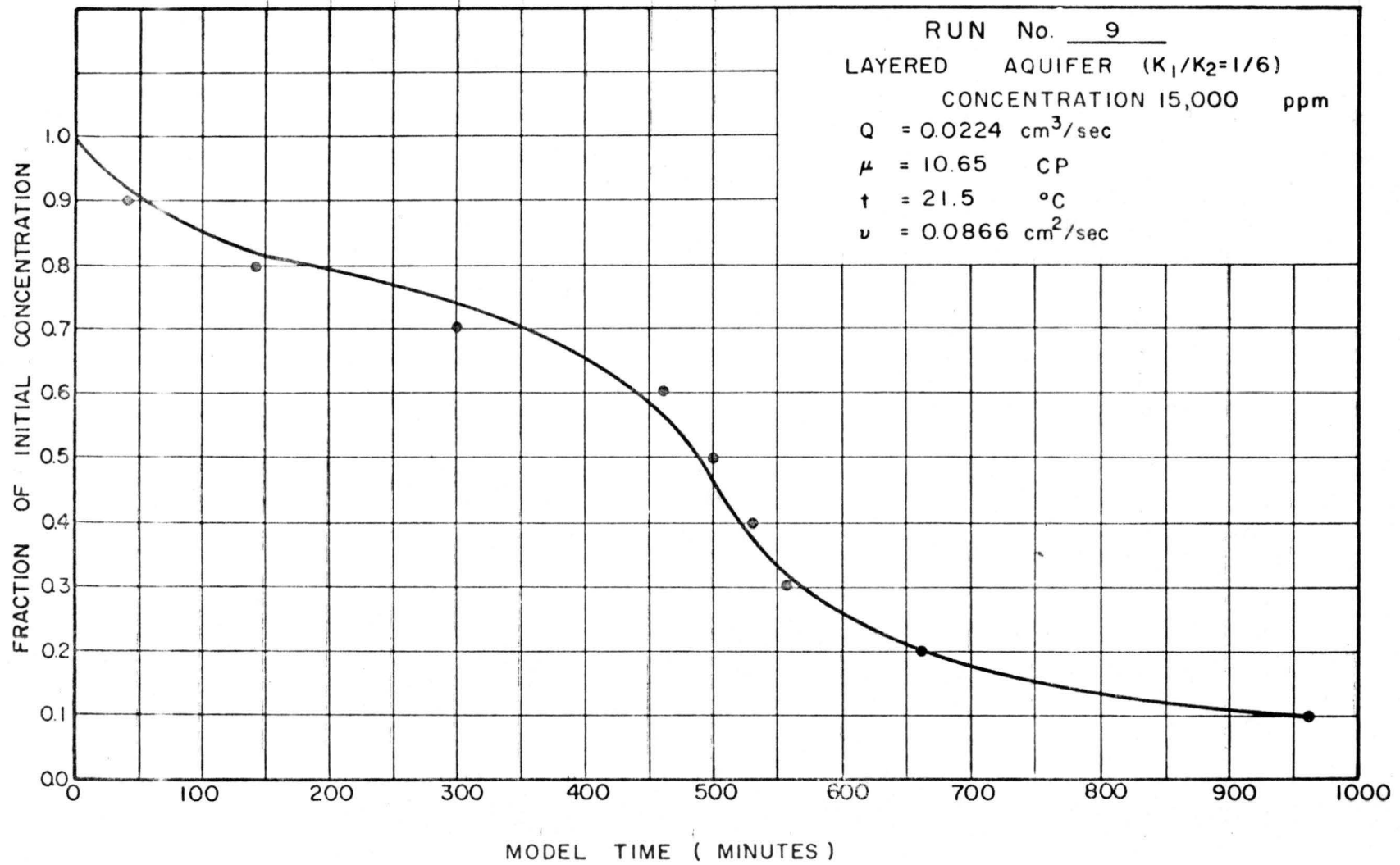


Fig. 69. Concentration versus time (Run 9, initial concentration 15, 000 ppm, layered aquifer,  $K_1/K_2 = 1/6$ ).

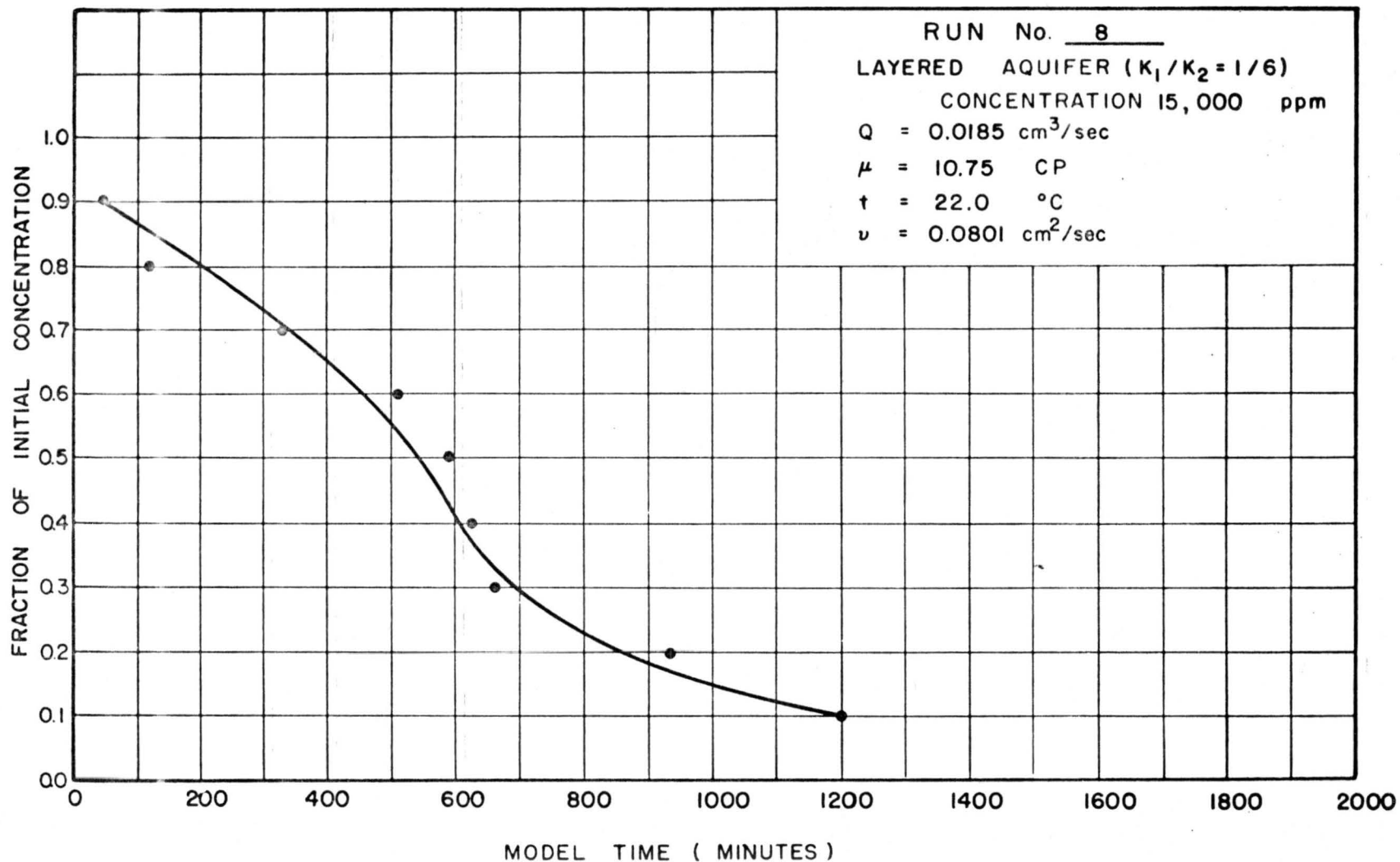


Fig. 70. Concentration versus time (Run 8, initial concentration 15,000 ppm, layered aquifer,  $K_1/K_2 = 1/6$ ).

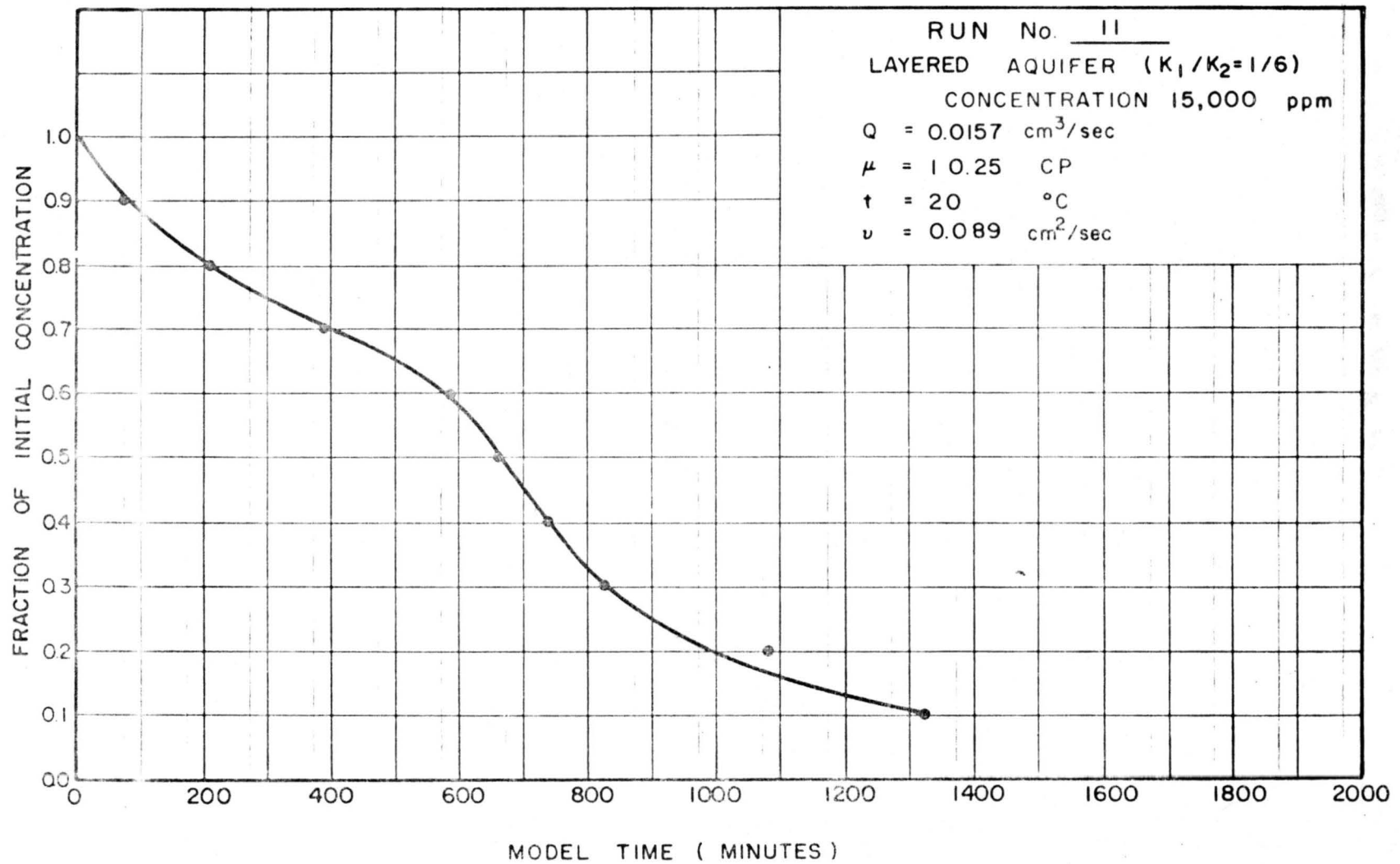


Fig. 71. Concentration versus time (Run 11, initial concentration 15,000 ppm, layered aquifer,  $K_1/K_2 = 1/6$ ).

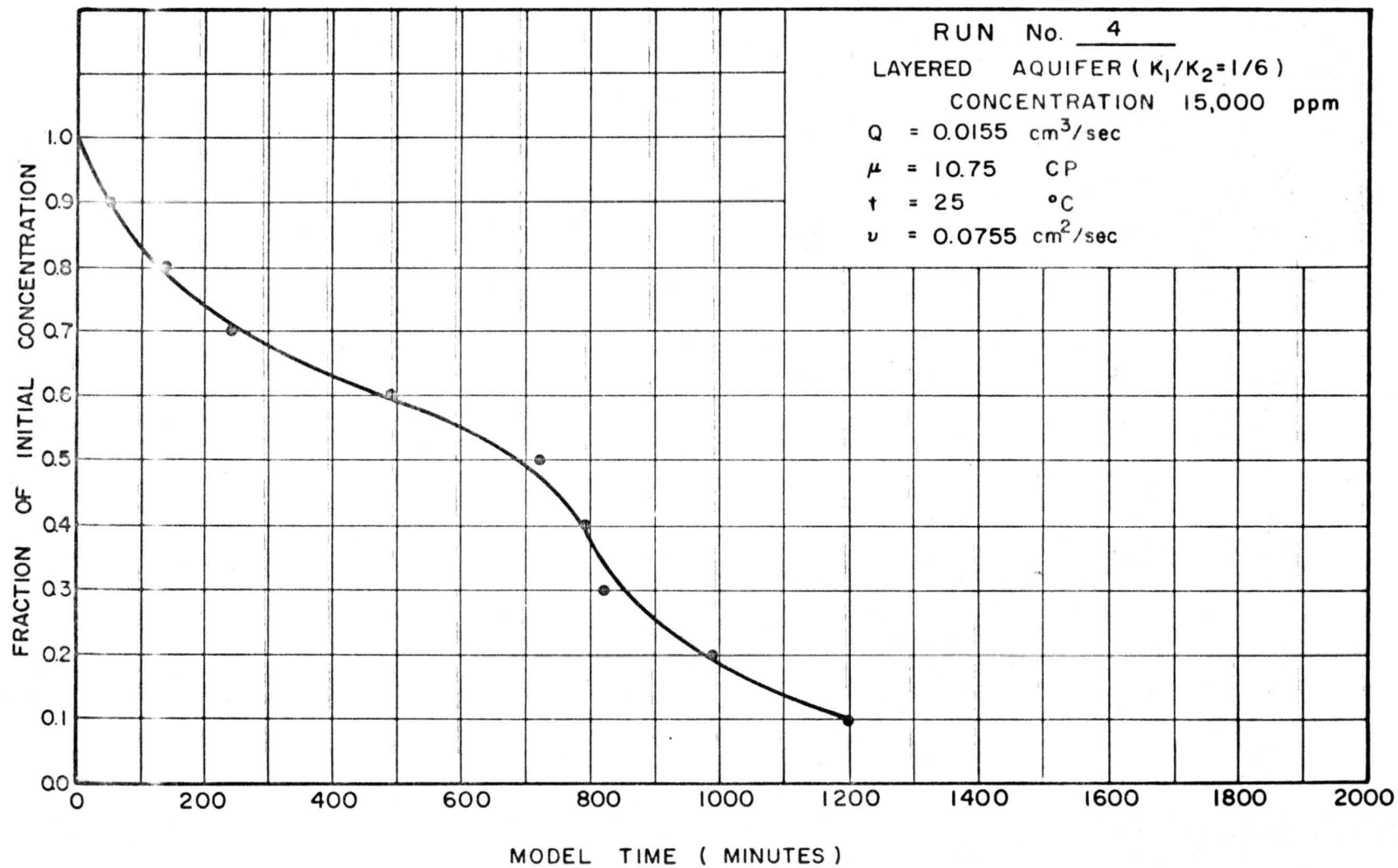


Fig. 72. Concentration versus time (Run 4, initial concentration 15,000 ppm, layered aquifer,  $K_1/K_2 = 1/6$ ).

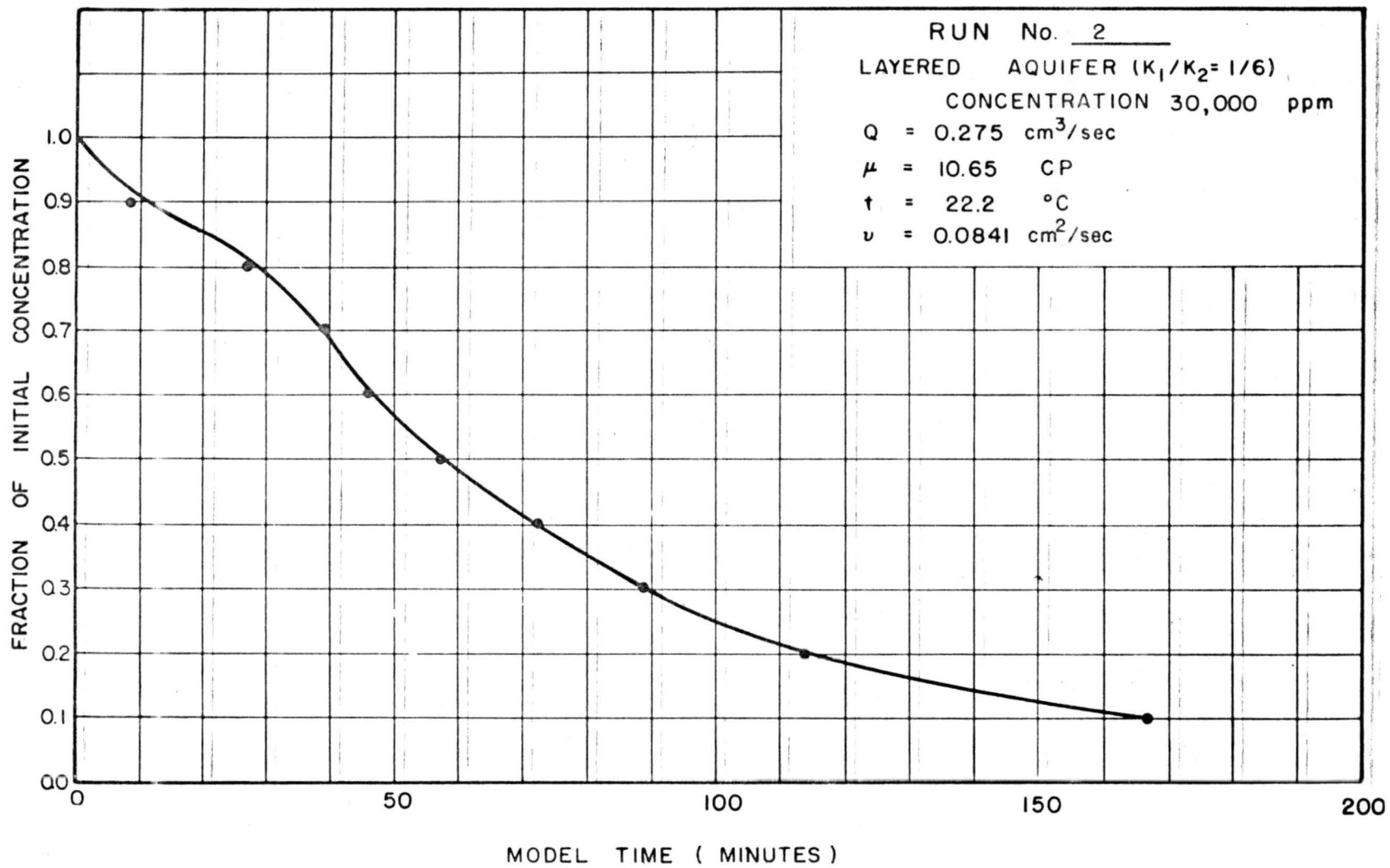


Fig. 73. Concentration versus time (Run 2, initial concentration 30,000 ppm, layered aquifer,  $K_1/K_2 = 1/6$ ).

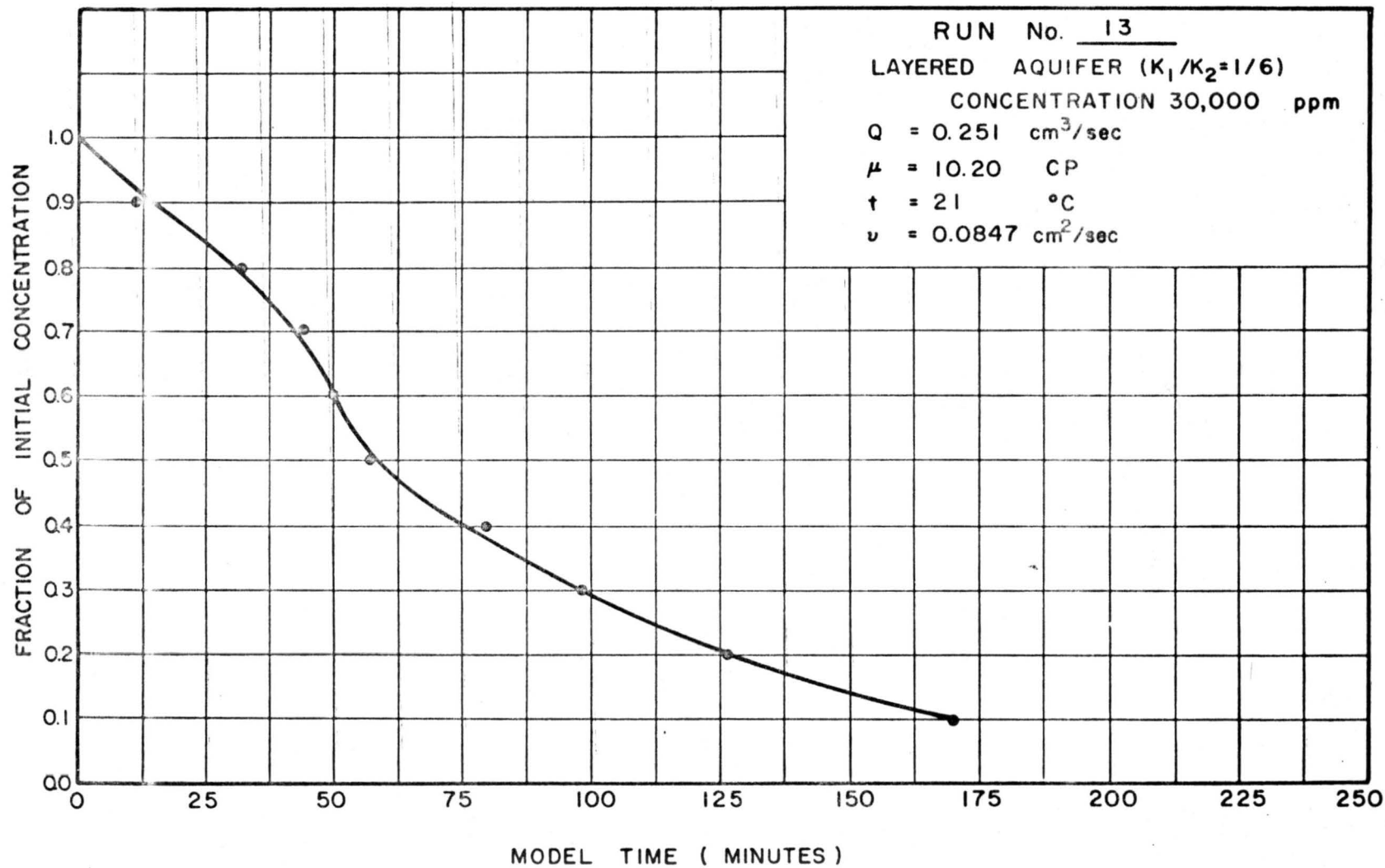


Fig. 74. Concentration versus time (Run 13, initial concentration 30,000 ppm, layered aquifer,  $K_1/K_2 = 1/6$ ).

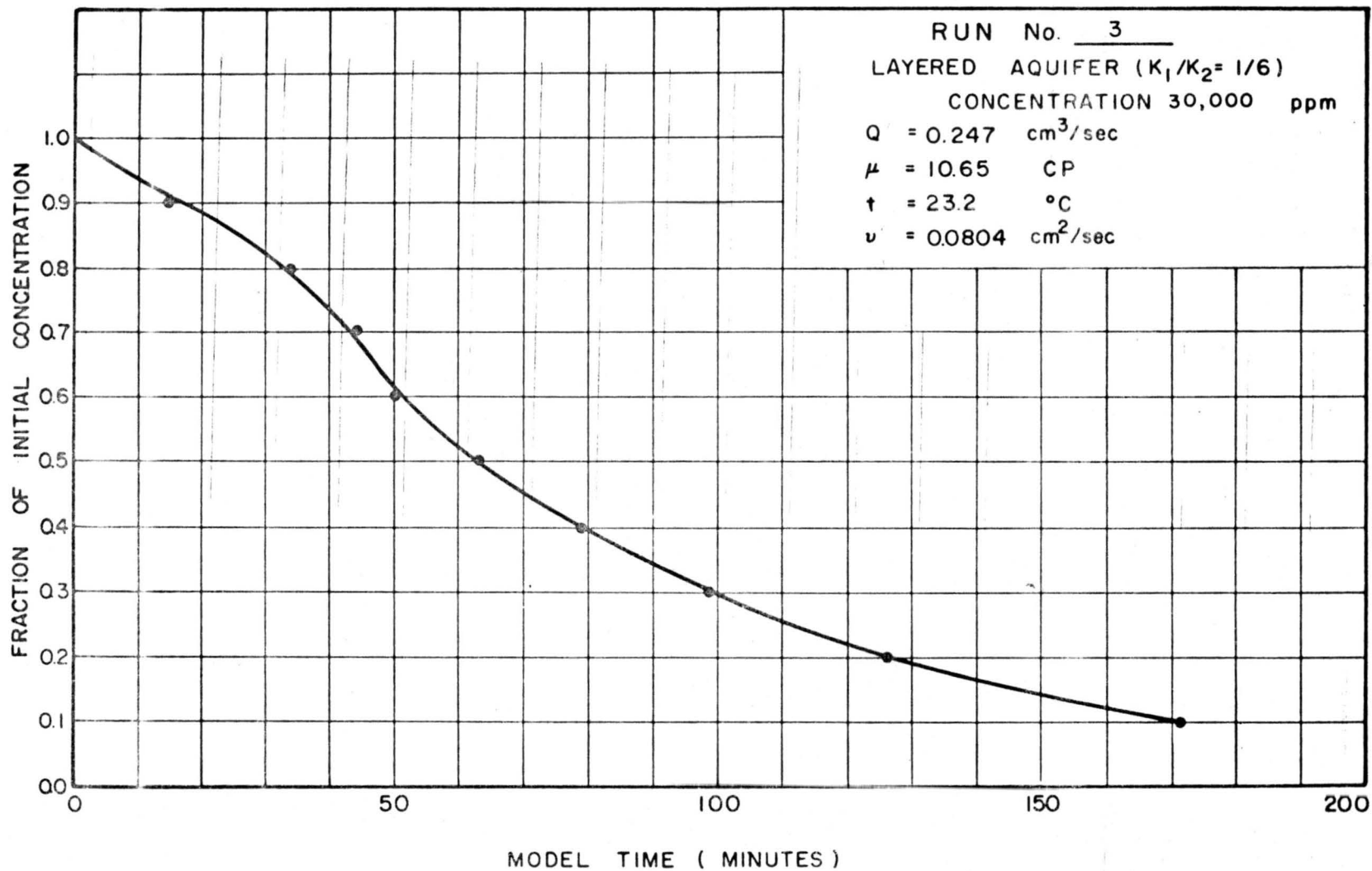


Fig. 75. Concentration versus time (Run 3, initial concentration 30,000 ppm, layered aquifer,  $K_1/K_2 = 1/6$ ).

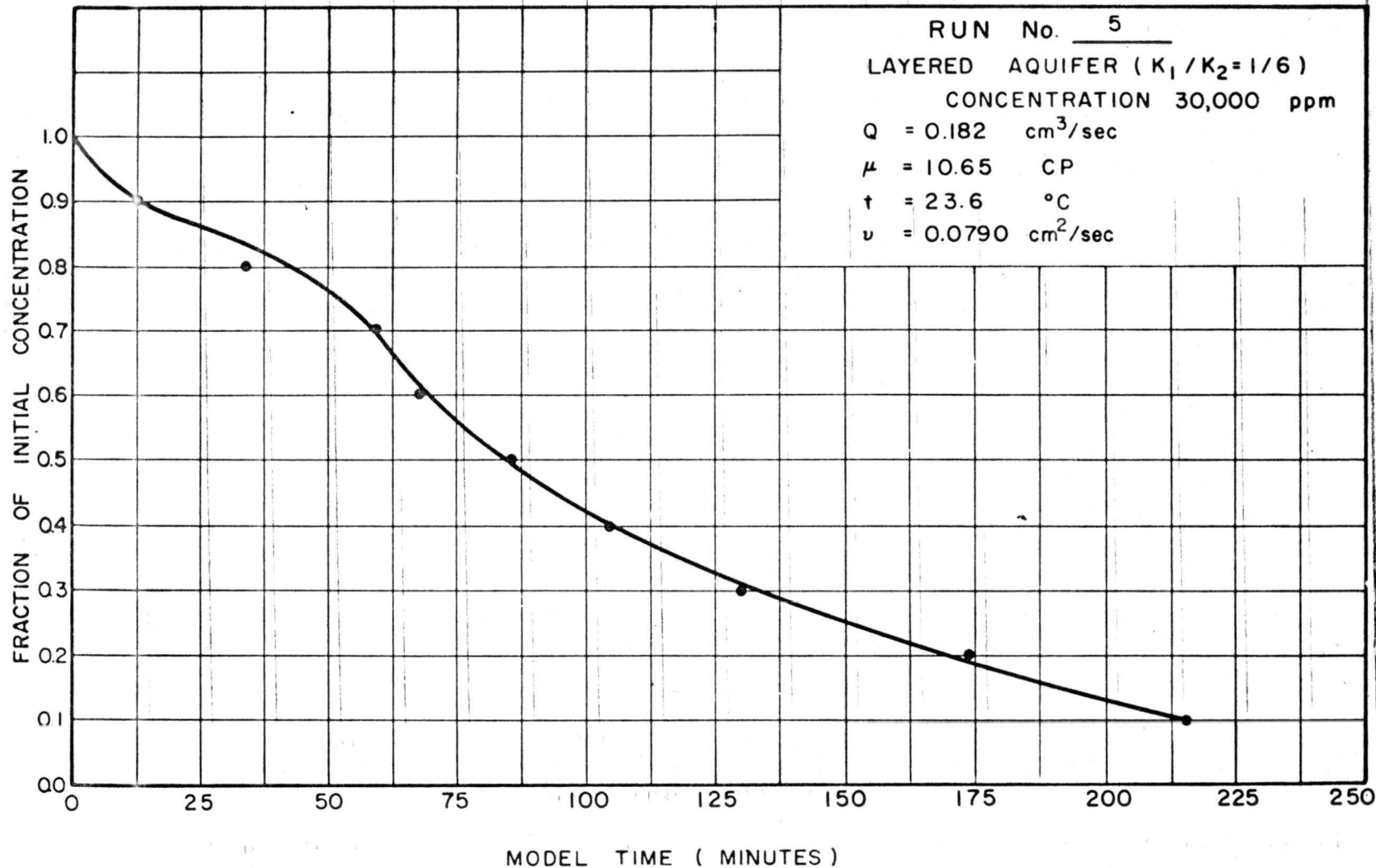


Fig. 76. Concentration versus time (Run 5, initial concentration 30,000 ppm, layered aquifer,  $K_1/K_2 = 1/6$ ).

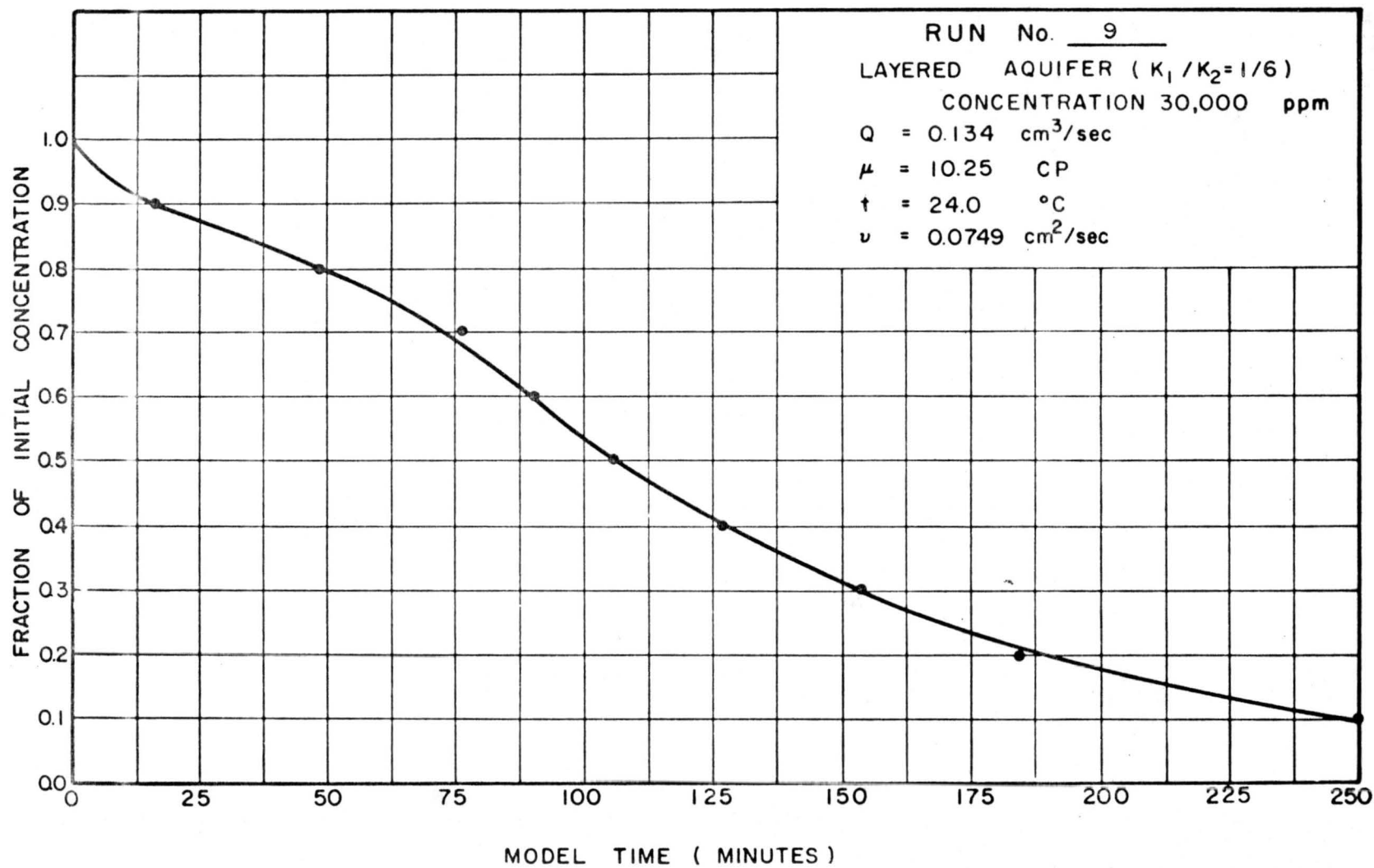


Fig. 77. Concentration versus time (Run 9, initial concentration 30,000 ppm, layered aquifer,  $K_1/K_2 = 1/6$ ).

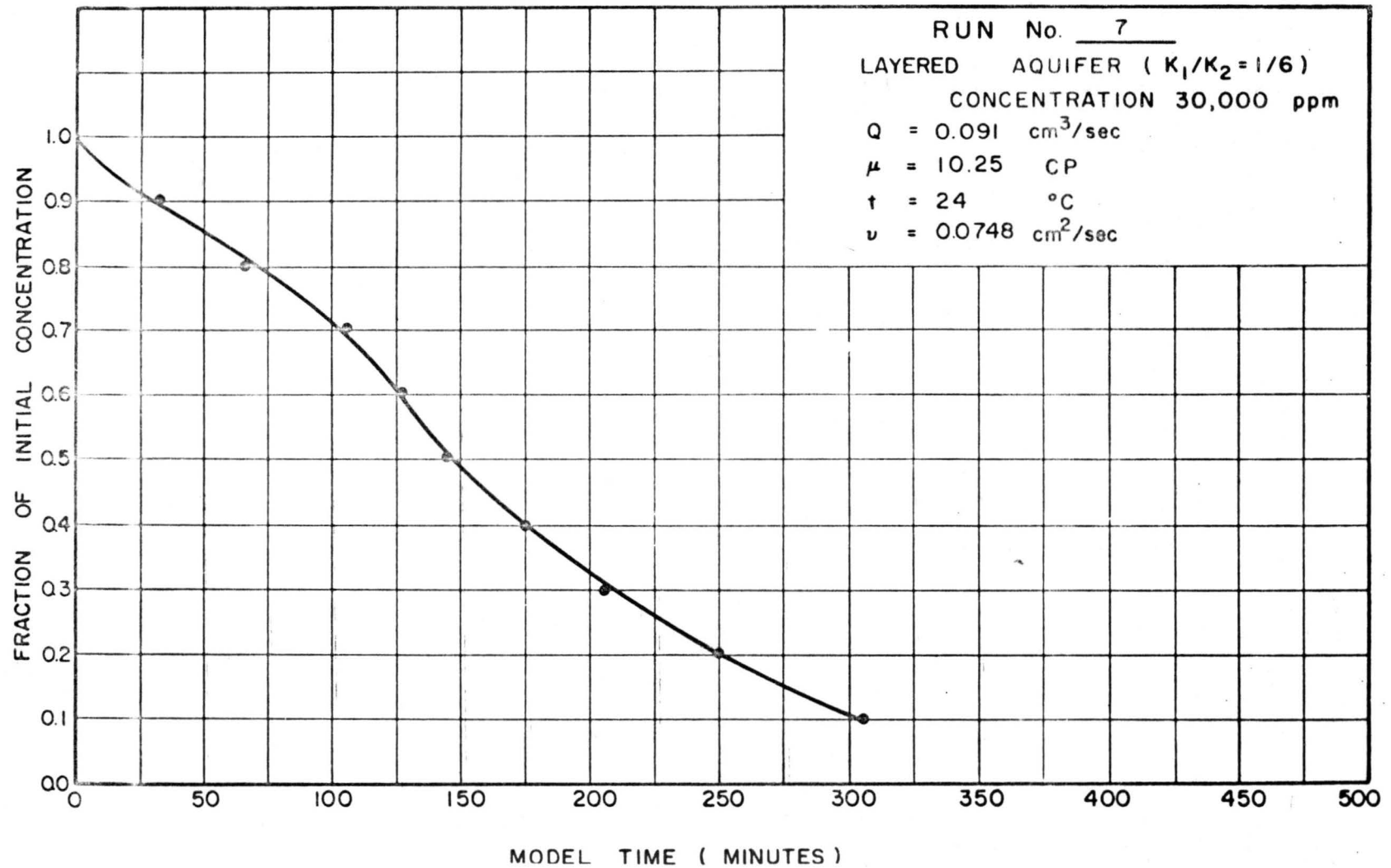


Fig. 78. Concentration versus time (Run 7, initial concentration 30,000 ppm, layered aquifer,  $K_1/K_2 = 1/6$ ).

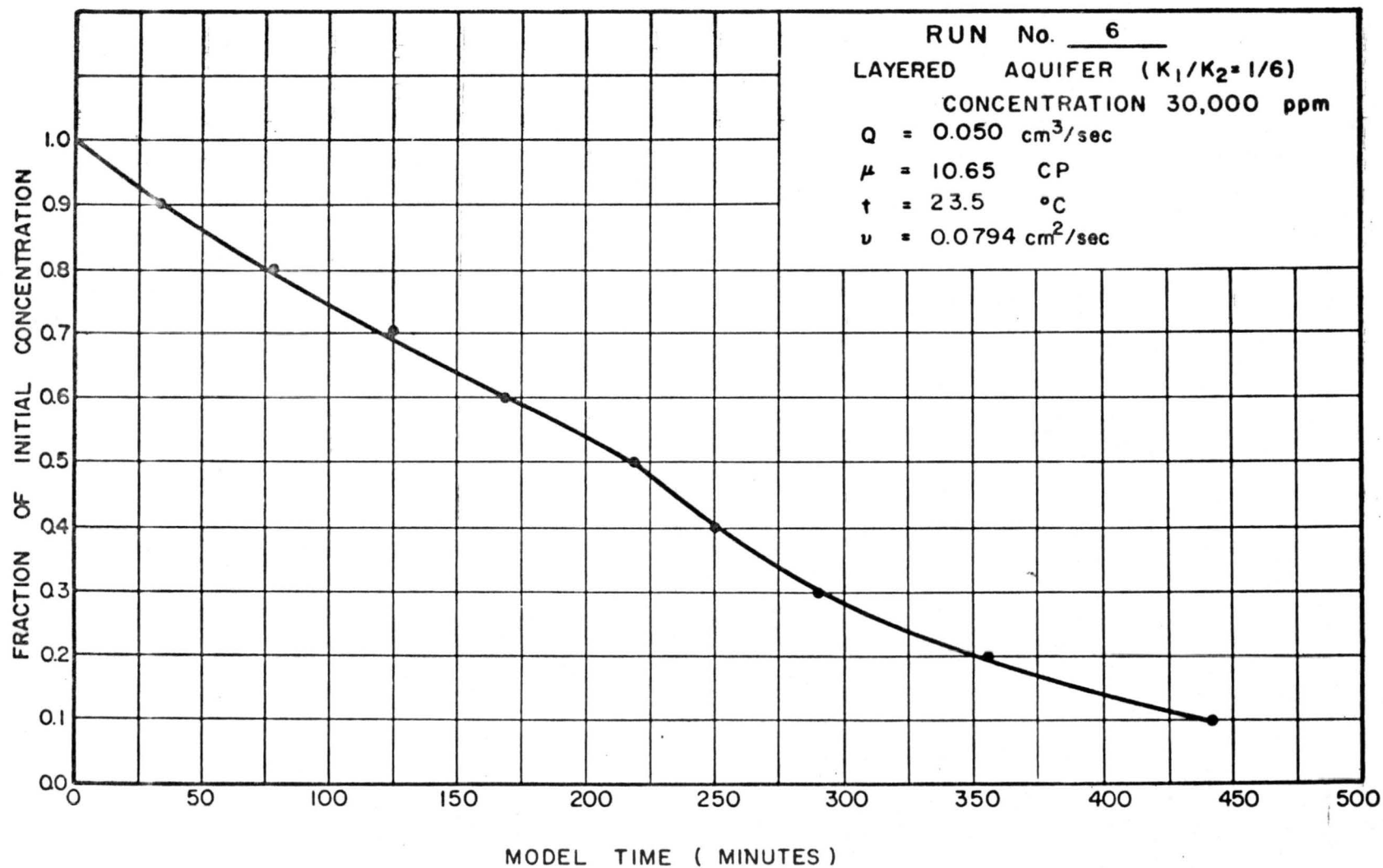


FIG. 19. Concentration versus time (Run 6, initial concentration 30,000 ppm, layered aquifer,  $K_1/K_2 = 1/6$ ).

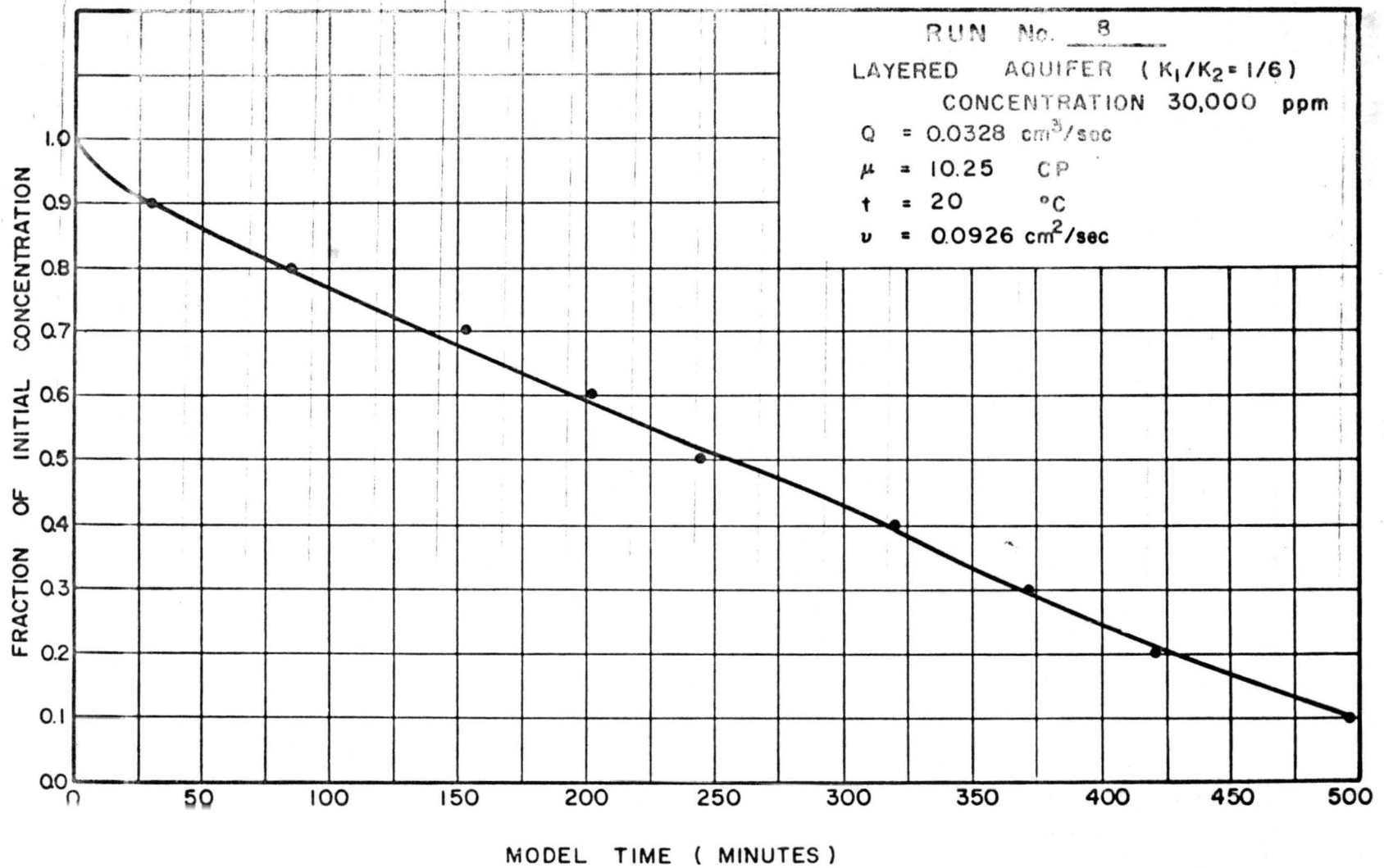


Fig. 30. Concentration versus time (Run 3, initial concentration 30,000 ppm, layered aquifer,  $K_1/K_2 = 1/6$ ).

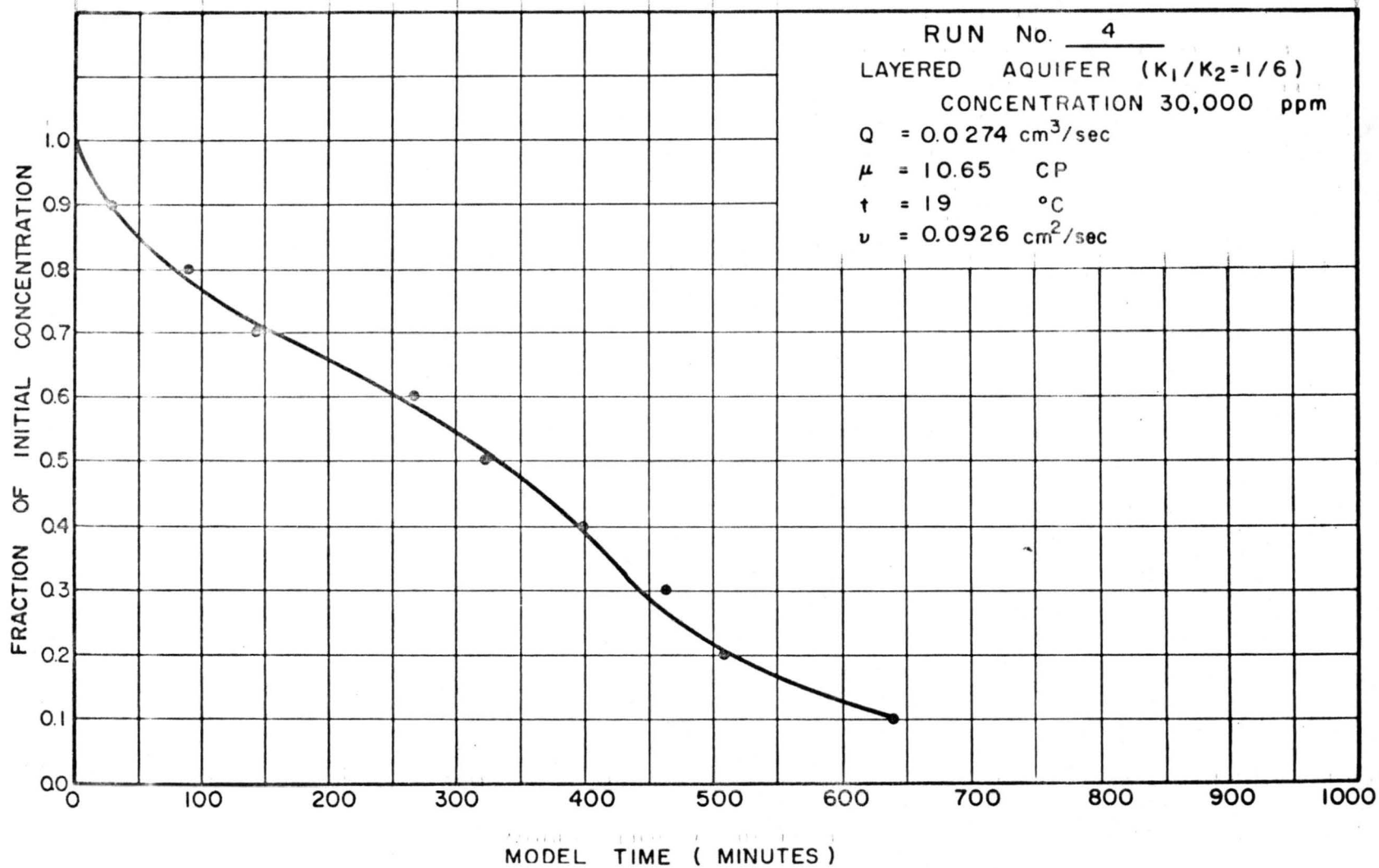


Fig. 31. Concentration versus time (Run 4, initial concentration 30,000 ppm.; layered aquifer,  $K_1/K_2 = 1/6$ ).

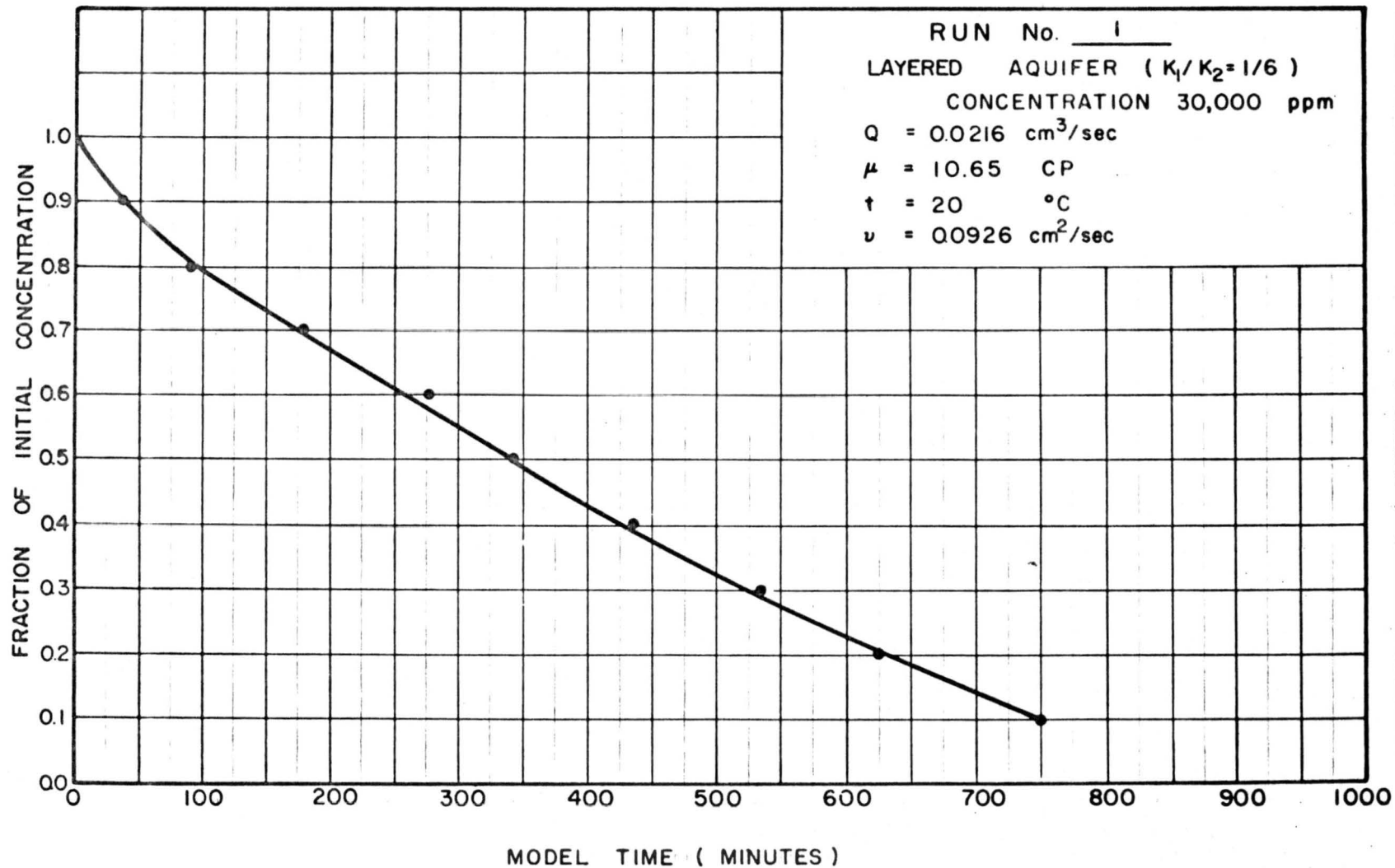


Fig. 32. Concentration versus time (Run 1, initial concentration 30,000 ppm, layered aquifer,  $K_1/K_2 = 1/6$ ).

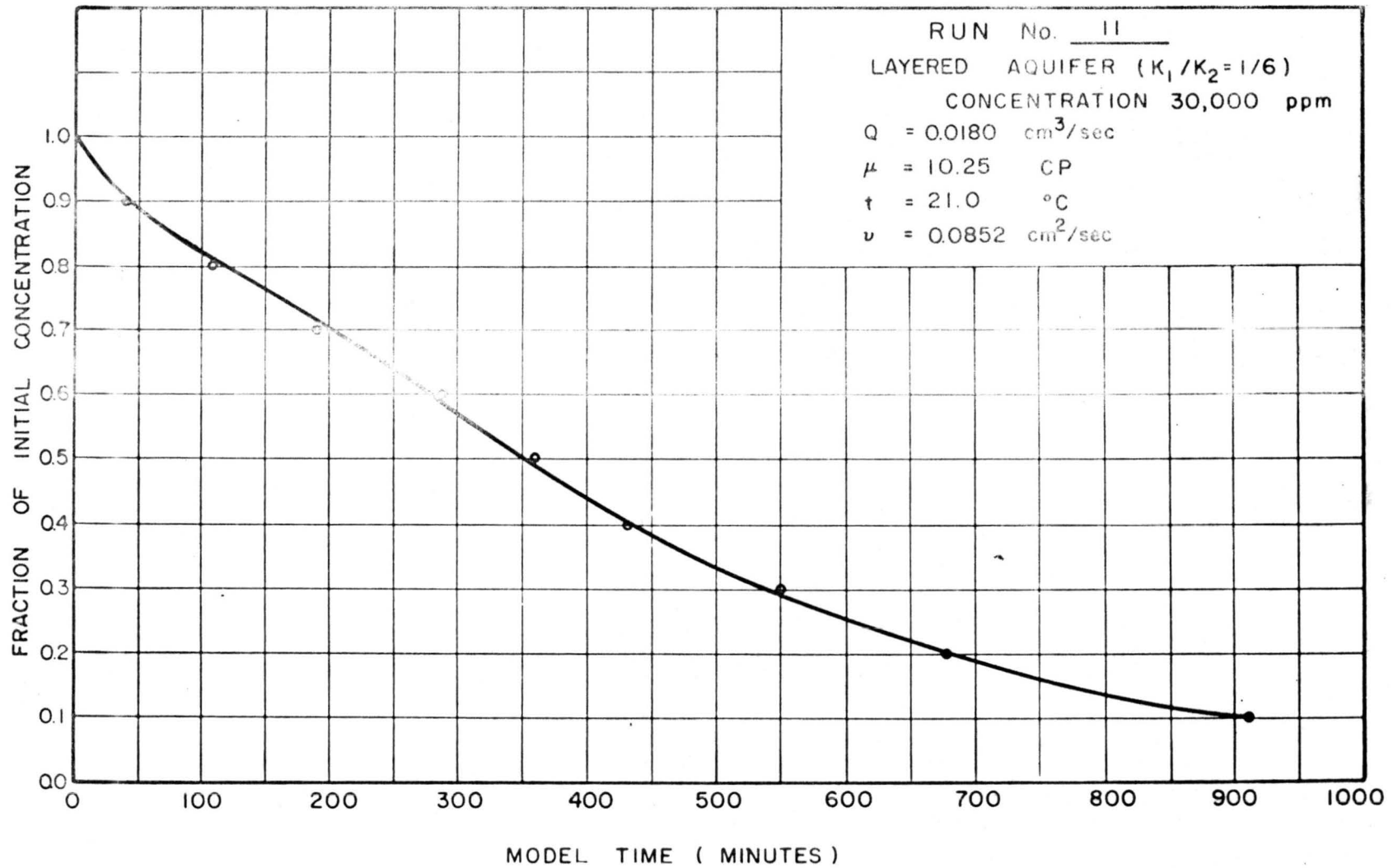


Fig. 83. Concentration versus time (Run 10, initial concentration 30,000 ppm, layered aquifer,  $K_1/K_2 = 1/6$ ).

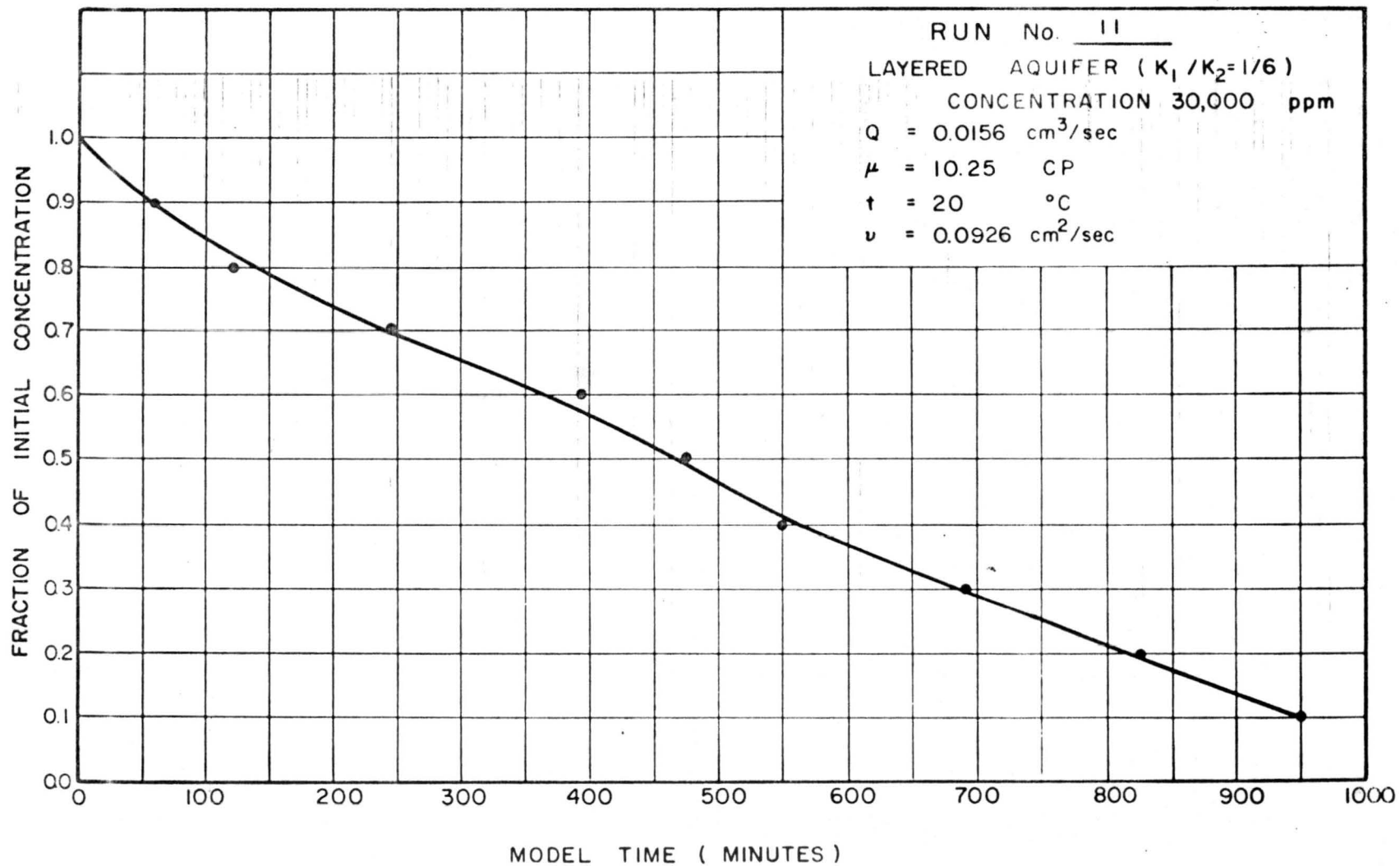


Fig. 34. Concentration versus time (Run 11, initial concentration 30,000 ppm, layered aquifer,  $K_1/K_2 = 1/6$ ).

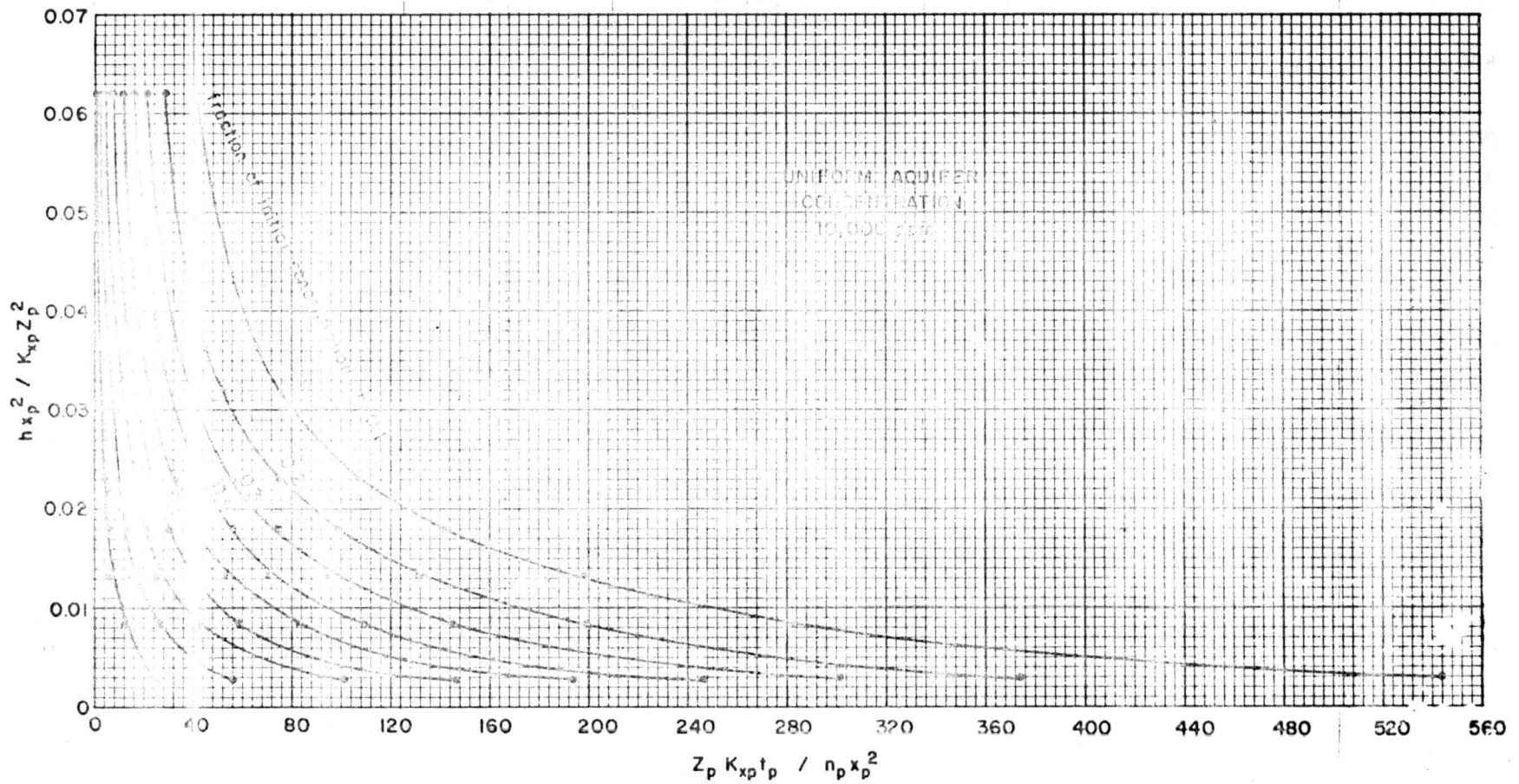


Fig. 85. Dimensionless chart of  $(h x_p^2)/(K_x p z_p^2)$  versus  $(z_p K_x p t_p)/(n_p x_p^2)$  uniform aquifer, initial concentration 10,000 ppm.

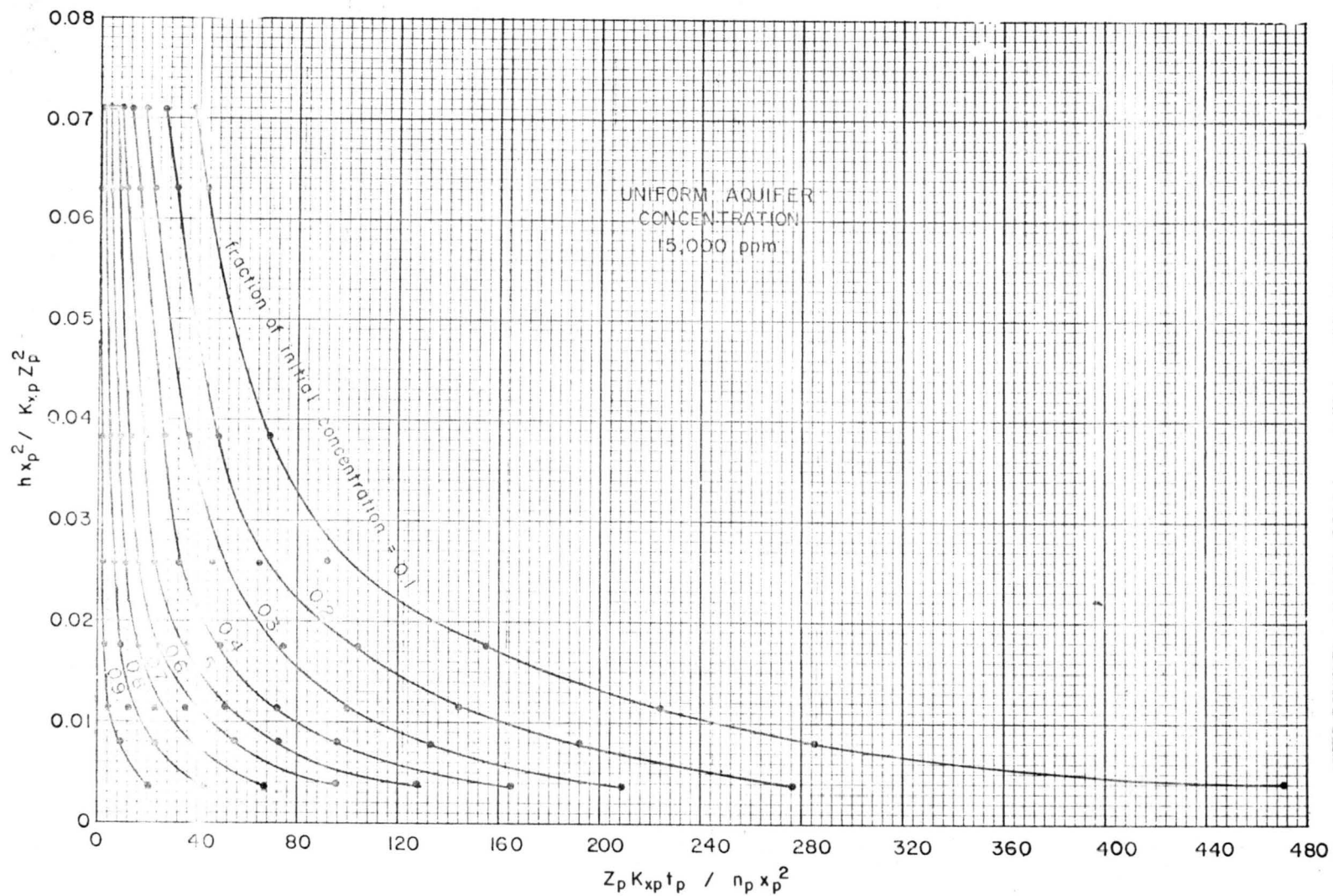


Fig. 36. Dimensionless chart of  $(h x_p^2) / (K_{xp} z_p^2)$  versus  $(z_p K_{xp} t_p) / n_p x_p^2$  (uniform aquifer, initial concentration 15,000 ppm).

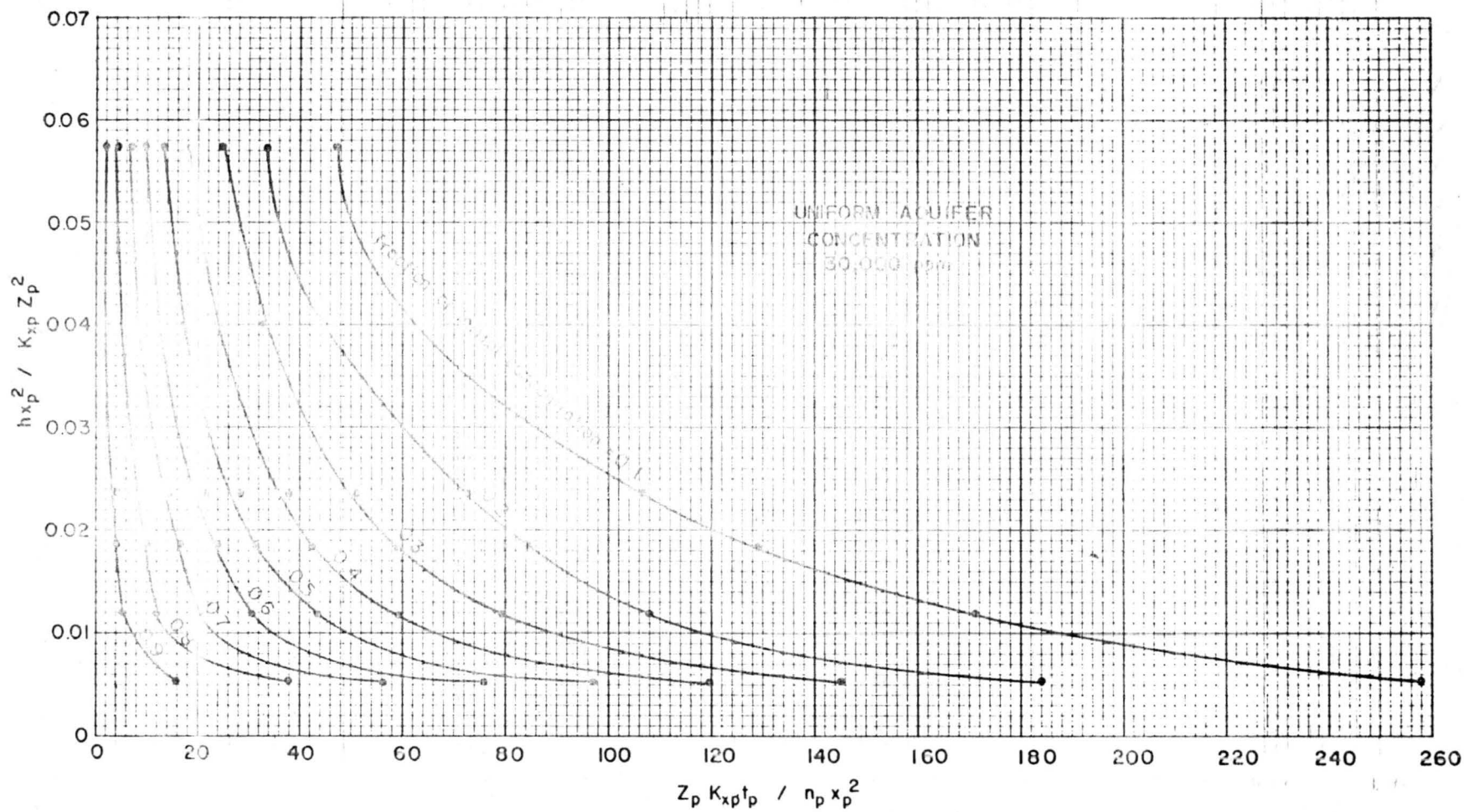


Fig. 37. Dimensionless chart of  $(h x_p^2) / K_{xp} z_p^2$  versus  $(z_p K_{xp} t_p) / (n_p x_p^2)$  (uniform aquifer, initial concentration 30,000 ppm).

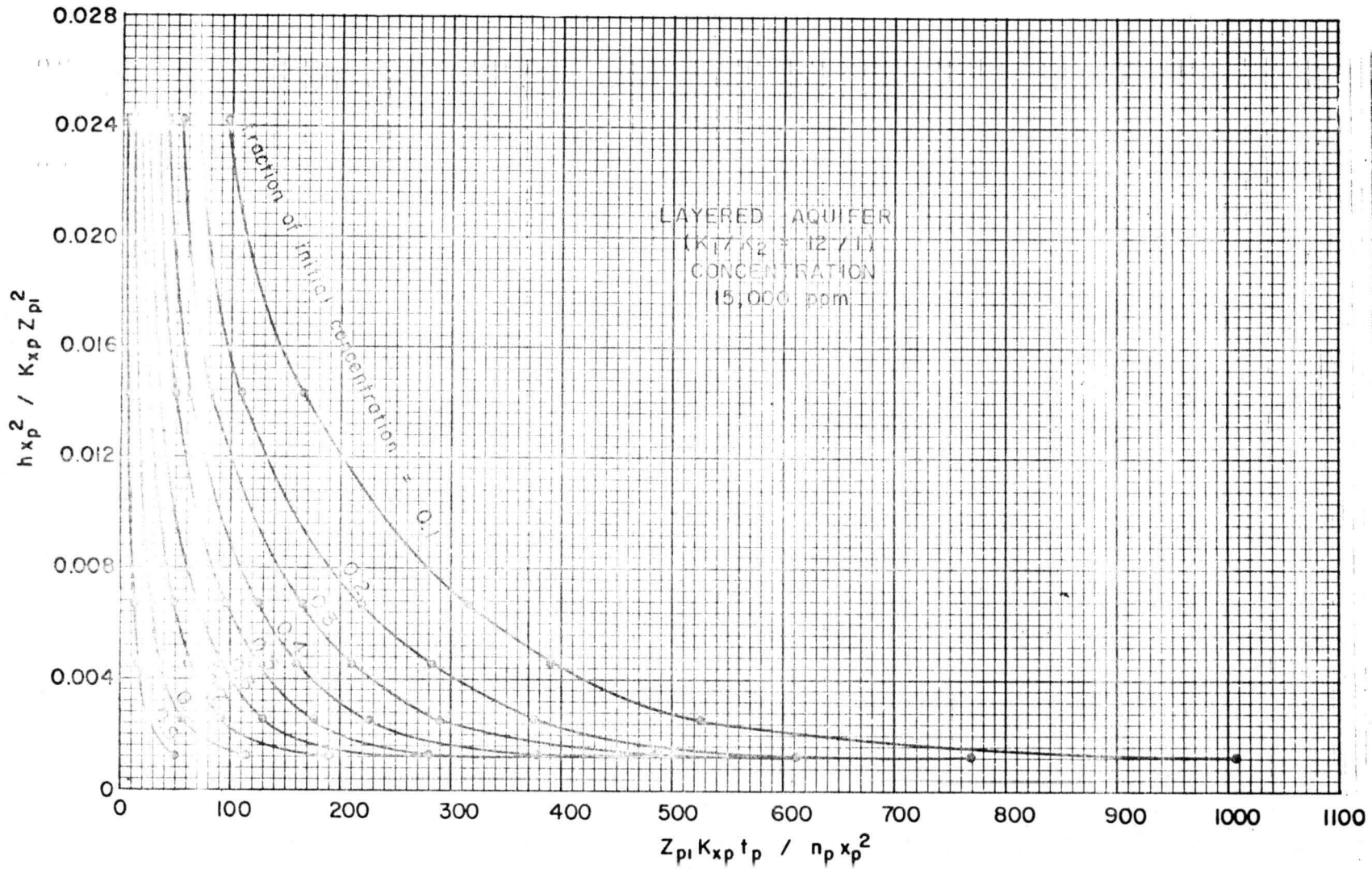


Fig. 83. Dimensionless chart of  $(hx^2)/K_{xp}z_{p1}^2$  versus  $z_{p1}K_{xp}t_p/n_p x_p^2$  (layered aquifer,  $K_1/K_2 = 12/1$ , initial concentration 15,000 ppm).

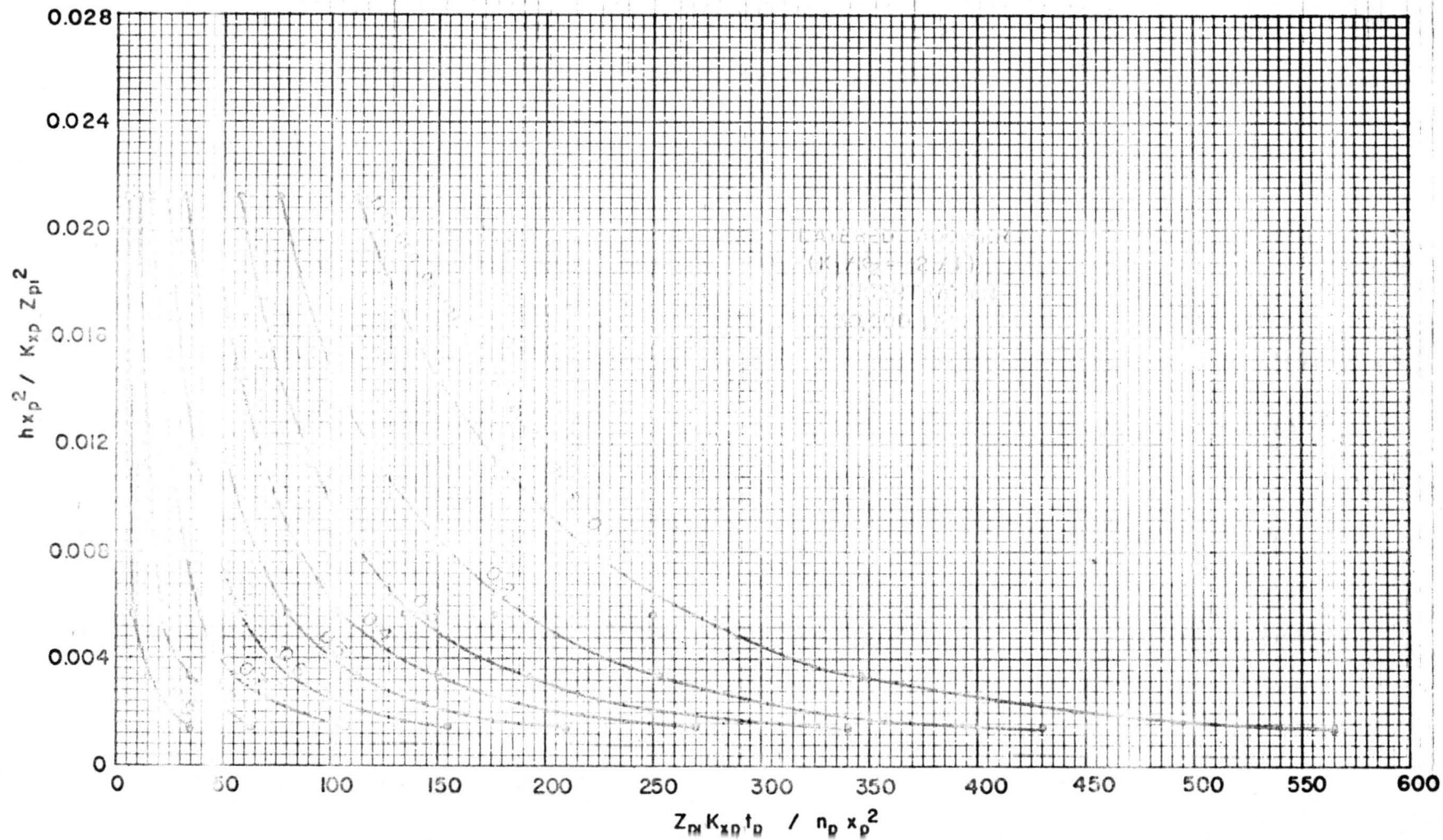


Fig. 89. Dimensionless chart of  $(h x_p^2) / (K_{xp} z_{p1}^2)$  versus  $(z_{p1} K_{xp} t_p) / (n_p x_p^2)$  layered aquifer,  $K_1 / K_2 = 12/1$ , initial concentration 30,000 ppm.

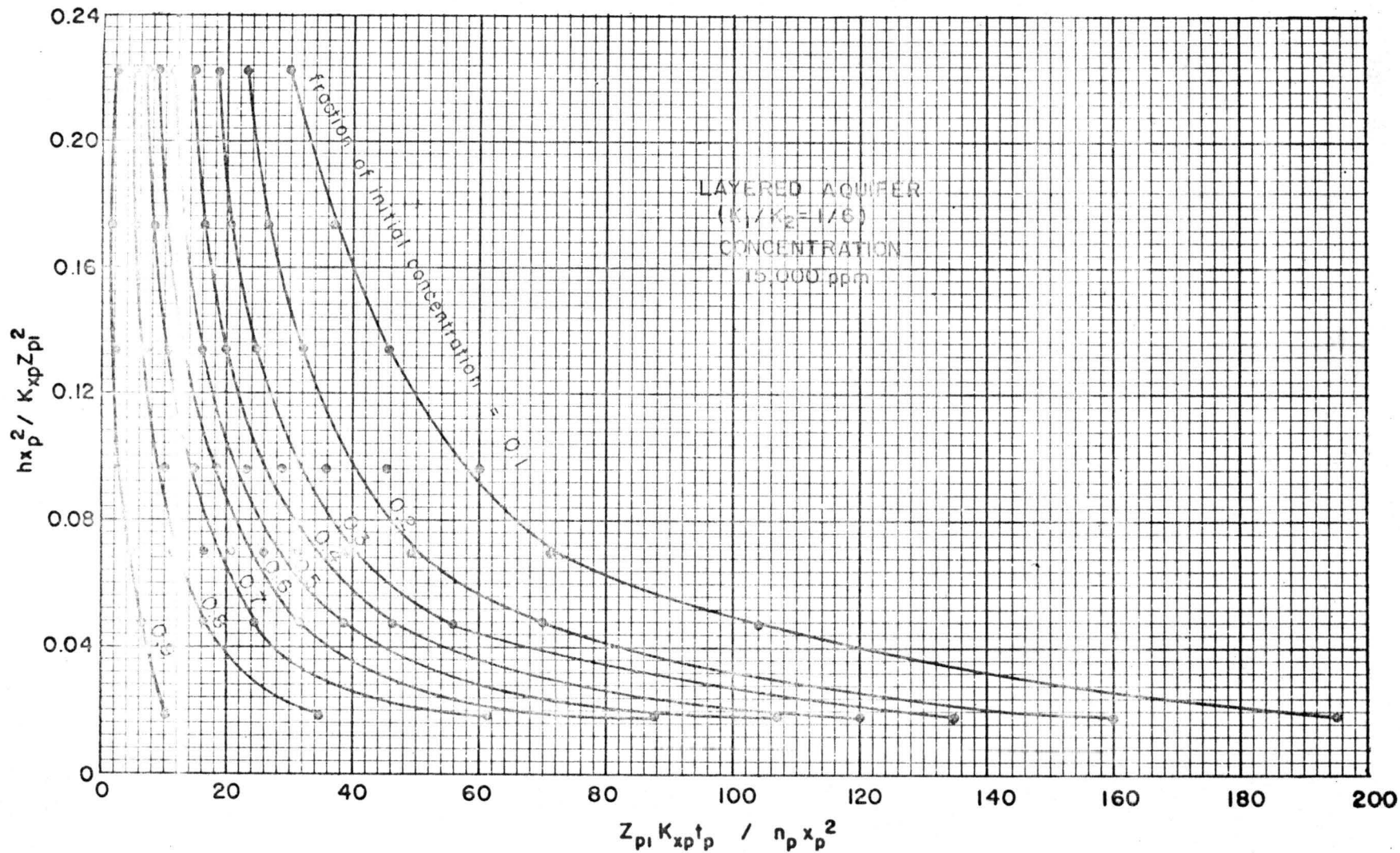


Fig. 90. Dimensionless chart of  $(hx_p^2)/(K_x p z_{p1}^2)$  versus  $(z_{p1} K_x p t_p)/(n_p x_p^2)$  (layered aquifer,  $K_1/K_2 = 1/6$ , initial concentration 15,000 ppm).

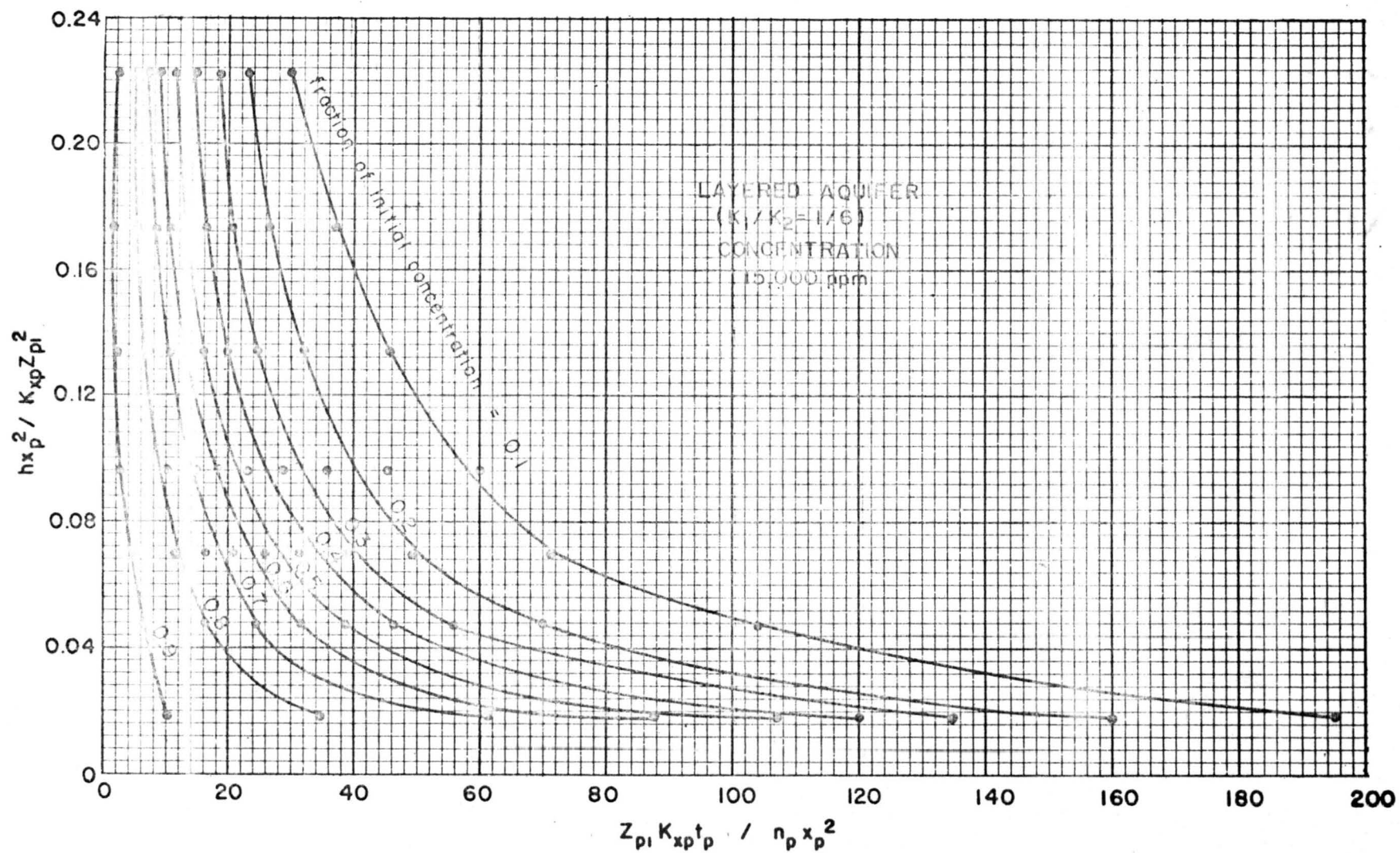


Fig. 90. Dimensionless chart of  $(hx_p^2)/(K_x p z_{p1}^2)$  versus  $(z_{p1} K_x p t_p)/(n_p x_p^2)$  (layered aquifer,  $K_1/K_2 = 1/6$ , initial concentration 15,000 ppm).

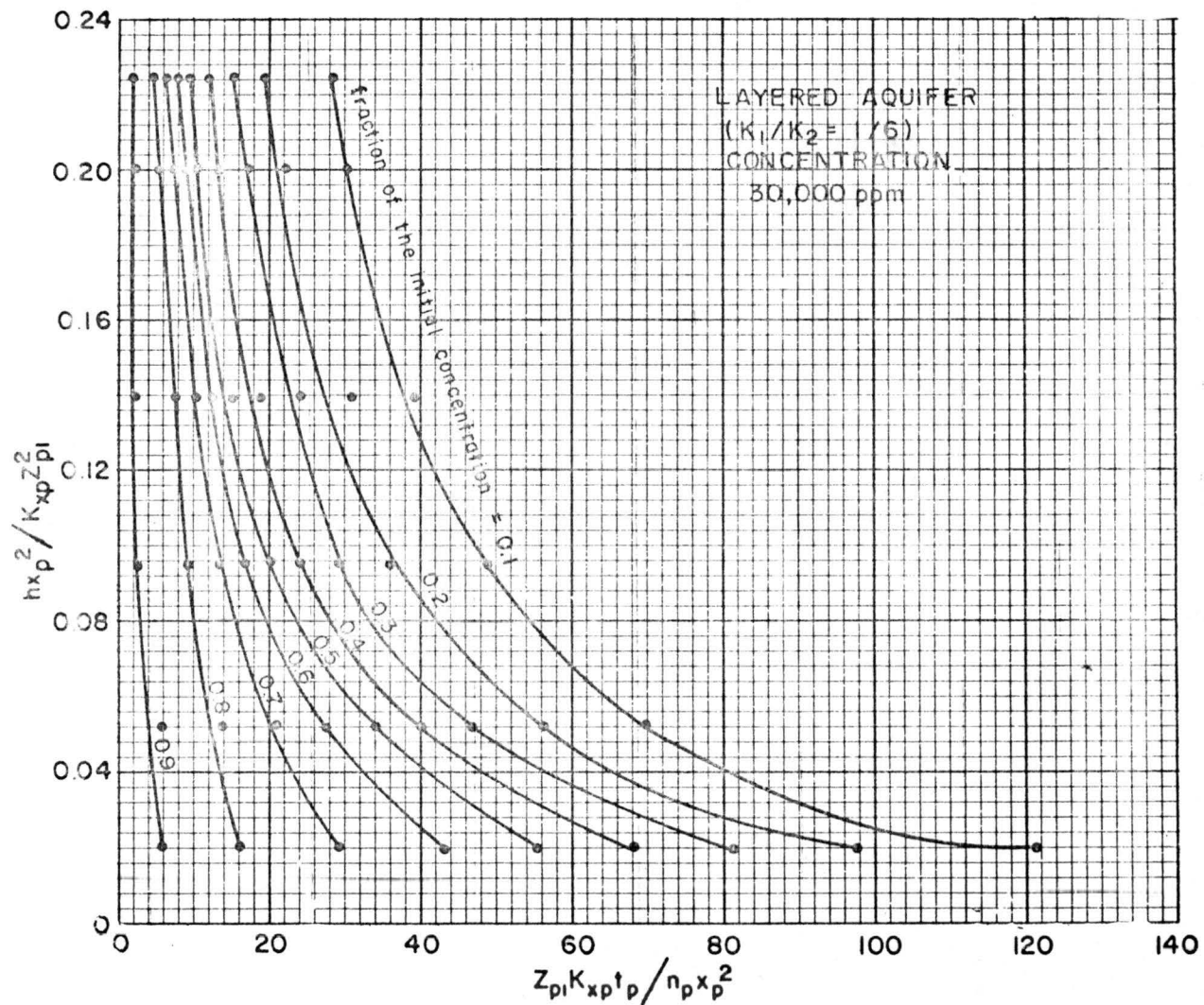


Fig. 91. Dimensionless chart of  $(hx_p^2)/(K_{xp} z_{pi}^2)$  versus  $(z_{pi} K_{xp} t_p)/(n_p x_p^2)$  (layered aquifer,  $K_1/K_2 = 1/6$ , initial concentration 30,000 ppm).

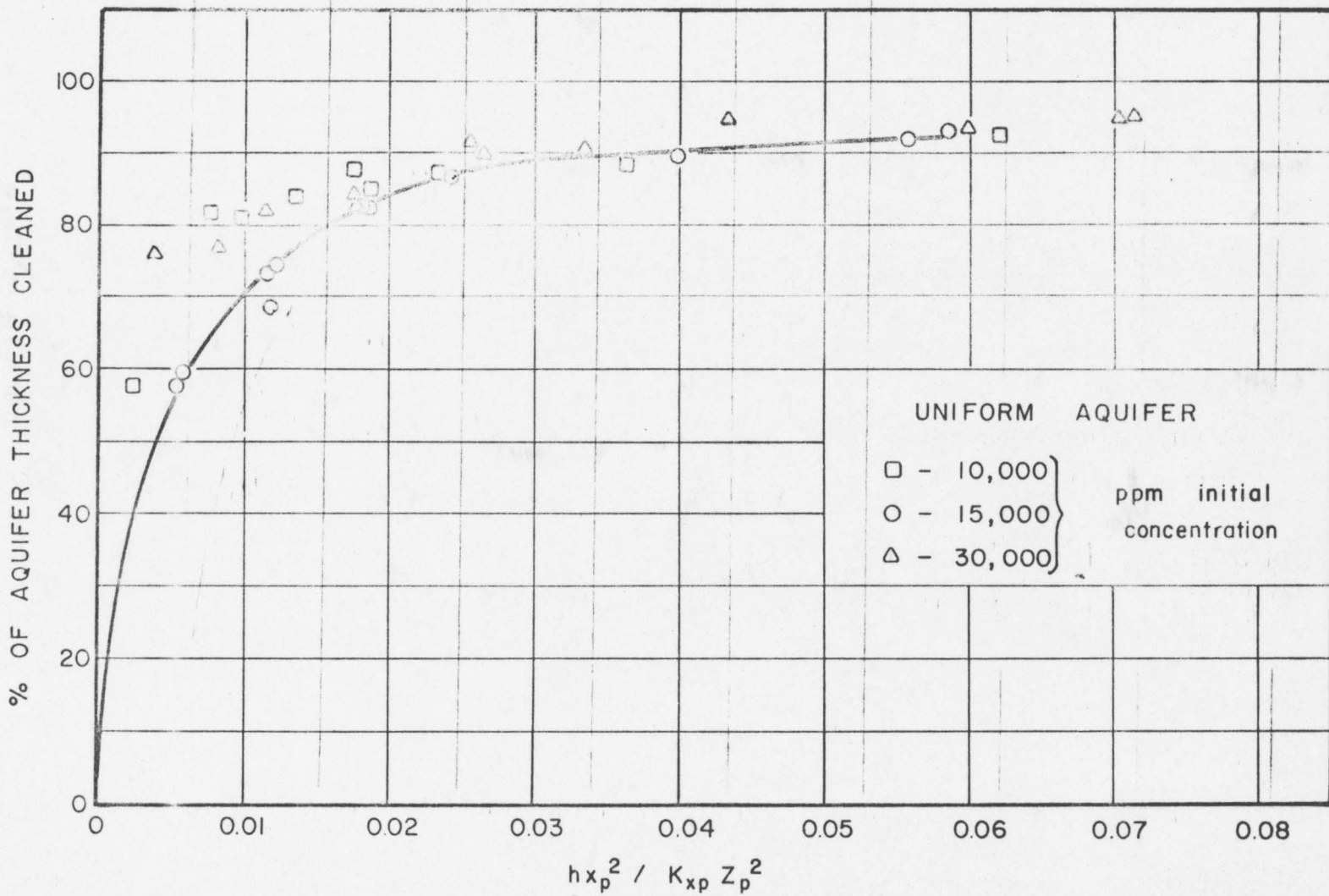


Fig. 92. Percent of aquifer thickness cleaned versus  $(hx_p^2)/(K_{xp} z_p^2)$  (uniform aquifer).

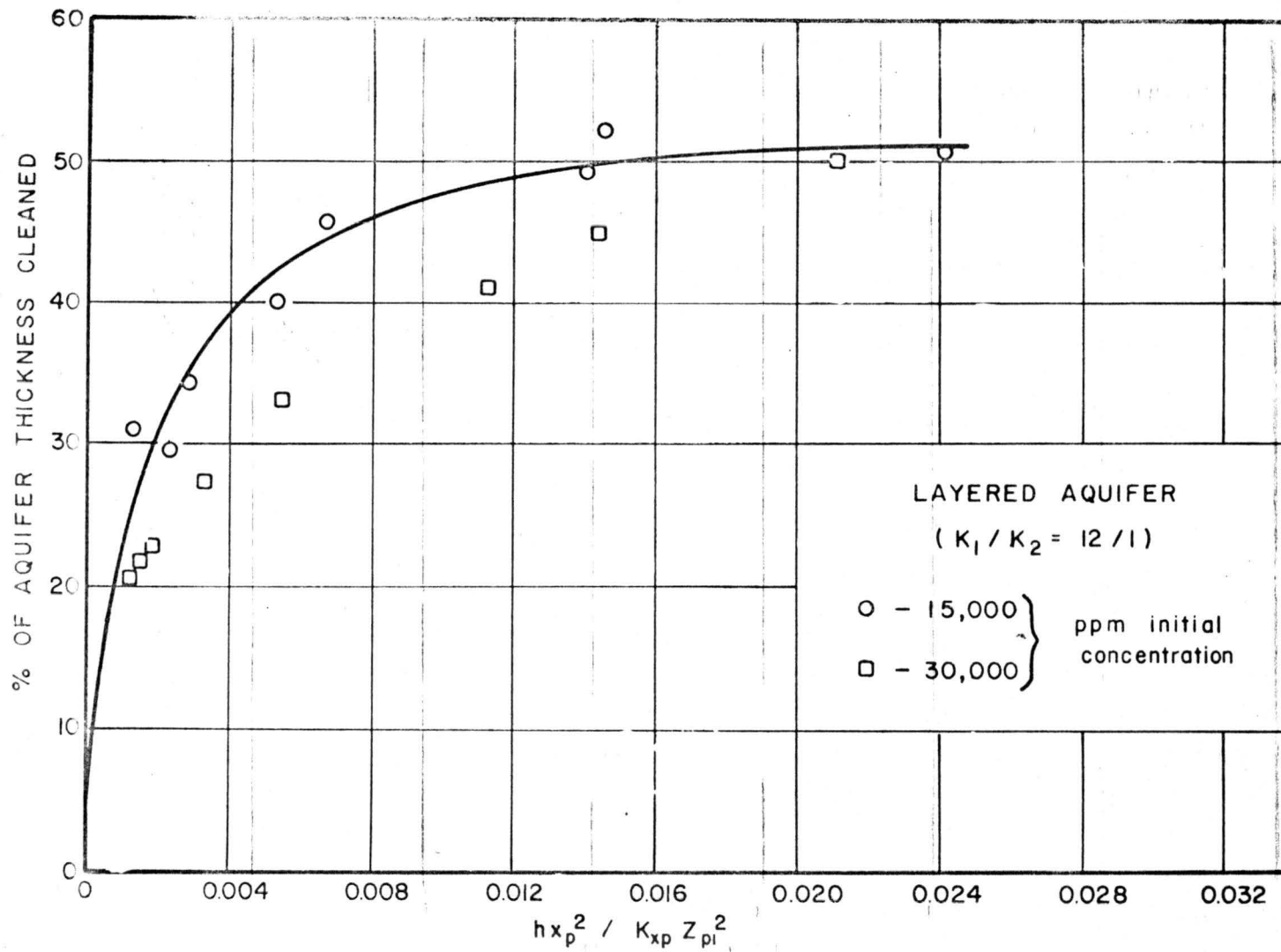


Fig. 93. Percent of aquifer thickness cleaned versus  $(hx_p^2)/(K_{xp} z_{p1}^2)$  (layered aquifer  $K_1/K_2 = 12/1$ ).

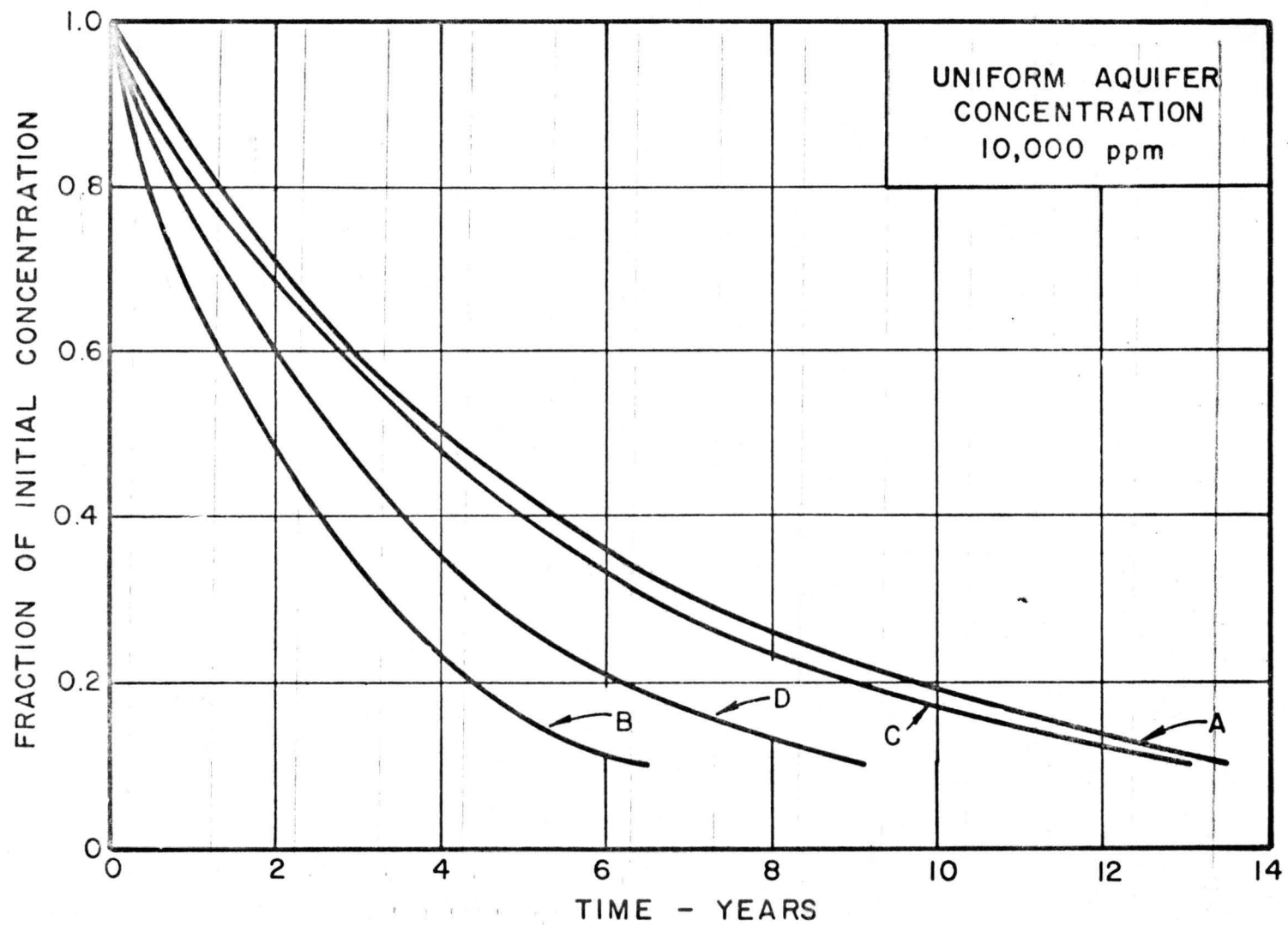


Fig. 94. Concentration versus time for some specific conditions (uniform aquifer, initial concentration, 10,000 ppm).

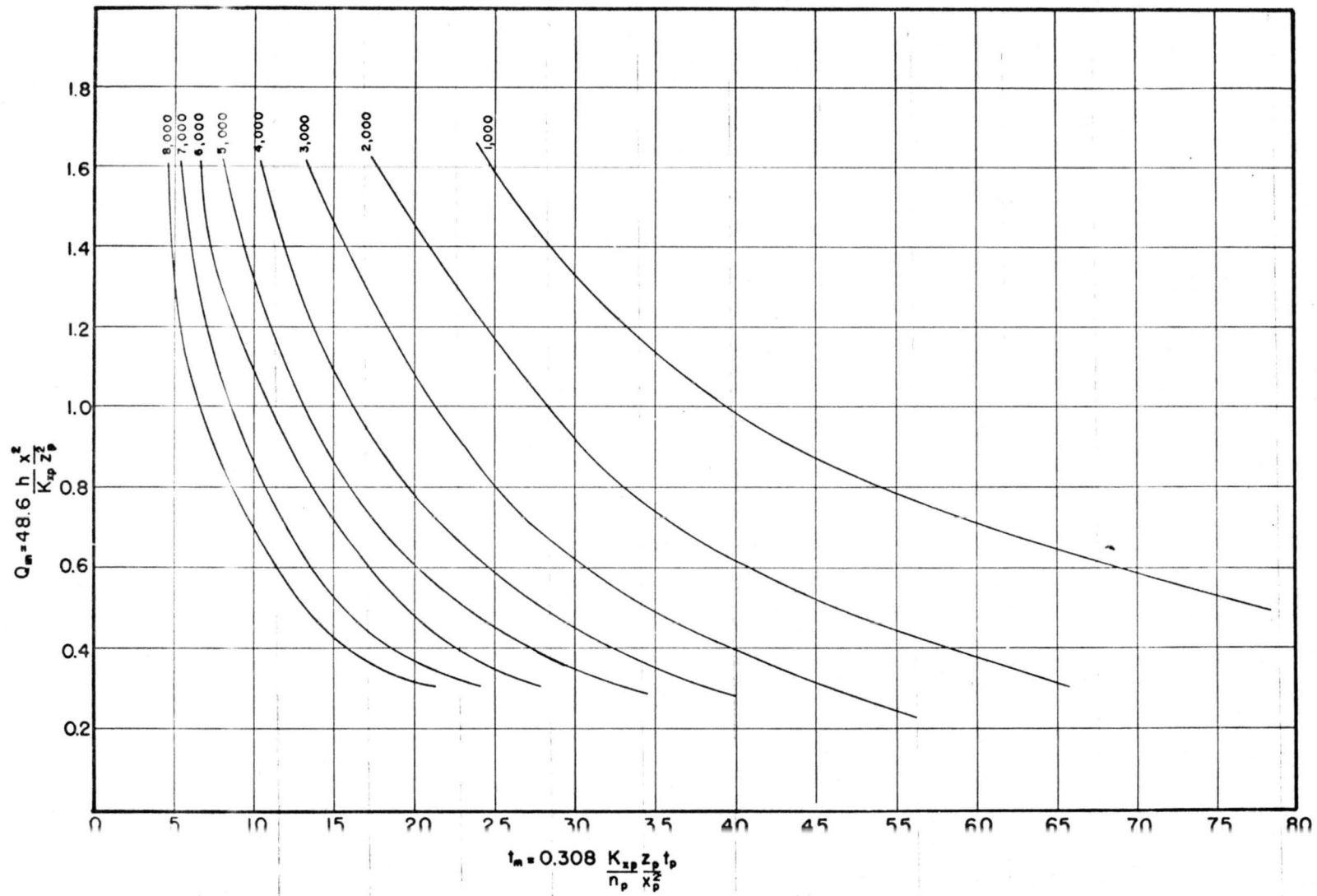


Fig. 95. Model discharge versus model time (uniform aquifer, water experiments).

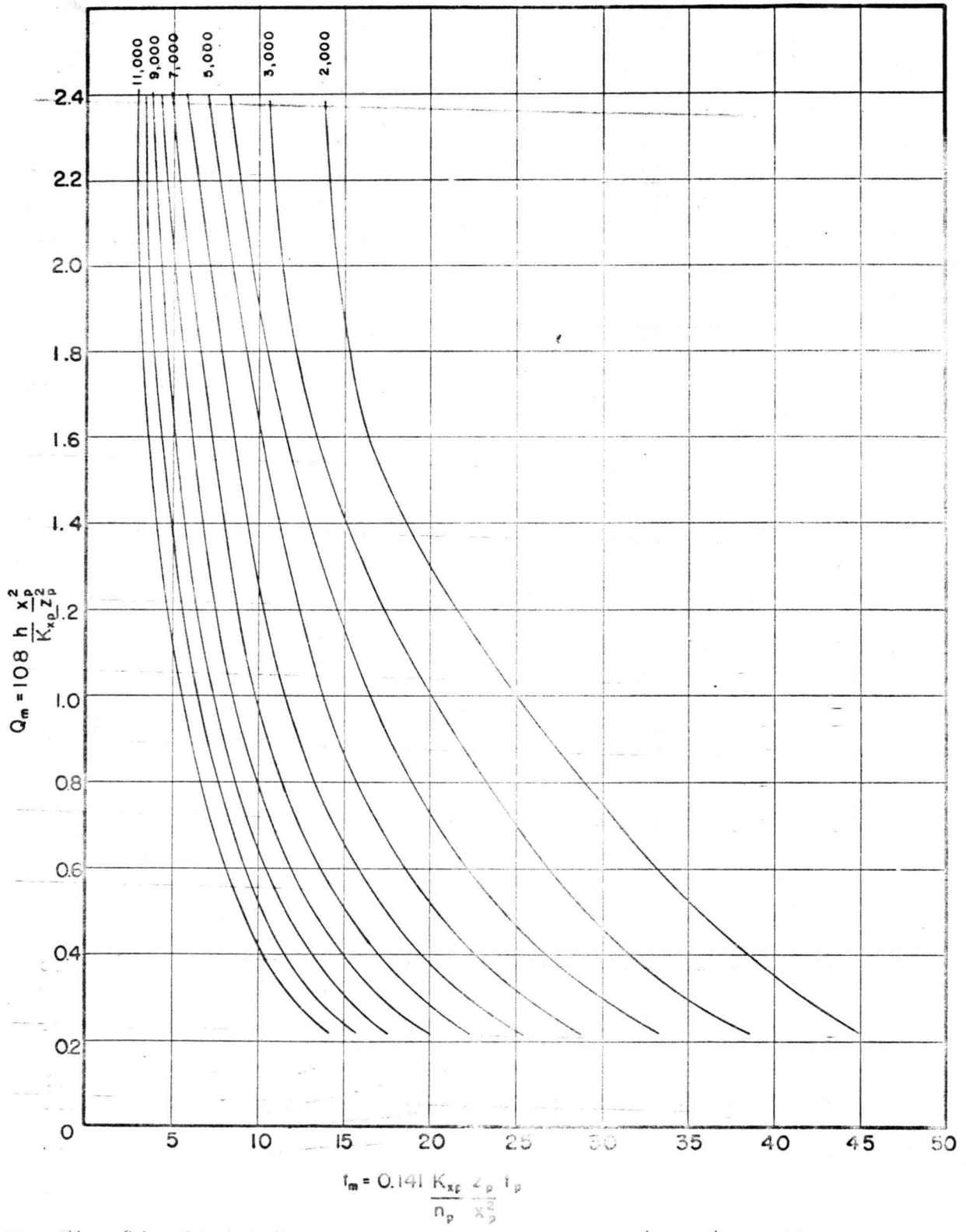


Fig. 96.—Model discharge versus model time (10.5/1 aquifer, water experiments).

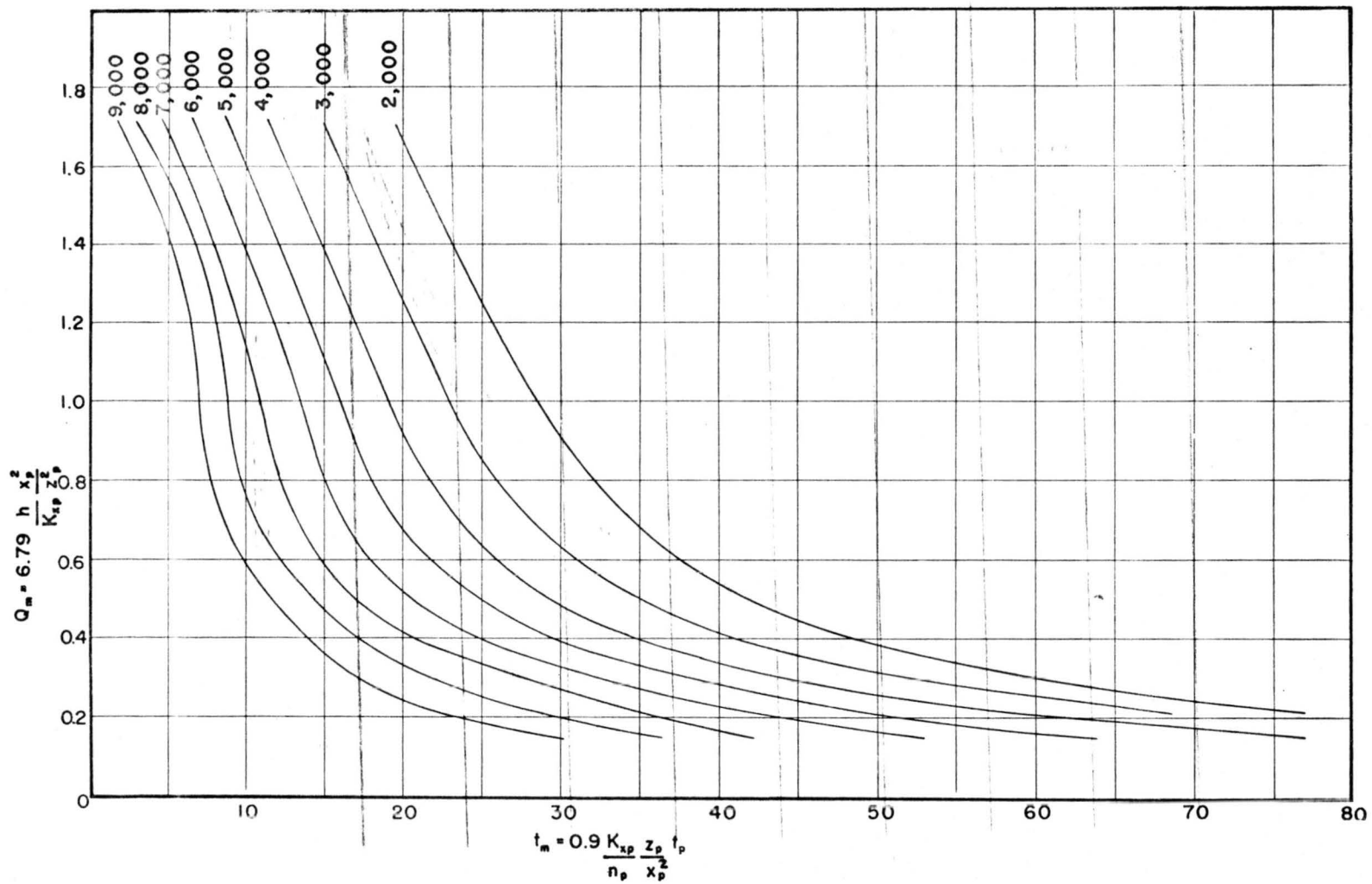


Fig. 97. Model discharge versus model time (1/11.5 aquifer, water experiments).

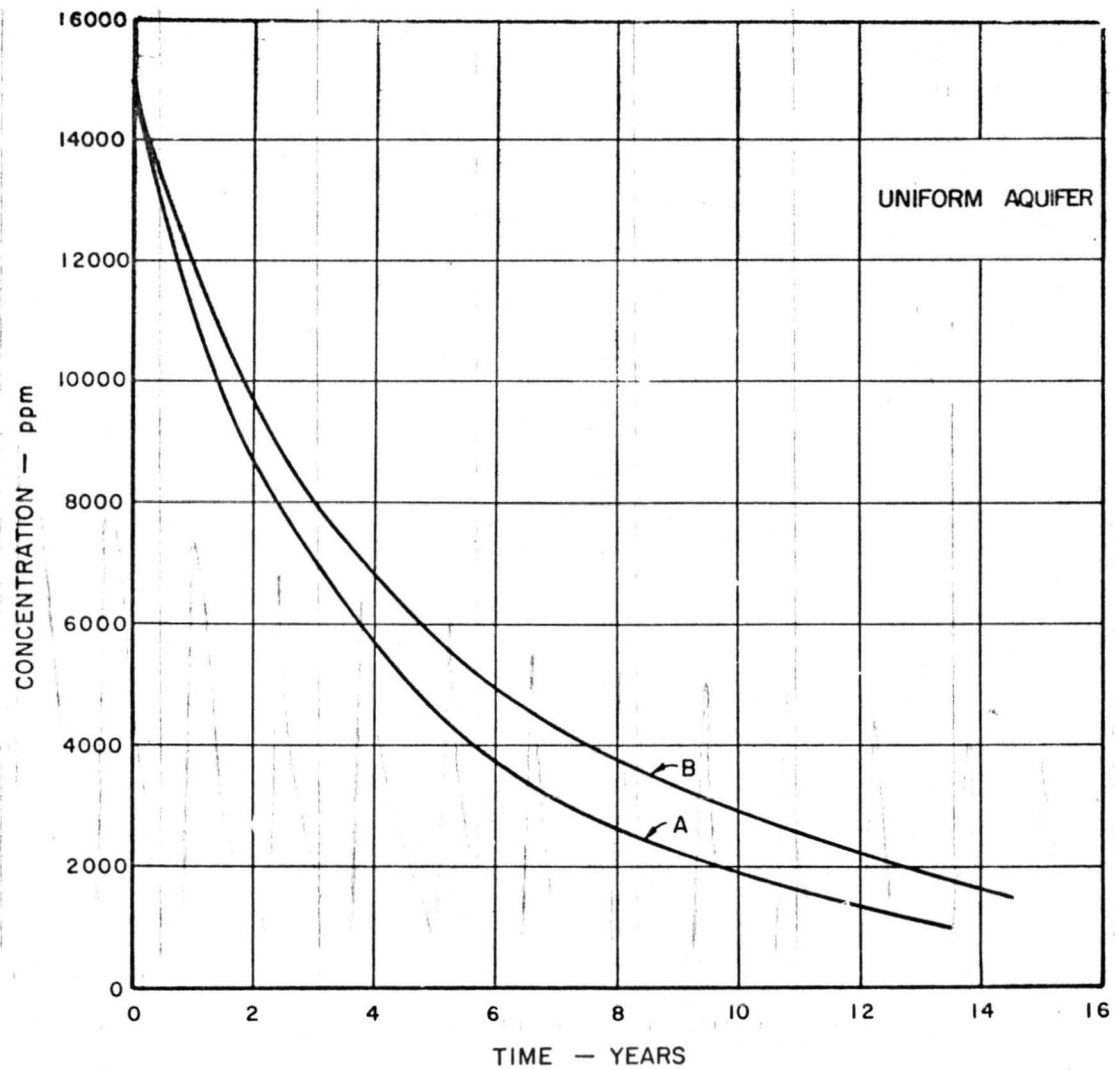


Fig. 98. Effluent concentration versus time.

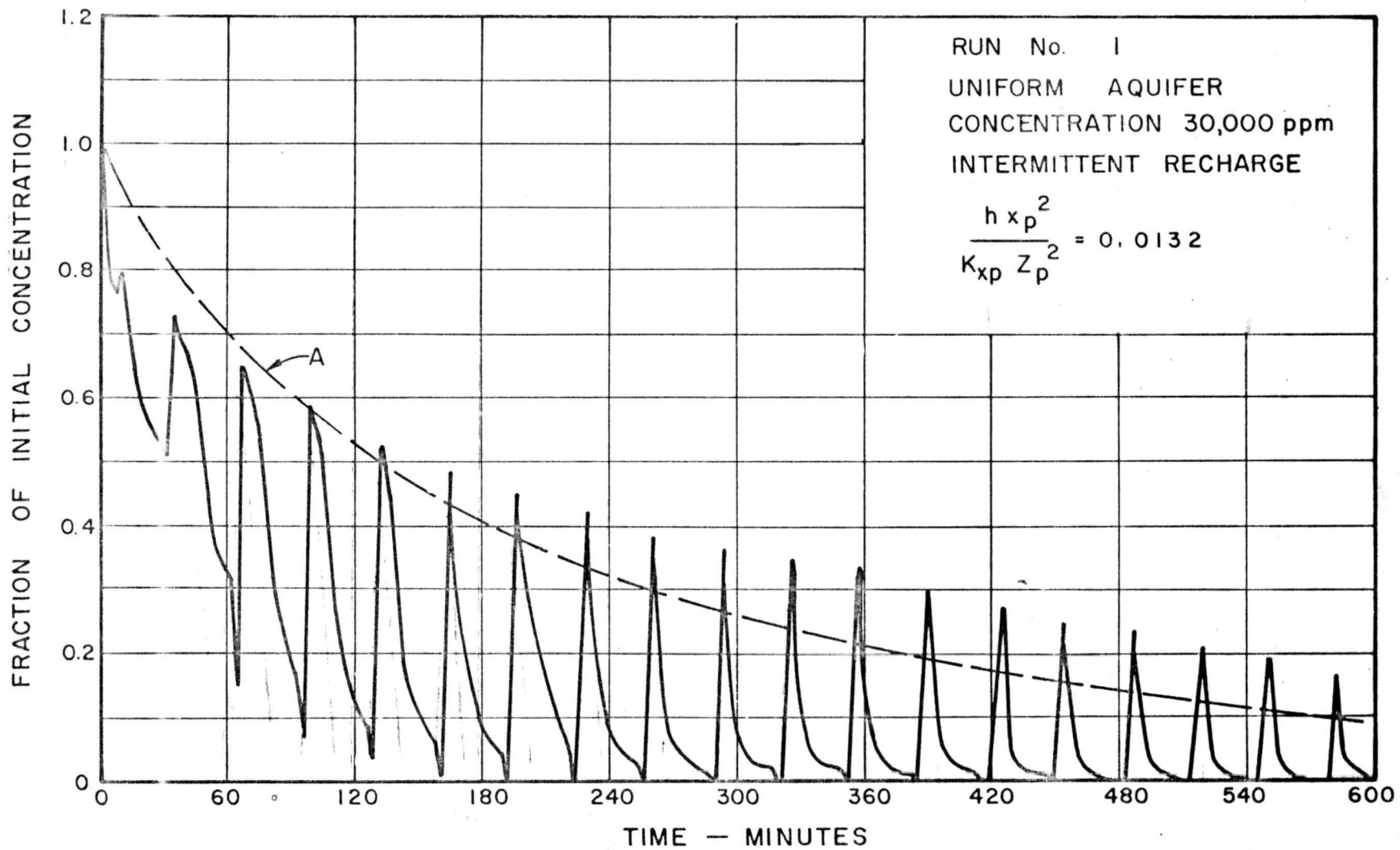


Fig. 99. Effluent concentration versus time (intermittent versus continuous recharge, initial concentration 15,000 ppm).

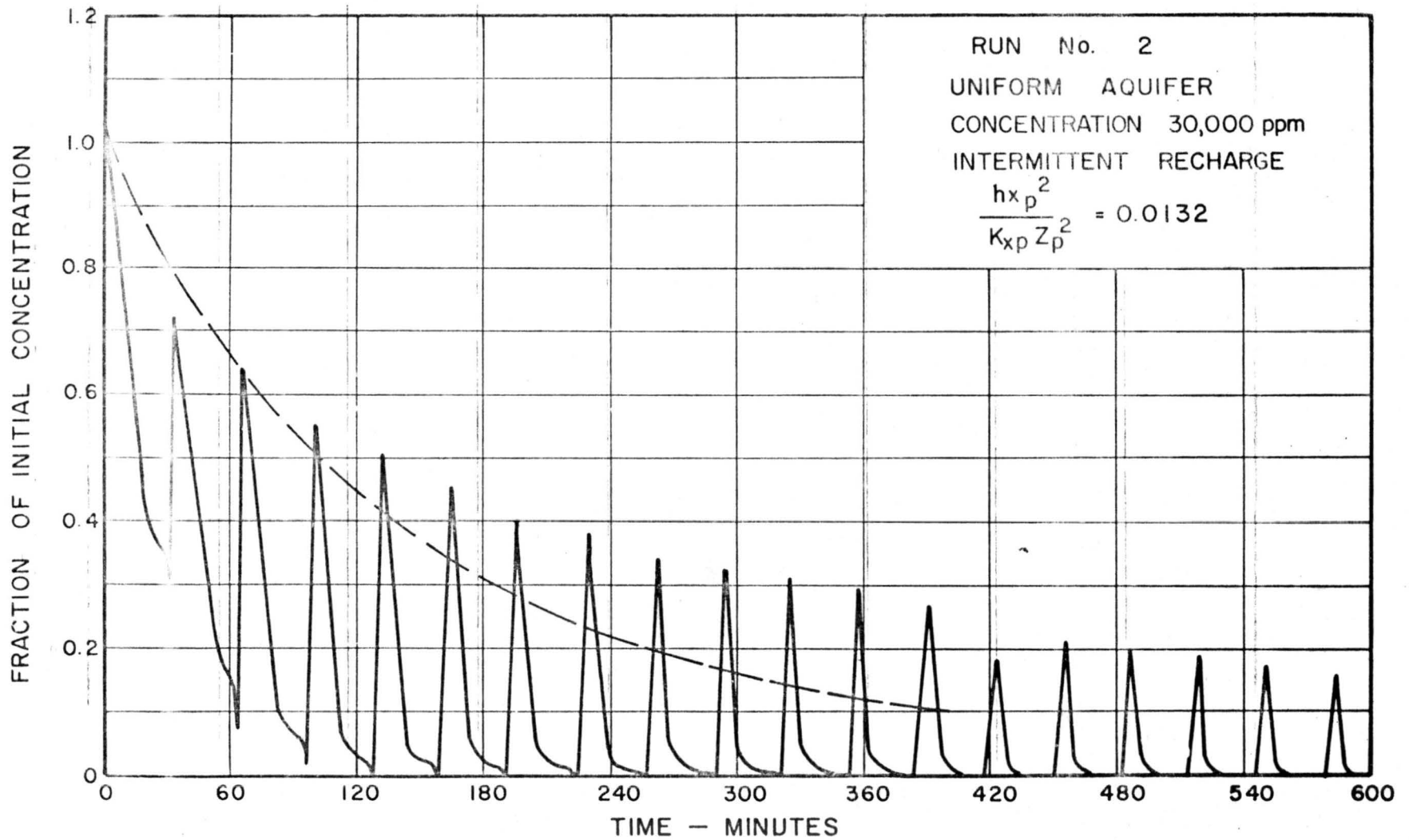


Fig. 100. Effluent concentration versus time (intermittent versus continuous recharge, initial concentration 30,000 ppm).

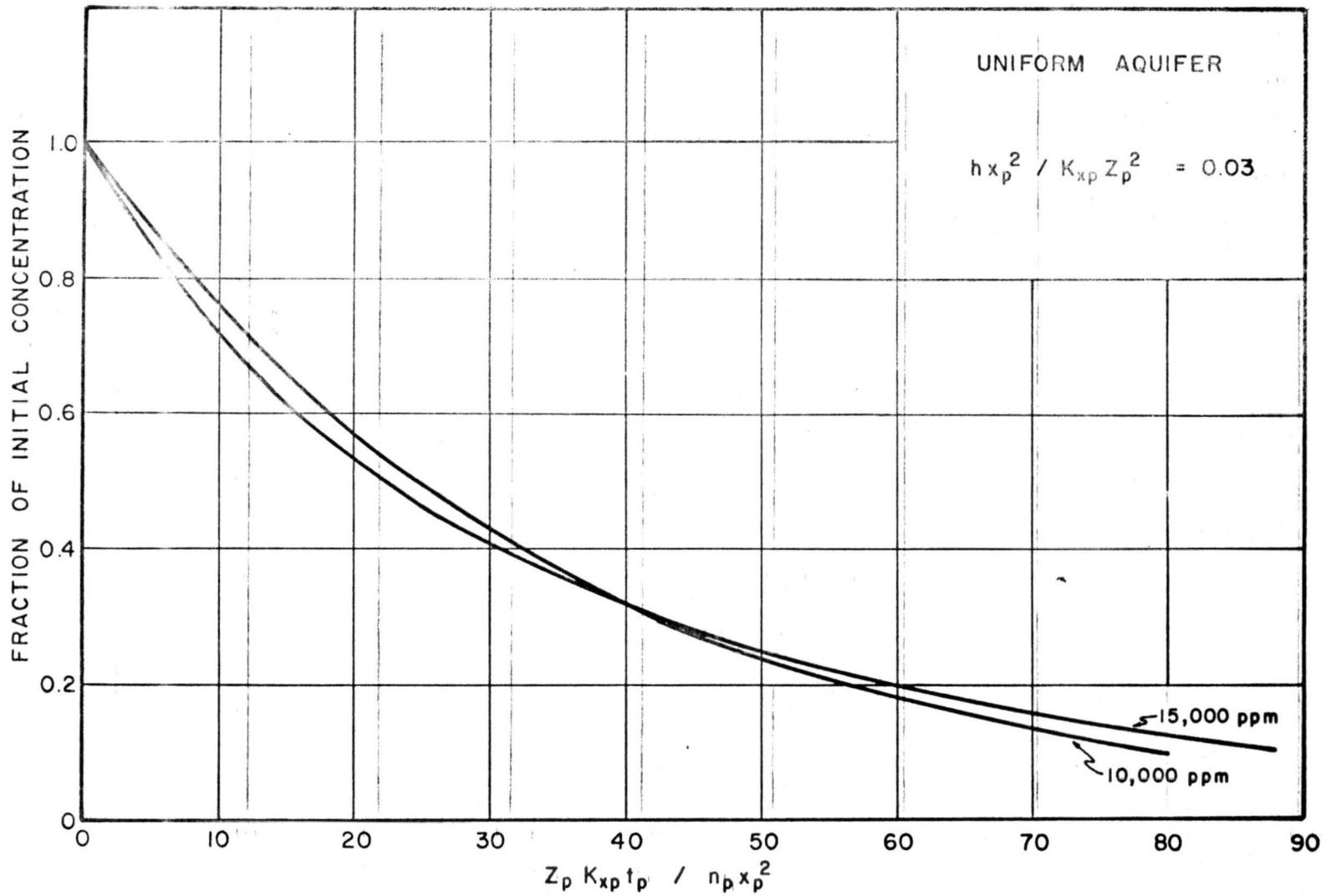


Fig. 101. Effluent concentration versus  $(z_p K_{xp} t_p) / (n_p x_p^2)$  for different values of initial concentration.

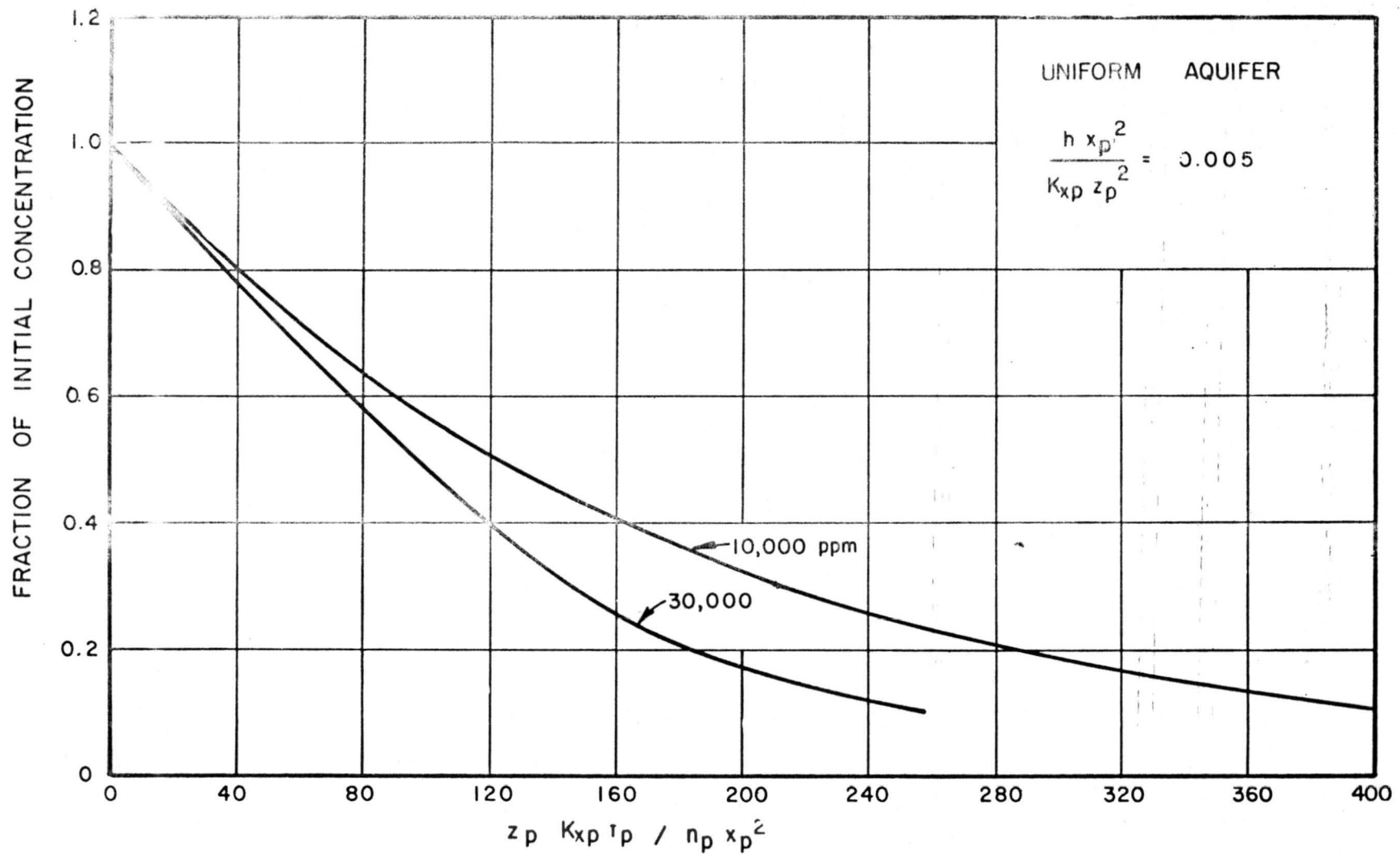


Fig. 102. Effluent concentration versus  $(z_p K_{xp} t) / (n_p x_p^2)$  for different values of initial concentration.

Final Report Supplement

COMPARISON OF VISCOUS ANALOGY MODEL  
RESULTS WITH USBR SAND TANK STUDIES

by

M. W. Bittinger and D. E. L. Maasland

## Introduction and Additional Objectives

Additional objectives of the studies performed under Contract Number 14-06-D-5254 included a comparison of results obtained from the Colorado State University Hele-Shaw Model with similar studies performed by the Bureau of Reclamation using a sand-tank model. At the time of the writing of Mr. Maasland's dissertation, results of the USBR studies were not available, therefore this supplement is attached in order to complete the final report.

## Description of U.S. Bureau of Reclamation Studies

Eight tests, using a sand-tank model, were conducted in 1963 by USBR Hydraulics Laboratory personnel. The tank was 15.71 feet long by 2.5 feet wide and 2.5 feet deep. Drains were placed by each end and at the center of the tank, thus providing drain spacings of 31.42, 15.71 and 7.86 feet by allowing one, two or three drains to flow. Sand with a permeability of about 17,200 feet per year was used to a depth of 2 feet for runs in which a uniform aquifer was simulated. For runs simulating a layered aquifer the lower one-half consisted of sand having a permeability of about 50 times that of the upper one-half. Initial concentrations of water stored in the aquifer ranged from about 4000 to 80,000 ppm of total dissolved solids. As with the CSU Hele-Shaw tests, water having a negligible concentration of dissolved solids was used for recharge.

Uniform Aquifer Comparisons

Run No. 7 by the Bureau of Reclamation utilized a uniform aquifer with an initial salinity in the aquifer of 79,770 ppm of total dissolved solids. The Hele-Shaw model at CSU was modified to duplicate the geometry of the sand-tank model as nearly as possible. Table 1 summarizes dimensions and flow rates of the two models and the prototype which both models represented. Four runs were made on the Hele-Shaw model using recharge rates representing from 2.3 to 3.5 ft/yr in the prototype. A comparison of results in terms of the initial concentration versus prototype time is shown in Figure 1.

The two curves represent average results from the USBR (three drains) and CSU (4 runs) models. Zero time did not correspond, so results from the Hele-Shaw model were adjusted so that the time to reach 0.90 of the initial concentration in each model corresponded (i.e. 10 months prototype time). The results do not compare as favorably as one would wish. However, if the effective porosity,  $M_p$ , of the prototype aquifer (and the USBR sand) is assumed at 0.3 instead of 0.4, thus changing the Hele-Shaw time scale to about  $1 \text{ min} = 16 \text{ months}$ , the two results compare within 2 months throughout the length of the curves.

In addition, it was assumed in computing the time scale for the Hele-Shaw model that water in the prototype (and the USBR model) was at 20°C and this was also the temperature at which the permeability of 17,200 feet/year was determined. Considering these possible erroneous assumptions the discrepancies in Figure 1 do not seem too serious.

TABLE 1

## UNIFORM AQUIFER COMPARISONS

	USBR Model Run No. 7	CSU Model Runs 1, 2, 4 and 5	Prototype
Initial Salinity	79,770 ppm	79,200 ppm	
Time Scale	$t_p = 1095 t_m$ (1 hr. = 1-1/2 mo)	$t_p = 92,000 t_m$ (1 min = 21 mo)	
Length Scale	$l_p = 40 l_m$	$l_p \approx 55 l_m$	
x	3.93 ft	87.8 cm (2.88 ft)	157.2 ft
z	1.8 ft	39.8 cm (1.30 ft)	72 ft
n	0.40	1.0	0.40
K	17,200 ft/yr (perm. to water assumed $\nu = 0.1$ )	6.66 cm/sec ( $6.89 \times 10^6$ ft/yr) (perm. to aqueous glycerin $\nu = 0.095$ )	17,200 ft/yr (perm. to water - assumed $\nu = 0.1$ )
Ave. Q	2.76 gal/hr (2.95 ft/yr in terms of proto- type	0.0085 cm <sup>3</sup> /sec (2.86 ft/yr in terms of proto- type	$h = 3$ ft/yr

Layered Aquifer Comparisons

The two-layered sand-tank model tests conducted by the USBR utilized sands of permeabilities in a ratio of about 1:50, with the higher permeability on the bottom.

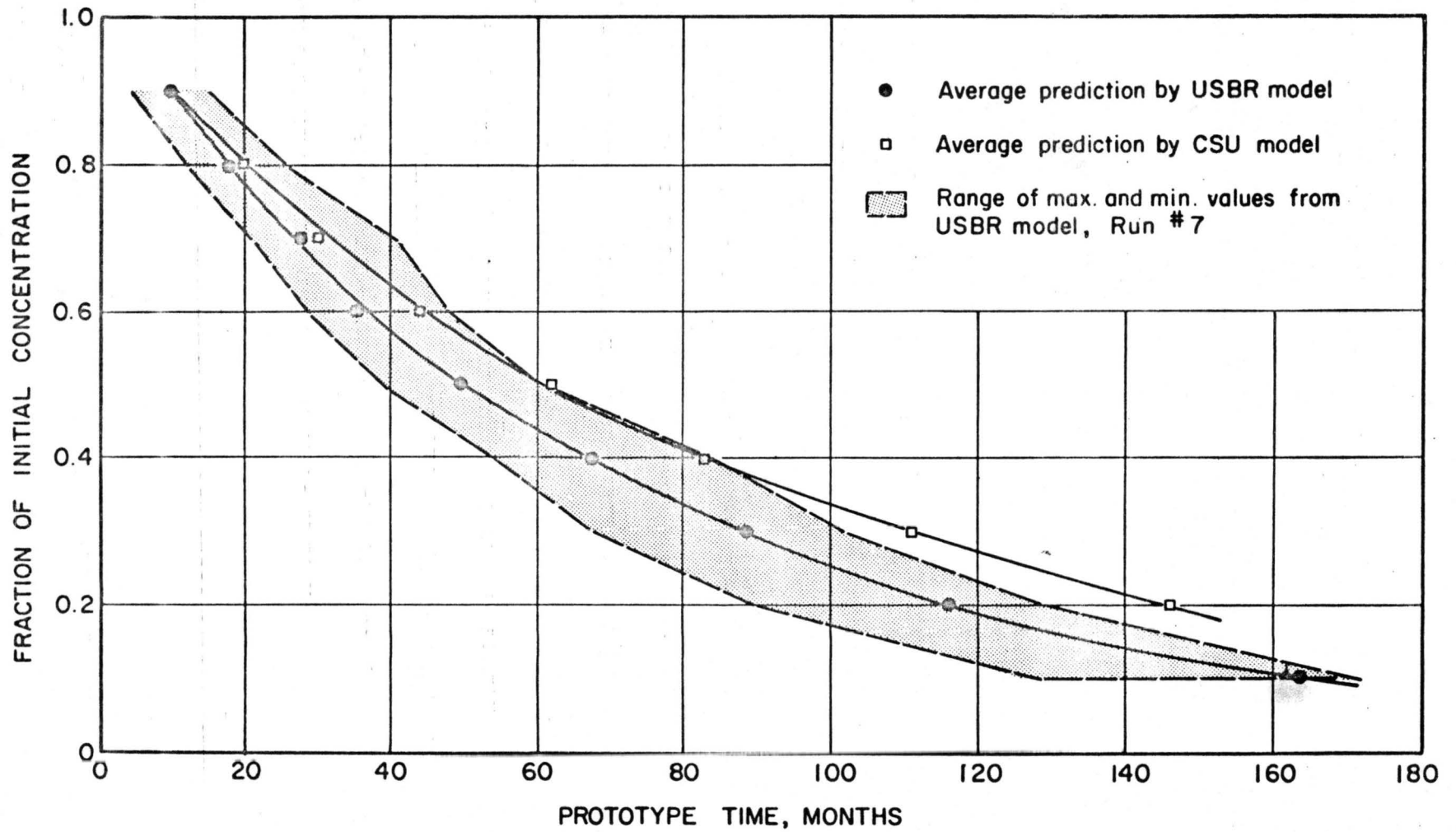


Figure 1. Comparison of USBR and CSU models, uniform aquifer.

The Hele-Shaw Model was modified to duplicate this situation by changing the interspace between the plates to achieve a one to fifty permeability relationship. Tests were attempted at several different initial salinities. The USBR test No. 4, which was attempted to be duplicated by the Hele-Shaw Model, had an initial permeability of about 7,000 ppm of total dissolved solids. Considerable difficulty was experienced in operating the Hele-Shaw Model at initial salinities of less than 15,000 parts per million because a good interface between the saline water and the fresh water could not be maintained at lower salinities. This is probably because the direction of flow in the upper aquifer was essentially vertical throughout the width of the aquifer in that most of the horizontal flow took place in the more permeable lower member. Thus, drops of the recharge water deposited on the surface of the saline water tended to move downward as a drop and create vertical fingers of fresh water. This did not occur at higher initial salinities. Two runs were accomplished at 15,000 and 20,000 parts per million of initial salinity, but results were erratic. A comparison with the USBR run No. 4 (which was also erratic) was attempted with little success. Therefore results of the 1 to 50 permeability runs are considered to be of no value.

#### Relative Advantages and Disadvantages of the Viscous Flow Analogy Model

A number of advantages are apparent in the utilization of the viscous flow analogy or Hele-Shaw model over the sand tank model for the type of studies described herein. These include:

1. A more rapid time scale, which allows a run simulating many years of prototype time to be accomplished in less than a day of model time.
2. Extreme versatility in changing permeability being simulated (by changing the viscosity of the fluid and/or the interspace between the parallel plates).
3. Better visualization of the pattern of flow.
4. Rapid take-down and setup time compared to changing of sand in a sand tank model.

Some of the disadvantages of the Hele-Shaw Model have already been discussed in the main part of the final report. Principal of these are the problem of requiring the ratio of the parallel plate spacing to the prototype porosity  $\left(\frac{b}{n_p}\right)$  to remain equal throughout the model. Whenever two or more permeabilities are being simulated in the model it necessitates assuming changes (possibly very unrealistic) in the porosity of the prototype aquifer. The second major disadvantage discussed above was the fingering effect occurring when the lower part of the model has a much higher permeability than the upper part. Thus, recharge fluid continually dropping on the same spot tends to form a vertical flow-line of recharge fluid through the more saline fluid giving erratic results. Another minor disadvantage, under some conditions, is the sensitivity of results to changes in temperature. Because the viscosity is related to the permeability being simulated, it is necessary that a constant temperature be maintained throughout any one test.